ANTIBODY BIOCONJUGATES FOR TARGETED THERAPEUTIC DELIVERY

A Dissertation

Presented to the Faculty of the Graduate School

of Cornell University

In Partial Fulfillment of the Requirements for the Degree of

Doctor of Philosophy in Chemical & Biomolecular Engineering

by

Dana Nicole Thornlow

May 2019

ANTIBODY BIOCONJUGATES FOR TARGETED THERAPEUTIC DELIVERY

Dana Nicole Thornlow, Ph. D.

Cornell University 2019

Monoclonal antibodies (mAbs) have emerged over the last 20 years as an invaluable biosensing, diagnostic, and therapeutic tool for targeting cancer. With their tight antigen binding and specificity, mAbs are a modular platform for a host of therapeutic modalities, most recently in bioconjugates. Bioconjugates are broadly defined as biological targeting moieties covalently linked with therapeutic molecules and are useful in targeting potent therapeutics to specific cells and tissues. In this work, we develop and investigate mAb bioconjugates for targeted delivery of small molecules, nucleic acids, peptides, and proteins. First, we establish methods for in-house expression, purification, and characterization of mAbs that undergo lysosomal and fast recycling endocytosis pathways upon binding to a target antigen. We then utilize biorthogonal reaction pairs to append various cargo to the mAbs. With an eye toward short-interfering RNA (siRNA) delivery, we conjugate siRNA and membrane disrupting agents to antibodies for co-delivery, targeted cytosolic localization, and gene knockdown of a luciferase reporter gene. Finally, we engineer antibodies with two, orthogonal conjugation sites and to attach sequentially cleavable cargos to a single mAb. With this, we demonstrate controlled, site-specific, dual-labeled antibodies with extracellular and intracellular cargo release mechanisms that can be implicated for sequential release antibody drug conjugates (ADCs).

BIOGRAPHICAL SKETCH

Dana Nicole Thornlow was born on November 2nd, 1991 and spent her childhood in Sayville, New York. She began dancing at age 4 and believed she would grow up to be a dancer, until she realized she couldn't make a career out of it and discovered she was actually pretty good at science. She graduated from Sayville High school in 2009 with a newfound love of chemistry.

In September 2009, she moved to Amherst, Massachusetts for her B.S. in Chemical Engineering with a concentration in biochemical engineering. In her freshman year, she joined the UMass dance team to maintain her sanity in the midst of lots of homework. In her sophomore year, she pursued undergraduate research under Prof. Neil S. Forbes, studying *Salmonella typhimurium* motility in tumor tissue, and continued throughout her undergraduate career.

In August 2013, she moved to Ithaca, New York to start her PhD research as the first cohort of students in Prof. Christopher A. Alabi's Lab. Under his direction, she worked on a variety of projects related to building antibody conjugates for delivering short-interfering RNA, as well as pioneering laboratory efforts to screen synthetic antimicrobial oligomers. In 2014, she received the NSF graduate research fellowship, followed by the inaugural Fleming Family Fellowship in 2015, and culminated her PhD by receiving the Austin Hooey Research and Service Award in 2018. She continued her passion for dance at Cornell when she literally stumbled upon the audition for Shadows Dance Troupe in 2013 while looking for the locker room in Teagle. She danced with Shadows for 10 semesters.

After her PhD, she will begin a postdoctoral research position in Prof. Judy Lieberman's Lab at Harvard Medical School, designing RNA aptamer conjugates for targeted siRNA delivery. She will also undoubtedly continue to dance.

For all the people at Cornell and elsewhere that made all of this possible. And to CTB for all the hazelnut coffee (and chapples).

ACKNOWLEDGMENTS

I would first like to acknowledge Prof. Chris Alabi for taking me on as a student and giving me the freedom to make this project my own. Though it was difficult, I learned a huge range of skills that have prepared me well for the next challenge I face after this PhD. He has been a constant source of ideas and none of this would be possible without his guidance.

Next, I would like to acknowledge my committee members, Prof. David Putnam and Prof. William Brown for their helpful feedback throughout this process. Though I should have utilized them much more, I appreciate their help in making this process as smooth and painless as possible.

I would like to also acknowledge the National Science Foundation, the PhRMA Foundation, and Sam and Nancy Fleming for their financial support of me and my work.

The entire Alabi Lab, past and present, have been an invaluable resource of knowledge and friendship throughout this PhD process. I would not be where I am now without the helpful conversations I've had with all of my lab mates, about experiments or otherwise, that have kept me moving forward over the past 5 years.

Additionally, I would like to acknowledge the several undergraduate researchers I've had the pleasure of mentoring and working with: Katherine Fein, Madeline Dalziel, Bryan Thornlow, Masoom Chainani, and Jacqueline Plesset. They have taught me how to be a mentor and dealt with my learning process along the way. I hope I was able to insight as much in them as they have in me.

Particular members of the fellow "bio" CBE groups have been invaluable to my success, including Emily Cox, Morgan Ludwicki, and Carolyn Shurer. I am very proud to be a part of this group of women who are incredible scientists, and I believe

that all of us have helped each other immensely in science and otherwise during our time in Ithaca.

I would like to also acknowledge all of the other Cornell students and post-docs that have helped me along the way, particularly the 2013 PhD cohort. I have made the best of friends that I know will stay with me long after we all leave Ithaca. I cherish all the time we've spent together, from long homework sessions in the penthouse, attending A exam practices and presentations, outreach events, and organizing committees, to beers at the Chapter House (RIP), summer kickball, birthday parties, and every single one of my dance performances.

I would also like to thank Shadows Dance Troupe for welcoming me as an old lady grad student to practice and perform with you all. Thanks for keeping dance as a constant source of joy in my life.

To Nick Lamson, who provided love, support, and a plethora of coffee shops for thesis writing.

Also, to the entire CBE family, for which I have truly felt a welcome member.

And finally, to acknowledge my parents, Dan and Robin Thornlow, and brother, Bryan Thornlow, for all of their support for as long as I can remember. They encouraged me to pursue this PhD and I know they will continue to support me beyond it.

TABLE OF CONTENTS

BIOGRAPHICAL SKETCH iv
TABLE OF CONTENTS viii
LIST OF ABBREVIATIONS ix
LIST OF FIGURES xi
LIST OF TABLES xiii
CHAPTER 1 – INTRODUCTION: PROTEIN CONJUGATES IN TARGETED DELIVERY OF BIOLOGICS 14
CHAPTER 2 – ANTIBODY EXPRESSION AND CONJUGATION METHODS 26
CHAPTER 3 – ANTIBODY-siRNA CONJUGATES 52
CHAPTER 4 - MEMBRANE DISRUPTING AGENTS FOR ENDOSOMAL ESCAPE 78
CHAPTER 5 – ANTIBODY CONJUGATES FOR DUAL-DELIVERY 110
CHAPTER 6 – DUAL-LABELED ANTIBODY DRUG CONJUGATES FOR ORTHOGONAL CARGO RELEASE 129
CHAPTER 7 – CONCLUSIONS AND FUTURE DIRECTIONS 152
APPENDIX 156
REFERENCES 186

LIST OF ABBREVIATIONS

MW – Molecular Weight
PEG – Polyethylene Glycol
LLO – Listeriolysin O
PFO – Perfringolysin O
MAL – Maleimide
OPSS – Ortho pyridyl disulfide
RP-HPLC – Reverse-phase High Performance Liquid Chromatography
HIC – Hydrophobic Interaction Chromatography
LCMS – Liquid chromatography-mass spectrometry
CDC – Cholesterol-dependent cytolysin
DTT – Dithiothreitol
βME – Beta-mercaptoethanol
DMSO – Dimethyl Sulfoxide
DMF – Dimethyl Formamide
SDS-PAGE – Sodium dodecyl sulfate-polyacrylamide gel electrophoresis
THF – Tetrahydrofuran
TFA – Trifluoroacetic Acid
MMP-2 – Matrix Metalloproteinase-2
CatB – Cathepsin B
siRNA – short interfering RNA
EEA – Endosomal Escape Agent
Ab – Antibody
mAb – Monoclonal Antibody
HC – Heavy chain
LC – Light chain
GalNAc – N-acetyl galactosamine
ASGPR – Asialoglycoprotein receptor
Tf – Transferrin
TfR – Transferrin Receptor
Tub – Tubulin
ASO – antisense oligonucleotide
CQ – Chloroquine
ADC – Antibody-drug conjugate
ADCC – Antibody-dependent cell-mediated cytotoxicity
CDC – Complement-dependent cytotoxicity
ADCP – Antibody-dependent cellular phagocytosis
NK – Natural Killer
mTG – Microbial Transglutaminase
LplA – Lipoic Acid Ligase A
LAP – LplA Acceptor Peptide
HEK – Human Embryonic Kidney
DOL – Degree of Labeling
DAR – Drug-Antibody Ratio

KD – Knockdown
MAL – Maleimide
SS – Disulfide
NHS – N-hydroxy succinimide
TCO – Trans cyclooctene
MeTzine – Methyl tetrazine
DBCO – Dibenzyl cyclooctyne
Az – Azide
DNA – Deoxyribonucleic Acid
RNA – Ribonucleic Acid
dsDNA – double-stranded DNA
dsRNA – double-stranded RNA
ssDNA – single-stranded DNA
ssRNA – single-stranded RNA
aa – Amino acid
His – Histidine
EtOH – Ethanol
MeOH – Methanol
EtOAc – Ethyl Acetate
IPA – Isopropanol
PBS – Phosphate-buffered saline
DMEM – Dulbecco's Modified Eagle Media
FBS – Fetal Bovine Serum
AF488 – Alexa Fluor 488
AF647 – Alexa Fluor 647
MDR – Multi-drug resistant
MMAE – Monomethyl auristatin E
MMAF – Monomethyl auristatin F
WT – Wild-type
Mut – Mutant
K_D – Dissociation Constant
kD – Kilodalton
CEA – Carcinoembryonic Antigen
EGFR – Epidermal growth factor receptor

LIST OF FIGURES

Figure 1.1 Antibody Structure and Function (adapted from Carter et. al[1]) (15)

Figure 1.2 Antibody Therapeutic Mechanisms (adapted from Weiner *et.* al[2]) (16)

Figure 2.1 Hybridoma Antibody Culture, Expression and Purification (31)

Figure 2.2 Trastuzumab Antibody Cloning, Expression, and Purification from HEK 293F Suspension Cells (33)

Figure 2.3 Uptake of Purified Antibodies in Target Cells (35)

Figure 2.4 Schematic of conjugation reactions (36)

Figure 2.5 Non-specific and Site-Specific PEGylation of Purified Antibodies (38)

Figure 3.1 Luciferase Expression via Viral Transduction (56)

Figure 3.2 RNA Chemical Stability Modification (58)

Figure 3.3 Transferrin-Nucleic Acid Conjugation and Purification (60)

Figure 3.4 Functionalized Nucleic Acids with Heterobifunctional Crosslinkers (62)

Figure 3.5 Conjugation and Uptake of Antibody-nucleic acid conjugates (63)

Figure 4.1 Peptide Endosomal Escape Agents with Amine Chemistry (82)

Figure 4.2 Peptide Endosomal Escape Agents with Thiol Chemistry (85)

Figure 4.3 Melittin Conjugation to Transferrin (Tf) Protein (86)

Figure 4.4 Peptide Conjugations with Chemical Linkers (88)

Figure 4.5 Characterization and Conjugation of R9K (90)

Figure 4.6 Conjugation of Peptides to Antibodies (92)

Figure 4.7 Perfringolysin O (PFO) Characterization (93)

Figure 4.8 Listeriolysin O (LLO) Characterization (96)

Figure 4.9 LLO Surface PEGylation- Studies on surface PEGylating LLO for reduced interaction with the outer cell membrane. (98)

Figure 4.10 LLO-Antibody (Ab) Conjugation and Uptake into Mammalian Cells (SKOV3 Cells) (101)

Figure 5.1 Schematic of Proposed Antibody Dual-Conjugate Delivery System (112)

Figure 5.2 Early Endosomal Fusion and Co-localization of TfR Antibody Conjugates (114)

Figure 5.3 Melittin-siRNA complexation for Luciferase Knockdown (115)

Figure 5.4 Transferrin (Tf)-siRNA and Tf-Melittin Conjugate Co-Delivery (116)

Figure 5.5 Antibody-siRNA Conjugate Delivery with Chloroquine Treatment (118)

Figure 5.6 Her2Ab-siRNA Conjugate Delivery with Chloroquine Treatment (119)

Figure 5.7 CD63Ab-siRNA and LLOmut Conjugate Co-Delivery: Simultaneous and Sequential Addition (121)

Figure 5.8 Conjugated LLOmut-siRNA Delivery (123)

Figure 5.9 Her2Ab-R9K-siRNA Non-covalent conjugate delivery (124)

Figure 6.1 Schematic for Dual-Labeled Antibody Conjugates and Orthogonal Cleavage (130)

Figure 6.2 LAP-Tag incorporation into pVitro vector for simultaneous transfection and expression of light chain (LC) and heavy chain (HC) tagged Trastuzumab (132)

Figure 6.3 Efficient conjugation of antibodies with pAz and TCO substrates and Click-able PEGs (PEG-Tz and PEG-DBCO) via LplA (133)

Figure 6.4 Dual-Labeled Antibodies via mTG and LplA (134)

Figure 6.5 Enzymatic Cleavage of Linkers via CatB and MMP-2 (137)

LIST OF TABLES

Table 3.1 of Dissociation Constants of Parent Antibodies and Antibody-DNA Conjugates (64)

CHAPTER 1 – INTRODUCTION: PROTEIN CONJUGATES IN TARGETED DELIVERY OF BIOLOGICS

Antibodies as a Cancer Therapeutic Class

Monoclonal antibodies (mAbs) have become an invaluable scientific tool in laboratory and pathological diagnosis since their discovery in 1975.[3] With their strong antigen specificity and affinity, antibodies are utilized in laboratory cell and tissue analysis, as well as a diagnostic tool for a host of disease biomarkers.

An antibody is a Y-shaped, tetrameric protein consisting of two identical heavy and light chains with constant and variable domains linked via disulfide bonds (Figure 1.1).[1] The constant region of the antibody contains 3 heavy chain domains (C_H1, C_H2, and C_H3) and one light chain domain (C_L), whereas the variable region consists of one heavy (V_H) and one light (V_L) chain domain. C_H2 and C_H3 domains exist in the Fc or "stem" region of the protein, and dictate the immunological response triggered by the antibody. This region also contains a conserved, single glycosylation site at Q297 which is vital for effector function. The Fab or "arm" region of the protein contains the C_H1, C_L, and variable domains, which dictate the antigen binding specificity and affinity. Manipulating and engineering the antibody structure can determine the mechanism and efficiency at which it can be used in cancer treatment.

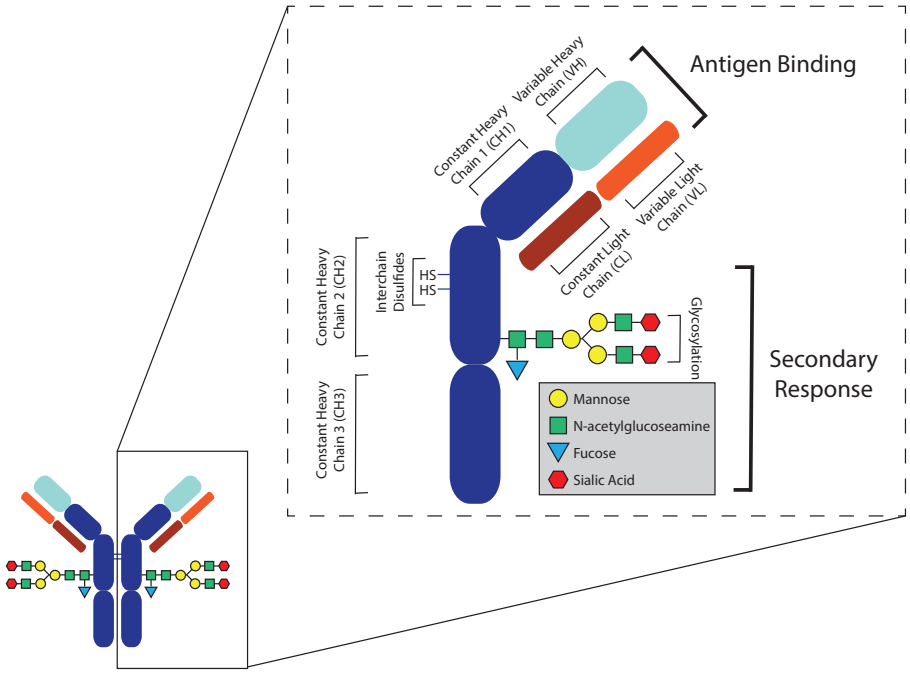

Figure 1.1 Antibody Structure and Function (adapted from Carter et. al[1]) - Schematic of full length IgG1 and Fc region glycosylation (not to scale). Zoom of symmetric half of IgG containing constant (dark blue, red) and variable (light blue, orange) domains. These two symmetric halves are connected via disulfide bonds in the CH2 domain. A single glycosylation site is present at the CH2 domain at Q297.

Monoclonal antibodies can be used in a variety of ways to treat cancer depending on the given antigen and cell type. The holy grail of monoclonal antibodies in treating cancer would be to identify a single antigen that is uniquely and abundantly present on cancerous tissue over normal tissue. However, this cancer-specific antigen has yet to be found. Nevertheless, a host of antibodies that bind cancerous cells specifically have been identified and have the highest tumor specificity of any other targeted therapy to date.[4]

In treating cancer, monoclonal antibodies can function via three main mechanisms:[5] Blocking/changing receptor function, modulating the immune system, or delivering a

chemotherapeutic cargo (Figure 1.2). Depending on the mechanism being targeted, the antibody-antigen pair requires a different set of properties. For example, antibodies eliciting an immune effector function response should bind to a highly abundant, non-internalizing, surface antigen; whereas antibodies carrying a chemotherapeutic drug need not be as abundant but should be highly specific and internalize rapidly via endocytosis. Several antibodies have been developed utilizing these mechanisms.

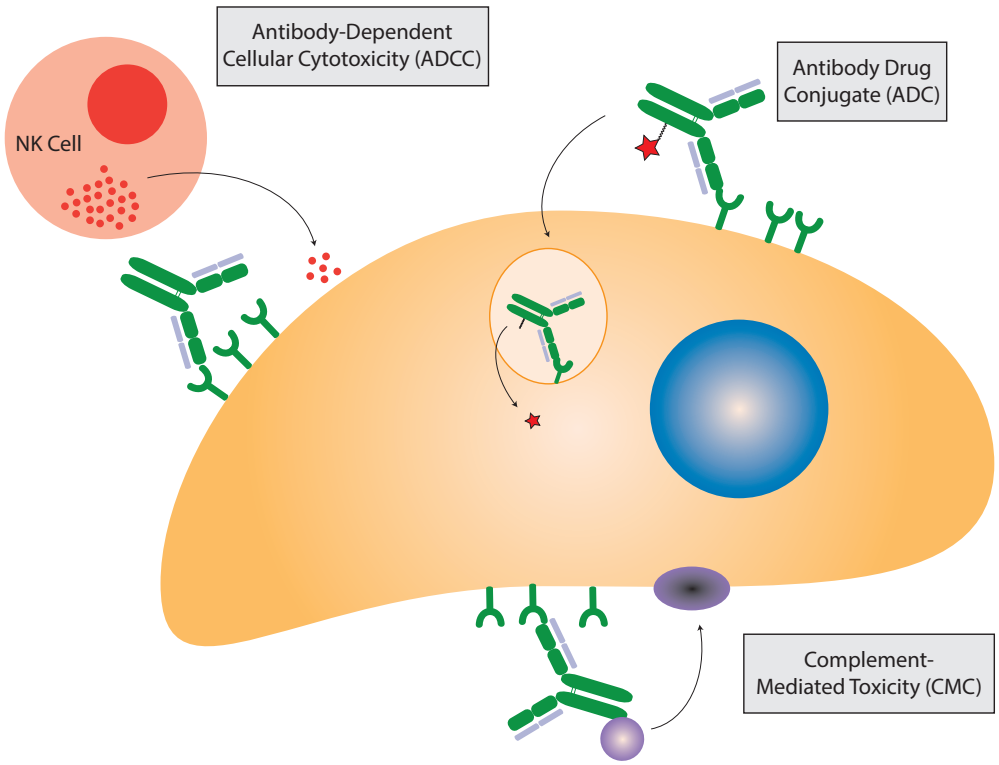

Figure 1.2 Antibody Therapeutic Mechanisms (adapted from Weiner *et.* al[2]) - Schematic of antibody therapeutic mechanisms on target cells including secondary effector responses (ADCC and CMC) and Antibody Drug Conjugates (ADCs). mAbs can signal effector cells through immunoreceptor tyrosine-based activation motifs (ITAMs), that recruit natural killer (NK) cells to secrete perforin and granzymes and induce apoptosis in the target cell for antibody-dependent cellular cytotoxicity (ADCC). mAbs can also induce complement-mediated cytotoxicity (CMC) in which the classical complement pathway is triggered and a membrane attack complex (MAC) is formed. Antibody drug conjugates (ADCs) can also induce cell killing by endocytosis of the ADC followed by release of the cytotoxic drug and subsequent cell death.

The most straight-forward mechanism for mAb-induced cancer cell killing is through direct transmembrane signaling, in which the antibody binds to its target and triggers a signaling cascade to induce apoptosis.[2] Rituximab is an FDA-approved chimeric antibody targeting the CD20 molecule for treatment of non-Hodgkin's lymphoma that functions via this mechanism.[6] Though it also works through a variety of other mechanisms, Rituximab binding was shown to induce activation of apoptosis-associated caspases 3 and 9 and a subsequent reduction in circulating lymphocytes.[7] This is one example of how the antibody can induce apoptosis directly, but more often the cell killing comes through a secondary response.

Antibodies can target cancer cells indirectly by recruiting effector cells to specifically kill cancerous cells. The Fc region of antibodies can trigger an effector cell response through antibody-dependent cell-mediated cytotoxicity (ADCC), complement-dependent cytotoxicity (CDC), or antibody-dependent cellular phagocytosis (ADCP).[1] These mechanisms bring in effector cells such as natural killer (NK) cells, which secrete granzymes to a target and induce apoptosis, or macrophages that can phagocytose, or engulf, the target cell. Antibodies can also manipulate the immune system by setting up an immunological checkpoint blockade. Antibodies like Ipilimumab block the CDLA4 receptor, which is expressed on the cell surface of T cells and stops T-cell activation and survival signals mediated by CD28. By blocking CTLA4 with Ipilimumab, activated T cells could now tag tumor cells for apoptosis, which lead to improved survival in patients with metastatic melanoma.[8]

The third mechanism in which antibodies can be used to kill cancer cells is through antibody drug conjugates (ADCs), in which a cytotoxic payload is covalently attached to a targeted antibody. Following antigen binding and internalization of the ADC into

the target cell, the drug is released and can induce cell death.[9] A notable example of a successful antibody drug conjugate is Trastuzumab-emtansine (T-DM1 or trade name: Kadcyla™), which delivers the cytotoxic drug, DM1, as a potent tubulin inhibitor to $Her2^+$ breast cancer cells, a particularly aggressive form of breast cancer.[10] ADCs are a relatively new class of antibody-based drugs and requires specific antibody and linker design to make them effective.

Antibody Drug Conjugates

ADCs have gone through several generations of conjugation strategies and linker designs since the first ADC was approved in 2000. This first-generation ADC, Gemtuzumab ozogamicin (Mylotarg®), used a CD33 targeted antibody conjugated to calicheamicin, a bacterial-derived antitumor agent that causes double-stranded DNA breaks,[11] for treatment of patients with acute myeloid leukemia (AML). The drug was connected to the antibody via an acid-labile hydrazone linker attached randomly to surface-exposed lysine residues on the protein, yielding an average drug:antibody ratio (DAR) of ~2-3. In 2010, this ADC was withdrawn from the market for high toxicity, presumably due to the heterogeneity of the conjugate and linker instability. However, Mylotarg was later re-introduced and re-approved in 2017 after modifications were made to the dosing regimen.[12] The next generation of ADCs, such as Brentuximab vedotin and Trastuzumab emtansine, incorporated more stable linkages such as thioether linkages, and protease specific release mechanisms such as endolysosomal protease-cleavable sites for targeted drug release.[86] Though these have been successful, they still utilized random conjugation to surface lysine residues or hinge region thiols, which result in statistical heterogeneous mixtures. The third generation of ADCs utilize engineered cysteine residues for site-specific conjugation to the constant heavy domain of the antibody, yielding conjugates with a fixed DAR and

homogeneous composition. By continuously improving conjugate homogeneity and reducing drug deconjugation in serum, ADCs can have an increased efficacy toward the target cells, reduced off-target effects, and increased tolerability.[13,14]

With a proven increase in tolerability of site-specific ADCs, researchers have explored several methods to site-specifically conjugate cargo to antibodies. With the rise of bio-orthogonal chemistry and chemoenzymatic ligation, research groups have developed chemo-enzymatic peptide tags[15-17] and non-natural amino acids[18-21] that can be incorporated into antibodies for site-specific conjugation. Beyond reactive thiol groups, as utilized in THIOMAb technology,[14] researchers have incorporated >50 non-natural amino acids into proteins.[19] Most commonly, p-acetophenylalanine (pAcF) and p-azidophenylalanine (pAzF) have been incorporated for oxime ligations or "click" reactions with ketone or alkyne functionalized substrates, respectively. However, codon optimization of efficient incorporation and expression can be difficult; therefore, chemoenzymatic tags can be an attractive alternative.

Chemoenzymatic ligation involves the ligation of a chemical substrate via an enzyme to a specific amino acid tag. These tags can vary in length and can be incorporated internally or terminally to the protein, depending on the tag. Many of these tags involve post-translational protein modification, in which the protein is modified with a substrate and enzyme after it is expressed and purified. For example, lipoate acid ligase,[22] transglutaminase,[23] and sortase[24] enzymes can incorporate a wide variety of substrates to a short tag incorporated into a target protein. The Bertozzi group has pioneered a co-translational enzymatic ligation method via formylglycine-generated enzyme (FGE), which oxidizes the cysteine residue in the CXPXR pentapeptide sequence to a reactive aldehyde residue.[25] This method is unique in that the enzymatic

ligation occurs co-translationally, thus eliminating a purification step in making the protein tag.

These site-specifically tagged antibodies have been utilized in various applications beyond ADCs. Antibodies tagged with fluorescent and radioactive molecules have become vital in cellular labeling in microscopy applications and immuno-PET.[26-29] Additionally, nucleic acids could be efficiently conjugated to antibodies for applications in immuno-PCR.[30,31] In addition to analytical applications, these conjugation strategies could be applied to other therapeutic cargo, like RNAs. These function similarly to ADCs for intracellular delivery of nucleic acids to target cells.

Nucleic-Acid Therapeutics

Oligonucleotide therapeutics, particularly RNA-based, provide a unique opportunity for transient genetic manipulation of target cells. Unlike CRISPR technologies that permanently edit the genome of cells and tissues and incur a host of ethical conundrums,[32] RNA therapeutics provide a means for transiently down or upregulating gene expression with antisense oligonucleotides (ASOs), short interfering RNAs (siRNAs), and mRNAs.[33] ASOs and siRNAs work by binding to a target mRNA and knocking down gene and protein expression through endonuclease-mediated transcript knockdown[34-36] or Ago2-mediated mRNA splicing.[37,38] mRNA delivery works through upregulating the expression of a target protein by introducing more transcript into the cell. Despite the promise of all of these strategies for gene and protein regulation, the main barrier to therapeutic efficiency is inefficient cytosolic localization, as the mRNA and target machinery are only present in the cell cytosol. Though all nucleotide-based therapeutics run into delivery problems crossing the cell

lipid bilayer, we will focus on ASOs and siRNAs as they are more accessible to conjugate-based delivery strategies.

ASOs and siRNAs have two major barriers in their efficiency of delivery: their serum instability and inability to diffuse through the cell membrane due to its size, charge, and hydrophilicity. To combat serum instability, there has been a wealth of research into chemical modifications to the nucleotide bases and phosphodiester backbone.[39,40] Most notably, modifications to the 2' base position, such as 2'-OMe and 2'-F base modifications, are biophysically similar to the native 2'-OH group, and can still load efficiently into the RNAi machinery, but stabilize the RNA from RNAse degradation and immune activation.[41] Additionally, changing a single oxygen in the backbone phosphodiester bond to a sulfur yields a phosphorothioate linkage,[42] which decreases susceptibility to phosophodiesterases and increases hydrophobicity and subsequent membrane permeability for ASOs.[43] Though these modifications were sufficient for ASO translocation, double-stranded siRNAs were still too hydrophilic for direct cellular uptake.

Conjugate-based therapeutics for siRNA have become increasingly popular with the emergence of GalNAc-siRNA conjugates that efficiently mediate targeted knockdown in hepatocytes.[44] This conjugate uses a trivalent N-acetylgalactosamine (GalNAc) ligand to target the asialoglycoprotein receptor (ASGPR) on the surface of hepatocytes. This conjugate is unique in that there is no obvious component or mechanism for translocation into the cytosol following endocytosis. It is believed however that this specific conjugate depends on the high expression (~10^6 /cell) and fast recycling (10-15 mins) of ASGPR.[33] Under these conditions, if only 0.01% of cargo escaped any endosome through natural leakage, this receptor pathway would

reach the threshold of 5,000 cytosolic siRNAs in less than 24 hours. However, most target receptors have much lower surface expression levels (10^4-10^5 /cell) and slower recycling rates (~90 mins), that reaching this critical threshold within a doubling time of a cell is not possible. Thus, for extra-hepatic delivery, efficiently translocating the endosomal membrane is a barrier that still must be overcome.[45-48]

Endosomal Escape

Lipid bilayers have evolved over billions of years to allow small (< 1kD), somewhat hydrophobic molecules to diffuse through, while preventing large, highly charged molecules, like nucleic acids, from passing through.[33,49] To circumvent a lack of passive uptake, nucleic acids can be encapsulated in a particle or conjugated with a targeting ligand so they can be endocytosed into a target cell. However, unless the oligo can escape the endosome that cargo is rapidly degraded by nucleases present in the endolysosomal compartment, rendering the cargo ineffective.

There are several mechanisms that researchers use to facilitate endosomal escape;[50] most commonly of which are pore formation, pH-buffering and osmotic disruption (i.e. proton sponge effect),[51-53] or membrane fusion[54-56] with the lipid bilayer. Pore formation occurs commonly with amphiphilic, helical peptides, that form a hole in the endosomal membrane that allows content to leak out. The "proton sponge effect" occurs when protonatable groups, such as ionizable amines, buffer protons in the endosome as they acidify, leading to an increase in osmotic pressure and subsequent endosomal membrane disruption and leakage.[51-53] Fusion occurs when pH-inducible lipids of a carrier fuse with the endosomal membrane and the contents are released into the cell cytosol.[54-56] Materials and chemicals that utilize these mechanisms have been identified and incorporated into drug carriers for this purpose.

Chloroquine (CQ) is small molecule lysosomotropic agent and anti-malarial drug commonly utilized for endosomal escape.[57] Mechanistically, CQ and its derivatives[58] are believed to facilitate cytosolic delivery of nucleic acids by inhibiting acidification and interacting with the nucleic acids for increased activity.[58] At high doses, it has been shown to increase endosomal disruption and therapeutic effect of the delivered cargo.[59,60] However, CQ isn't naturally targeted to a cell and has major toxicity at the high concentrations at which it is effective. Thus, researchers have incorporated buffering functional groups into polymers for delivery,[52] or resorted to other mechanisms for endosomal disruption, like through pore forming agents.

Pore forming agents derived from bacterial or viral infectious agents have been utilized for targeted disruption of the endosomal membrane. A common pore-forming agent utilized in delivery systems is Melittin, which is a 26-amino acid peptide and the primary toxic component of bee venom.[61,62] Melittin forms a tetrameric structure in solution,[63] and upon binding to a target cell membrane, forms an amphipathic helical structure and pore perpendicular to the cell membrane.[64,65] Melittin and analogs have been incorporated into various delivery systems including polyplex[66,67] and notably dynamic polyconjugate (DPC) systems.[68-70] In DPCs, a Melittin derivative was masked with a maleic anhydride derived polymer and a GalNAc targeting ligand. The masking step is critical to prevent Melittin from non-specific membrane disruption. This conjugate was co-delivered with a cholesterol-conjugated siRNA cargo for specific delivery to hepatocytes. Following co-localization in the early endosome, the Melittin derivative is unmasked in the acidic environment of the endosome, which enabled Melittin to induce pore formation and subsequent escape of the cargo siRNA into the cytosol. Arrowhead pharmaceuticals pioneered this technology, but later placed a hold on clinical trials, likely due to the toxicity of Melittin.[33]

In addition to amphiphilic, lytic peptides, bacterial toxins have also emerged as another class of pore-forming agents for endosomal escape. Notable in this class are the family of cholesterol-dependent cytolysins,[71] which are soluble in aqueous solution, but readily form large pores (~300A) in lipid membranes with cholesterol. These toxins are secreted by several gram-positive bacteria and are important in their pathogenicity.[72] Two examples of these pore forming toxins are Perfringolysin O (PFO) and Listeriolysin O (LLO) from *Clostridium perfringens* and *Listeria monocytogenes*, respectively. These toxins are both ~52kD in size and have a similar tetrameric structure.[73,74] They have a high affinity (K_D ~10^{-9} M) for cholesterol, and oligomerize to form 20-30nm ring-shaped pores.[71] Uniquely, LLO is utilized for endosomal escape of Listeria following uptake into a host cell. The toxin is secreted from the endocytosed bacterium to form a pore in the endosome so the bacteria can replicate in the cytosol of the host. However, following endosomal escape, the toxin becomes inactive at the neutral pH of the cytosol as to not kill the host, making it a unique target for endosomal escape in biologics delivery.

LLO and PFO have been utilized for targeted intracellular delivery of immunotoxins[75-77] and siRNA.[78] In these studies, conducted in the Wittrup Lab, they generated a bispecific antibody that both neutralized the bacterial toxin and targeted EGFR for specific endocytosis. When co-delivered with the immunotoxin, gelonin, or an siRNA, the two conjugates co-localized and the bacterial toxin facilitated release of the cargo into the cytosolic space. They found this was an effective method for targeted delivery and endosomal escape *in vitro*. However, this study likely did not move *in vivo* because of the immune response that would be generated from the bacterial toxin.

These studies emphasize the importance of incorporating a well-protected endosomal escape agent into a conjugate delivery system.

Despite the promise of RNA therapeutics, the translation of these therapeutic entities continues to be limited by delivery. Because of their natural cell impermeability, endosomal escape remains the major hindrance to the translational potential of therapeutic nucleic acids. Until a method for safely incorporating endosomolytic agents becomes clear, disease targets are still limited to hepatocytes. Antibody conjugates are an effective means to target tissues beyond the liver specifically but incorporating siRNA and endosomal escape agents into antibody conjugates effectively remains difficult. In this dissertation, we will discuss methods for expressing, purifying, and conjugating antibodies with therapeutic cargo. We hope to use this work to inform the design of antibody conjugates carrying both siRNA and protected, potent endosomal escape agents for targeted delivery and endosomal escape.

CHAPTER 2 – ANTIBODY EXPRESSION AND CONJUGATION METHODS

Background

Antibodies have emerged over the last ~25 years as an important new class of drugs to treat cancer, infectious diseases, chronic inflammatory diseases, and several other classes of disease.[1] Antibodies are an intriguing class of therapeutics because they are target specific, well-tolerated in humans, modular, and can work through a variety of mechanisms. The first monoclonal antibody was approved in 1986 (Muromonab), and since then, more than 50 antibody-based drugs have been FDA approved for various applications.[79] The design and production of antibodies is constantly evolving as the utility of this class of drugs continues to grow.

Hybridoma technology was the first method for generating monoclonal antibodies (mAbs). With this method, B cells from mice immunized with a particular antigen are fused with an immortalized myeloma cell line to produce stable antibody-expressing cells.[3] These hybridoma cells generate mouse monoclonal antibodies, which have had huge success in research applications, but a minimal success rate (3%) in drug development[80] due to the immunogenicity of mouse antibodies in humans. This has been largely solved though through chimeric or humanized antibodies.[82-85] Generating these humanized antibodies can be done through phage-,[81-83] ribosome-,[84-88] and yeast-display libraries,[89,90] human hybridomas, or transgenic mice.[91,92] Following their discovery and affinity maturation, antibodies can be genetically manipulated for better effector function with glycoengineering,[93-95] constant region amino acid manipulation,[96] and isotype modulation.[97] The engineered antibodies can then be expressed in HEK293T, and the suspension HEK293F cells for lab scale testing.[98,99] Nearly all late-stage clinical antibodies are then produced recombinantly in Chinese

hamster ovary (CHO) or NS0 mouse myeloma cells because of their high antibody titres.[1]

mAbs are most commonly utilized for their effector function and generating a secondary immune response to a target cell. The Fc region of the antibody can trigger effector cells like NK cells, monocytes, granulocytes, or macrophages to kill the target cell.[100-103] However, over the last 10 years researchers have also developed antibody drug conjugates (ADCs) in which a chemotherapeutic drug is linked through a chemical linker.[9,104] With the specificity of the antibody and the potent activity of the small molecule drug, these conjugates can target specific cancer cells with chemotherapeutic drugs without the broad toxicity of delivering the drug systemically. To generate these conjugates, biorthogonal chemistry is used to covalently attach various molecules to proteins.[16,105] Here, we utilize "click chemistry" groups with fast kinetics and aqueous stability for protein conjugation.

"Click chemistry" is a term coined in 2001 to define reactions that have high yields, form stable products in physiological solutions, are wide in scope, and form only "inoffensive byproducts".[106] The main reactions that fall under this scope are the Huisgen[107] and Diels-Alder[108] cycloaddition reactions between azide and alkyne groups, and tetrazine and diverse dienophiles, respectively. These pairs are bio-orthogonal, stable in aqueous solutions, have fast kinetics, and are commercially and synthetically accessible. In this chapter, we utilize all of these functional groups for antibody bioconjugation.

Antibodies, like other proteins, can be conjugated in two major ways: non-specifically to accessible and abundant surface residues, or to a specific region or residue.

Commonly, researchers take advantage of surface primary amine groups on lysine residues in the protein and utilize N-hydroxysuccinimide functionalized crosslinkers to attach cargo. In contrast, methods for site-specific conjugation[9] on antibodies include maleimide conjugation to native cysteines in the hinge region of IgG1's, and engineering additional cysteines[14,109-111] or other reactive non-natural amino acids[18,112,113] into the constant region domains. Chemoenzymatic ligation involves the ligation of a chemical substrate via an enzyme to a specific amino acid sequence tag. These tags can vary in length and can be incorporated internally or terminally to the protein, depending on the tag.[15] Post-translational site-specific enzymatic conjugation strategies include microbial transglutaminase (mTG)[13,23,94,95] and lipoic acid ligase (LplA).[114] Here, and throughout this dissertation, we utilize both non-specific and site-specific methods for conjugating various therapeutic cargo to antibodies.

Microbial transglutaminase (mTG) is a bacterial derived enzyme that can crosslink glutamine and lysine residues of proteins. This enzyme has also been shown to specifically crosslink Q295 on the Fc region of humanized antibodies with amino-containing substrates for site-specific conjugation.[23] This enzyme is commercially accessible and very cheap, as it is also used as "meat glue" for binding together meat products. It also has promiscuous substrate specificity including a variety of click chemistry, fluorescent, or even small molecule drug substrates.[115-117] Thus, a variety of conjugates can be easily developed without genetic manipulation.

An alternative method for site-specific conjugation involves incorporating an amino acid tag to the genetic antibody sequence. The LplA Acceptor Peptide (LAP) sequence (GFEID**K**VWYDLDA) is a short, 13aa tag that can be incorporated anywhere into a target protein. The LplA enzyme can couple a valeric acid substrate specifically to the

lysine residue in the LAP tag sequence. This chemoenzymatic ligation has fast kinetics, variety of compatible substrates, and flexibility in sequence location.[22,114,118-122] However, to our knowledge it has not yet been incorporated into an antibody conjugate. In this chapter, we manipulate and express mouse and humanized antibodies targeting CD63 and Her2. We then use non-specific and specific conjugation strategies to generate antibody conjugates with functional cargo for targeted delivery to cells.

Hybridoma Antibody Expression and Purification

Antibodies can commonly be expressed and purified from hybridoma cells, which are a cross between antibody-expressing B-cells recovered from a mouse challenged with a specific antigen, and immortal B cancer cells called myelomas. These hybridomas are convenient in that they secrete monoclonal antibodies into the media they are cultured in, and the cells can be cultured indefinitely. Generating hybridomas can be a very lengthy process, but they can be acquired through shared networks such as the Developmental Studies Hybridoma Bank (DSHB) through the University of Iowa. Here, we purchased the H5C6 hybridoma cell line[123] to produce an antibody targeting the ubiquitous tetraspanin CD63, which is known to traffic to the late endosome/lysosome.

Hybridoma cell culture and antibody purification is a slow expansion process in full serum media, followed by a reduced serum production phase, antibody precipitation and column purification (Figure 2.1). Cells are cultured in a way such that they begin in a 24-well plate and are expanded continuously until they reach a desired density to purify antibody from. When the cells move from the well plate to a larger vessel, the wells of the 24-well plate are replenished with fresh media, and the remaining cells

that were not transferred from the well expand in the new media so the process can begin again. In growth phase, the hybridomas are cultured in high serum (20%) media to maintain viability. Following the growth phase when the cell density is high enough, the media can be exchanged to low serum (5%) media for the antibody production phase. This is done in order to reduce the amount of residual protein in the media that the antibody is purified from.

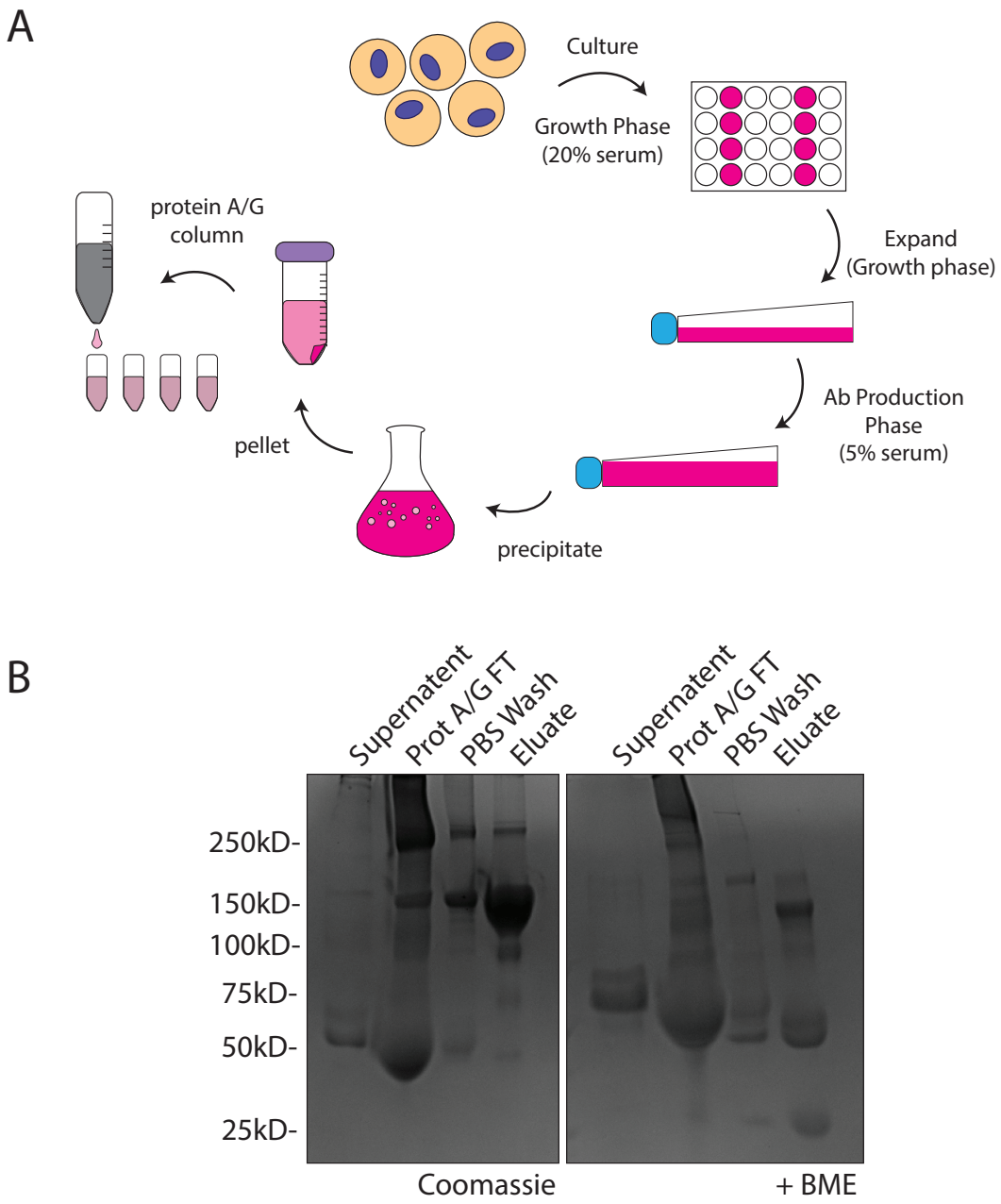

Figure 2.1 Hybridoma Antibody Culture, Expression and Purification (CD63Ab) – (a)Schematic of cell culture and expansion of CD63 antibody-expressing hybridoma cells from 24-well plate to large culture flask. Upon proper cell density and viability, antibody is precipitated with saturated ammonium sulfate, pelleted, and re-suspended in buffer and purified on a protein A/G affinity column. (b) Analysis via SDS-PAGE showed no antibody remaining in the supernatant, but some remaining in the flow-through (FT) over the protein A/G column. Following PBS washed and elutions, the pure antibody was detected in its full length and reduced to the proper heavy and light chain fragments.

When the hybridoma cells have died from the reduced serum, the antibody must be purified from the media. Because of the large volume of media recovered from these cells, the protein is first precipitated from the media using ammonium sulfate. Once the protein has precipitated and pelleted, the recovered pellet can be re-suspended in a smaller volume for affinity purification. That volume can be flowed over a protein A/G resin, which binds specifically to the Fc region of antibodies, and can be eluted at low pH's. Following precipitation and purification, we see no antibody remains in the precipitate, and only pure antibody leaves in the eluate (Figure 2.1B). Some antibody was detected in the affinity column flow-through, which could be further optimized with more resin and a longer incubation time to load on the resin. The entire purification process takes 2-3 days and generates yields of ~3.3mg/L.

HEK293F Cloning, Expression, and Purification of Trastuzumab

Though hybridoma technology is an efficient means for antibody production, manipulation of the antibody at the genetic level in a hybridoma cell line can be difficult. The emergence of CRISPR technologies has made manipulation possible, but the design of CRISPR RNAs is non-trivial, and hybridoma cells can be slow to expand. Therefore, we moved to a platform where we could genetically manipulate the antibody in *E. coli* and produce the antibody in an alternative cell line.

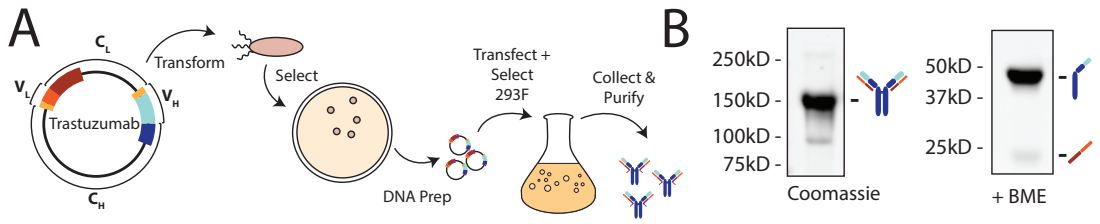

Figure 2.2 Trastuzumab Antibody Cloning, Expression, and Purification from HEK 293F Suspension Cells – (a) Schematic of cloning and expression of Trastuzumab antibodies (with and without LAP Tag) in 293F Expression Cells. (b) SDS-PAGE of full length Trastuzumab antibody (left) and reduced to heavy and light chain fragments (right).

Dodev and colleagues at King's College London developed a platform for genetic manipulation of an antibody sequence in *E. coli* and expression in an Freestyle-293F suspension cell platform.[98] Ilieva took this platform and generated a plasmid for expressing the FDA-approved Her2-targeting antibody, Trastuzumab[99]. With this plasmid, we were able to generate a stable, Freestyle-293F suspension cell line to produce full-length Trastuzumab antibody for use in our targeted delivery studies (Figure 2.2). This platform uses PIPE or Gibson style cloning techniques to swap variable and constant antibody regions in *E. coli*. Then, the purified plasmid can be easily transfected, and is stably incorporated into HEK293F cells using a commercial transfection reagent. These cells can have a range of expression levels and yields, as the level of integration into the cell genome is random. With this platform we were able to generate antibodies targeting Her2 and poly-Sialic acid (ch735) [124] to make conjugates with. Additionally, we were able to incorporate a LAP tag at the variable heavy or light chain region of the antibody. Having genetic manipulation capabilities on this antibody allowed us to use site-specific conjugation techniques rather than random labeling techniques as was done with the commercial and hybridoma expressing antibodies.

CD63Ab and Her2Ab Internalization into Target Cell Lines

In order for the target antibodies to be useful in internalizing cargo, we verified their uptake into cells with immunofluorescence and flow cytometry. SKOV3 cells were incubated with CD63 and Her2 targeted antibodies for 1 hour, then permeabilized and labeled with a corresponding secondary antibody to determine cellular localization (Figure 2.3). Both antibodies were detected in the intracellular space, with Her2 antibody also detected significantly at the cell surface, which is consistent with literature.[125] CD63 was primarily present as punctate intracellular spots, which is expected as a late endosomal marker.[126]

Relative uptake of the CD63 and Her2 targeted antibodies was analyzed in MCF7, HeLa, and SKOV-3 cells via flow cytometry. Each antibody was labeled with a green, Alexa Fluor 488 NHS-ester, and added to varying cell types to examine relative expression levels. CD63 expression levels were approximately equal across all three cell lines (Figure 2.3 B,C,D). CD63 is a ubiquitous tetraspanin that internalizes via a lysosomal pathway.[126] Targeting this receptor with antibody conjugates would allow us to analyze the same pathway across a variety of cell lines to determine cell type dependence. Her2 expression levels varied across cell lines, with significantly higher expression levels in SKOV3 cells over the other two lines (Figure 2.3 B,C,D). Her2/ErbB2 has varying expression levels and is a primarily recycling receptor.[125] Targeting this receptor would allow us to examine expression level dependence and look at a fast recycling pathway which has been shown to be effective in hepatocytes. These two antibodies gave us a variety of pathways and expression levels to examine antibody conjugate efficacy.

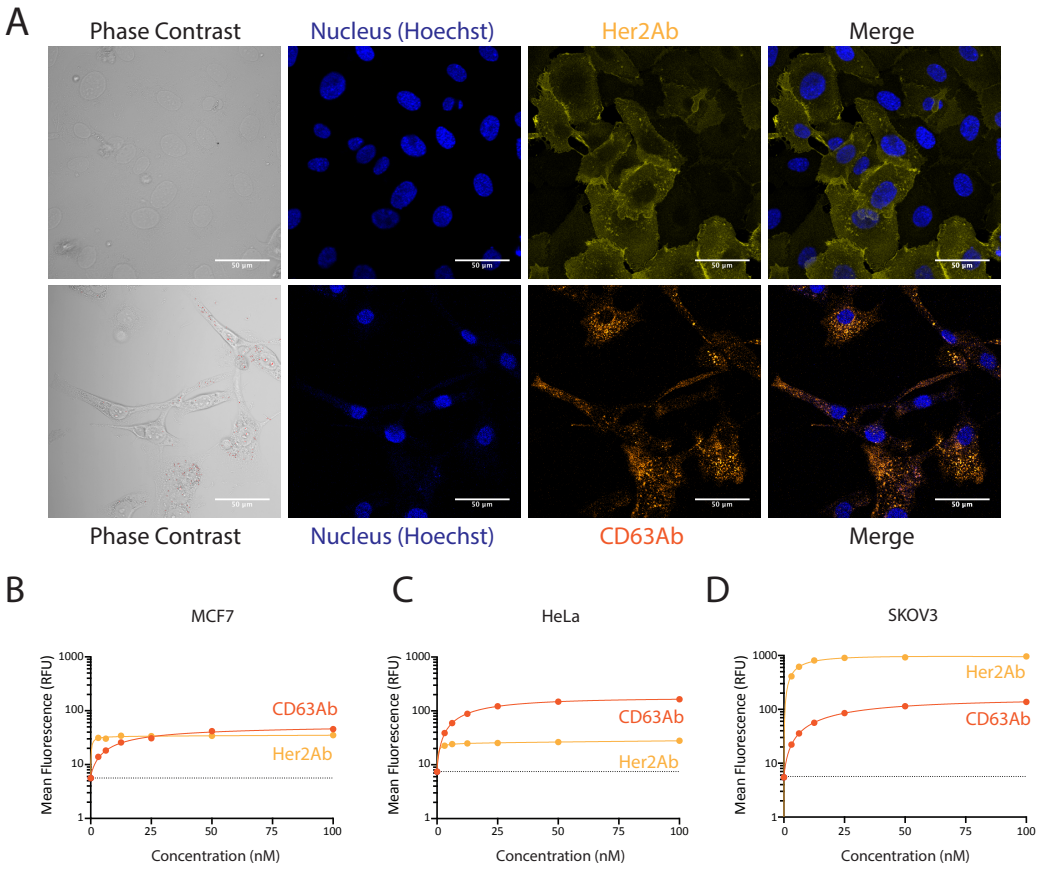

Figure 2.3 Uptake of Purified Antibodies in Target Cells – (a) Immunofluorescence of Her2 antibody (top) and CD63 antibody (bottom) internalization into SKOV3 cells. Phase contrast images (left), Hoechst-stained nuclei (blue), Her2 antibody (yellow), CD63 antibody (orange), and merged images (right). (b-d) Flow cytometry uptake of AlexaFluor 488 (AF488) labeled antibodies into MCF7 (b), HeLa (c), and SKOV3 (d) cells. Antibodies showed similar affinities across cell lines, but varying uptake levels relative to expression levels.

PEGylation of Antibodies with Click Chemistry

Protein drugs often suffer from a short half-life within the body, as they are rapidly excreted or degraded by serum proteases. This then leads to more frequent dosing, and an increased immune response among treated patients. One major way that these issues can be alleviated is through surface PEGylation, in which a PEG (polyethylene

glycol) molecule is added to the protein, increasing its hydrodynamic radius and "shielding" the protein from the body.[127] With a variety of conjugation techniques at hand, we used both non-specific and site-specific methods to PEGylate the surface of antibodies. We utilized two-step click chemistry methods for conjugation, so we could expand the PEGylation technique to other functional cargo like nucleic acids and proteins.

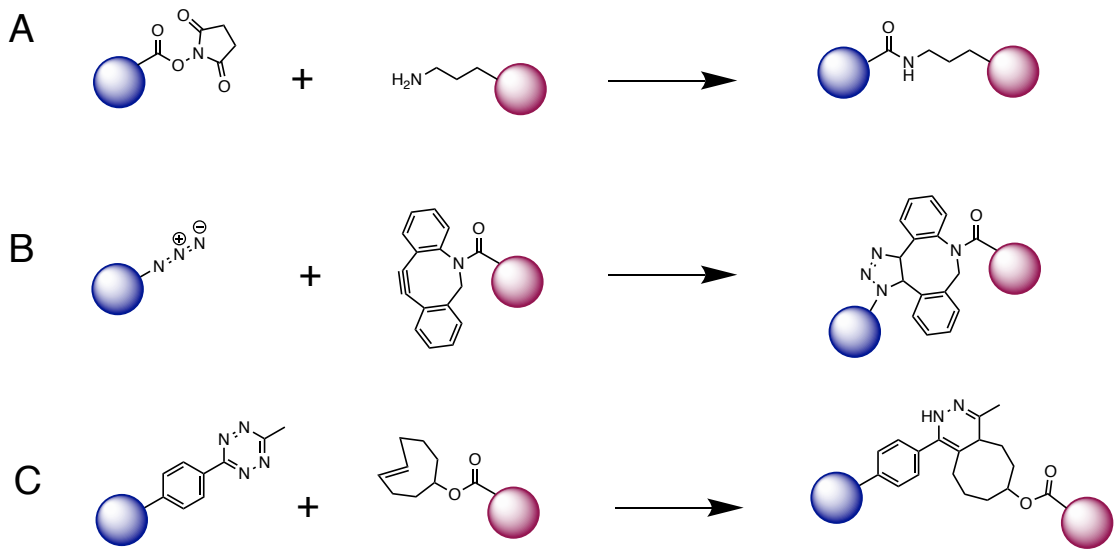

Figure 2.4 Schematic of conjugation reactions. (A) N-hydroxy succinimidyl ester (NHS ester) reaction with primary amine. (B) Copper-free click reaction between azide with dibenzyl cyclooctyne (DBCO) (C) Inverse electron demand Diels-Alder reaction between methyltetrazine (MeTzine) and trans cyclooctene (TCO)

We began with the statistical surface labeling via N-hydroxy succinimidyl (NHS)-ester functionalized PEGs. These NHS-ester PEGs react with the primary amine present on solvent exposed lysine residues on the surface of the antibody (Figure 2.4A). The number of available residues is dependent on the antibody sequence, making this method polydisperse and highly variable. However, this is a single-step conjugation, in which the cargo is connected directly to the antibody and is not reliant on a second reaction step. This method is ideal over a two-step if the NHS-ester

functionalized cargo exists. However, the NHS-ester readily undergoes hydrolysis in aqueous solution, therefore, synthesizing the NHS-ester form of a reagent isn't always feasible. The NHS-ester PEG is commercially available, and thus we examined the resulting DOL from this reaction. As seen in Figure 2.5D, a degree of labeling range from 0-3 was detected via SDS-PAGE for this particular reaction condition, but this can be variable dependent on the equivalencies of NHS-ester substrate, concentration, and reaction time for a given conjugate. Additionally, even with a similar degree of labeling, the location of the sites is highly variable, leading to a very heterogeneous mixture of conjugates. Though generating homogeneous antibody conjugates is ideal, these antibodies are still functional and can be made quickly and easily.

Following the statistical conjugation, we optimized mTG-based PEGylation of antibodies with an Azide-DBCO click chemistry pair (Figure 2.4B). This method specifically conjugates a single PEG chain to Q295 residue in each symmetric Fc region of the antibody. [23] With this method, we saw a near-quantitative PEGylation of Trastuzumab specific to the heavy chain of the antibody as visualized with SDS-PAGE (Figure 2.5E). However, this method requires a near stoichiometric amount of enzyme, long reaction time (6-24 hours), and a rigorous enzyme removal step. Additionally, this method requires removal of the single glycan present on the Fc region of the antibody, which is very important for complement immunity. Therefore, ADCs synthesized in this way cannot elicit a targeted complement immune response. Nevertheless, this method does not require genetic manipulation and can be used on any humanized antibody.

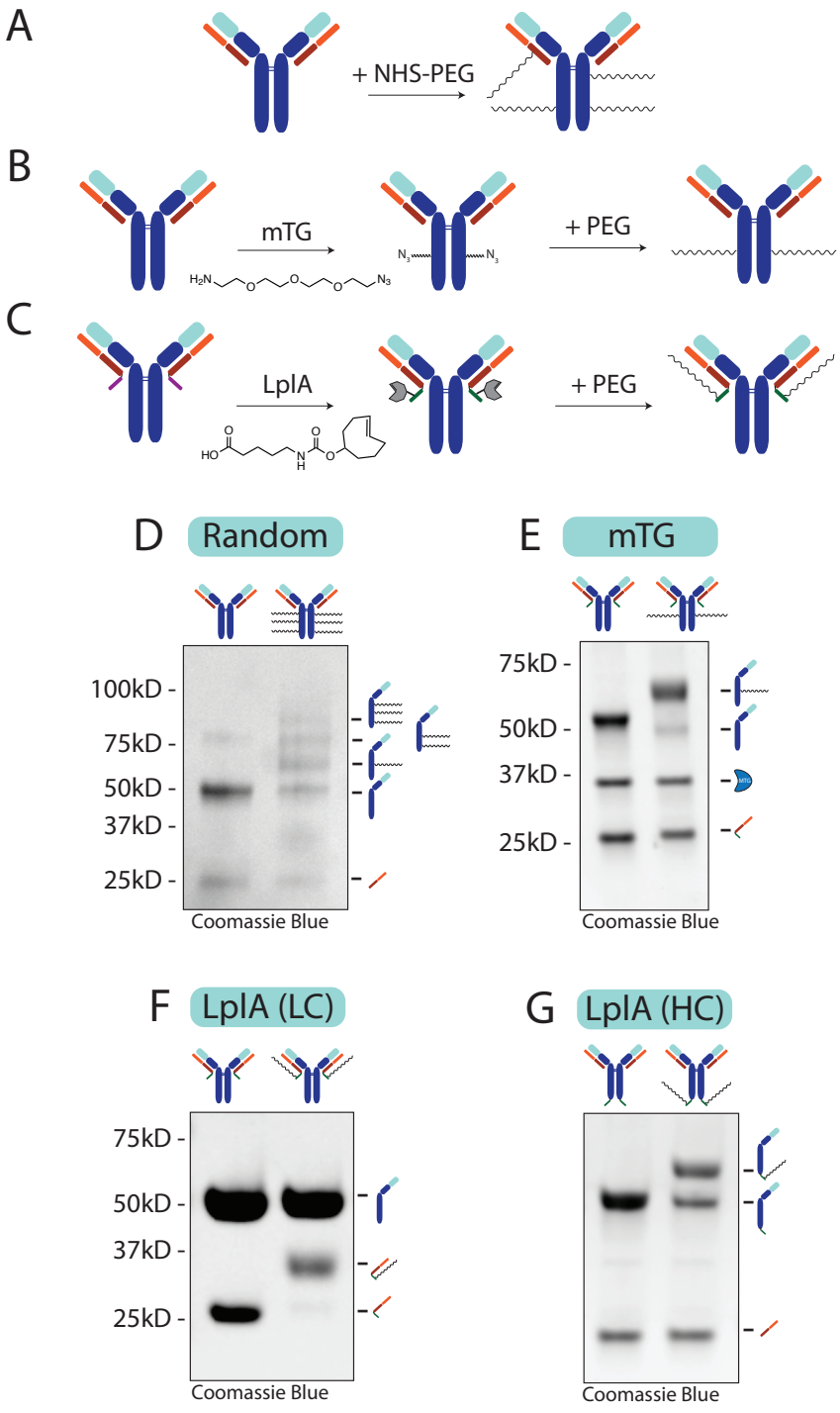

Figure 2.5 Non-specific and Site-Specific PEGylation of Purified Antibodies – (a-c) Schematic of non-specific (a), mTG site-specific (b), and LplA site-specific (light-chain) (c) modified antibodies with PEG. (d-g) SDS-PAGE analysis of extent of PEGylation of antibodies, stained with Coomassie blue. Random surface PEGylation

(d) showed a distribution of labeling on both heavy (HC) and light chain (LC) fragments. mTG labeling (e) showed quantitative labeling specifically to the heavy chain fragment. LplA labeling showed quantitative labeling at the light chain (f) and approximately 50% labeling at the heavy chain (g).

Finally, we optimized the LplA-based PEGylation of antibodies at the heavy or light chain constant region domains. The LAP-tag (GFEID**K**VWYDLDA)[114] along with a GGGS flexible spacer was cloned into the heavy chain (HC) and light chain (LC) C-termini of Trastuzumab. The C-termini of each constant region chain was chosen for ease of swapping variable regions to generate LAP-tagged antibody conjugates against a new antigen, and for minimal inhibition of protein folding and antigen binding. Addition of the LAP-tag was verified with Sanger sequencing. Using the TCO-functionalized substrate,[121] we could PEGylate the antibody at the light or heavy chain C-terminal specifically with a tetrazine-functionalized PEG (Figure 2.5C). With this conjugation, we saw near-quantitative conjugation of the light chain, and only ~50% conjugation of the heavy chain (Figure 2.5F&G). Further optimization or different substrates could help promote the quantitative conversion at the heavy chain site. This method requires a low enzyme concentration (10mol%) and short reaction time (1-2 hours) relative to the mTG reaction. Also, since the LAP tag is genetically incorporated, it can be moved to theoretically anywhere throughout the protein. However, the reaction conversion site-dependent and required time-consuming genetic manipulation to be incorporated into the antibody. This ligation is also orthogonal to the mTG reaction and thus can be in combination with LplA for dual conjugation, which will be discussed further in chapter 6.

Conclusions & Discussion

In this chapter, we examined various expression platforms and conjugation methods for PEGylation of antibodies. These methods are necessary in making antibody drug

conjugates (ADCs) or other antibody conjugates carrying various cargo to a specific cell of interest. Though commercial antibodies are available, they can be very expensive (~$400/100μg Ab) to generate conjugates from and deliver to cells. Therefore, for antibody conjugation labs it is necessary to explore platforms for making and purifying antibodies.

We analyzed two expression platforms: Hybridoma and Freestyle-293F cells. These cell lines are both cultured in suspension, which is necessary to achieve cell densities high enough to generate enough antibody without a large surface area. Hybridoma cell lines can be difficult to generate however, as they are dependent on mouse immunization and fusion with myeloma cells and several selection steps. Nonetheless, this method can generate antibodies without knowing the protein sequence, so can be used in discovering and expressing new antibodies. The alternative requires first acquiring the sequence of the antibody but can then be genetically incorporated easily into HEK293F cells using commercial transfection reagents and without the design of CRISPR RNAs or viral transduction. These cells are easy to grow and produce antibody in serum-free media and are simple to purify. Both strategies suffer from low yields (~2-3mg/L Ab), thus, future studies should consider ExpiCHO-S® (Life Technologies) cells. Though generation of a stable line of these cells is less trivial, transient transfection generates yields of up to 3 g/L, well beyond those of Freestyle-293F cells that stable incorporation may not be necessary.

Finally, we examined random and site-specific conjugation methods for labeling antibodies. We utilized TCO-tetrazine and DBCO-azide cycloaddition pairs for their bio-orthogonality and fast kinetics to tag a large variety of cargo to antibodies. As a first, easy conjugation cargo, we examined simple PEGylation and analyzed the pros

and cons of each conjugation method. Random NHS-ester conjugation methods are very simple and easy, can achieve high DOL, and use a one-step conjugation, which does not require intermediate purification steps, whereas a two-step conjugation method would. This method requires no enzyme, therefore simple size-based separations should be sufficient to remove the added substrate. However, this method yields heterogeneous conjugates that can have varying antigen affinities, efficacies, and pharmacokinetic/pharmacodynamic properties *in vivo*. Also, synthesizing NHS-ester functionalized cargo is not always feasible, since the ester is easily hydrolyzed.

The site-specific conjugation strategies using mTG and LplA generate homogeneous conjugates. These homogeneous conjugates should have a better affinity for their antigen, since the conjugation should not block the binding site. The mTG conjugation showed a near-quantitative conversion clicking a DBCO-functionalized PEG onto an azide-functionalized antibody. This was more efficient than the LplA reaction attaching a TCO substrate to the heavy chain C-terminal and clicking on a Tzine-functionalized PEG. It appears that when labeling the heavy chain, the mTG reaction is more efficient. However, given a different set of substrates, it may be possible to get conversion of the HC LplA reaction equal to that of the mTG. Also, moving the LAP-tag to a different place within the heavy chain may also improve reaction conversion. Light chain labeling, however, was quantitative using LplA and the TCO substrate. This illustrates that the "click" reaction is quantitative, and the difference in labeling is due to substrate incorporation into the antibody. LC labeling currently cannot be achieved with the mTG, thus the LplA reaction is vital for labeling the light chain specifically. Labeling the LC allows for the Fc to remain untouched, and therefore can still trigger effector response. Additionally, when comparing ADCs labeled at the LC vs the HC, the LC-labeled ADCs were more stable.

These site-specific modification methods, though generate more consistent, homogeneous conjugates, can be more difficult to implement. Both the mTG and LplA coupling reactions require more stringent purification to remove the enzyme. Additionally, the LplA requires additional genetic manipulation by incorporating the LAP tag into the antibody sequence, which is not always possible unless the antibody is in a genetically tractable plasmid. This is necessary though, if the cargo needs to be at a specific site on the antibody. Depending on the application, one strategy may be more beneficial than the other and it is on the researcher to decide which method is necessary for a given application. For preliminary characterization, it is best to begin with non-specific conjugation methods. However, following proof of concept studies, researchers should take advantage of site-specific methods whenever possible for optimization, especially *in vivo*.

Materials & Methods

Cell Culture and Reagents: Hybridoma cells were cultured in Iscove's Modified Dulbecco's Media (IMDM) and RPMI Media purchased from Life Technologies with 20% heat-inactivated fetal bovine serum (FBS; Atlanta Biologics) and 100 U/mL Penicillin and Streptomycin (Pen/Strep; Life Technologies). SKOV3 and HeLa cells were cultured in Dulbecco's Modified Eagle Media (DMEM; Life Technologies) with 10% FBS. MCF7 cells were cultured in DMEM + 10% FBS with 10µg/mL insulin. Freestyle-293F cells were maintained in Freestyle 293 Expression medium with 100U/mL Pen/Strep.

All chemicals and solvents were purchased from Millipore-Sigma and VWR unless stated otherwise. Chemical crosslinkers were purchased from BroadPharm (Az-PEG3-NH2, Cat#BP20580; TCO-NHS ester, BP-22417; NHS-PEG4-TCO, Cat# BP-22418; MeTzine-PEG5-NHS, BP-22945; DBCO-PEG4-NHS, BP-22288). DNA Primers were

purchased from Integrated DNA Technologies (IDT). Materials for PCR and cloning were purchased from New England BioLabs. Gel electrophoresis materials were purchased from Bio-Rad. Plasmid for Trastuzumab antibody generation was purchased from Addgene (Plasmid# 61883). All sequencing was done by the Cornell Genomics Facility using the Applied Biosystems Automated 3730xl DNA Analyzer using Big Dye Terminator chemistry and ApliTaq-FS DNA Polymerase.

Hybridoma Culture and CD63Ab Purification: H5C6 Hybridoma cells (Developmental Studies Hybridoma Bank) expressing a CD63/LAMP-1 Antibody were quickly thawed from frozen into IMDM Media + 20% FBS + Pen/Strep, centrifuged at 500xg for 5 mins, then transferred to 4 wells of a 24 well plate (Costar). Cells were incubated overnight at 37°C with 5% CO_2, then split into 8 wells of the 24 well plate. Upon confluency, cells were transferred to a T75 (Thermo Fisher), followed by a T175 (Thermo Fisher). The emptied wells were refilled with IMDM media to recover and expand remaining cells. During growth phase, cells were fed with IMDM Media + 20% FBS + Pen/Strep. During antibody production phase, cells were fed RPMI Media + 5% FBS + Pen/Strep. Production is complete when cells are 50% viable by Trypan Blue.

200mL of media and cells from the T175's were collected and centrifuged at 3750xg at 4°C to pellet cells. The supernatant was carefully decanted and mixed 1:1 with a saturated ammonium sulfate (SAS) solution to precipitate the proteins. The mixture was stirred overnight at 4°C, then pelleted at 12,000xg (JA-12 rotor) for 30mins at 4°C. The pelleted precipitate was resuspended in 10mL PBS, then purified on a protein A/G column. The eluted fractions were pooled and concentrated using Amicon 30kDa spin filters and concentration was measured via absorbance at 280 nm.

Cloning of LAP-tagged Antibodies. The "LAP Tag" and spacer (GGGS-GFEID**K**VWYDLDA) was incorporated into the heavy and light chain C-terminal of the pVITRO-ch735-IgG1 vector [124] using 4 sequential PCR steps. The tag was added through the reverse primer, adding ~17-20 bases at a time. The following primers were used:

Heavy Chain LAP Tag:

FWD (ch735): ccgccacaggcgcgcactcccagattcagctgcagcaatc

REV1: aagccagatcctccgccTTTACCCGGAGACAGGGAGAGGC

REV2: accacaccttgtcgatctcgaagccagatcctccgccTTT

REV3: ACATCAggcgtccaggtcgtaccacaccttgtcgatctcg

REV4: ATGTCTGGCCAGCTAGCTGTACATCAggcgtccaggtcgt

Light Chain LAP Tag:

FWD (ch735): gggttccagctagccgcggtgatgtagtcatgacgcagac

REV1: aagccagatcctccgccACACTCTCCCCTGTTGAAGCTCT

REV2: accacaccttgtcgatctcgaagccagatcctccgccACA

REV3: TCCCTAggcgtccaggtcgtaccacaccttgtcgatctcg

REV4: CTGCTCCTAGGCGTACGGGATCCCTAggcgtccaggtcgt

PCR amplification was done with the Flash-Phusion enzyme master mix with an initial denaturation step for 30 sec at 98°C, followed by 30 cycles with denaturation for 10 sec at 98°C, and extension for 15 sec/kb at 72°C. The product was gel purified, and reamplified with 10ng of template for the 4 sequential amplifications.

To assemble the final vector, the following primers were used:

FWDvector: TCCCGTACGCCTAGGAGCAGGTTTCCCCAATGACACAAAA

REVvector: accgcggctagctggaacccagagcagcagaaacccaatg

FWDch735V_L: gggttccagctagccgcggtgatgtagtcatgacgcagac

REV4V_L: CTGCTCCTAGGCGTACGGGATCCCTAggcgtccaggtcgt

PCR amplification was done with the Flash-Phusion enzyme master mix with an initial denaturation step for 30 sec at 98°C, followed by 5 cycles with denaturation for 10 sec at 98°C, annealing for 15 sec starting at 55°C and decreasing 1°C per cycle, and extension time at 90% of the recommended 15 sec/kb which was 107 sec for the vector piece (FWDvector and REVvector) and 10 seconds for the light chain piece (FWDch735V_L and REV4V_L) at 72°C. The product was gel purified, and reamplified with 10ng of template for the 4 sequential amplifications. Following the touchdown protocol, 30 cycles of PCR were performed with denaturation for 1 sec at 98°C, annealing for 5 sec at 55°C and extension for 107 sec or 10 sec at 72°C respectively. Resulting PCR products were DpnI digested for 1 hour at 37°C. Then the digests were combined 1:1 to a total volume of 100 uL and incubated at RT for 1 hour. The reactions were cleaned up with the Qiagen PCR clean up protocol and eluted in 30 uL of water. The volume was brought to 100 uL with water and 2 uL of this reaction was used to transform NEB 10-beta chemically competent cells according to the manufacturer's protocol. After recovery, the cells were plated onto 300 µg/mL HyroB LB plates. Colonies were picked and grown in LB + 300µg/mL HygroB, mini-prepped, and verified with sanger sequencing.

To swap the variable regions from ch735 to Trastuzumab, the following primers were used:

TrasV$_H$Fwd: ccgccacaggcgcgcactccGAGGTGCAGCTGGTGGAGTC

TrasV$_H$Rev: GATGGGCCCTTGGTGCTAGCTGAGGAGACGGTGACAAGAG

TrasV$_L$Fwd: gggttccagctagccgcggtGACATCCAGATGACCCAGTC

TrasV$_L$Rev: GATGGCGCCGCCACCGTACgtttgatCTCCAGCTTGGTAC

C$_H$Fwd: GCTAGCACCAAGGGCCCATCGGTCTTCCCCCTGGCACCCT

C$_H$Rev: accgcggctagctggaacccagagcagcagaaacccaatg

C$_L$Fwd: cgtacggtggcggcgccatctgtcttcatcttcccgccat

C$_L$Rev: ggagtgcgcgcctgtggcggccgccaccaagaagaggatc

Variable region pieces were amplified from pVitro1-Trastuzumab-IgG1 (Plasmid# 61883), and constant region pieces were amplified from the LAP-tag incorporated ch735 vector. PCR amplification was done with the Flash-Phusion enzyme master mix with an initial denaturation step for 30 sec 98°C, followed by 30 cycles with denaturation for 10 sec at 98°C, annealing for 15 sec at 60°C, and extension for 6 and 60 sec at 72°C for variable and constant region pieces, respectively. Resulting PCR products were DpnI digested for 2 hours, cleaned-up, and quantified via 260/280nm absorbance on a Tecan Nanoquant Plate. The purified pieces were mixed at a 1:1:1:1 molar ratio, ligated via Gibson, and transformed into NEB 10-beta chemically competent cells and plated onto 300µg/mL HygroB LB plates. Colonies were picked and grown in LB + 300µg/mL HygroB, mini-prepped, and verified with sanger sequencing.

Recovered pVITRO-Trastuzumab-IgG1-LAP vectors were re-transformed, midi-prepped, and transfected into HEK 293F suspension cells.

Stable Transfection of 293F Cells and Her2Ab Purification: Methods for genetic incorporation of the LAP tag to the Trastuzumab plasmid are discussed in chapter 6.

For stable transfection of the Trastuzumab plasmid (with and without LAP Tag), 293F cells were cultured in suspension in Freestyle 293 Expression Media (Life Technologies) for at least 3 passages maintained at 1M cells/mL prior to transfection. 30M cells in 30mL of Freestyle Media were transferred to a new flask in fresh media and transfected using Freestyle MAX Transfection reagent with 37.5µg of ethanol precipitated DNA using the standard transfection protocol. After 24 hours, cells were replaced with selection media (50µg/mL Hygromycin B; Life Technologies) and passaged every two days maintaining at 1M cells/mL for two weeks and/or until control cells were no longer viable. Media was tested for antibody using a dot blot, and cells were maintained at 1M cells/mL passaging every 3 days with selection media (25µg/mL). Approximately 0.5-1L of media was purified on 1mL of protein A/G column. Media was flowed continuously over the resin, washed with ~50mL of PBS, then eluted with 5mL of 0.1M Glycine (pH 2) into 1mL of 1M Tris (pH 8). The antibody was concentrated and buffer exchanged to PBS with 3 centrifuge steps at 14K x g for 8 mins using 500 µL Amicon 30 kDa MWCO (Millipore Sigma) spin columns.

Sanger sequencing of constant heavy and light chain domains with LAP tag sequences.

BLACK & UPPERCASE – constant region DNA sequence

red & lowercase – LAP tag DNA sequence

C_H Region:

GCTAGCACCAAGGGCCCATCGGTCTTCCCCCTGGCACCCTCCTCCAAGAGC
ACCTCTGGGGGCACAGCGGCCCTGGGCTGCCTGGTCAAGGACTACTTCCCC
GAACCGGTGACGGTGTCGTGGAACTCAGGCGCCCTGACCAGCGGCGTGCA

CACCTTCCCGGCTGTCCTACAGTCCTCAGGACTCTACTCCCTCAGCAGCGT

GGTGACCGTGCCCTCCAGCAGCTTGGGCACCCAGACCTACATCTGCAACGT

GAATCACAAGCCCAGCAACACCAAGGTGGACAAGAAAGTTGAGCCCAAA

TCTTGTGACAAAACTCACACATGCCCACCGTGCCCAGCACCTGAACTCCTG

GGGGGACCGTCAGTCTTCCTCTTCCCCCCAAAACCCAAGGACACCCTCATG

ATCTCCCGGACCCCTGAGGTCACATGCGTGGTGGTGGACGTGAGCCACGA

AGACCCTGAGGTCAAGTTCAACTGGTACGTGGACGGCGTGGAGGTGCATA

ATGCCAAGACAAAGCCGCGGGAGGAGCAGTACAACAGCACGTACCGGGT

GGTCAGCGTCCTCACCGTCCTGCACCAGGACTGGCTGAATGGCAAGGAGT

ACAAGTGCAAGGTCTCCAACAAAGCCCTCCCAGCCCCCATCGAGAAAACC

ATCTCCAAAGCCAAAGGGCAGCCCCGAGAACCACAGGTGTACACCCTGCC

CCCATCCCGGGATGAGCTGACCAAGAACCAGGTCAGCCTGACCTGCCTGG

TCAAAGGCTTCTATCCCAGCGACATCGCCGTGGAGTGGGAGAGCAATGGG

CAGCCGGAGAACAACTACAAGACCACGCCTCCCGTGCTGGACTCCGACGG

CTCCTTCTTCCTCTACAGCAAGCTCACCGTGGACAAGAGCAGGTGGCAGCA

GGGGAACGTCTTCTCATGCTCCGTGATGCATGAGGCTCTGCACAACCACTA

CACGCAGAAGAGCCTCTCCCTGTCTCCGGGTAAAggcggaggatctggcttcgagatcga

caaggtgtggtacgacctggacgcc

C_L Region:

GTACGGTGGCGGCGCCATCTGTCTTCATCTTCCCGCCATCTGATGAGCAGT

TGAAATCTGGAACTGCCTCTGTTGTGTGCCTGCTGAATAACTTCTATCCCA

GAGAGGCCAAAGTACAGTGGAAGGTGGATAACGCCCTCCAATCGGGTAAC

TCCCAGGAGAGTGTCACAGAGCAGGACAGCAAGGACAGCACCTACAGCCT

CAGCAGCACCCTGACGCTGAGCAAAGCAGACTACGAGAAACACAAAGTCT

ACGCCTGCGAAGTCACCCATCAGGGCCTGAGCTCGCCCGTCACAAAGAGC
TTCAACAGGGGAGAGTGTggcggaggatctggcttcgagatcgacaaggtgtggtacgacctggacgcc

Immunofluorescence of Antibody Internalization to SKOV3 Cells: SKOV3 cells were cultured via standard cell culture methods and plated 75K cells to each quadrant of a segmented 35mm dish, 24 hours prior to incubation. Cells were incubated with 100nM of antibody, or Tf-AF488 positive control, for 1 hour at 37°C. Cells were washed with PBS then fixed with 4% paraformaldehyde for 15 mins at RT. The cells were then blocked overnight with blocking buffer (5% Normal Goat Serum + 0.3% Triton-X in PBS) at 4°C, followed by an incubation with a 1:200 dilution of Alexa Fluor 568-labeled anti-mouse 2° Ab (for CD63Ab) or AlexaFluor 488-labeled anti-human 2° Ab (for Her2Ab) for 1 hour at RT. Nuclei were stained with 2µM Hoechst 33342 for 15 mins at RT. The slide was then imaged on a Zeiss LSM880 Confocal/Multiphoton Inverted Microscope.

Antibody Functionalization: *Non-specific conjugation*: For random surface conjugations, 25µM of antibody was incubated with 250µM of either NHS-PEG4-TCO or NHS-PEG4-MeTzine (Broadpharm) in PBS overnight at 37°C. The reaction mixture was purified via 30 kDa amicon spin columns (500 µL) 3 times, and quantified via absorbance using a quartz NanoQuant (Tecan) plate using beers law for the TCO conjugates (no detectable absorbance of TCO) and the following formula for Tzine DOL:

cAb = (A278*eTz294-A294*eTz278)/[(eAb278*eTz294-eAb294*eTz278)*L]

cTz = (A278*eAb294-A294*eAb278)/[(eTz278*eAb294-eTz294*eAb278)*L]

Where: eTz294 = 29,578 $M^{-1}cm^{-1}$, eTz278 = 21,672 $M^{-1}cm^{-1}$, eAb294 = 93,710 $M^{-1}cm^{-1}$, eAb278 = 217,900 $M^{-1}cm^{-1}$, L=0.05cm (on the Tecan Quartz Nanoquant).

Antibodies were sought to have an approximate degree of labeling (DOL) of 5 Tzines per antibody.

mTG Site-specific Conjugation: 500µg of LplA-reacted antibody was incubated at 12.5 µM with 200 wt% Moo Gloo (10U/g Ab; Modern Pantry), 160 molar equivalencies of NH_2-PEG_3-Az, and 0.6µL of PNGase F for 7 hours at 37°C. The reaction mixture was purified via Amicon 30kDa MWCO centrifugal columns and quantified via 280nm absorbance using a quartz NanoQuant plate (ext. $coeff_{280nm}$ = 210,000 M^{-1} cm^{-1}).

LplA Site-specific Conjugation: 500µg of antibody was incubated at 20µM with 10mol% LplA, 200µM pAz or TCO-LAP, 1mM ATP, and 5mM $Mg(OAc)_2$ in PBS for 1.5 hours at 37°C. The reaction mixture was quenched with EDTA at a final concentration of 30mM.

Antibody PEGylation: Following antibody functionalization with a click chemistry substrate, the antibody was examined for extent of reaction with a gel shift assay following conjugation of a large PEG. Recovered antibodies following substrate addition with mTG or LplA were incubated with a large excess (25 molar equivalencies) of 5,000 MW DBCO-PEG or MeTzine-PEG reagents overnight at 37°C. Reaction mixtures were then reduced, boiled, and run on a 4-20% Mini-Protean TGX pre-cast protein gels (Bio-Rad) at 120V for 60 mins. Gels were stained with Bio-Safe® Coomassie, de-stained with water, and analyzed for a gel shift indicating a successful click reaction.

Antibody-Fluorophore Labeling: 25µM of antibody was incubated with 250µM of either NHS-AlexaFluor488 (AF488) (Life Technologies) in PBS overnight at 37°C. The reaction mixture was purified via 30 kDa amicon spin columns (500 µL) 3 times

and quantified via absorbance using a quartz NanoQuant (Tecan) plate (ext. coeff$_{280}$ = 210,000 M^{-1} cm^{-1}; ext. coeff$_{488}$ = 71,000 M^{-1} cm^{-1}; CF = 0.11).

Antibody Uptake via Flow Cytometry: 50,000 cells of a designated cell type (HeLa, SKOV3, and MCF-7) cells were plated to 24-well plates 24 hours prior to the assay. Green, fluorescently-labeled antibodies were incubated at varying concentrations on cells for 1 hour at 37°C and 5% CO_2. Cells were washed with PBS, trypsinized, quenched with media, and pelleted at 1,000 x g for 5 mins. Trypsin and media were removed via aspiration and resuspended in 500μL PBS. Samples were then analyzed for green fluorescence intensity on each individual cell using flow cytometry.

CHAPTER 3 – ANTIBODY-siRNA CONJUGATES

Background

RNA interference (RNAi) has emerged over the last 15 years as a specific and potent means of targeted gene silencing at the mRNA level. Since its initial discovery in *C. elegans*, researchers have sought to harness this mechanism, by way of short interfering RNAs (siRNA), as an efficient route to silencing disease-causing genes.[37,128] Because of their large size and charge, siRNAs cannot passively diffuse through cell membranes. However, siRNAs are small enough to be filtered by the kidney and are rapidly excreted following IV injection. Additionally, unmodified siRNAs are rapidly degraded by nucleases in serum. Consequently, siRNAs need to be encapsulated or conjugated to a large macromolecule to avoid kidney filtration and induce active cellular uptake.

The most widely used delivery strategy currently involves synthetic materials to encapsulate the siRNA cargo into a particle, deliver it to the cell, and facilitate endosomal release to the cytoplasm. Among these materials are cyclodextrin polymer particles,[129-135] lipid and lipid-like nanocarriers,[136-146] and cationic polymers.[147-152] Although optimization of these delivery vehicles has been slow and limited to the liver, few successes have emerged. The first FDA-approved RNAi drug, Patisiran, was just recently approved in August 2018 to treat transthyretin (TTR) amyloidosis, a liver disease which leads to nerve damage and impaired heart function. Expansion to diseases beyond the liver has been even slower.[153] This is because particle-based formulations can be difficult to target away from the liver.[154] Preferential deposition in the liver is due to protein adsorption to the particle surface, followed by rapid clearance by phagocytic cells abundant in the liver and spleen. [155] Other types of

delivery modalities, such as bioconjugates,[156] are now being explored to treat extra-hepatic targets.

The most successful bioconjugate thus far is the GalNAc-siRNA conjugates. Developed by Alnylam, this conjugate includes a trivalent N-acetylgalactosamine (GalNAc) and showed specific targeting and robust knockdown efficiency in cells containing the asialoglycoprotein receptor (ASGPR).[44,157] This conjugate is unique in that endosomal escape is proposed to be solely dependent on endosomal leakage, but has a higher escape rate than other pathways because of the high expression levels, rapid uptake, and fast recycling rate of the ASGPR pathway.[33] Unfortunately, this receptor is solely present on hepatocytes. To go beyond the liver, several conjugates are being explored with RNA-aptamer[158-160] and antibody targeting ligands.[161-167] These conjugates can target a variety of cell types and surface antigens and carry the siRNA cargo into a cell.

Antibody (Ab) and antibody fragment bioconjugates have garnered particular interest due to their specificity, range of receptor targets, and clinical success in antibody-drug conjugates (ADC's).[104] Several antibody-based bioconjugates have successfully delivered siRNA to epithelial tumors[162,164,168] and specific leukocytes[161,167,169] while utilizing nucleic acid binding proteins like polyarginine and protamine for siRNA complexation and endosomal escape. Song et al. were the first to demonstrate cell-type specific targeted siRNA delivery via an antibody-protamine fusion, and saw targeted knockdown of reporter and endogenous gene targets in HIV-infected T cells and Her2 expressing breast cancer cells.[161] These protamine fusions however, were difficult to express and never proceeded to the clinic. Later, researchers at Genentech generated directly conjugated (i.e. no protamine/arginine) antibody-siRNA conjugates

targeting various cell surface antigens and internalization pathways and systematically evaluated their knockdown efficiency. Only a limited number were able to deliver functional amounts of siRNA to the cytosol, with unclear dependence on endocytosis pathway.[165] This systematic evaluation illustrates that there is a significant lack of understanding in the critical components of siRNA conjugates, and more must be done to understand the impact of endocytic pathway, conjugation method, and membrane disrupting agents on efficient delivery. Understanding the individual component contributions for efficient cytosolic trafficking will help inform the design of bioconjugates to meet the therapeutic potential of RNAi.

In this chapter, we develop antibody-siRNA conjugates for a modular dual-delivery strategy that decouples cellular internalization from endosomal escape through the use of antibody (Ab) conjugates. Cellular internalization of these conjugates is dictated solely by the antibody, while endosomal escape is attained with an endosomal escape agent (EAA), which will be explored in chapter 4. First, we generated luciferase-expressing cells as a reporter gene in knockdown experiments. Then, we stabilized the siRNA to serum proteins with chemical backbone and base modifications. Next, we generated and characterize protein-siRNA conjugates using the native Transferrin protein, and antibodies against Transferrin, CD63, and Her2 receptors. These surface ligands are present across a variety of cell lines and cover both fast recycling and lysosomal endocytosis pathways. These conjugates covalently bind the siRNA and protein using various click chemistries and incorporate cleavable sites for siRNA release by endosomal enzymes including gamma-interferon-inducible lysosomal thiol reductase (GILT) and cathepsin B (CatB). These conjugates effectively internalize siRNA to target cells as measured by flow cytometry and confocal microscopy. Later, these can be co-delivered with Ab-EEA conjugates for targeted knockdown.

Results

Generating Luciferase-Expressing Cell Lines: For preliminary studies, we examined knockdown of a reporter gene before moving to an endogenous gene target due to its higher throughput. Firefly luciferase is a widely-used reporter gene. It can be read easily in a well-plate format, the substrate is commercially available, and has a low background signal. To generate cell lines with luciferase expression, we cloned the Luc2 gene (replacing the GFP gene previously in the vector) into a lentiviral pCDH vector under a CMV promoter, then used a second-generation lentiviral transfection to generate stably Luc2-expressing HeLa, SKOV3, HEK293T, and MCF7 cell lines (Figure 3.1A). Second generation lentiviral transfection methods, for safety reasons, split the viral genome into three vectors: a packaging vector (psPAX2), an envelope plasmid (pMD2.G), and the transfer plasmid carrying the gene of interest (pCDH-Luc2) (Figure 3.1). HEK293T cells were transfected with lentiviral components via a calcium phosphate transfection,[170] then the virus generated from the 293T's were used to infect HeLa, SKOV3, MCF-7, and fresh HEK293T cells. Following infection, cell lines were selected with Blasticidin and expanded. We then examined their luciferase expression levels with the ONE-GLO/Tox Luciferase Assay kit. We saw that these cells had a signal increase of 5 orders of magnitude over the wild-type cells (Figure 3.1B&C). To verify that our siRNA was compatible, we treated cells with our luciferase-targeting siRNA via Lipofectamine and saw a 90% knockdown, and no detectable knockdown with the dummy siRNA targeting a different strain of luciferase (Figure 3.1D&E). These cells were used for knockdown studies with our conjugates.

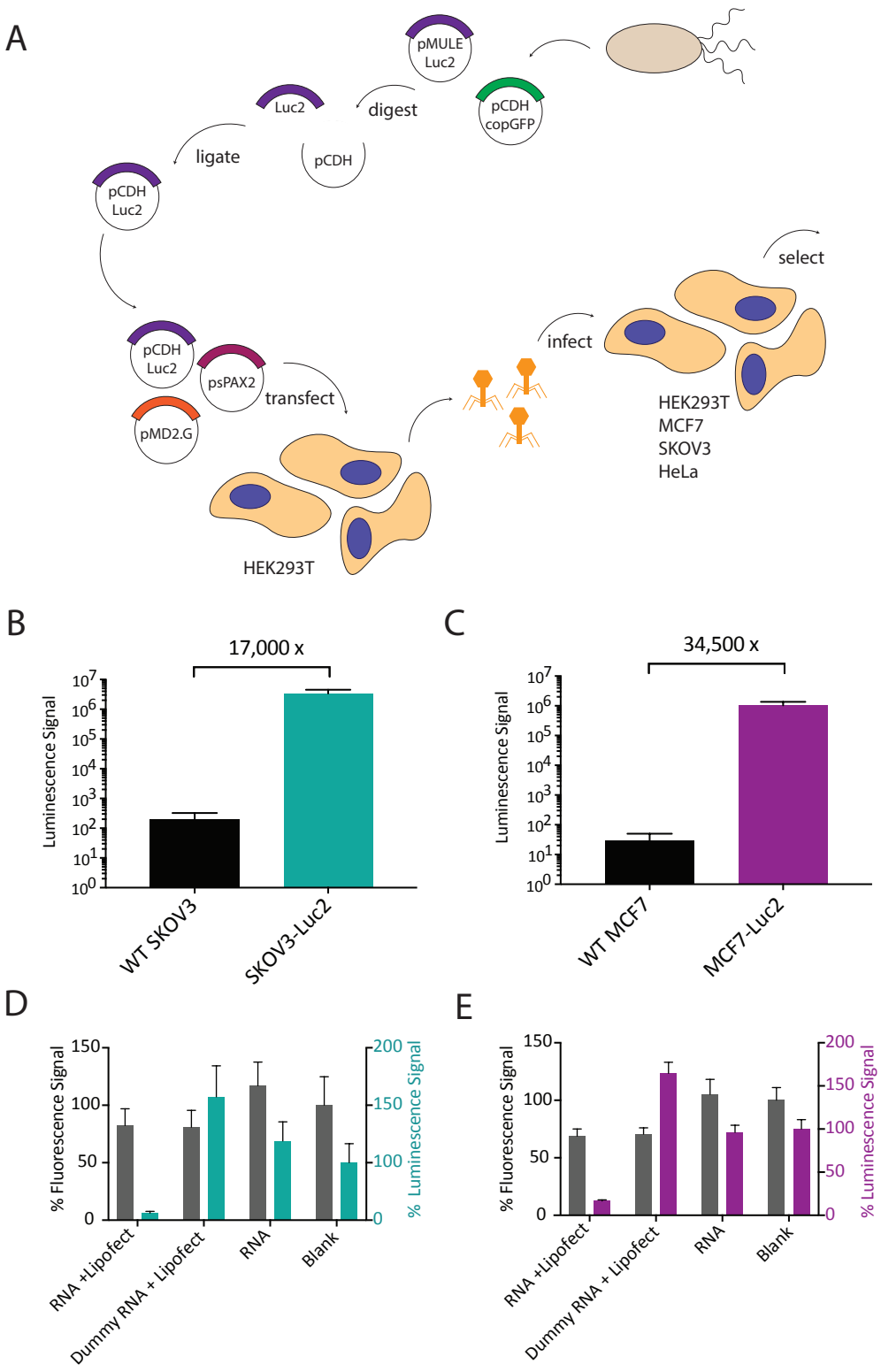

Figure 3.1 Luciferase Expression via Viral Transduction – (a) Schematic of viral transduction of select cell lines with Luc2. Luc2 was cloned into a pCDH vector (from Paszek Lab), then transduced into HEK293T cells via a 3rd generation method with

three plasmids: Transfer plasmid, packaging plasmid, and envelope plasmid. Virus generated from HEK293T cells were used to infect HeLa, SKOV3, MCF7, and HEK293T cells. (b-c) Luciferase expression levels as measured by Promega ONE-GLO reagent in Luc2 expressing SKOV3 (teal) and MCF7 (purple) cells over wild-type. (d-e) Cell Viability (left; gray) and luciferase expression (right; teal – SKOV3, purple – MCF7) of treated cells with Luc2-targeting siRNA. Efficient knockdown with target siRNA indicated successful transduction with proper Luc2 vector.

Stabilization of siRNA through base and backbone chemical modifications: Unlike more common delivery vehicles like polyplexes or nanoparticles, siRNAs conjugated to antibodies are not encapsulated and are thus more easily susceptible to serum nucleases. Researchers at Alnylam® Pharmaceuticals Inc. found chemical modification to be critical to the success of their GalNAc-siRNA conjugates for targeting hepatocytes and screened a large number of siRNAs with various modifications.[171] We utilized 2'methyoxy (MeO) modifications to the 2' hydroxyl (OH) group, and phosophorothioate backbone linkages at the 3' overhangs to stabilize the siRNA in the presence of mouse serum (Figure 3.2). The location and number of modifications present on the siRNA determine the stability, but also have an impact on knockdown efficiency. Therefore, we made a variety of sense and anti-sense RNA strands with modifications at various locations, duplexed them, and looked at their subsequent knockdown efficiency and serum stability.

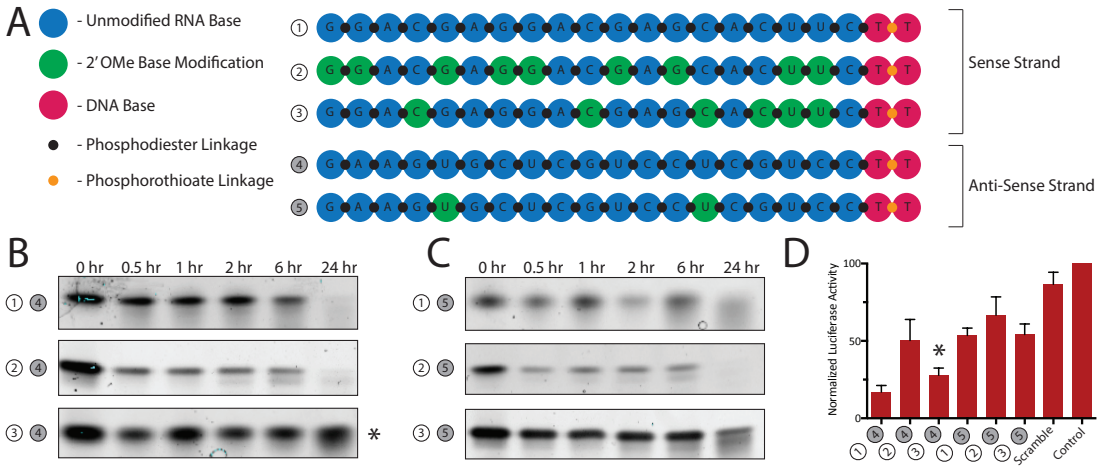

Figure 3.2 RNA Chemical Stability Modification – (a) Schematic of available RNA sense strand (top) and antisense strand (bottom) sequences and locations of modifications to RNA bases (large circles; blue and green) or DNA bases (large circles; pink) and backbone linkages (small circles; blank and orange). Sense strand sequences are labeled 1-3, and antisense strand sequences are labeled 4 & 5. (b) Time course serum stability PAGE gels stained with SYBR gold of sense strand sequences 1-3 duplexed with antisense strand 4. Asterisk (*) indicates the most stable duplex. (c) Time course serum stability PAGE gels stained with SYBR gold of sense strand sequences 1-3 duplexed with antisense strand 5. (d) Luciferase expression normalized to cell viability of SKOV3 cells treated with 6 available duplexes, scramble sequence, and untreated control. Asterisk (*) indicates luciferase expression of cells treated with most stable duplex 3-4.

In this study, we included 3 sense strands variations with either no modifications (1), 2'OMe modifications to G and U bases (2) or C and U bases (3). For the anti-sense strand, we had two variations with either no modifications (4), or with 2'OMe modifications to positions 5 and 14 (5) (Figure 3.2A). We chose these modifications to examine the effect of antisense vs. sense strand modifications, pyrimidine vs. purine base modification, and location dependence on stability and knockdown efficiency. All strands had DNA base (dTdT) overhangs with a phosphorothioate linkage at the 3' end, as is a common modification for siRNAs.[39] This yielded 6 possible combinations of double-stranded siRNAs. Each combination was incubated in mouse serum for 24 hours and analyzed via SDS-PAGE for stability. After 24 hours, only the (3-4) and (3-

5) combinations could be significantly detected after 24 hours (Figure 3.2B&C). From this we deduced that modifications to the sense strand had the greatest impact on serum stability, and modifications to the pyrimidine bases was more effective than modifying the purine bases, which is consistent with literature.[172] We then examined the knockdown efficiency of these duplexes against a target luciferase gene via lipoplexing with Lipofectamine™, a commercial transfection reagent to deliver siRNA. At a concentration of 50 nM, we observed a range of efficiencies from 40-80% knockdown across the duplexes (Figure 3.2D). As expected, the unmodified sense and anti-sense pair had the greatest knockdown, but the lowest stability. The next best knockdown efficiency was observed with the 3-4 duplex, which also had the greatest stability. This 3-4 duplex was used for all future siRNA conjugates. We purchased the modified siRNA with a 3' terminal protected thiol or terminal primary amine on the sense strand for conjugation to protein carriers.

Transferrin Protein-Nucleic Acid Conjugates: Transferrin (Tf) is a ubiquitous iron-chelating protein responsible for iron transport into cells. Transferrin binds to its receptor, Transferrin Receptor (TfR), and is internalized into a cell via clathrin-dependent endocytosis. Following internalization, the acidic pH of the endosome induces the chelated iron to be released from the protein. The endosomes containing the protein are then recycled back to the cell surface quickly (15-30 mins), where the Tf then detaches from its receptor and is released back to the extracellular space to chelate more iron. The TfR is expressed on a variety of mammalian cell lines and has been shown to have elevated expression in cancerous cells. Therefore, the Tf-TfR pair was an ideal system to begin building conjugates.

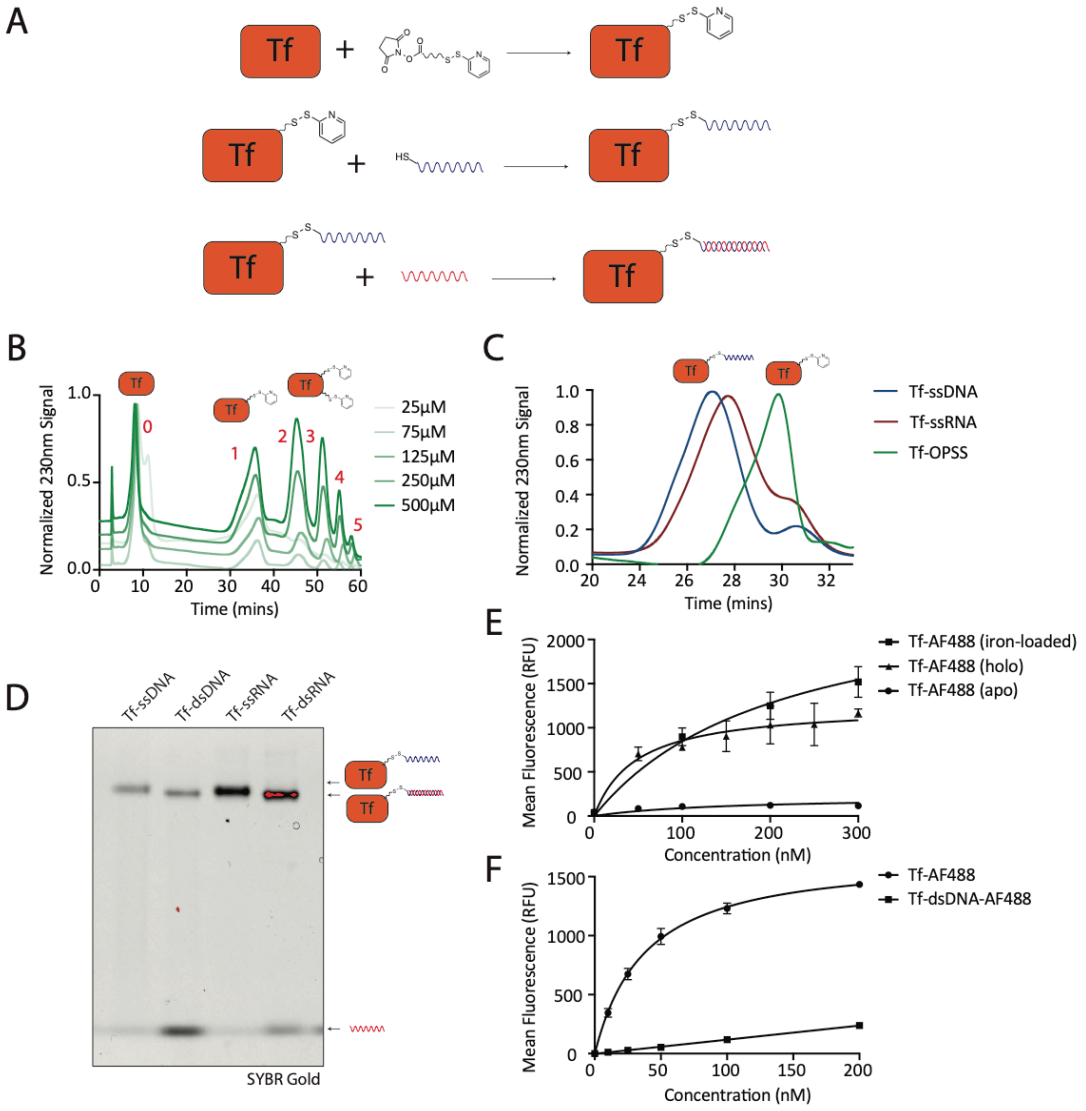

Figure 3.3 Transferrin-Nucleic Acid Conjugation and Purification – (a) Schematic of conjugation scheme for Transferrin (Tf) protein-nucleic-acid conjugates. Tf is first modified with an NHS-PEG-OPSS crosslinker. The purified, mono-conjugated Tf-OPSS is then mixed with a thiolated single stranded sense DNA/RNA, purified, then duplexed with the antisense strand for the final conjugate. (b) Hydrophobic interaction chromatography (HIC) trace of Tf reacted at increasing concentrations with NHS-PEG-OPSS crosslinker. Red box indicates mono-conjugated product. (c) HIC trace of Tf-OPSS before (green) and after thiolated DNA (blue) or RNA (red) addition. A hydrophilic shift (i.e. earlier time) is indicative of conjugation. (d) Native PAGE of single-stranded (ss) and double-stranded (ds) Tf-RNA and Tf-DNA conjugates, stained with SYBR Gold for nucleic acids. A small, quantitative, gel shift down from the single-stranded conjugate is indicative of hybridization, and excess, non-hybridized antisense strand runs at the bottom of the gel. (e) Flow cytometry analysis of Transferrin with varying iron-loading levels. Commercial holo-transferrin

(triangle), apo-transferrin (circle), and iron-loaded apo-transferrin (square). (f) Flow cytometry analysis of Tf protein (circle) and Tf-dsDNA-AF488 conjugates (square). Uptake of DNA conjugates was significantly less than that of the protein.

To conjugate siRNA to Tf, we utilized an ortho-pyridyl disulfide (OPSS) linker that reacts with thiol groups via thiol-disulfide exchange (Figure 3.3A). The resulting disulfide bond can be cleaved in the reducing environment in the endosome to release the siRNA. To functionalize the protein, we used an N-hydroxysuccinimide (NHS) ester and OPSS heterobifunctional crosslinker to add OPSS groups to the solvent-accessible surface lysine residues of Tf, of which there are 7. We optimized our reaction conditions for the mono-conjugated product and purified it via hydrophobic interaction chromatography (HIC) (Figure 3.3B). The mono-conjugated Tf-OPSS eluted at ~35 mins on a gradient of 100-25% 1M ammonium in phosphate buffer over 45 mins. We then added single stranded DNA or RNA with a 3' thiol to the mono-conjugated Tf-OPSS and saw a characteristic hydrophilic shift via HIC (Figure 3.3C). After purification of the Tf-nucleic acid conjugate, positive staining for nucleic acid was seen via native PAGE with no free nucleic acid detected (Figure 3.3D). This indicated that the conjugates were made and purified successfully.

Because iron is also released from Tf in high salt conditions of the HIC purification, the Tf conjugate was iron-loaded with iron citrate solution[173] and screened for uptake in TfR-expressing cells (HeLa cells) (Figure 3.3E). Efficiency of iron loading was measured by the absorbance ratio at 465nm and 280nm and normalized to commercial holo-transferrin. The iron-loaded Tf (IL Tf; 212 +/- 26nM kD) showed greater uptake than the apo Tf but showed approximately 5-fold lower affinity than the native holo-Tf (47 +/- 16nM kD). Furthermore, following the DNA conjugation, the uptake of these conjugates was very low relative to the control Tf (Figure 3.3F). We concluded that

the combination of inefficient iron-loading and steric hindrance by the presence of the nucleic acid had a negative impact on uptake efficiency.

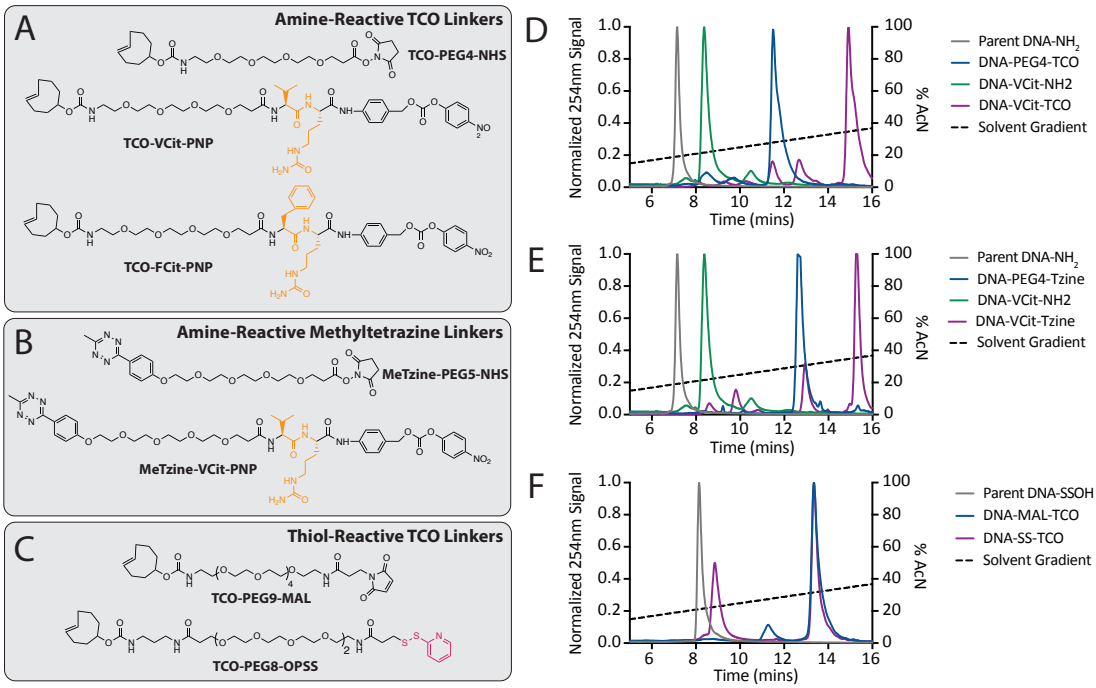

Figure 3.4 Functionalized Nucleic Acids with Heterobifunctional Crosslinkers – (a-c) Chemical structures of heterobifunctional crosslinker used in antibody-nucleic acid conjugates. (a) TCO-functionalized linkers with and without a CatB-cleavable site (Valine Citrulline – VCit; Phenylalanine – FCit). Reactive with amine-functionalized nucleic acids (b) Tetrazine-functionalized versions of the stable and VCit linkers in (a). (c) Stable and reducible, TCO-functionalized linkers that are reactive with thiolated nucleic acids. (d-f) RP-HPLC traces of nucleic acids. Parent DNA traces (gray) reacted with stable linkers (blue) and cleavable linkers (purple). Green traces show trace of intermediate product formed during CatB-cleavable oligo synthesis. Minor peak in purple trace in (f) is likely partially reduced biproduct.

Functionalized Nucleic Acids for Antibody Conjugation: Antibody conjugates are an appealing modality for siRNA delivery because of the wide range of receptor targets and their high binding specificity. However, commercial antibodies are very expensive (~$400/100µg), so we sought to make conjugates at a small scale, low concentrations, and near 1:1 molar equivalency. We chose the trans-cyclooctene (TCO) and

methyltetrazine (MeTzine) reaction pair that undergo Inverse Electron Demand Diels-Alder (IEDDA) reaction. This pair has the fastest reported reaction kinetics of any "click chemistry" pair (2,000 M^{-1} s^{-1}),[108] is bio-orthogonal, stable in aqueous solution, and commercially and synthetically accessible. We synthesized and purified a variety of heterobifunctional crosslinkers with TCO or MeTzine groups to crosslink antibodies and nucleic acids (Figure 3.4). These crosslinkers contained (1) a reactive group for amines or thiol and (2) a stable PEG linkage or a protease-cleavable or reducible site. These crosslinkers were reacted with 3' functionalized nucleic acids and purified via RP-HPLC.

	Parent Antibody	Antibody-DNA Conjugate
Transferrin Receptor (TfR)	13.3 +/- 2.0 nM	39.2 +/- 11.0 nM
CD63/LAMP-3	7.6 +/- 1.5 nM	12.2 +/- 0.4 nM
Her2/ErbB2	1.74 +/- 0.5 nM	1.54 +/- 0.5 nM

Table 3.1 Dissociation Constants of Parent Antibodies and Antibody-DNA Conjugates

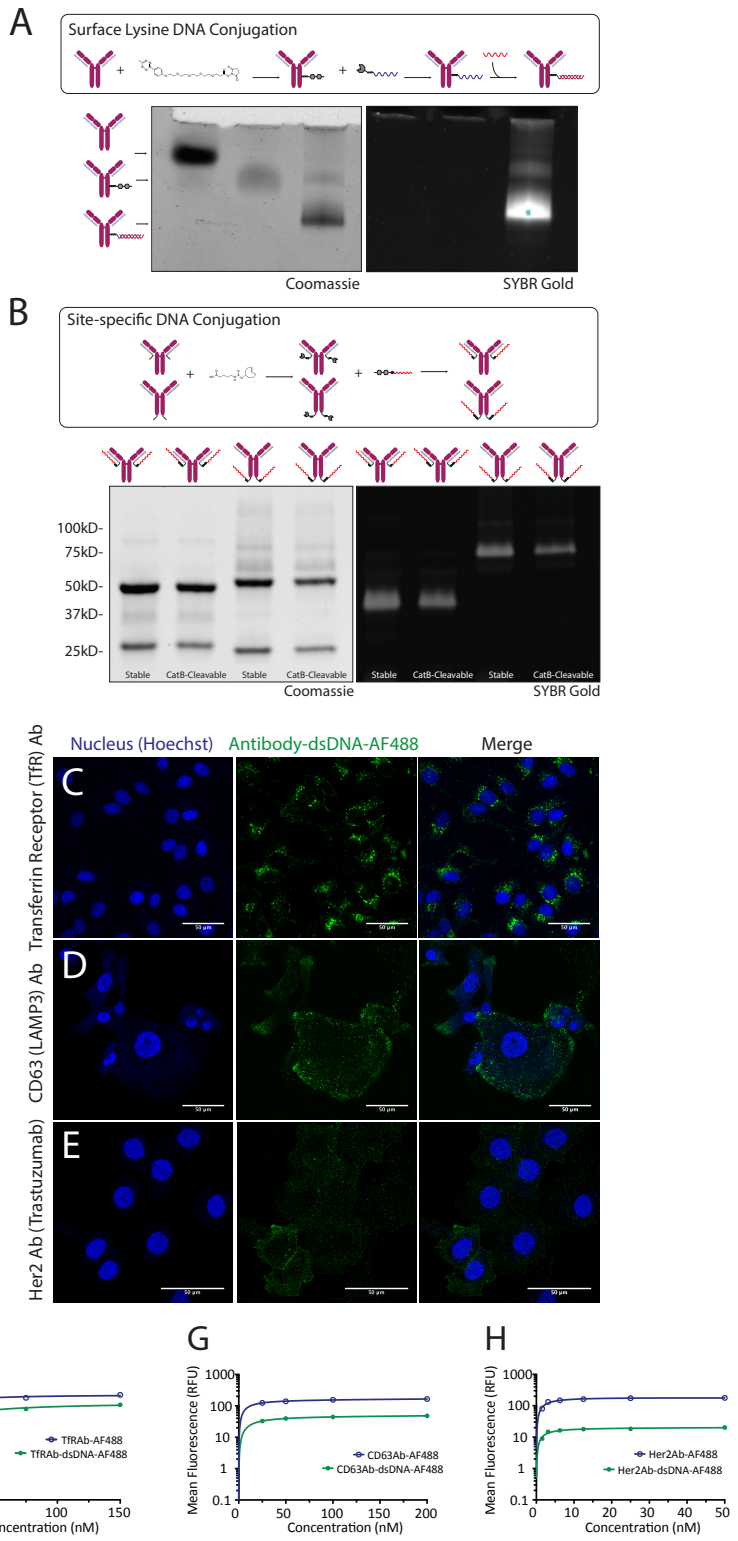

Figure 3.5 Conjugation and Uptake of Antibody-nucleic acid conjugates – (a) Non-specific antibody-siRNA conjugation. (top) Schematic of conjugation protocol with surface tetrazine functionalization, followed by a click reaction with a TCO-functionalized oligo. The single stranded conjugate is purified, quantified, then hybridized with the corresponding antisense strand. (bottom) Native PAGE gel stained

with Coomassie (left) for protein and SYBR gold (right) for nucleic acid. Downward shifts and positive nucleic acid staining are indicative of conjugation and hybridization. Protein band shifts are near quantitative indicative of complete conjugation. (b) Site-specific antibody-siRNA conjugation. (top) Schematic of conjugation protocol to LC-LAP tagged antibody with a TCO-substrate, followed by a click reaction with a Tzine-functionalized oligo. (bottom) SDS-PAGE gel stained with Coomassie (left) for protein and SYBR gold (right) for nucleic acid. Gel shifts upward and positive nucleic acid staining are indicative of conjugation. Faint bands at ~37kD and ~60kD that stain positively for protein and nucleic acid are conjugate, however conversion is low. (c-e) Confocal microscopy for uptake of antibody-oligo conjugates. Antibody-DNA conjugates with the TfRAb (c; HeLa), CD63Ab (d; SKOV3), and Her2Ab (e; SKOV3). Blue = Hoechst (nuclei stain). Green = Alexa Fluor 488 (Antibody-oligo conjugates, fluorophore on oligo). (f-h) Flow cytometry uptake of labeled antibodies and nucleic-acid conjugate counterparts. Antibody-DNA conjugates with the TfRAb (f; HeLa), CD63Ab (g; SKOV3), and Her2Ab (h; SKOV3). Blue traces = labeled antibody. Green traces = Antibody-oligo conjugates.

Antibody-Nucleic Acid Conjugation and Cellular Uptake: After purifying the DNAs and RNAs, these nucleic acids could then be conjugated to a targeting antibody. To analyze the effect of pathway dependence on efficient siRNA delivery, we looked at antibodies against three different surface antigens: for the Transferrin receptor (TfR), CD63/LAMP-3, and the Her2 receptor. These encompass recycling and late endosomal pathways and have varying receptor surface densities on the cell lines present in the Alabi Lab. We generated Ab-nucleic acid conjugates on these antibodies via either a site-specific (Figure 3.5B) or random conjugation (Figure 3.5A). Unlike the Transferrin conjugates, these are randomly conjugated but have a DOL greater than 1 as measured via absorbance of the methyltetrazine group. Thus, there could be several DNAs conjugated to the antibody. This was verified via SDS-PAGE to see a gel shift on native PAGE and positive staining for nucleic acids (Figure 3.5A). We also tried conjugating via site-specific methods utilizing a TCO LAP tag substrate on the antibody heavy or light chain (Figure 3.5B). These also showed a gel shift via SDS-PAGE and positive staining for nucleic acids, but the extent of reaction was much lower, presumably because of the lower TCO DOL of the antibody. Therefore, we proceeded with the non-specifically conjugated antibodies. We analyzed their

uptake in cells expressing the given antibody receptor. For the TfRAb, CD63Ab, and Her2Ab, we saw that these antibodies internalized DNA into the cell via confocal microscopy (Figure 3.5C-E) and flow cytometry (Figure 3.5F-H). As expected though, these conjugates had comparable dissociation constants (K_D) values (Table 3.1) relative to the parent antibody, but lower overall uptake. However, the decreased uptake is likely due to a combination of the lower relative DOL and steric hindrance by attaching the double-stranded nucleic acid. Nevertheless, the conjugates were effectively internalized and could be used in future co-delivery studies.

Conclusions & Discussion

In this chapter, we examined methods for conjugating nucleic acids to targeting proteins and antibodies via various chemistries and examined their uptake in receptor-expressing cells. This is important for targeted delivery of nucleic acids to specific cell types as the protein-receptor pair both dictates the cell type being targeted and mediates internalization of nucleic acids into cells. We used both endogenous proteins (Transferrin protein, Tf), as well as antibodies targeting a variety of surface receptors, including TfR, CD63, and Her2. This range of targets would then allow us to examine the effect of receptor density, cell type, and endocytic pathway on nucleic acid delivery efficiency.

First, we stabilized the siRNA via chemical modifications to the backbone and bases, and optimized degree of stabilization with knockdown efficiency. This has been shown to be vital in siRNA conjugate success, particularly with non-encapsulated siRNAs. While the base sequence dictates the gene target, oligonucleotide chemical structure dictates delivery and potency.[174] In this chapter, we performed a small screen of chemically-modified siRNAs (6 total duplexes) with a single targeting sequence for

the luc2 gene (pgL4 vector; Promega). We were able to determine a sequence that was stable after 24 hours incubated in serum and showed ~75% knockdown at 50nM when delivered with Lipofectamine. This was viable for stability in serum, but it is unclear as to whether these were sufficient for protection from endolysosomal enzymes and could be a contributing factor later as to why the protein-siRNA conjugates were not viable in eliciting knockdown even in the presence of chloroquine, a known lysosomotropic agent (see Chapter 5). Given more resources, it would be useful to further optimize the sequence and location and number of chemical modifications to the siRNA to be sure this not a contributing factor.

Following stability modifications of the siRNA, we moved to making conjugates with the endogenous Transferrin protein. Tf protein has been utilized in conjugates and on the surface of nanoparticles as a cancer-cell targeting protein, particularly for targeting the brain. It served as a simple protein for proof-of-concept studies in building the conjugates. However, because Tf is an iron-chelating protein and the purification of the conjugates with a high salt buffer caused the iron to dissociate, it was difficult to generate high-affinity conjugates that undergo endocytosis via the TfR. We did generate a protocol for iron-loading Tf, however, we still observed low uptake of the Tf-nucleic acid conjugates. This was likely due to a combination of inefficient iron-loading of Tf and steric hindrance by attaching the nucleic acid non-specifically to the surface of the protein. Future studies could perhaps be performed with a mutant Tf with slower iron-release kinetics,[175] or with other well-characterized internalizing proteins such as low density lipoprotein (LDL).

To circumvent the difficulties encountered with iron-loading, we generated similar conjugates with antibodies. We chose TfR, CD63, and Her2-targeting antibodies. We

began with commercial TfR-targeted antibodies as an easy transition from the endogenous Tf protein. We then moved to CD63 where we were able to purchase a hybridoma cell line for expression and purification. Finally, we generated the Her2-targeted antibody, Trastuzumab, because of its high expression levels on SKOV3 cells and ability to genetically manipulate the protein. We were able to generate Ab-siRNA conjugates via the efficient TCO-tetrazine click chemistry ligations. These conjugates internalized into receptor-expressing cell lines with lower efficiency than their parent antibody, as anticipated. This was likely due to a discrepancy in labeling efficiency of the parent antibody with the conjugate as well obstruction of the binding site due to the presence of a large double-stranded nucleic acid. Labeling efficiency could be improved with higher concentrations of both components, which is dependent on having greater amounts of antibody and DNA. Site-specific conjugations may also be able to circumvent this and make sure the DNA does not block the antigen binding site of the antibody. It might be necessary to include 4 conjugation sites rather than 2 as well, to obtain a higher DOL and better uptake. Also, the location of these sites would also perhaps need to be optimized to minimize interference with the antigen binding site on the antibody.

In conclusion, we have determined that these chemical conjugation methods are viable for attaching nucleic acids to antibodies for internalization into mammalian cells. These conjugates though, have no explicit mechanism for endosomal escape and as is are not sufficient for cytosolic delivery of siRNA. Endosomal escape conjugates will be discussed in Chapter 4.

Materials & Methods

Cell culture and reagents: HeLa, SKOV3, and HEK293T cells were maintained in Dulbecco's modified eagle media (DMEM; Life Technologies) supplemented with 10% Fetal bovine serum (FBS; Atlanta Biologics). MCF-7 cells were maintained in DMEM + 10% FBS with 10µg/mL insulin. All DNA and RNA oligos were purchased from IDT with any base and backbone modifications noted. All cloning materials were purchased from New England Biolabs (NEB). Alexa Fluor NHS-ester reagents were purchased from ThermoFisher Scientific.

Cloning and DNA preparation: The luciferase gene (Luc2) was stably incorporated into SKOV3, HeLa, MCF-7, and HEK293T cells via viral transfection using a pCDH vector under a CMV promoter. Plasmid containing Luc2 (Addgene Plasmid #62170) was mini-prepped from DH5alpha cells. Luc2 and pCDH vectors were digested at EcoRI and NotI sites, run on an agarose gel, and the insert and backbone were extracted and ligated overnight at 37°C. Ligated plasmid (pCDH-Luc2) was transformed into Mix-and-go competent cells and plated to LB-agar plates with ampicillin. Plasmid DNA was mini-prepped from colonies for viral transfection.

Lentiviral Transfection: 800K HEK293T cells were plated in 1.6mL media in a 6-well plate the evening before transfection. 800µL of media from each well was replaced with fresh media the following morning. 3.25µg of pCDH-Luc2, 2.43µg psPAX2 (packaging vector), and 0.97µg pMD2.G (VSVG vector) were mixed in HBSS buffer with 58mM $CaCl_2$ and added dropwise to the 6-well plate and incubated overnight. Media was changed the following morning to 1.6mL fresh media to collect virus for 36 hours. Cells to be infected were also plated at this time such that they reach 50% confluency by time of infection (36 hours later). After 36 hours, 1.5mL

media with virus was mixed with 1.2µL polybrene, then centrifuged at 2K RPM for 5 mins to pellet any cells. 1mL of this was diluted 1:6 with fresh media and added to infection cells. Media was changed following an overnight incubation and incubated for another 36 hours. Following this, selection media (Blasticidin) was added to cells and following death of control cells, selected cells were expanded and frozen stocks were prepared.

Luciferase Expression Test: To examine Luciferase expression levels in transfected cells, 10K cells were plated in FluoroBrite™ to a white, 96-well plate 24 hours prior to reading. 20µL of CellTiter-Fluor™ was added to wells, then incubated for 30 mins at 37°C. Fluorescence intensity was measured at 400/505nm Ex/Em and normalized to an untreated control for cell viability/count. Luciferase activity was measured by adding 20µL ONE-GLO™ reagent to wells, incubating for 5 mins at RT, then measuring on for luminescence with a 100ms integration time. Luciferase signal was normalized to an untreated control.

siRNA Stability Analysis: For stability analysis, 10µM stocks of each RNA strand were mixed 1:1 to anneal in Milli-Q H_2O for 30 mins at RT. RNA duplexes were then mixed 1:1 with non-heat inactivated mouse serum at 37°C for 0.5, 1, 2, 6, or 24 hours. Untreated controls and treated samples were then loaded onto native 4-20% PAGE gels, run at 100V for 60 mins, stained with SYBR Gold, and imaged on a ChemiDoc MP Imaging system (Bio-Rad). Gels were examined qualitatively by band intensity.

siRNA Knockdown Efficiency: To examine knockdown efficiency of siRNA duplexes, Luc2-expressing SKOV3 cells were treated with Lipofectamine encapsulated siRNA and analyzed for Luciferase expression levels. 15K SKOV3 cells

were plated in a white, 96-well plate 24 hours prior to reading. siRNA duplexes were mixed at a ratio of 75µL Lipofectamine per nmole of siRNA for 20 mins at RT, then added to cells in 100µL DMEM + 10% FBS at a final concentration of 50nM siRNA. The cells incubated at 37°C in 5% CO_2, then were washed with PBS after 16 hours, replaced with fresh DMEM + 10% FBS with no phenol red for the remaining 32 hours. Cells were analyzed with the Promega ONE-GLO/Tox Luciferase Assay Kit. First, 20µL of fluorescent reagent was added to wells and incubated for 30 mins at 37°C, followed by a fluorescent measurement at 400nm/505nm Ex/Em. Then, 20µL of luminescent reagent was added and incubated for 5 mins at RT, followed by a luminescence measurement at 100ms integration time. Luminescence signals were normalized by fluorescence signal (cell viability), then normalized to an untreated control for % luciferase expression.

Cathepsin-B Labile Linker Synthesis and Purification (Appendix A.6-A.9):

Fmoc-FCit-OH: 200mg of the Fmoc-protected phenylalanine pentafluorophenyl ester (Fmoc-F-OPfp) was solubilized in 2.5mL THF. 1.05 equivalents of Citrulline (H-Cit-OH) and sodium bicarbonate were solubilized in 1mL DI water. The Fmoc-F-OPfp solution was added to the H-Cit-OH and $NaHCO_3$ and stirred at 40°C overnight. THF was then dried via rotary evaporation, and the remaining water layer was diluted to 5mL with DI water and 0.5mL IPA and acidified to pH~1 with HCl. The product was extracted with (9:1) Ethyl Acetate:IPA 5 times, rinsed with brine, dried with sodium sulfate, and dried via rotary evaporation. The product was triturated with Diethyl Ether and the final product was recovered and verified with LCMS.

*Fmoc-FCit-PABA***:** 35mg of Fmoc-FCit-OH was mixed with 2 equivalents each of 4-aminobenzyl alcohol (PABA) and N-Ethyoxycarbonyl-2-ethyoxy-1,2-dihydroquinoline (EEDQ) in 3:1 DCM:MeOH and stirred at RT overnight. The DCM

and MeOH were dried via rotary evaporation, followed by trituration with diethyl ether. The product was verified with LCMS (data not shown).

TCO-PEG$_4$-FCit-PABA: 14.5mg of Fmoc-FCit-PABA was incubated with 8 equivalents triethylamine (TEA) and 1.25 equivalents NHS-PEG$_4$-TCO in DMSO at 50mM at RT overnight. The TCO-PEG$_4$-FCit-PABA was purified via semi-preparative RP-HPLC with a gradient of water and acetonitrile with 0.1% trifluoroacetic acid (TFA). The product was dried immediately with argon and verified with LCMS (data not shown).

TCO-PEG$_4$-FCit-PABC: 5.2mg of TCO-PEG$_4$-FCit-PABA was solubilized in dioxane with 6 equivalents of bis-4-nitrophenyl carbonate ((PNP)$_2$CO) and 3.6 equivalents N,N-diisoproylethylamine (DIEA) at 25mM overnight at 50°C. The reaction mixture was dried immediately with argon, purified via RP-HPLC, and verified with LCMS (Appendix A.9).

The Valine-Citrulline linker followed the same protocol with the following changes:

(1) Fmoc-Valine-OPfp ester was used instead of Fmoc-F-OPfp
(2) EEDQ coupling was performed in 2:1 DCM:MeOH instead of 3:1

Thiol-Reactive Linker Synthesis and Purification:

Non-cleavable TCO-PEG9-MAL Linker was purchased from Broadpharm (Cat# BP23872)

TCO-PEG$_8$-OPSS: 2.5 mg (9.51 µmol) of TCO-NH$_2$ was incubated with 6.63 µL (47.6 µmol) TEA and 7.35mg (9.99µmol) NHS-PEG$_8$-OPSS in 107µL anhydrous DMSO overnight at RT. The reaction mixture was purified on a semi-preparative RP-HPLC on a gradient of 5-95% AcN in water over 30 mins. The product eluted at 17.3 mins and was verified via LC-MS (Appendix A.22).

Nucleic-Acid Functionalization with heterobifunctional crosslinkers: All functionalized DNAs were purified on an analytical C18 RP-HPLC column on a gradient of 5-65% 0.1M triethylammonium acetate (TEAA) buffer (pH 7.0) in acetonitrile over 30 minutes. Product peaks were recovered and dried in a speed-vac and re-suspended in PBS buffer for conjugation. The recovered DNA was quantified via absorbance at 260nm on a quartz Nanoquant™ plate.

DNA-PEG4-TCO Synthesis: 100µg of single strand (ss)DNA-NH_2 (14.5 nmol) was incubated with 373µg of TCO-PEG_4-NHS (725 nmol) in 280mM HEPES buffer in 53µL of 50% DMSO overnight at 37°C and purified via RP-HPLC.

DNA-PEG4-Tzine Synthesis: 150µg of ssDNA-NH_2 (21.7 nmol) was incubated with 580µg of MeTzine-PEG_5-NHS (1.09 µmol) in 200mM HEPES buffer in 72µL of 60% DMSO overnight at 37°C and purified via RP-HPLC.

DNA-VCit-PEG4-TCO/Tzine Synthesis: 100µg of ssDNA-NH_2 (14.5 nmol) was incubated with 274µg of Fmoc-VCit-PABC (Broadpharm; 290 nmol) in 110 mM HEPES buffer in 71µL of 75% DMSO overnight at 37°C. The mixture turned a bright yellow color following reaction. The mixture was then passed through a Zeba 7kD MWCO 500µL spin column one time at 1,500 x g for 2 mins. The recovered DNA was then mixed with 314µg (610 nmol) of TCO-PEG_4-NHS or 310 µg (610 nmol) MeTzine-PEG_5-NHS in 100mM HEPES buffer in 79% DMSO overnight at 37°C and purified via RP-HPLC.

DNA-MAL-TCO Synthesis: 100µg of DNA (14.4 nmol) with a protected thiol (ssDNA-SSOH) was mixed 1:1 with 100mM DTT in PBS at a final concentration of 5 mg/mL DNA for 1 hour at RT. The mixture was washed three times with 100µL ethyl acetate (EtOAc) to remove excess DTT, then the remaining aqueous layer was incubated with 220µg (289 nmol) MAL-PEG_9-TCO in 84mM HEPES in 60µL of 75% DMSO overnight at 37°C and purified via RP-HPLC.

DNA-SS-TCO Synthesis: 100µg of DNA (14.4 nmol) with a protected thiol (ssDNA-SSOH) was mixed 1:1 with 100mM DTT in PBS at a final concentration of 5 mg/mL DNA for 1 hour at RT. The mixture was washed three times with 100µL ethyl acetate (EtOAc) to remove excess DTT, then the remaining aqueous layer was incubated with 244µg (289 nmol) OPSS-PEG_8-TCO in 250mM HEPES in 20µL of 25% DMSO overnight at 37°C and purified via RP-HPLC.

Antibody Functionalization:

Non-specific conjugation: Antibodies were functionalized non-specifically with methyltetrazine groups by incubating 100µg of antibody at 25µM with 250µM NHS-PEG_4-methyltetrazine in PBS overnight at 37°C. Excess linker was removed by washing three times with PBS in Amicon 30kDa spin columns. Recovery was quantified via absorbance at 280nm using a quartz NanoQuant plate (ext. $coeff_{280nm}$ = 210,000 M^{-1} cm^{-1}). Degree of labeling of the tetrazine was quantified via absorbance at 294nm (ext. $coeff_{294nm}$ = 93,710 M^{-1} cm^{-1}) and calculated using the formula under "degree of labeling calculation".

mTG Site-specific Conjugation: 200µg of LplA-reacted antibody was incubated at 12.5µM with 200 wt% Moo Gloo (10U/g Ab), 160 molar equivalencies of NH_2-PEG_3-Az, and 0.6µL of PNGase F for overnight at 37°C. Excess linker was removed by washing three times with PBS in Amicon 30kDa MWCO centrifugal columns. Recovered antibody was quantified via 280nm absorbance using a quartz NanoQuant plate (ext. $coeff_{280nm}$ = 210,000 M^{-1} cm^{-1}).

LplA Site-specific Conjugation: 200µg of LC or HC LAP-tagged antibody was incubated at 20µM with 10mol% LplA, 200µM pAz, 1mM ATP, and 5mM $Mg(OAc)_2$ in PBS for 1.5 hours at 37°C. The excess linker was either removed by washing three times with PBS in Amicon 30kDa MWCO centrifugal columns. Recovered antibody

was quantified via 280nm absorbance using a quartz NanoQuant plate (ext. coeff$_{280nm}$ = 210,000 M^{-1} cm^{-1}).

Ab-siRNA Conjugation: Three molar equivalencies of RNA-TCO or RNA-DBCO, with or without a cleavable site, was added to the methyltetrazine- or azide-functionalized antibody, respectively, overnight at 37°C. Conjugates were run on 4-20% Tris-Glycine polyacrylamide gels under native conditions for non-specific conjugates, and denatured and reducing conditions for site-specific conjugates. Native gels were stained with 1:10,000 diluted SYBR gold in Tris-Glycine buffer for 15 mins, then imaged on a ChemiDoc MP Imaging system (Bio-Rad). These gels were then stained with Bio-Safe™ Coomassie Stain, de-stained with water, and imaged on a ChemiDoc MP Imaging system (Bio-Rad). For denatured gels, gels were rinsed two times with 5% Triton-X in Tris-Glycine buffer for 30 mins before SYBR Gold and Bio-Safe staining, de-staining, and imaging.

Degree of Labeling Calculation: Degree of labeling measurements were taken on a TECAN M1000pro plate reader using a quartz Nanoquant™ plate and calculated using the formula below. This formula was adapted for protein, antibody, DNA, and linkers with an absorbance.

$$c_{mAb} = (A_{280}\varepsilon_{Tzine}^{294} - A_{294}\varepsilon_{Tzine}^{280}) / [(\varepsilon_{mAb}^{280}\varepsilon_{Tzine}^{294} - \varepsilon_{mAb}^{294}\varepsilon_{Tzine}^{280})l]$$
$$c_{Tzine} = (A_{280}\varepsilon_{mAb}^{294} - A_{294}\varepsilon_{mAb}^{280}) / [(\varepsilon_{Tzine}^{280}\varepsilon_{mAb}^{294} - \varepsilon_{Tzine}^{294}\varepsilon_{mAb}^{280})l]$$

$$\varepsilon_{DNA}^{260} = 190{,}900 \quad \varepsilon_{mAb}^{260} = 102{,}346 \quad \varepsilon_{Tzine}^{260} = 7{,}102$$
$$\varepsilon_{DNA}^{280} = 100{,}855 \quad \varepsilon_{mAb}^{280} = 217{,}900 \quad \varepsilon_{Tzine}^{280} = 21{,}672$$
$$\varepsilon_{DNA}^{294} = 23{,}480 \quad \varepsilon_{mAb}^{294} = 93{,}710 \quad \varepsilon_{Tzine}^{294} = 29{,}578$$

$$DOL = c_{Tzine} / c_{mAb}$$
$$\lambda_{\max}(Tzine) = 294nm$$

Equations for Degree of Labeling calculations (above).

Purification of Ab-RNA Conjugates: Ab-RNA conjugates were purified using Millipore NanoSep® 100kDa columns via the following protocol. Columns were soaked in 500µL Milli-Q H_2O for 1 hour prior to purification. Water was then removed and 50µL of Ab-RNA reaction mixture was added to each column. Columns were centrifuged at the 2,500 x g for 5 minutes. Sample was recovered using two washes of 20µL of PBS over the membrane surface. Conjugates were run on 4-20% Tris-Glycine polyacrylamide native gels and stained with SYBR GOLD to assess purity. Following purification, Ab-RNA conjugates were quantified via absorbance at 260nm and 280nm for protein and nucleic acid concentrations, respectively.

Confocal Microscopy Uptake Analysis of Ab-dsDNA-AF488 Conjugates: HeLa (TfRAb conjugates) or SKOV3 (CD63Ab or Her2Ab conjugates) cells were plated to ~75% confluency on 35mm MatTek glass bottom dishes 24 hours prior to antibody incubation. The cells were then treated with 100nM antibody-dsDNA-AF488 conjugates for 1 hour in DMEM + 10% FBS at 37°C in 5% CO_2. Cells were washed

with PBS, fixed with 4% paraformaldehyde for 15 mins at RT, followed by staining with 2μM Hoechst for 10 mins at RT, then stored at 4°C in PBS prior to imaging. Dishes were imaged on a Zeiss LSM880 inverted confocal microscope with 405nm and 488nm lasers at 40X magnification.

Flow Cytometry Uptake Analysis of Ab-dsDNA-AF488 Conjugates: 25K HeLa (TfRAb conjugates) or SKOV3 (CD63Ab or Her2Ab conjugates) cells were plated to a 24-well plate 1 day prior to antibody incubation. Cells were incubated at the varying concentrations in 200μL DMEM + 10% FBS media for 1 hour at 37°C in 5% CO_2. The cells were then washed with PBS, trypsinized, quenched with media, and resuspended in 500μL PBS for flow cytometry analysis on a BD FACSCalibur flow cytometer. Data was analyzed with FlowJo software and plotted in PRISM. All measurements were blanked with an untreated cell control.

CHAPTER 4 - MEMBRANE DISRUPTING AGENTS FOR ENDOSOMAL ESCAPE

Background

Biologics have emerged as a growing class of therapeutics in the drug market, encompassing 40% of the total market and growing at a rapid pace. This field encompasses protein- and nucleic acid-based drugs that often bind to a specific target on, or in, a cell to mediate a cellular function.[176] However, delivery of biologics is difficult, particularly for intracellular targets. Short-interfering RNA (siRNA), in particular, must enter the cytosolic space of a target mammalian cell in order to function.[153,177] Because most delivery vehicles utilize endocytosis for cellular uptake, the delivery cargo often resides in the endosome, where, in the absence of a membrane-permeating reagent, it will remain in the endosome until the cargo is degraded by proteases/nucleases as the endosome matures to a lysosome. Thus, facilitating escape from the endosomal compartment remains the major barrier to nucleic acids delivery.

There are several mechanisms and reagents used to translocate across the endosomal membrane.[50] Some pathways rely on natural leakage events that occur during fusion and fission of endosomes during endocytosis.[47] Others depend on reagents that disrupt the membrane via direct pore-formation, pH-buffering and osmotic disruption (proton sponge effect),[51-53] or carrier membrane fusion[54-56] with the endosome bilayer. Materials and chemicals derived from pathogens, as well as biomimetics, that utilize these mechanisms have been identified and incorporated into drug carriers to facilitate this process. In this study, we sought to incorporate a variety of endosomal escape agents into a non-viral delivery system, namely an antibody bioconjugate, for co-delivery with siRNA to facilitate targeted endosomal escape. To begin this study, we

examined agents that mechanistically lead to escape via pore formation in the endosomal membrane.

A common pore-forming agent utilized in delivery systems is Melittin, which is a 26-amino acid peptide and the primary toxic component of bee venom.[61,62] Melittin forms a tetrameric structure in solution,[63] and upon binding to a target cell membrane, forms an amphipathic helical structure and pore perpendicular to the cell membrane.[64,65] Melittin and several analogs have been incorporated into liposomes, polyplexes,[67,178-181] and conjugates,[66,182] most notably the dynamic polyconjugate (DPC) system.[68-70] In DPCs, Melittin was decorated with an acid-labile, maleic anhydride-derived polymer, and a targeting ligand for specific delivery to hepatocytes. When co-delivered with a cholesterol-siRNA conjugate, the endosomally unmasked Melittin induced pore formation and subsequent escape of the co-localized siRNA cargo into the cytosol. Taking inspiration from this system, we conjugated Melittin and analogues to an antibody for targeted extra-hepatic delivery.

In addition to amphipathic helical peptides such as Melittin, arginine-rich cell-penetrating peptides[183] have also been successful in delivering functionally active macromolecular cargos such as proteins,[184] oligonucleotides,[185] and plasmid DNA. It is believed that the positively-charged guanidine groups in these arginine rich peptides enhances cellular uptake and endocytosis, and possibly also facilitate endosomal escape. Recently, Najjar and colleagues showed that that polyarginines were in fact endosomolytic and facilitate the release of cargo into the cytosolic space with pulse-chase microscopy.[186] They also showed that these affects were strongly affected by the number of charges and the nature of the charged group. By covalently incorporating

arginine-rich peptides onto antibody conjugates, we can study the efficiency of endosomal escape decoupled from uptake and stability.

Bacterial-derived toxins are another class of pore-forming agents for endosomal escape. Cholesterol-dependent cytolysins[71] (CDCs) are a family of toxins which are soluble in aqueous solution, but readily oligomerize to form large pores (~300A) in lipid membranes with cholesterol. These toxins are secreted by gram-positive bacteria and are important in their pathogenicity.[72] Two examples of these pore forming toxins are Perfringolysin O (PFO) and Listeriolysin O (LLO) from *Clostridium perfringens* and *Listeria monocytogenes*, respectively. Both toxins are tetrameric proteins, approximately ~52kD in size,[73,74] with a conserved 4th domain undecapeptide responsible for its high affinity (K_D ~10^{-9} M) for cholesterol. Approximately 30-40 toxin molecules then come together on the membrane surface and oligomerize to form a pore to allow the cargo to translocate the membrane. These toxins have been used for cytosolic delivery of both cytotoxic proteins[75,77,187] and nucleic acids.[78,188]

In this chapter, we examine pore-forming activity and cytotoxicity of both peptide- and bacterial toxin-based endosomal escape agents (EEAs). We analyzed their pore-forming ability through hemolysis assays, in which we exposed these agents to red blood cells, and measured hemoglobin release as a function of agent concentration. We then explored various conjugation strategies, taking advantage of heterobifunctional linkers to specifically link EEAs to antibodies. Finally, we examined masking strategies to prevent outer membrane disruption and target these agents to the endosomal membrane. Though we were not able to effectively target these agents specifically to the endosome, we describe the steps taken to conjugate these agents and insights for how to utilize other escape agents in a similar system.

Results

Melittin and Melittin Analog Characterization: We began our investigation of EEAs with the known lytic peptide, Melittin, and two analog structures. We characterized these structures for membrane pore formation, followed by conjugation to targeting ligands. Our crosslinkers (Figure 4.4A and B) take advantage of primary amine or thiol conjugation handles, therefore, we modified the peptides to be amenable to that chemistry.

In order to utilize amine-reactive chemical crosslinkers, we needed to address the multiple lysine residues present on the native Melittin peptide (Figure 4.1A; top), as this would lead to heterogeneous crosslinking. We proposed two Melittin analogues, MK7R and MS18R (Figure 4.1A; center & bottom), each with a truncated C-terminal to remove the two lysine and two arginine residues present there. Previous work has demonstrated that though N-terminal truncation obviates Melittin activity, C-terminal truncation was well-tolerated.[67,189] The remaining amine at the 7th position was substituted with an arginine residue to preserve charge. In the MS18R analog, the 18th position serine was substituted with an arginine residue for additional charge. Both analogs left a single primary amine at the N-terminal for conjugation. The removal of charged residues from the peptides caused a rather dramatic shift in hydrophobicity, as indicated by RP-HPLC (Figure 4.11B). The second analog, MS18R, was more hydrophilic though as was expected with the additional charge.

These peptides were then analyzed via hemolysis assay at varying pH (physiological and endosomal) to test their pore-forming activity and pH-selectivity. MS18R and MK7R peptides showed similar hemolytic activity relative to the parent Melittin with

HC_{50} values around 1-2.5μM at physiological pH (Figure 4.1C) and 2-5μM at endosomal pH (Figure 4.1D). However, these peptides had a slight increase in activity ratio toward endosomal pH, i.e. the differential in HC_{50} between endosomal and physiological pH was smaller (Figure 4.1E). This data indicated that these peptide analogs would behave similarly to the parent peptide in terms of endosomal disruption, but with the ease of a single conjugation handle at the N-terminal.

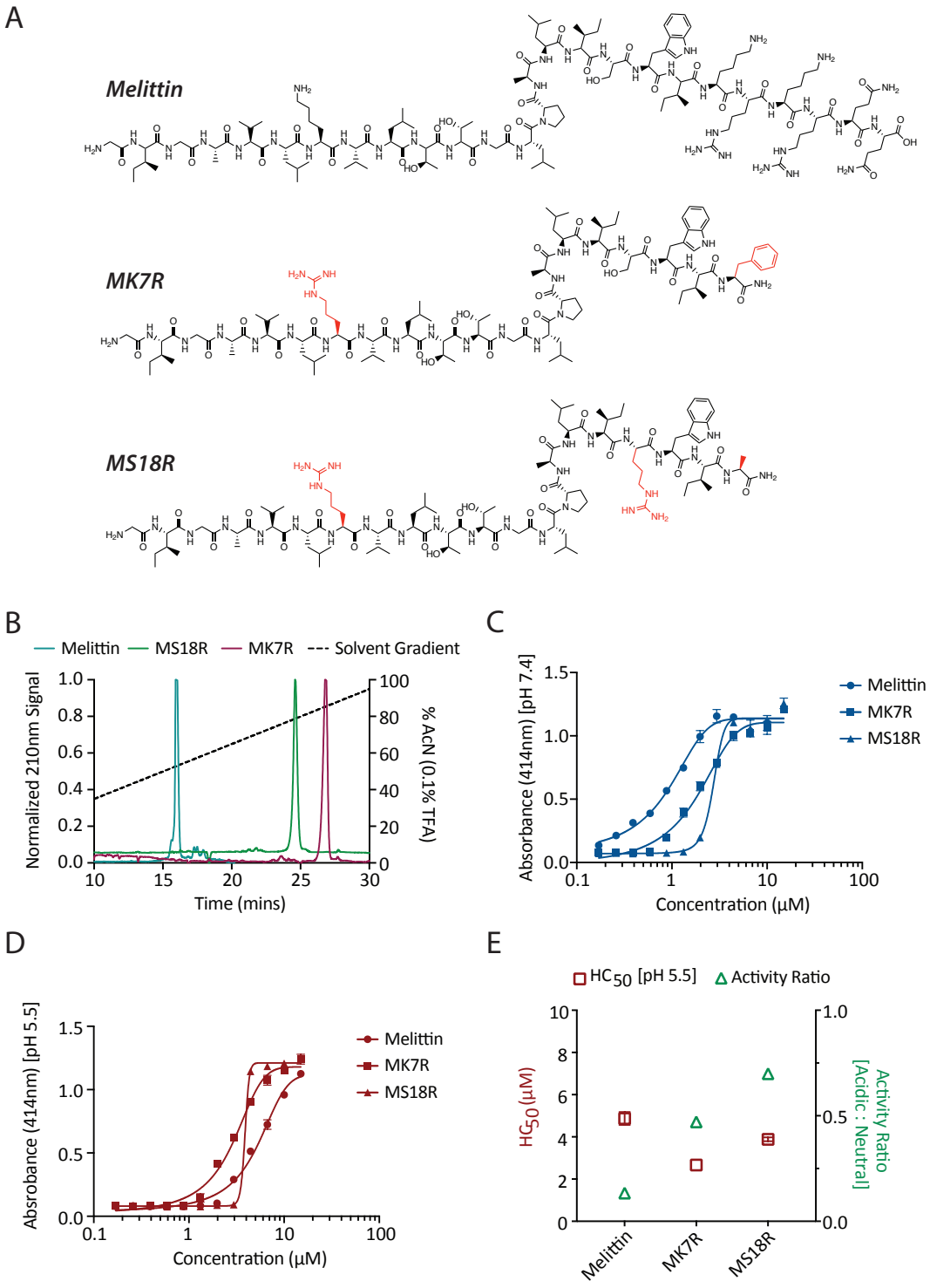

Figure 4.1 Peptide Endosomal Escape Agents with Amine Chemistry – Melittin and melittin analogs (MK7R and MS18R) with amine functionality for conjugation to antibodies. (A) Chemical structures of parent melittin peptide (top), MK7R (middle),

and MS18R (bottom). (B) RP-HPLC trace of peptides [Melittin (teal); MS18R (green); MK7R (maroon)] on a C18 column. (C) Hemolytic activity of Melittin [circle], MK7R [square], MS18R [triangle] at physiological pH (PBS buffer; pH 7.4). (D) Hemolytic activity of Melittin [circle], MK7R [square], MS18R [triangle] at endosomal pH (CBS buffer; pH 5.5).

We also utilized peptides with a thiol handle for conjugation, as the intracellular reducing environment can serve as a cleavage cue for conjugates. We received a potent melittin analog, C6M3, and parent Melittin, both with a C-terminal cysteine residue (Figure 4.2A) from a collaborator in the Pun Lab at the University of Washington. The C-terminal cysteine residue allowed us to use orthogonal chemistry to amine-reactive functional groups, therefore did not require any peptide truncation. The C6M3 peptide was more hydrophilic than the parent Melittin peptide via HPLC (Figure 4.2B) and had previously been shown by our collaborator to be active only at pH < 6.5. Additionally, this peptide showed a decrease in activity when conjugated to polymers in the Pun Lab, therefore would need to be cleaved off of its carrier in order to be active. With the four lytic peptides available, we proceeded to conjugate them to proteins and antibodies.

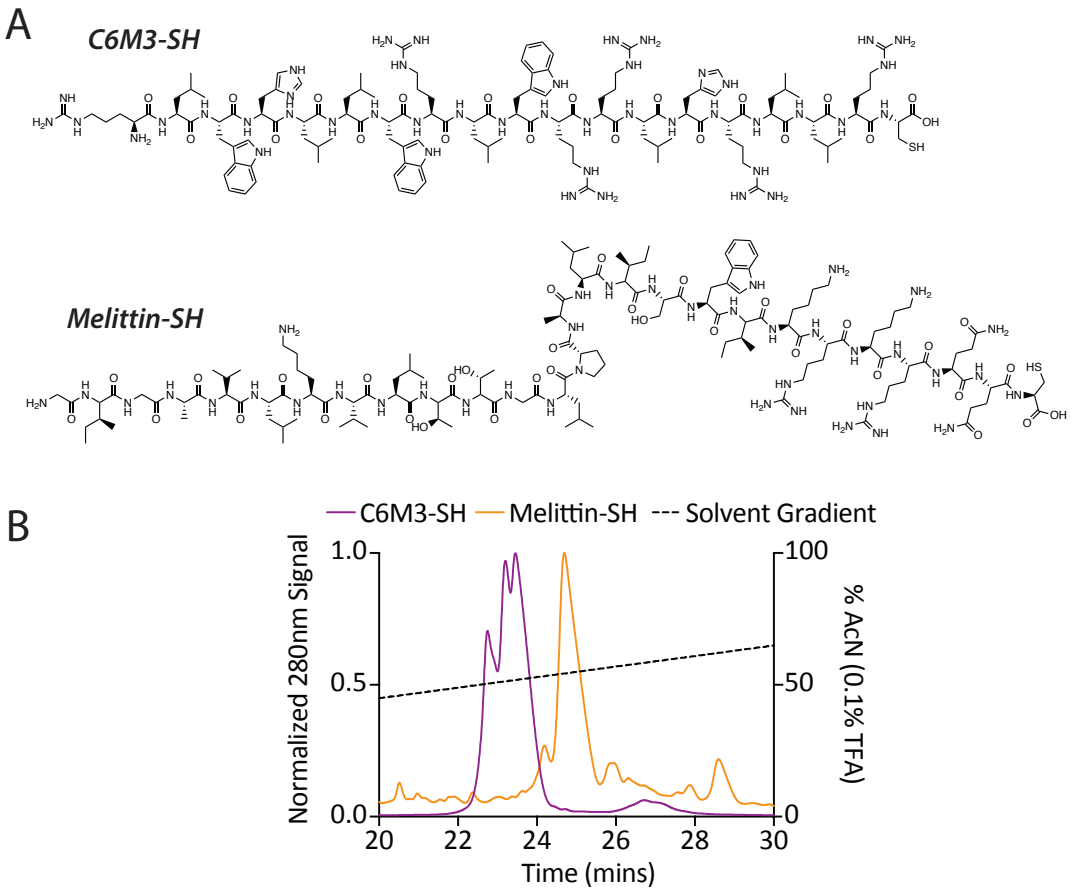

Figure 4.2 Peptide Endosomal Escape Agents with Thiol Chemistry – Melittin and "venom" peptide from Pun Lab with thiol functionality for conjugation to antibodies (A) Chemical structures of C6M3 with C-terminal cysteine (top) and Melittin with C-terminal cysteine (bottom). (B) RP-HPLC trace of peptides [C6M3 (purple); Melittin (orange)] on a C18 column.

Melittin Conjugation to Transferrin Protein: To make Transferrin conjugates we used the mono-conjugated, OPSS-functionalized Transferrin generated in chapter 3, and reacted it with Melittin-SH (Figure 4.3A). We took the Tf-OPSS and added increasing amounts of Melittin-SH and saw a shift via SDS-PAGE indicating an increase in molecular weight indicative of successful conjugation (Figure 4.3B). This conjugate was purified with dialysis to remove excess Melittin-SH and to be used for co-delivery with the Tf-siRNA conjugates made in chapter 3.

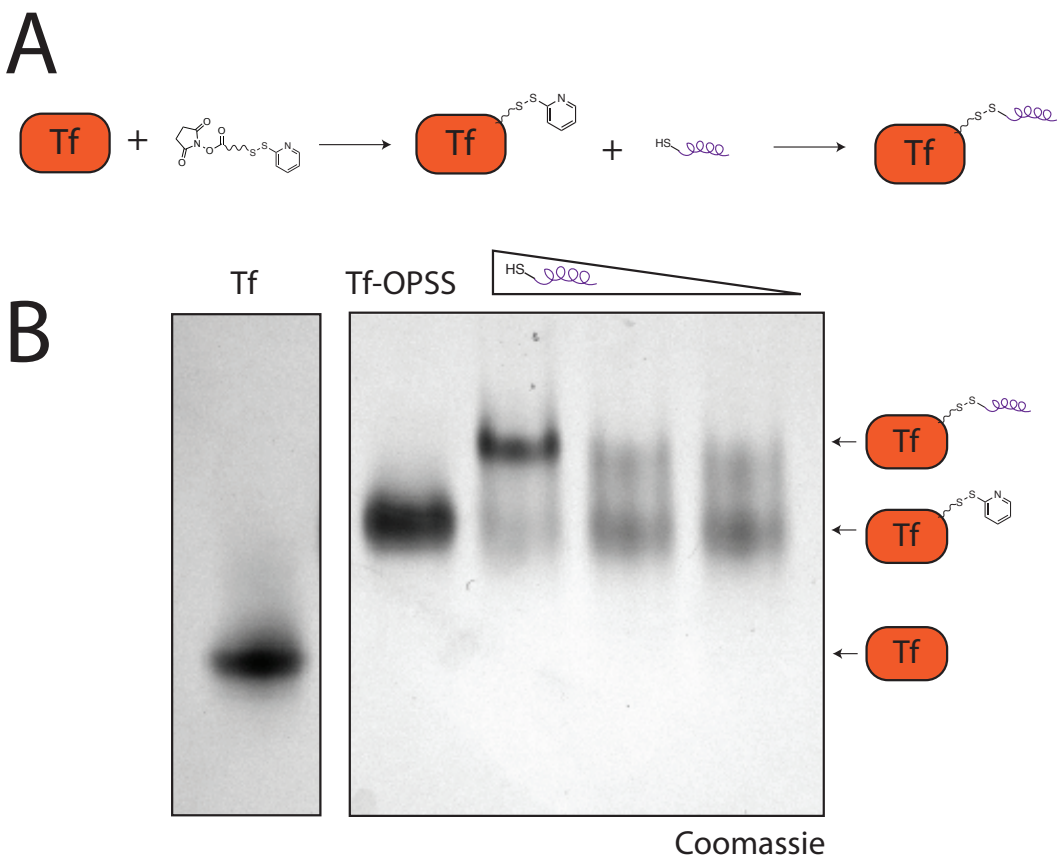

Figure 4.3 Melittin Conjugation to Transferrin (Tf) Protein – (left) Schematic of Tf functionalized with a single ortho-pyridyl disulfide (OPSS) crosslinker, followed by thiol-disulfide exchange with a thiolated Melittin peptide. (right) Native page of Tf-Melittin conjugation. Left panel shows native Tf protein. In the next panel, there is a shift upward indicative of OPSS crosslinker addition. With varying amounts of thiolated Melittin addition, there is a concentration dependent gel shift upward indicative of successful Melittin conjugation.

Peptide functionalization with heterobifunctional crosslinkers: Similar to the siRNA conjugation used in chapter 3, we used heterobifunctional crosslinkers with click chemistry groups for conjugation to antibodies. First, we functionalized the peptides with a reactive group, then clicked them onto antibodies with the opposite functionality. For the melittin analogs, we utilized amine-reactive crosslinkers (Figure 4.4A), and for the C-terminal cysteine peptides, we utilized thiol-reactive crosslinkers (Figure 4.4B). As expected, the parent melittin became heavily crosslinked and

precipitated with the addition of amine-reactive crosslinkers and could not be used. The MK7R proved to be too hydrophobic after addition of the crosslinker that it crashed out onto the HPLC column. Therefore, we purified the MS18R analog with a stable linker (MS18R-PEG4-TCO), and with two cleavable linkers with a Cathepsin-B labile Valine-Citrulline (VCit) or Phenylalanine-Citrulline (FCit) site within the linker (Appendix A.6-A.9). These peptides were still quite hydrophobic though, eluting near ~95% acetonitrile on a C4 RP-HPLC column for all three variations (Figure 4.4C). The thiol-reactive peptides were much more hydrophilic after addition of a stable maleimide-peg4-DBCO crosslinker, eluting near 60% acetonitrile on a C18 RP-HPLC column (Figure 4.4D). All peptide masses were verified with LCMS (Appendix A.1-A.5, A.10-A.16). Some oxidation of the W19 residue was observed on the purified peptide MS18R peptide conjugate, however we proceeded with conjugation anyway.

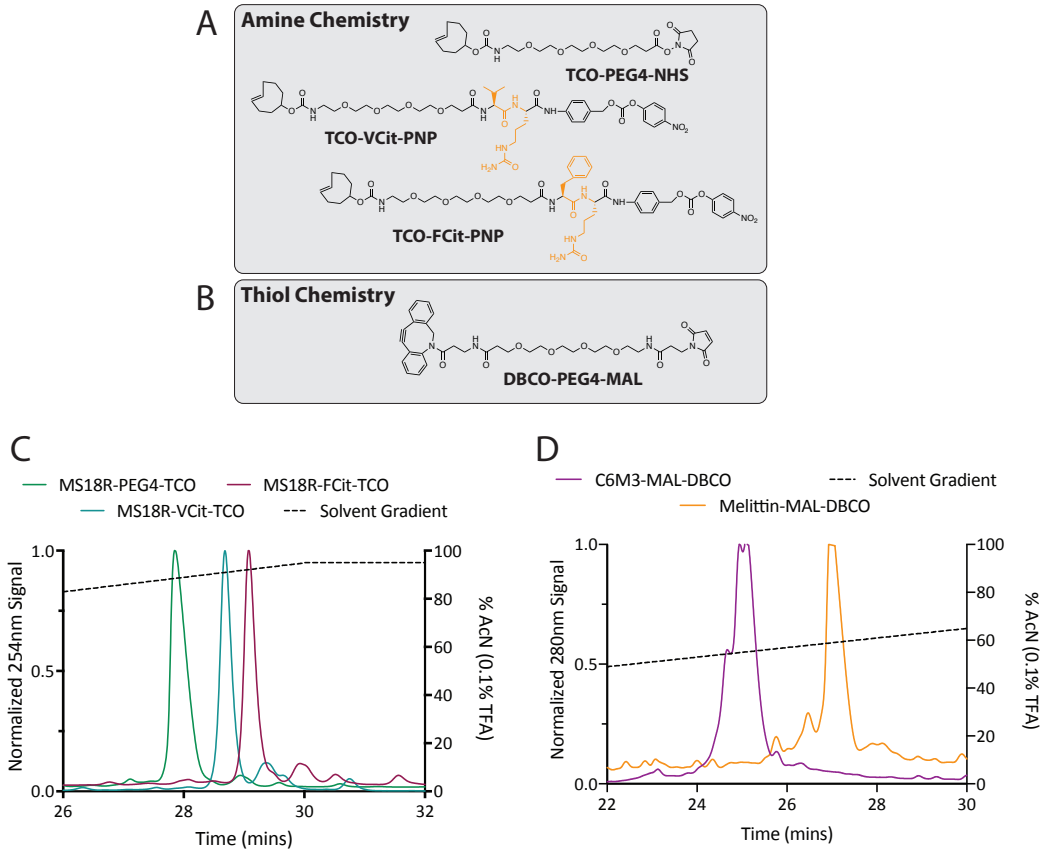

Figure 4.4 Peptide Conjugations with Chemical Linkers – Lytic peptides and chemical linker structures for conjugation to antibodies via "click chemistry" groups. (A) Chemical structures of stable (top) and Cathepsin B labile (middle & bottom) linkers functionalized with trans-cyclooctene (TCO) groups for reaction with tetrazine and para-nitrophenyl ester groups for reaction with amines. (B) Chemical structure of chemical linker with DBCO group for reaction with azides and maleimide groups for reactions with thiols. (C) RP-HPLC trace of MS18R peptide reacted with linkers in (A). (D) RP-HPLC trace of C6M3 (purple) and Melittin (orange) reacted with linker in (B).

Following successful crosslinker addition with the lytic peptides, we followed a similar methodology with a non-lytic peptide, R9K (Figure 4.5A).Though this peptide did not display any hemolytic activity at either pH (Figure 4.5C), it has been shown previously by us[190] and others[183,186] that guanidine-rich oligomers are efficient at cell membrane translocation. Therefore, we used a similar conjugation approach and a

DBCO crosslinker (Figure 4.4B) via an NHS-ester conjugation to the lysine group on the c-terminal end of R9K. This peptide mass was purified via RP-HPLC (Figure 4.5D) and verified with LCMS (Appendix A.17-A.19). This R9K-DBCO could then be used with the other lytic peptides and conjugated to antibodies.

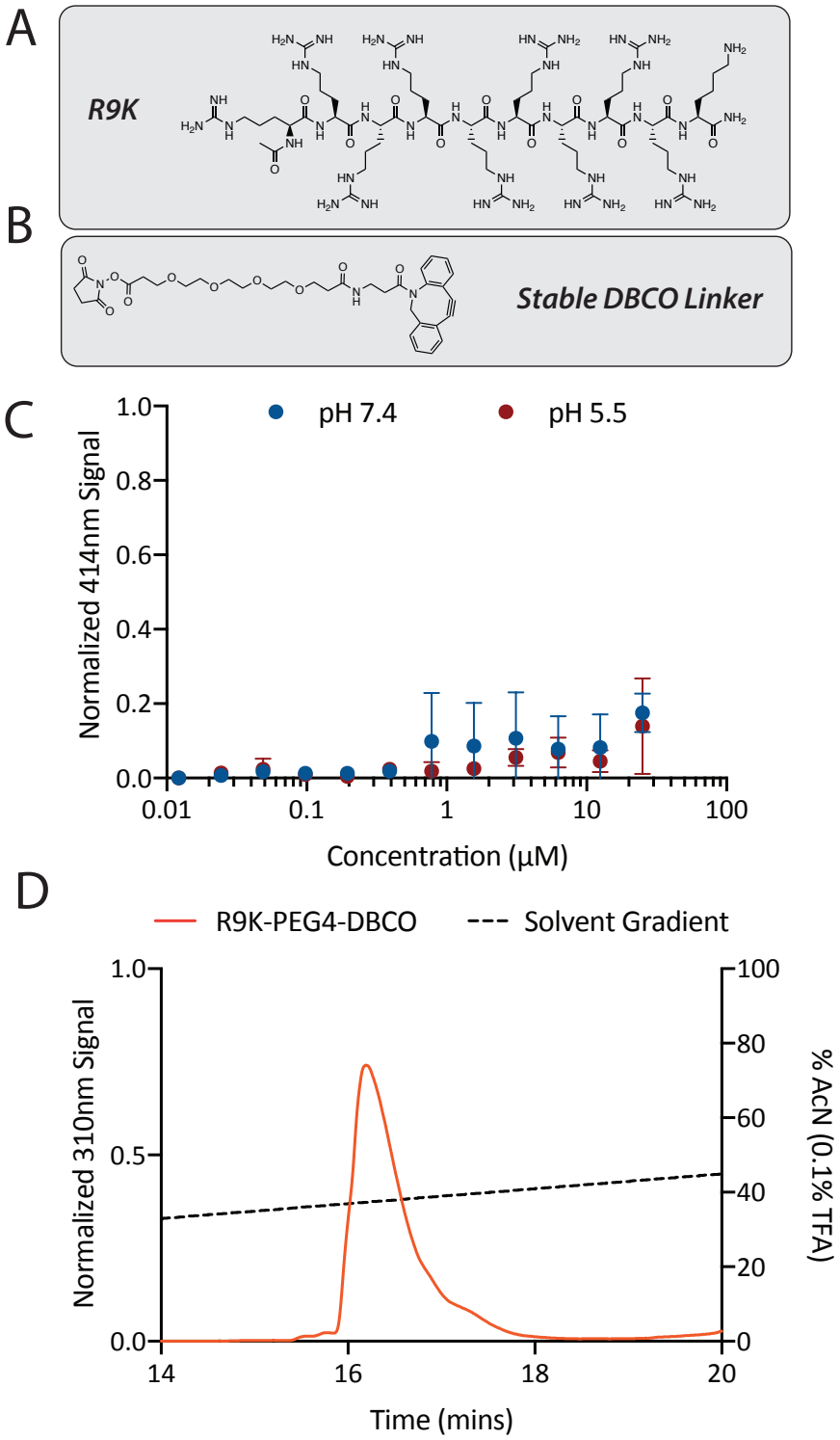

Figure 4.5 Characterization and Conjugation of R9K – Arginine reach peptide with amine functionality (R9K) characterization on red blood cells and conjugation with a chemical linker. (A) Chemical structure of R9K peptide. (B) Chemical structure of amine-reactive NHS-PEG$_4$-DBCO group for reaction with azides. (C) Hemolytic

activity of R9K at physiological pH (blue) and endosomal pH (maroon). (D) RP-HPLC trace on a C18 column of R9K reacted with the linker in (B).

Lytic Peptide Conjugation Methods to Cell Receptor Targeting Antibodies: In order to deliver these peptides in a targeted manner, we conjugated them to cell-surface targeting antibodies via several conjugation methods; non-specific, Fc-region specific, and light-chain specific (Figure 4.6A).

To non-specifically conjugate the MS18R peptide to an antibody, we took the TCO-functionalized MS18R peptide and added increasing molar ratios to a randomly tetrazine-functionalized antibody. This resulted in a gel shift and band intensity increase on both the heavy and light chains of the antibody, indicating that the peptide was successfully conjugated (Figure 4.6B). It also however, indicated that the peptide was conjugating indiscriminately all over the antibody, with little control over stoichiometry. Additionally, because the MS18R peptide was so hydrophobic, the resulting conjugated antibody precipitated out of solution.

With this result, we performed site-specific conjugation with azide-functionalized antibodies specifically on the Fc domain on the heavy chain, or the constant light chain (LC) domain with mTG and LplA enzymes, respectively. For this we used the two, more hydrophilic peptides, C6M3 and R9K and analyzed via SDS-PAGE. In this case, when the peptide was conjugated via mTG or LplA there was a very small specific shift in just one domain of the antibody (HC for the mTG conjugation, LC for the LplA conjugation), and no observable difference in band intensity (Figure 4.6C and D). This difference is very small and should be further verified with MALDI-TOF, but was encouraging enough to proceed. These antibody conjugates did not precipitate out of solution and could potentially be functional for delivery.

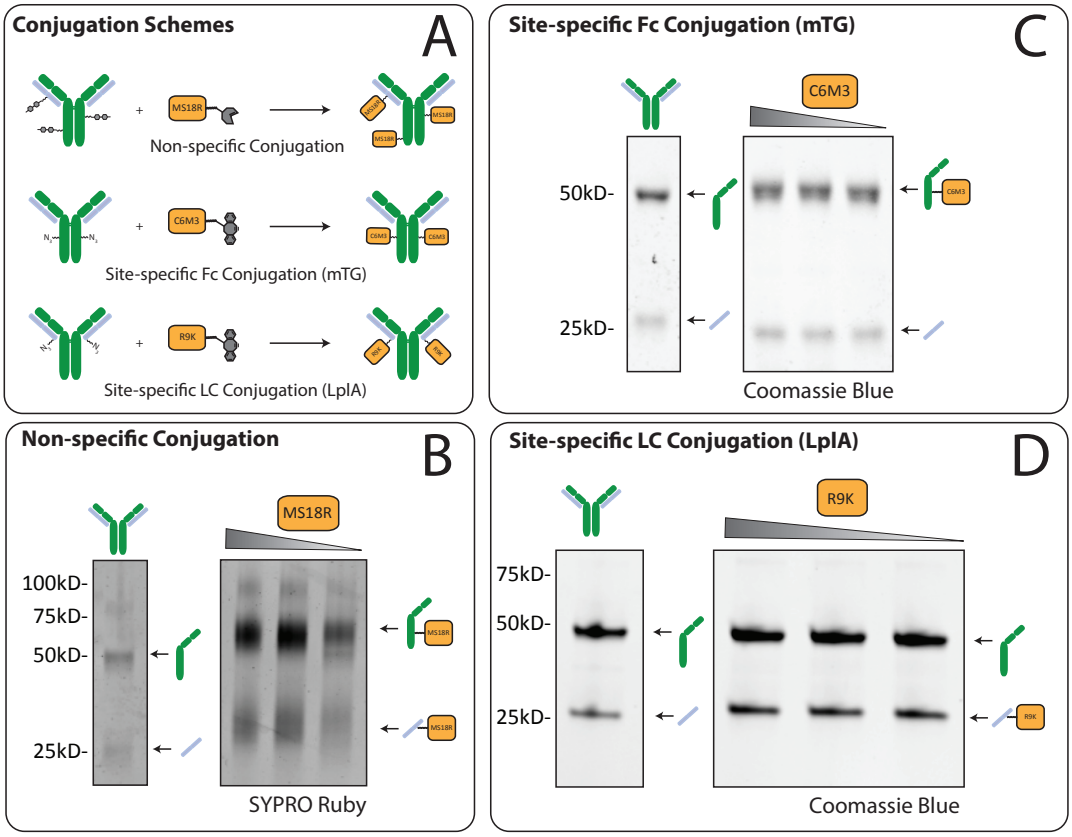

Figure 4.6 Conjugation of Peptides to Antibodies – SDS-PAGE analysis of antibodies conjugated to antibodies via random and site-specific conjugation methods. (A) Gradient conjugation of MS18R, functionalized with TCO, to a randomly tetrazine-labeled antibody. (B) Gradient conjugation of C6M3 peptide, functionalized with DBCO, to a Fc-region azide-labeled antibody. (C) Gradient conjugation of R9K peptide, functionalized with DBCO, to a LC-region azide-labeled antibody.

Bacterial Toxins in Endosomal Escape – Perfringolysin O (PFO): In addition to membrane-disrupting peptides, we investigated bacterial toxins for endosomal escape agents, specifically the cholesterol-dependent cytolysin (CDC) family of toxins. These toxins are unique in that they are aqueous soluble yet still have a strong membrane-affinity for pore formation. First, we considered Perfringolysin O (PFO), a secreted toxin from *Clostridium perfringens*, to characterize and investigate.

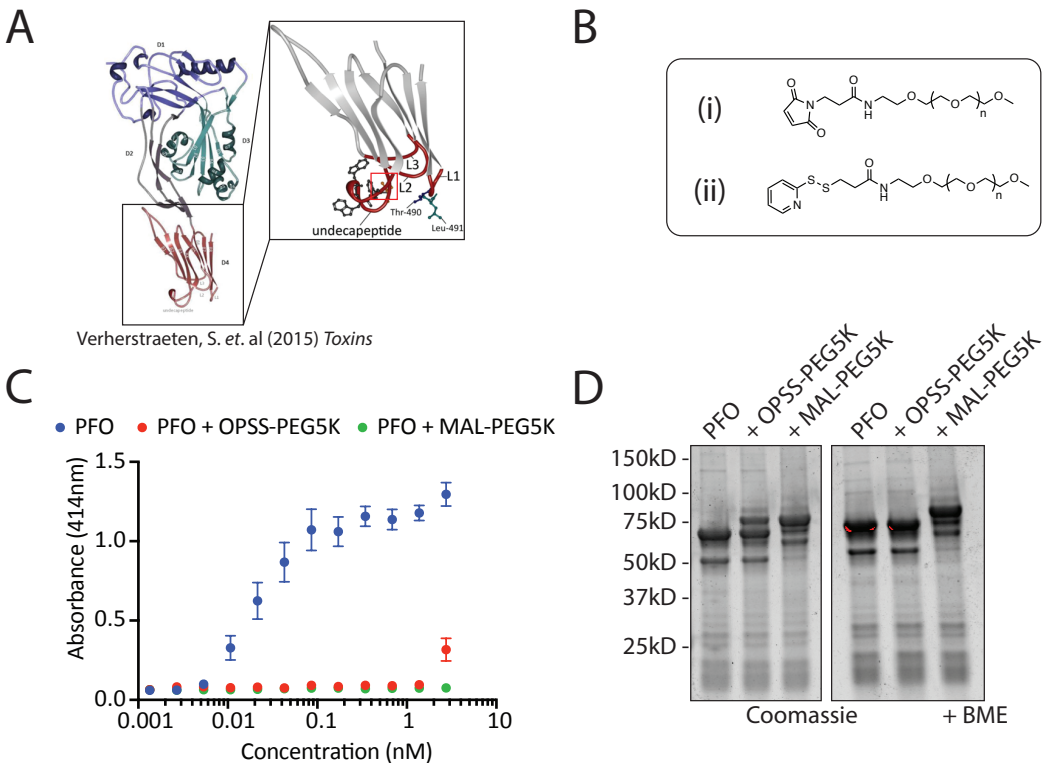

Figure 4.7 Perfringolysin O (PFO) Characterization – Characterization of commercial PFO hemolytic activity and PEGylation. (A) Crystal structure of full-length PFO[191] and zoom on domain four. Red box highlights single cysteine residue, shown in orange. (B) PEGylation reagents used for non-reducible (i) and reducible (ii) PEGylation of LLO on fourth domain cysteine. (C) Hemolytic activity of PFO and PEGylated counterparts with reducible (OPSS) and non-reducible (MAL) PEGs. (D) SDS-PAGE of control and PEGylated (reversible and stable) with and without βME. Expected mass of PFO+Tag = 66.2 kD

PFO, like other CDCs contains a characteristic, single, cysteine residue in the fourth domain of the protein (Figure 4.7A[191]). This domain and the undecapeptide within it has been shown to be responsible for cholesterol binding and membrane incorporation into a target cell membrane.[192] This cysteine residue thus served as a convenient reversible handle for both activity attenuation and conjugation. To demonstrate the activity attenuation, we incubated PFO with non-reducible (MAL)(Figure 4.7Bi) and reducible (OPSS)(Figure 4.7Bii) PEGylating agents and examined subsequent changes in hemolytic activity. As expected, the PEG addition significantly reduced the toxin

hemolytic activity up to 2.5 nM, with a small amount of detectable activity at 5 nM with the reducible linker (Figure 4.7C). When analyzed via SDS-PAGE, we observed a gel shift corresponding to the addition of the PEG chain (Figure 4.7D). When treated with a reducing agent, beta-mercaptoethanol (βME), the band corresponding to the toxin with the reducible PEG returned to the position of the parent toxin, while the non-reducible linkage was not affected. This is expected because the thiosuccinimide linkage is stable to reducing agents. After demonstrating that the toxin could be reversibly attenuated, we moved to a similar bacterial toxin that is known to be more active at endosomal pH, Listeriolysin O (LLO).

Bacterial Toxins in Endosomal Escape – Listeriolysin O (LLO): LLO is a member of the same family of CDCs as PFO, however; LLO is derived from the intracellular pathogen, *Listeria monocytogenes*. LLO is unique among CDCs in that it is used for endosomal escape of the *Listeria* and is more active in the endosomal compartment than the cytosolic or extracellular space. Using a plasmid generously donated by Dr. Daniel Portnoy's Lab at UC Berkeley, we were able to express and purify His-tagged WT LLO from BL21 *E. coli* cells. We characterized LLO for hemolytic activity and determined an HC_{50} value of 30 pM at endosomal pH. We also observed a pH differential in lytic activity of about 3.3X between physiological and endosomal pH (Figure 4.8A). This was consistent with literature and an indicator that LLO would be more active on the endosomal membrane than the outer cell membrane. Additionally, LLO also has the single, conserved cysteine residue at the fourth domain of CDCs that attenuates activity. We conjugated LLO with a reducible PEGylating agent (Figure 4.8Gii) and saw efficient PEGylation of the toxin via SDS-PAGE that was reversible with βME (Figure 4.8B). This PEGylation corresponded to a reduction in hemolytic activity by an order of magnitude at both physiological (Figure 4.8C) and endosomal

pH (Figure 4.8D) that was reversible with the addition of dithiothreitol (DTT). We saw a similar activity modulation with the toxin was conjugated with a reducible, heterobifunctional crosslinker for antibody conjugation (Figure 4.8E&F). This attenuation via the D4 cysteine was effective, but only attenuated the active range of the toxin to between 1-10nM. Unfortunately, the potency is higher than the dosing concentration of the antibody conjugates. Therefore, we needed to further attenuate the toxin.

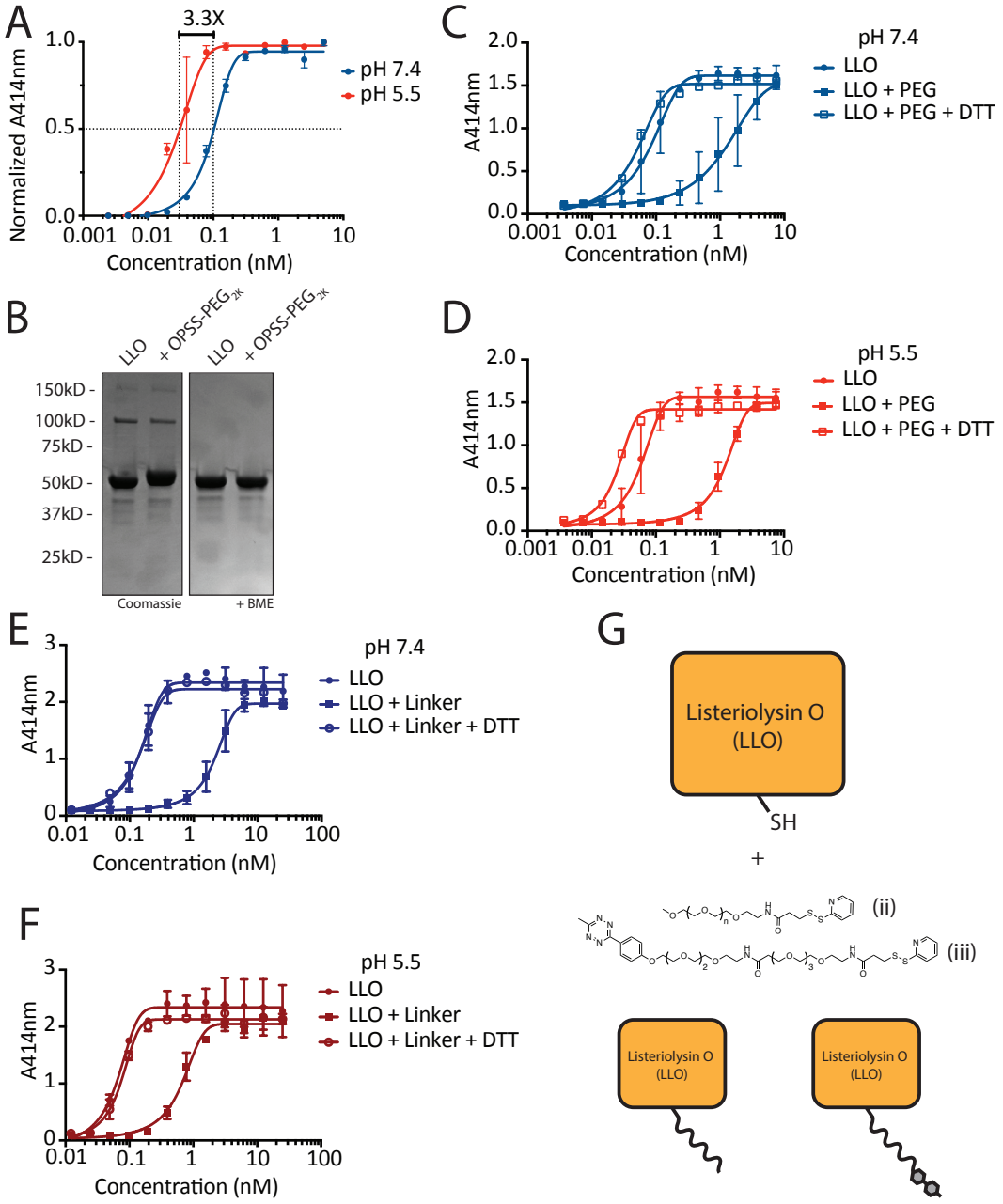

Figure 4.8 Listeriolysin O (LLO) Characterization – Characterization of LLO hemolytic activity, pH differential, and PEGylation. (A) Hemolytic activity of LLO at physiological [PBS buffer (pH 7.4)] and endosomal [CBS buffer (pH 5.5)] pH. Has a differential of 3.3-fold between endosomal and physiological pH. (B) SDS-PAGE of LLO with and without reducible PEGylation reagent (G-ii) and before and after treatment with βME. (C&D) Hemolytic activity of LLO with reducible PEG (G-ii) at physiological [blue; PBS buffer (pH 7.4)] and endosomal [red; CBS buffer (pH 5.5)] pH and reduced with DTT. (E&F) Hemolytic activity of LLO with reducible bi-functional PEG linker (G-iii) at physiological [blue; PBS buffer (pH 7.4)] and endosomal [red; CBS buffer (pH 5.5)] pH and reduced with DTT. (G) Schematic of

PEGylation of LLO with two PEG structures used in this figure. G-ii; PEG-OPSS. G-iii; MeTzine-PEG_8-OPSS

Surface PEGylation of LLO for Reduced Outer Membrane Affinity: Surface PEGylation has been shown previously to decrease adherence of several materials, including proteins, by adding an extra "water" layer around the given material[117,127]. Therefore, to decrease the affinity of the toxin for the target membrane, we first examined PEG length and PEG degree of labeling (DOL) on hemolytic activity. We screened mono- and poly-disperse NHS-PEGs with 1,200, 2,000, and 5,000 molecular weights (MW) (Figure 4.9B; top) at a range of molar equivalencies (3-10 fold) for attenuation of the toxin via surface PEGylation. Via SDS-PAGE, we saw a band shift to higher molecular weights with both increasing molar equivalencies of PEG (Figure 4.9A; left) and increasing PEG length (Figure 4.9A; right), as anticipated. This surface PEGylation correlated with decreasing amounts of hemolytic activity along the same trend (Figure 4.9C and D). The greatest decrease in activity was observed with the longest PEG chain length and highest equivalencies (10-fold molar excess). With this information, we generated an amine-reactive, para-nitrophenol functionalized PEG that is self-immolative following reduction of the internal disulfide (Figure 4.9B; bottom). We then showed via SDS-PAGE (Figure 4.9G) and hemolysis assay (Figure 4.9F) that this linker could PEGylate the surface of the toxin and is reversible with βME and DTT (Figure 4.9E and F).

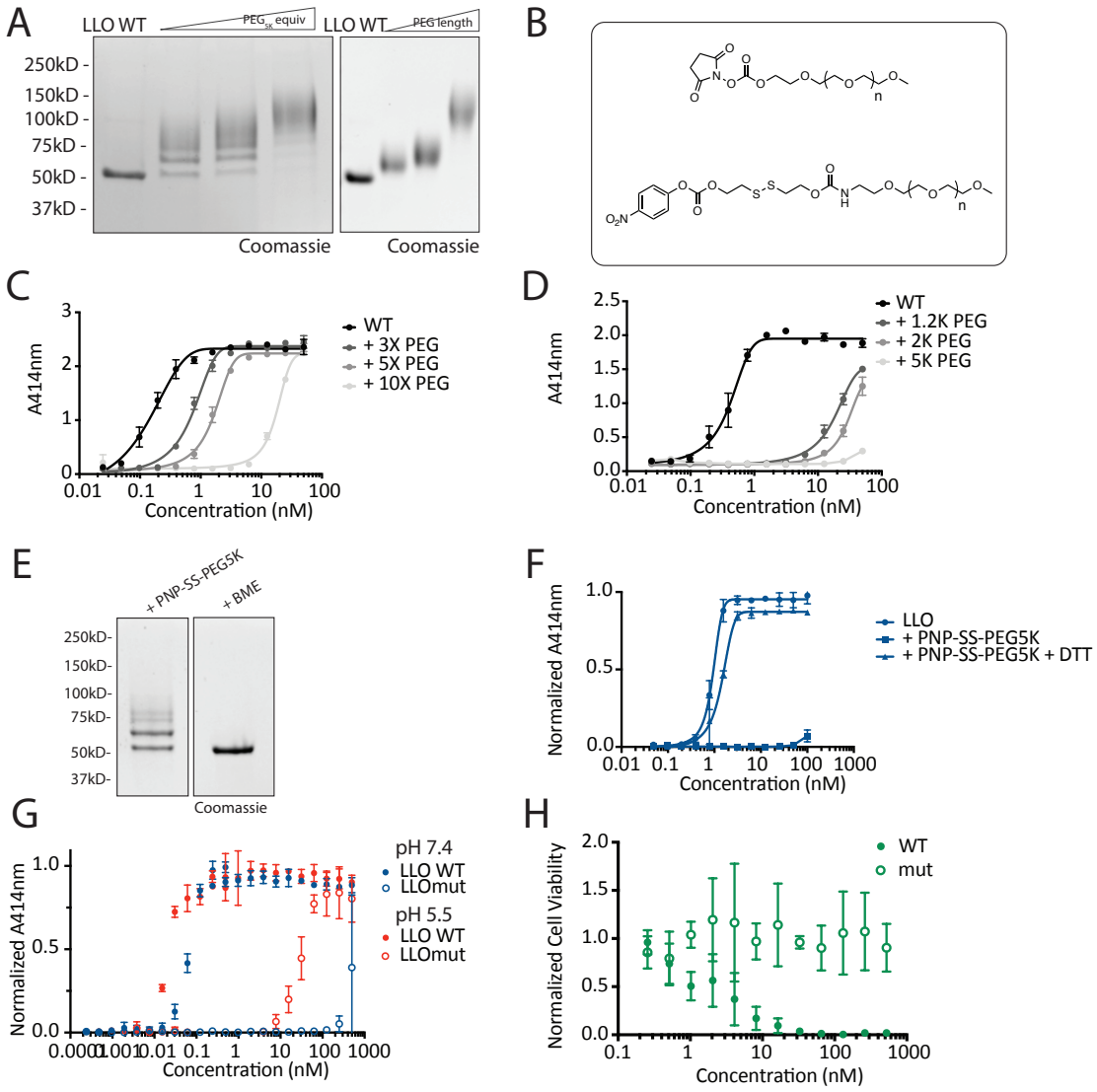

Figure 4.9 LLO Surface PEGylation- Studies on surface PEGylating LLO for reduced interaction with the outer cell membrane. (A) SDS-PAGE of LLO reacted with NHS-PEGs (B; top) with varying molar equivalencies (left) and varying molecular weights (right). (B) Chemical structures of non-reducible (top) and reducible (bottom) surface PEGylation reagents. (C&D) Hemolytic activity of LLO with non-reducible surface PEGylation with varying molar excess (C) and varied PEG length (D). (E) SDS-PAGE of LLO reacted with reducible surface PEGylation reagent (B; bottom) before and after treatment with βME. (F) Hemolytic activity of LLO reacted with reducible surface PEGylation reagent (B; bottom) before and after treatment with DTT. (G) Hemolytic activity of LLO WT (closed circle) and W491AW492A mutant (open circle) at physiological (blue) and endosomal (red) pH. (H) MTS assay for cytotoxicity on mammalian cells of WT LLO (closed circle) and mutant (open circle).

Site Directed Mutagenesis to 4th Domain Undecapeptide for Toxin Attenuation: To further reduce LLO's potency above the dosing concentration (~100 nM), we performed site-directed mutagenesis to mitigate overall toxicity to mammalian cells. In a similar targeted dual-delivery system in which a CDC was used for endosomal escape of a protein therapeutic, Gelonin, and later for siRNA, Yang and colleagues found that when PFO was mutagenized at T490A and L491V positions, the toxin had drastically reduced toxicity toward the mammalian cell target, but comparable activity to the WT in the targeted delivery system.[77,78] Taking inspiration from this system, we mutagenized W491A and W492A on LLO via Quik-change® mutagenesis and observed the change in lytic activity. After mutagenesis, the toxin showed a decrease in hemolytic activity at physiological pH by 4-orders of magnitude, and a decrease at endosomal pH by 2,000-fold (Figure 4.9G). This yielded a mutant toxin that had an activity range of 10-100nM at endosomal pH, and greater than 1μM for physiological pH, which increased the pH differential from 3.3- to 20-fold compared to the wild type, and in the ideal concentration range for our delivery system. Additionally, this mutant showed no detectable toxicity via MTS assay on SKOV3 cells on concentrations up to 1μM (Figure 4.9H). Next, we combined the mutagenesis and PEGylation and examined uptake of the toxin into mammalian cells.

Outer Membrane Binding of Attenuated and PEGylated LLO: CDCs have a very high affinity for cholesterol,[192] which is what makes them very potent membrane disruptors. However, the cholesterol binding by LLO to the cell surface competes with antibody binding and endocytosis of the entire conjugate. Therefore, we examined the impact of the mutagenesis and PEGylation of the toxin on the outer membrane binding. To do this, we labeled the toxin on the fourth domain cysteine with a maleimide AlexaFluor 488 (AF488) and PEGylated the surface, which corresponded

to an increase in MW and positive fluorescent signal (Figure 4.10A and B). We took these fluorescently-labeled toxins and examined their interaction with SKOV3 cells via flow cytometry. Following the trend in hemolytic activity, we observed a decrease in cellular uptake with increased PEG length and DOL. This uptake however, was still detectable above the BSA control even at the most extreme PEGylation condition (Figure 4.10C and D). Additionally, when we took the mutagenized toxin and conjugated it to Her2-targeted antibody via non-specific conjugation (Figure 4.10E), we saw uptake into mammalian cells that was receptor-independent (Figure 4.10F&G). In a final attempt to reduce surface interaction, we PEGylated the toxin and specifically conjugated it to the LC of Her2-targeted antibodies (Figure 4.10H) and examined uptake into SKOV3 cells. Unfortunately, the overall uptake of the conjugate was low and on-order with the PEGylated toxin alone (Figure 4.10J). This was indicative that the cholesterol affinity was greater than the antibody affinity, or the addition of the toxin was blocking the binding site of the antibody. With this information, we concluded that although the toxin was no longer toxic, it was too "sticky" to deliver via this antibody conjugation system.

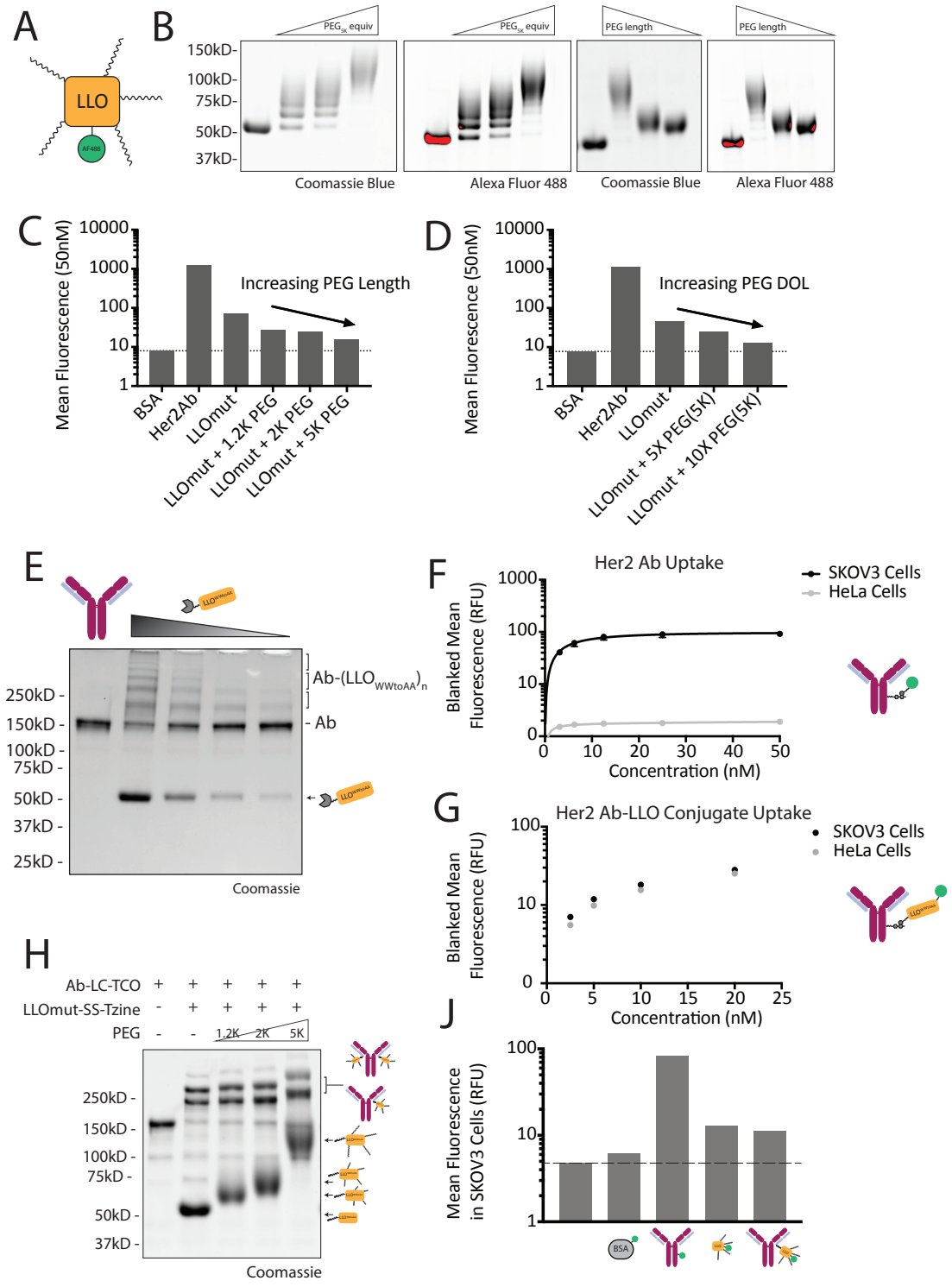

Figure 4.10 LLO-Antibody (Ab) Conjugation and Uptake into Mammalian Cells (SKOV3 Cells) – Studies examining the effect of surface PEGylation and conjugation to a targeting antibody on uptake into mammalian cells. (A) Schematic of simultaneous labeling of LLO with fluorescent AlexaFluor 488 (AF488) on the D4 cysteine and PEGylation via surface lysine residues. (B) SDS PAGE of fluorescently-labeled LLO with varying molar excess of PEG and varying PEG length under

Coomassie and fluorescence imaging. (C&D) Flow cytometry analysis of fluorescently-labeled and PEGylated LLOmut as a function of PEG length (C) and extent of surface labeling (D). Labeled BSA and Her2-targeted Ab are negative and positive controls for uptake in SKOV3 cells, respectively. (E) SDS-PAGE stained with Coomassie of non-specific conjugation of LLO to Her2-targeted antibodies as a function of increasing LLO excess. Mass LLO – 52kD; Mass Ab – 150kD; Mass conjugate – 200+ kD. (F) Surface Her2 receptor expression as depicted by flow cytometry measured Her2Ab uptake in SKOV3 cells (black) and HeLa cells (gray). (G) Uptake of Her2Ab-LLO conjugates in SKOV3 cells (black) and HeLa cells (gray) as a function of concentration. (H) SDS-PAGE stained with Coomassie of site-specific conjugation of PEGylated LLO (with varying PEG lengths) to light-chain tagged antibodies. (J) Uptake of PEGylated LLO and PEGylated LLO-Antibody conjugates in SKOV3 cells as measured by flow cytometry. Uptake of antibody conjugate and free LLO are comparable and well below antibody control, therefore uptake is not driven by antibody, only by LLO.

Conclusions & Discussion

In this chapter, we characterized both peptide and bacterial toxin endosomal escape agents (EEAs) with different potencies and conjugated both to antibodies for later use in an antibody conjugate delivery system. Lytic peptides included Melittin, a bee-venom derived peptide, and analogs, whereas bacterial toxins were cholesterol-dependent cytolysins (CDCs) derived from *Clostridium perfringens* and *Listeria monocytogenes*. To characterize these agents, we examined their hydrophobicity, hemolytic activity, and mammalian cellular uptake, and were able to conjugate them to antibodies using amine-reactive or thiol-reactive heterobifunctional crosslinkers. The hemolytic activity spanned picomolar to micromolar range, allowing us to screen agents with a range of membrane potencies and how efficiently they can induce endosomal escape. However, despite the hope that this conjugate system could de-couple uptake and stability from endosomal escape, the two were still indeed coupled.

We found that when the Melittin and Melittin-like peptides were too hydrophobic and non-specifically conjugated, the conjugates precipitated out of solution and could not be effectively delivered. However, when we took more hydrophilic peptides and

conjugated them specifically, the conjugates were much more stable in solution. Due to the chronology of this study, the site-specific antibody-peptide conjugates were never tested for uptake and endosomal escape. It is very likely that these conjugates would not have the same "sticky" fate as the antibody-LLO conjugates, as the potency of these lytic peptides was much lower than that of the bacterial toxins. However, these peptides may not be potent enough in the endosome, as these peptides had HC_{50} values in the low μM range, and it may be necessary to have a high peptide:antibody ratio to reach critical endosomal concentration for efficient lysis This could be achieved, through multifunctional crosslinkers like those developed in our lab, which would allow for a high DOL while still maintaining site-specificity on the antibody.

Out of concern of a lack of lytic potency, we transitioned from lytic peptides to water-soluble, highly potent, cholesterol-dependent cytolysins. The high affinity for cholesterol and potency was to our detriment though, as these toxins still showed receptor-independent uptake into mammalian cells despite significant attenuation attempts. Structural evidence[74,192] suggests this may be due to the toxin forming a pre-pore complex on the surface of the cell, but not converting to a final pore. This would make the toxic non-toxic, but still "sticky". The most effective means of attenuation is still held by the Wittrup lab[77,78,193] where an evolved fibronectin (Fn3) domain reversibly attenuates the toxin and releases it in the endosome. To extend this system to other EEAs would be difficult though as new Fn3 evolution would be required for each toxin. Chemical means of attenuating these toxins, or synthetic alternatives, could be an approach for future work.

From this study, we have learned that it is difficult to engineer conjugates to target lytic agents specifically to the endosomal membrane. This field is on-going, as there

currently is no antibody-conjugate based delivery system in the literature that effectively screens endosomal escape agents. Future studies should utilize a previously-validated receptor target, escape agent, and a highly stabilized cargo to more efficiently address this problem. This can then be expanded to new surface receptors, escape agents, and therapeutic cargos.

Materials & Methods

Reduction Sensitive Linker Synthesis and Purification (Appendix A.20-A.27):

TCO-PEG$_4$-OPSS: 2.1 mg (7.99 µmol) of TCO-NH$_2$ was incubated with 5.57µL (40.0 µmol) TEA and 4.7mg (8.39 µmol) NHS-PEG$_4$-OPSS in 90µL anhydrous DMSO overnight at RT. The reaction mixture was purified on a semi-preparative RP-HPLC on a gradient of 5-95% AcN in water over 30 mins. The product eluted at 18.5 mins and was verified via LC-MS. (Appendix A.21)

TCO-PEG$_8$-OPSS: 2.5 mg (9.51 µmol) of TCO-NH$_2$ was incubated with 6.63 µL (47.6 µmol) TEA and 7.35mg (9.99µmol) NHS-PEG$_8$-OPSS in 107µL anhydrous DMSO overnight at RT. The reaction mixture was purified on a semi-preparative RP-HPLC on a gradient of 5-95% AcN in water over 30 mins. The product eluted at 17.3 mins and was verified via LC-MS (Appendix A.22).

TCO-PEG$_{24}$-OPSS: 1.2 mg (4.57 µmol) of TCO-NH$_2$ was incubated with 3.18µL (22.8 µmol) TEA and 6.9mg (4.79 µmol) NHS-PEG$_{24}$-OPSS in 51µL anhydrous DMSO overnight at RT. The reaction mixture was purified on a semi-preparative RP-HPLC on a gradient of 5-95% AcN in water over 30 mins. The product eluted at 18.4 mins and was verified via LC-MS (Appendix A.23).

MeTzine-PEG$_8$-OPSS: 6.5 mg (17.9 µmol) of methyltetrazine-PEG$_4$-NH$_2$ was incubated with 12.5µL (89.4 µmol) TEA and 10.5mg (18.8 µmol) of NHS-PEG$_4$-OPSS in 248µL anhydrous DMSO overnight at RT. The reaction mixture was purified

on a semi-preparative RP-HPLC on a gradient of 5-95% AcN in water over 30 mins. The product eluted at 18.0 mins and was verified via LC-MS (Appendix A.25).

MeTzine-PEG$_{28}$-OPSS: 2.5mg (6.88 µmol) of methyltetrazine-PEG$_4$-NH$_2$ was incubated with 4.8µL (34.4 µmol) TEA and 10.4mg (7.22 µmol) NHS-PEG$_{24}$-OPSS in 159µL anhydrous DMSO overnight at RT. The reaction mixture was purified on a semi-preparative RP-HPLC on a gradient of 5-95% AcN in water over 30 mins. The product eluted at 18.3 mins and was verified via LC-MS (Appendix A.26).

PNP-SS-PEG5K: 4mg (800 nmol) of PEG5K-NH$_2$ was incubated with 1.12µL (8 µmol) TEA and 3.88 mg (8µmol) bis-SS-PNP in 121µL anhydrous DMSO for 3 hours at RT. The reaction mixture was purified on a semi-preparative RP-HPLC on a 5-95% gradient of AcN (0.1% TFA) in water (0.1% TFA) over 72 mins. The product eluted at 47 mins (Appendix A.27).

Truncated Melittin Linker Conjugation: 200µg of the truncated Melittin peptide (MS18R) was incubated with 2 equivalencies CatB cleavable linkers in DMSO with 20 equivalencies triethylamine (TEA) overnight at 37°C. The reaction mixture was purified on an analytical C4 HPLC column with a gradient of acetonitrile in water with 0.1% trifluoroacetic acid (TFA). Product was verified with LCMS. (Appendix A.10-A.11)

Non-specific Ab Functionalization: Purified anti-CD63 antibody (CD63Ab) or mouse isotype control (mAb) was functionalized at 25µM with 10 equivalencies NHS-PEG4-MeTzine in PBS overnight at 37°C. The reaction mixture was purified via 30kD amicon spin columns 3 times, and quantified via absorbance at 280nm and 294nm for concentration and DOL, respectively.

Site-Specific Ab Functionalization:

LplA Conjugation: 500µg of antibody was incubated at 20µM with 10mol% LplA, 200µM pAz or TCO-LAP, 1mM ATP, and 5mM $Mg(OAc)_2$ in PBS for 1.5 hours at 37°C. The reaction mixture was purified via Amicon 30kDa MWCO centrifugal columns and quantified via 280nm absorbance using a quartz NanoQuant plate (ext. $coeff_{280nm}$ = 210,000 M^{-1} cm^{-1}).

Transglutaminase (mTG) Conjugation: 500µg of antibody was incubated at 12.5µM with 200 wt% Moo Gloo (10U/g Ab), 160 molar equivalencies of NH_2-PEG_3-Az or NH_2-PEG_5-MeTzine, and 0.6µL of PNGase F for overnight at 37°C. The reaction mixture was purified via Amicon 30kDa MWCO centrifugal columns and quantified via 280nm absorbance using a quartz NanoQuant plate (ext. $coeff_{280nm}$ = 210,000 M^{-1} cm^{-1}).

PFO PEGylation with OPSS-PEG_{2000}: 5µg of recombinant PFO (MyBioSource.com) in PBS and 10% glycerol was incubated at 5µM with 10 equivalents of OPSS-PEG_{2000} for ~3 hours at RT. Conjugation was verified with gel electrophoresis and stained for protein with SYPRO Ruby. Activity changes due to conjugation were analyzed with red blood cell assays.

Red Blood Cell Assay: Single-donor human red blood cells were washed two times with PBS, then diluted to 4% v/v in PBS or CBS buffers at pH 7.4 and 5.5, respectively. Samples were serial diluted 1:1 in buffer, then 50µL was mixed 1:1 with RBC's in a v-bottom 96-well plate and incubated at 37°C for 1 hour shaking. The plate was then centrifuged at 500xg for 5 mins at 4°C, and 75µL of supernatant was transferred to a fresh plate and measured on a plate reader at 414nm.

His-tagged LLO Toxin Purification: Listeriolysin O (LLO) was expressed and purified from BL21 E. coli cells as previously described. Briefly, LLO-expressing BL21 cells were cultured in LB + Kan overnight, then subcultured into 300mL LB + Kan to mid-exponential phase (~ OD_{600}=0.5). At that point, cells were induced for LLO expression with 1mM IPTG for 6 hours. Cells were pelleted, re-suspended in lysis buffer (50mM phosphate (pH 8.0), 1M NaCl, 20mM imidazole, 10mM βME), homogenized, and the insoluble material was pelleted at 12Kxg for 30 mins. The soluble portion was purified over a Ni-NTA column and eluted with elution buffer (lysis buffer, pH 6.0) with varying amounts of imidazole (25mM, 50mM, 100mM, 250mM, and 500mM). Fractions verified for purity with gel electrophoresis were dialyzed into storage buffer (elution buffer – imidazole + 1mM EDTA). LLO was quantified via absorbance at 280nm (ext. coeff = 77,407).

LLO "Quik-Change" Site-Directed Mutagenesis: Mutants of LLO with a small number of amino acid changes can be done via "Quik-change" mutagenesis. Primers were designed to target the undecapeptide region of LLO, specifically Tryptophan residues at positions 491 and 492. These residues were changed to Alanine with the following primers:

FWD: GGTTTAGCTTGGGAA**GCGGCG**AGAACGGTAATTGATGACCGGAAC

REV: GTTCCGGTCATCAATTACCGTTCT**CGCCGC**TTCCCAAGCTAAACC

25ng of template LLO DNA was used for two PCR's, one with forward primer and one with reverse primer at a 50µL reaction volume. These strands were amplified with Phusion HF polymerase with standard Phusion thermocycle conditions for 10 cycles. 25µL of each PCR product was mixed together with an additional 0.5µL of

polymerase and run again through the thermocycler for 18 cycles. The PCR product was digested with 1µL DpnI to remove methylated template DNA at 37C for 1 hour. This mixture was cleaned up with Qiagen mini-prep columns and quantified via absorbance at 260/280nm. Final DNA was electroporated into DH5a cells and plated to Kan agar plates. DNA from a single colony was mini-prepped and the product was confirmed with sequencing. LLOmut DNA was then chemically transformed into BL21 cells for protein expression and purification.

Surface PEGylation of LLO: 100µg of LLO was incubated with varying equiv. and lengths of NHS-mPEG at 40µM overnight at RT. Degree of labeling of the unpurified reaction mixture was analyzed via SDS-PAGE. In the cases where LLO is conjugated to a thiol-reactive linker or fluorophore, the LLO was incubated with 20 or 10 equiv. linker or fluorophore, respectively, overnight at RT at 40µM the day after or day before the LLO PEGylation, respectively.

Linker Conjugation to Listeriolysin O (LLO): 100µg of LLO (WT or mut) was incubated at 40µM with 20 equiv. of OPSS-PEG-TCO or OPSS-PEG-MeTzine in phosphate buffer pH 6.0 overnight at RT. The mixture was purified of excess linker via three washes in Amicon 30kD spin columns. The recovered protein was quantified via absorbance at 280nm (and 294nm for MeTzine Linker) for subsequent reaction with antibody.

Flow Cytometry Analysis of Cellular Uptake: To verify uptake of the conjugates to mammalian cells, SKOV3 WT cells were plated at 25K cells per well 2 days prior to the assay. Varying concentrations of Ab-LLO-AF488 conjugates LLO were incubated on cells in full serum media for 1.5 hours at 37°C with 5% CO_2. Cells were washed

with PBS, trypsinized, quenched with media, pelleted, and resuspended in 400μL PBS for FACS analysis. Mean fluorescence values of histograms were plotted as a function of concentration to determine binding affinity.

CHAPTER 5 – ANTIBODY CONJUGATES FOR DUAL-DELIVERY

Background

Antibody bioconjugates have emerged as an efficient modality for targeted delivery of siRNA. Antibodies can efficiently bind and internalize via a specific surface antigen on a target cell and bring with it an siRNA cargo. Following endocytosis though, the antibody and its cargo are either degraded by intracellular enzymes or recycled back to the surface before it can be utilized by RISC for gene knockdown. Inefficient cytosolic localization of delivered siRNA continues to be a key challenge in RNAi therapeutic development[50]. Some antibody conjugates fused to protamine or other nucleic-acid binding peptides have shown efficacy in eliciting knockdown in target cells,[161-163,168] but were difficult to manufacture into drugs.[153] Other covalently conjugated antibody-siRNA conjugates also showed very limited knockdown and no obvious dependence on endocytosis pathway.[165] Thus, the correlation between internalization pathway and endosomal escape agent efficacy still remains largely unknown.

One unique strategy to incorporate and evaluate endosomal escape agents in bioconjugate vehicles is through a dual-delivery strategy, in which the endosomal escape agent and the siRNA are conjugated to two carriers and co-delivered. Both vehicles internalize into a target cell, co-localize, and the escape agent facilitates the release of the cargo into the cytosolic space. This method decouples the escape agent and the therapeutic cargo, thus enabling manipulation of the delivery ratio and avoiding the chemical complexity of combining both cargo into a single conjugate. There are two prime examples of this method in the literature, the first of which are Dynamic Polyconjugates (DPCs).

DPCs were introduced by Rozema *et. al*[68,69,194] and consists of multiple components for targeted delivery. The backbone of the DPC is a butyl and amino vinyl ether (PBAVE) endosomolytic polymer to facilitate the endosomal release of the siRNA cargo. This polymer is masked using an acid-labile carboxy dimethyl maleic anhydride (CDM)[195] functionalized PEG and N-acetylgalactosamine (GalNAc) ligand, which targets the asialoglycoprotein receptor (ASGPR) on hepatocytes. In later iterations, the masked polymer was co-delivered with a cholesterol-conjugated siRNA for efficient knockdown of apolipoprotein-B (apoB) in non-human primates.[70] The co-delivery method was 500-fold more efficacious than the cholesterol-siRNA alone and proved the co-delivery system as a viable strategy.

A similar co-delivery strategy was evaluated by the Wittrup group with two conjugates targeting carcinoembryonic antigen (CEA) and epidermal growth factor receptor (EGFR) for delivery of a protein toxin[71-73] and siRNA[78]. They developed a bispecific, neutralizing antibody directed to EGFR and Perfringolysin O and co-delivered a CEA-targeted gelonin toxin. They saw an increase in efficacy in the co-delivery system over the CEA-targeted gelonin alone. In later studies, they co-delivered an siRNA-binding protein targeted to a different epitope of EGFR for maximum co-localization and saw subsequent siRNA-mediated knockdown. With inspiration from these works, we sought to develop a similar co-delivery strategy to screen agents that facilitate endosomal escape across a range of cellular targets.

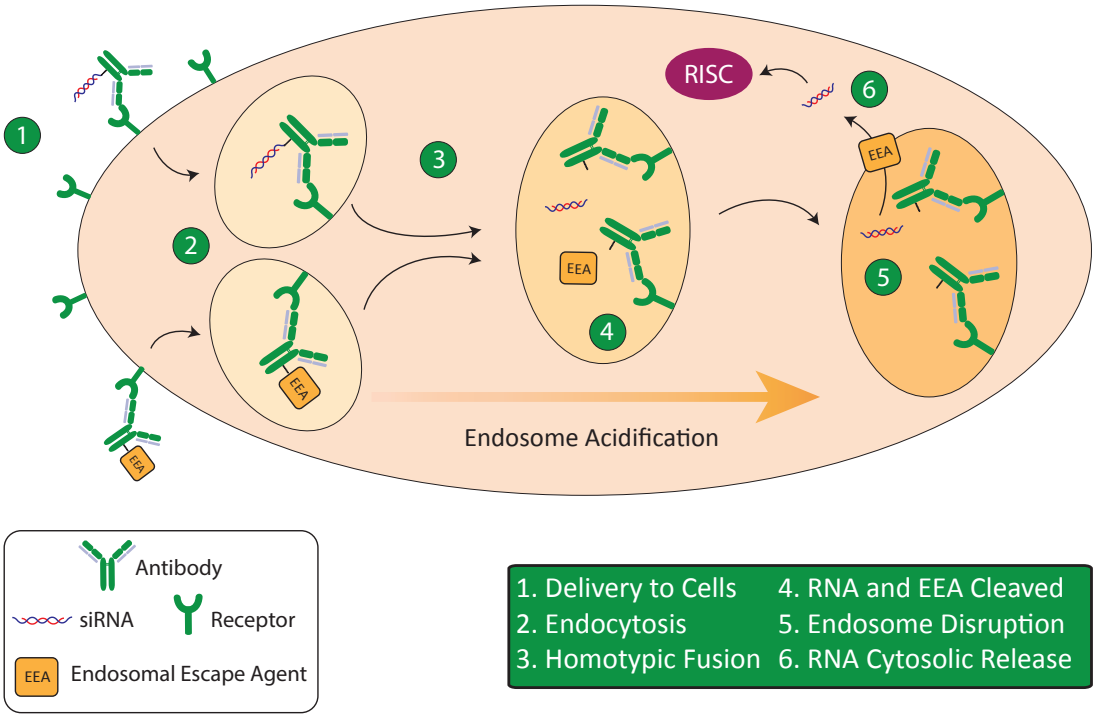

Figure 5.1 Schematic of Proposed Antibody Dual-Conjugate Delivery System – Antibodies carrying siRNA and an endosomal escape agent (EEA) are co-delivered to a target cell for intracellular co-localization and endosomal escape. (1) Antibody conjugates bind to their corresponding receptor on the surface of a target cell (2) Antibody conjugates are internalized via endocytosis (3) Early endosomes fuse, co-localizing both conjugates to the same intracellular compartment (4) siRNA and EEA cargo are cleaved from their antibody carrier via an endosomal cue (5) EEA induces pore formation and facilitates release of siRNA into the cytosol (6) siRNA binding to RISC complex, triggering target gene knockdown.

We began developing a modular dual-delivery strategy using antibody (Ab) conjugates (Figure 5.1). Cellular internalization of these conjugates is dictated solely by the antibody, while endosomal escape is attained with an endosomal escape agent (EAA). Two bioconjugates, an antibody-siRNA and antibody-EEA, were prepared using the same antibody to ensure compartmental co-localization[196,197] within the cell, then co-delivered to initiate RNAi. Decoupling internalization from escape enables us to screen EEAs that disrupt membranes for cytosolic translocation of siRNA independently of its endocytic pathway. The modularity of this system then allows us

to then explore the effect of entry pathway on gene silencing by substituting the targeting antibody. This approach could then be used as a platform to elucidate structure-activity relationships of potent EEAs and effects of entry pathway on the efficient delivery of siRNAs. In this chapter, we discuss the effort of testing the efficacy the antibody-siRNA and antibody-EEA conjugates developed in chapters 3 and 4 in a co-delivery system.

Results

Homotypic Fusion and Co-localization of Antibody Conjugates: Antibody conjugate co-delivery system hinges on the co-compartmentalization of the both conjugates in a single endosome following endocytosis. To verify that homotypic fusion occurs with the same type of antibodies carrying two different cargos, we examined co-localization of a green fluorescently labeled TfRAb-dsDNA-AF488 conjugate with a red fluorescently labeled TfRAb-AF647 conjugate (Figure 5.2A). We proposed that because the antibodies target the same receptor, their endosomes should fuse in the early endosomal pathway. To observe the fusion of endosomes, we looked for co-localization of the green signal (from the DNA conjugate) and the red signal (from the AF647 conjugate) to give a yellow, overlaid spot (Figure 5.2B). The overlay of these in punctate spots and quantification via Fiji Coloc2 plug-in showed that the two conjugates co-localized with 59% efficiency and verified that the dual-delivery method is viable.

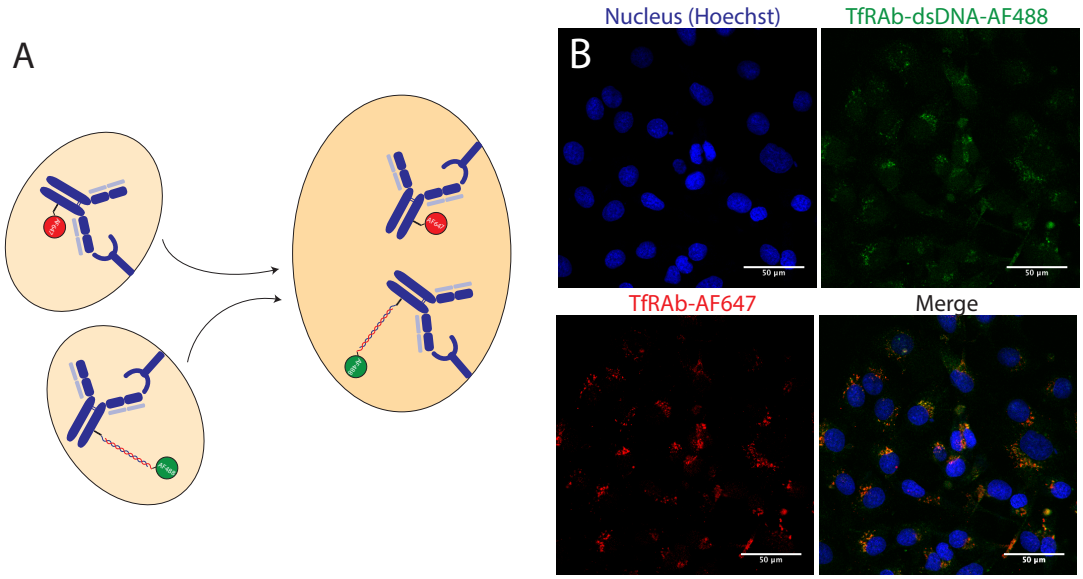

Figure 5.2 Early Endosomal Fusion and Co-localization of TfR Antibody Conjugates – Antibodies carrying two different cargo and targeting the same surface receptor co-localized to the same endosomal compartment. (a) Schematic of homotypic fusion of endosomes carrying green-labeled TfRAb-dsDNA conjugates and red-labeled TfRAb conjugates. (b) Confocal microscopy images of TfRAb co-localization into HeLa cells. From left to right: nuclei (blue), TfRAb-dsDNA-AF488 conjugates (green), TfRAb-AF647 (red), and merged images. Yellow spots are indicative of co-localized endosomes.

Melittin-siRNA Conjugate Delivery: We began our studies with an untargeted system in which we complexed Melittin directly with siRNA and delivered it to cells. Melittin has previously been shown to penetrate cell membranes and localize siRNA to the cytosol, and therefore is a good positive control for our experiments. The siRNA and Melittin were complexed at different concentrations and ratios, added to Luc2-expressing SKOV3 cells, and examined for knockdown efficiency of luciferase (Figure 5.3). We found that the amount of Melittin in the complex had a greater impact than the amount of siRNA, as samples with 2 μM Melittin had the same level of knockdown with either 50 nM or 100 nM siRNA. Similarly, complexes with 500 nM Melittin had the same level of knockdown with either 50 nM or 100 nM siRNA, and less knockdown than the 2 μM Melittin counterpart. With this data, we knew that

Melittin was an effective agent for membrane translocation and could move forward in making protein conjugates to decouple the action of cellular uptake and endosomal escape.

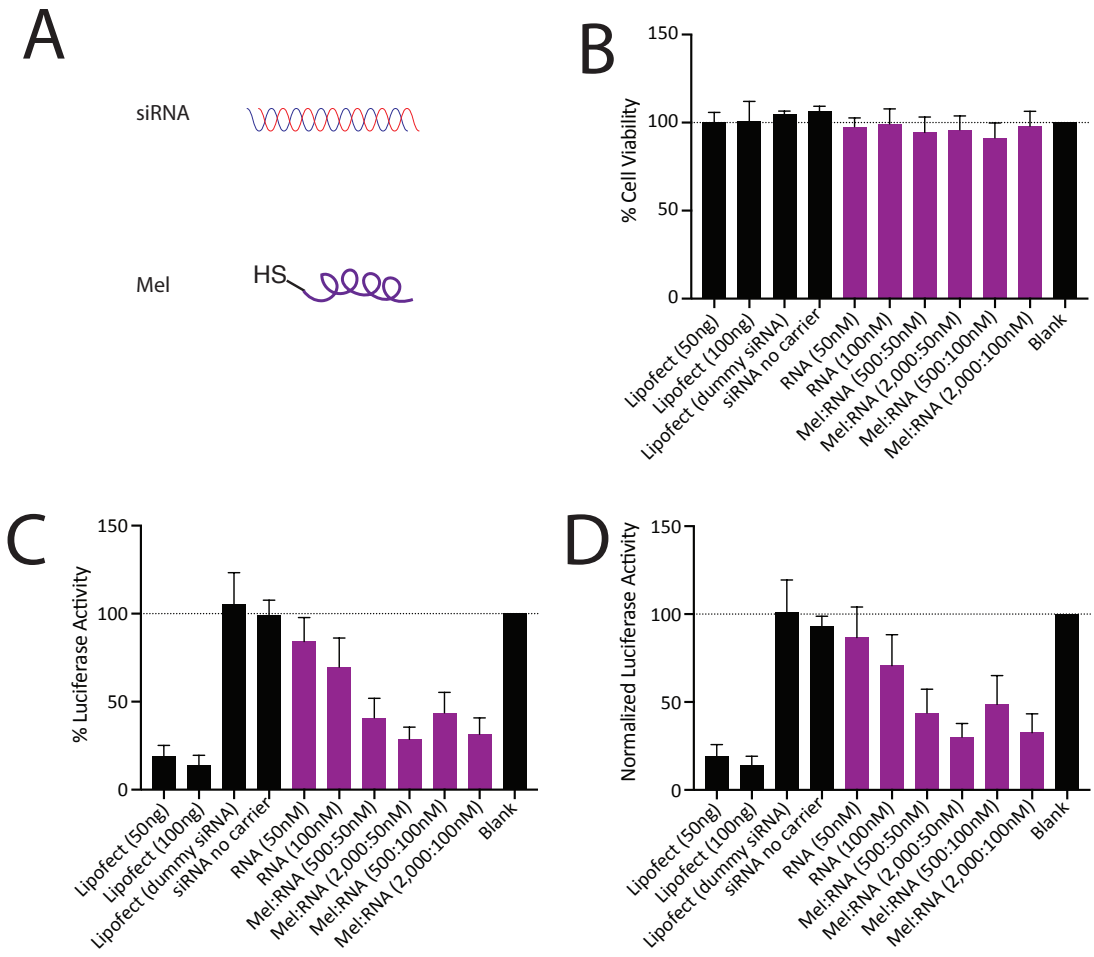

Figure 5.3 Melittin-siRNA complexation for Luciferase Knockdown – Melittin and Luc2-targeted siRNA were complexed and delivered to SKOV3-Luc2 cells and analyzed for knockdown. (a) Melittin and siRNA components (b) Cell viability of treated cells (c) Luciferase expression of treated cells (d) Luciferase Expression normalized to cell viability.

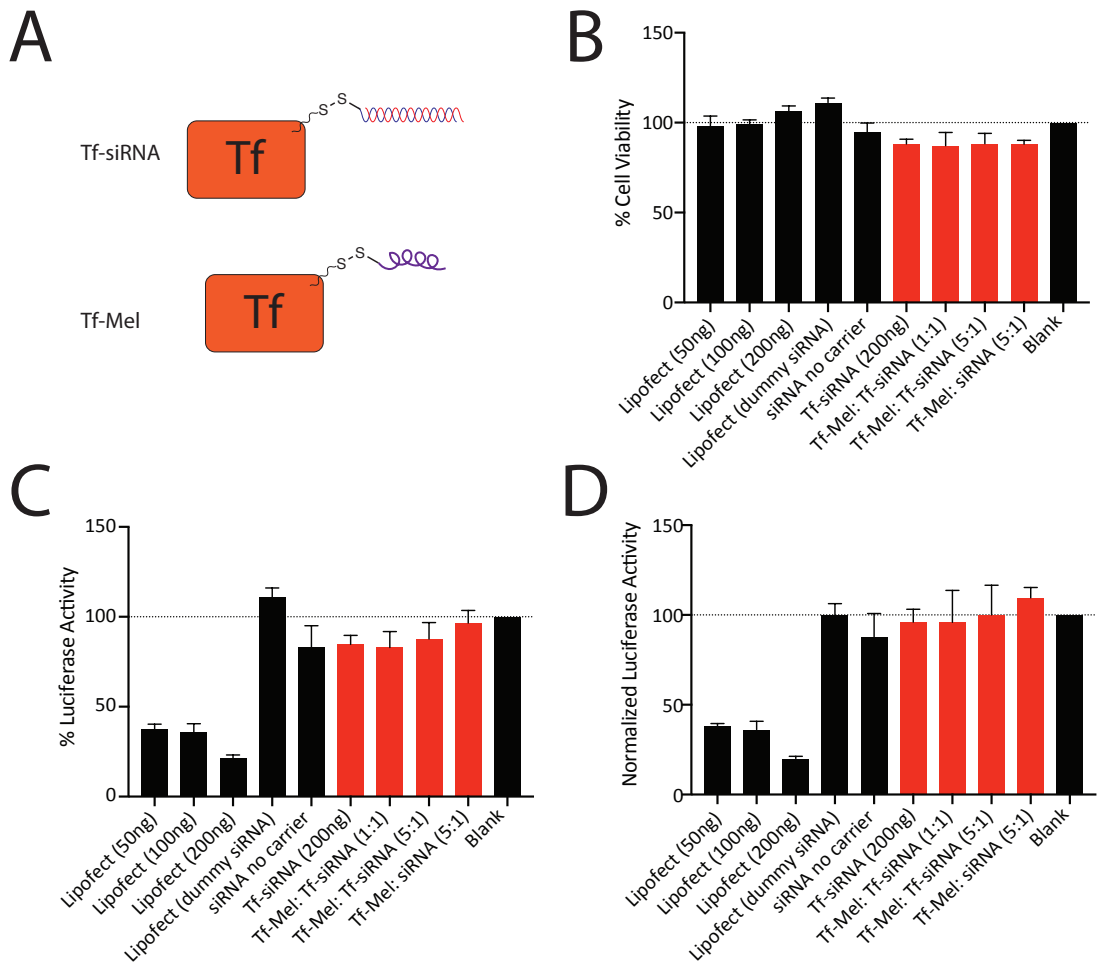

Figure 5.4 Transferrin (Tf)-siRNA and Tf-Melittin Conjugate Co-Delivery – Transferrin conjugates carrying siRNA and Melittin co-delivered to SKOV3-Luc2 cells. Black bars are controls and orange bars are Transferrin conjugate treated cases. (a) Schematic of Tf conjugates carrying siRNA and Melittin, each with a reducible disulfide linker. (b) Cell viability of treated cells (c) Luciferase expression of treated cells (d) Luciferase Expression normalized to cell viability.

Transferrin Conjugate Delivery: In chapter 3 and 4, we generated Transferrin conjugates carrying either siRNA or Melittin and co-delivered them to SKOV3-Luc2 cells (Figure 5.4). We co-delivered the two conjugates carrying 200ng of siRNA per well with 1:1 and 5:1 molar ratios of Melittin:siRNA to see if the Melittin conjugate was able to facilitate endosomal escape of the siRNA conjugate. As anticipated, the siRNA conjugate alone elicited no knockdown, but neither did the co-delivery with the

Melittin conjugate at any condition. This was either an indication that the Melittin is not effective in this format, or perhaps the uptake levels or endocytic pathway of these conjugates were not sufficient. Thus, we moved forward with the antibody-based bioconjugates.

Antibody Conjugate Delivery with Chloroquine: After successfully generating antibody-siRNA conjugates on antibodies targeting TfR, CD63, Her2, and Tubulin (negative control), we screened their efficiency when delivered with a known lysosomotropic agent, chloroquine (CQ) (Figure 5.5 and 5.6). CQ is thought to induce endosomal escape by the "proton-sponge effect" in which the tertiary amine in the structure absorbs protons as the endosome acidifies, inducing an influx of protons and a disruption of osmotic pressure of the endosome and leakage in the membrane. We dosed all the Ab-siRNA conjugates at 100nM with 100 or 150μM of CQ. In all antibodies, there was no detectable knockdown observed with or without CQ. Interestingly though, we did discover in this study that knockdown could be observed when the Ab-siRNA was complexed with Lipofectamine. This was observed with and without a cleavable linker for the siRNA (data not shown), indicating that the lipofectamine works independently of what the siRNA is attached to, and the siRNA can still be effectively loaded into RISC.

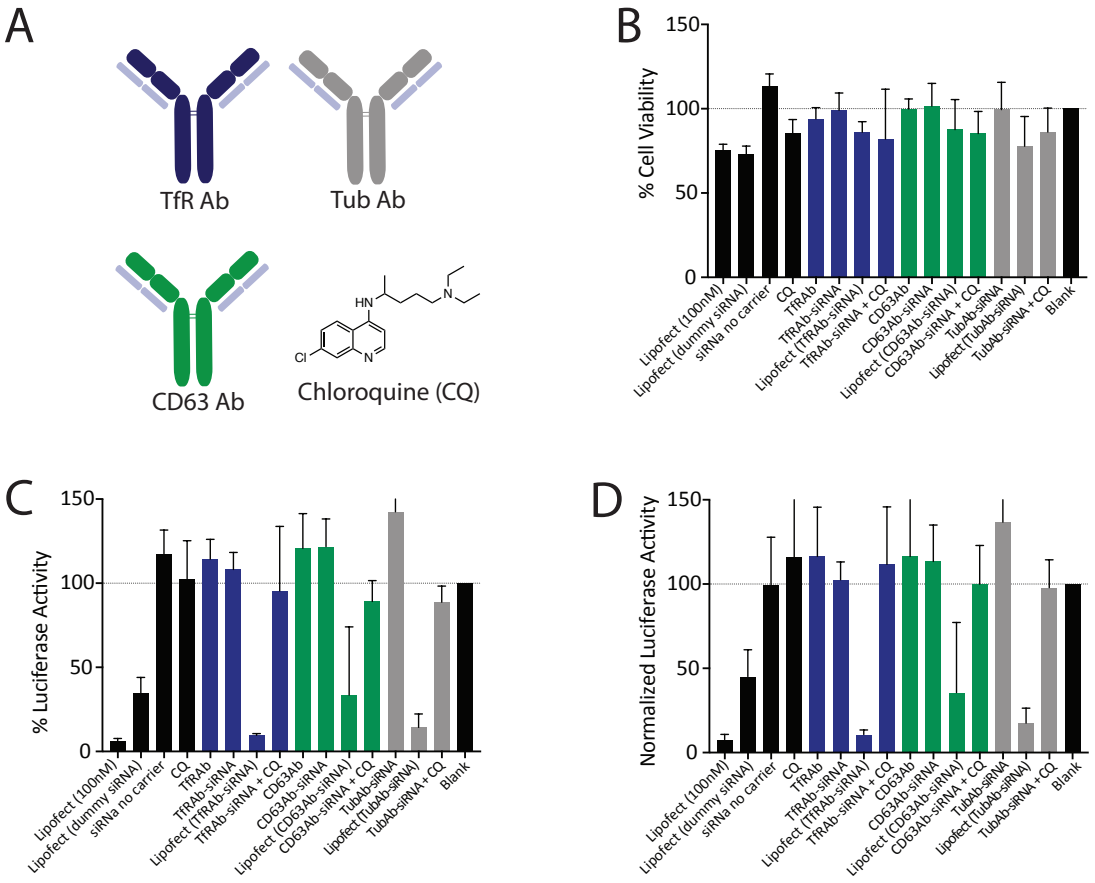

Figure 5.5 Antibody-siRNA Conjugate Delivery with Chloroquine Treatment – Antibody conjugates targeting TfR, CD63, and Tubulin Control (dosed at 100nM Ab and ~100-200nM siRNA) for knockdown in SKOV3-Luc2 cells. Chloroquine was added at 100μM as a small molecule endosomal escape agent. Black bars are controls, blue bars are TfRAb treated, green bars are CD63Ab treated, and gray bars are Tubulin Ab treated. Conjugates were either treated alone, encapsulated in lipofectamine, or co-treated with 100μM CQ. (a) Schematic of antibodies with color designation (left) and chemical structure of chloroquine (CQ) endosomal escape agent. (b) Cell viability of treated cells (c) Luciferase expression of treated cells (d) Luciferase Expression normalized to cell viability.

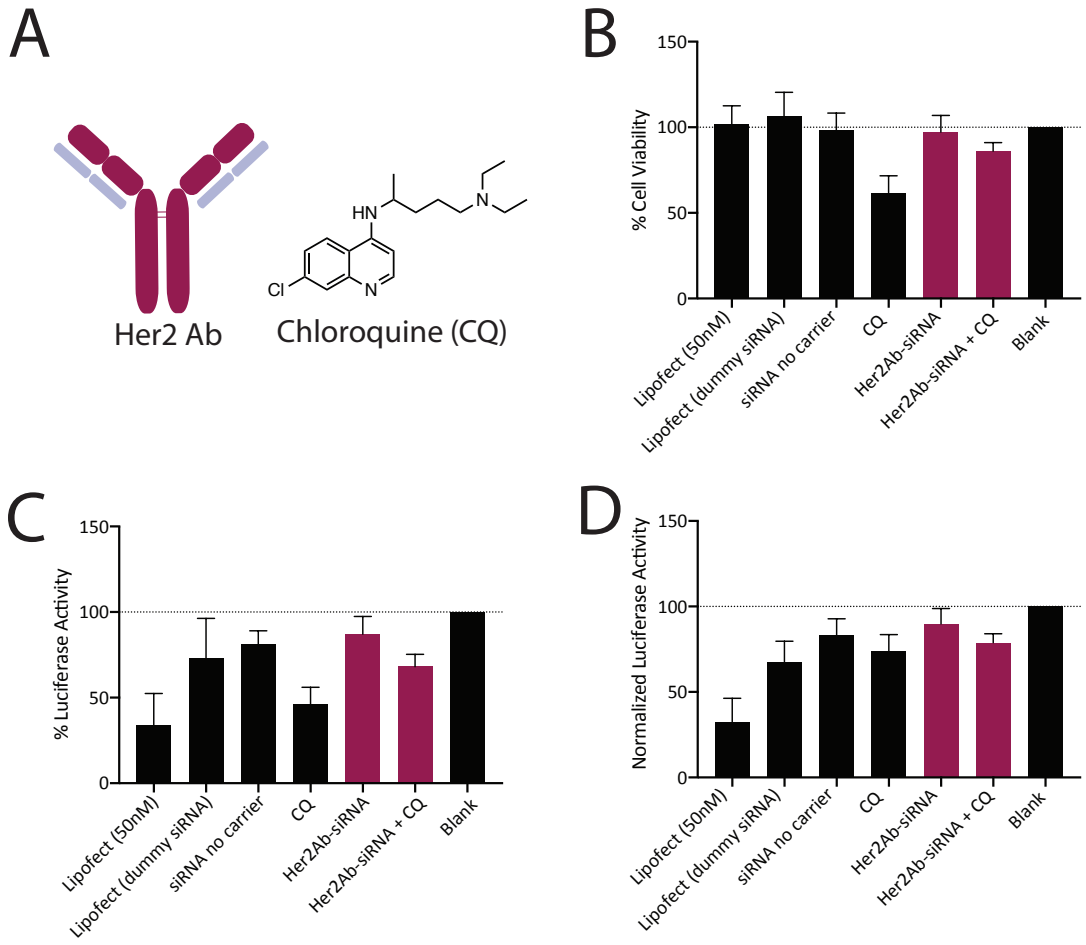

Figure 5.6 Her2Ab-siRNA Conjugate Delivery with Chloroquine Treatment – Antibody conjugates dosed at 100nM antibody (100-200nM siRNA) targeting the Her2 receptor on SKOV3-Luc2 cells, co-treated with small molecule endosomal escape agent, chloroquine (CQ), at 150μM. Chloroquine showed some toxicity but no detectable increase in knockdown relative to the controls. (a) Schematic of antibodies with color designation (left) and chemical structure of chloroquine (CQ) endosomal escape agent. (b) Cell viability of treated cells (c) Luciferase expression of treated cells (d) Luciferase Expression normalized to cell viability.

Antibody-LLO Conjugate Delivery: We attempted the co-delivery strategy again with a more potent endosomal escape agent, Listeriolysin O (LLO). As discussed in chapter 4, we discovered that the WT toxin was alone very toxic to mammalian cells, and had to mutate the 4th domain to be able to dose at the proper concentrations. We conjugated this mutant to the CD63Ab for co-delivery with the CD63Ab-siRNA conjugate. In this study, we looked at the effect of simultaneous addition (Figure 5.7A

and B) and sequential addition of conjugate (Figure 5.7C and D), as there was a concern that because the conjugates target the same receptor, they could be out-competing each other for uptake. We also looked at varying dosing ratios and total concentrations. In all cases, though we did not observe any apparent toxicity, there was no observed knockdown either. As we learned in chapter 4, this could be due to the membrane binding of the LLOmut being greater than that of the antibody. With that information, we decided to tag the LLOmut directly with siRNA and deliver it to cells.

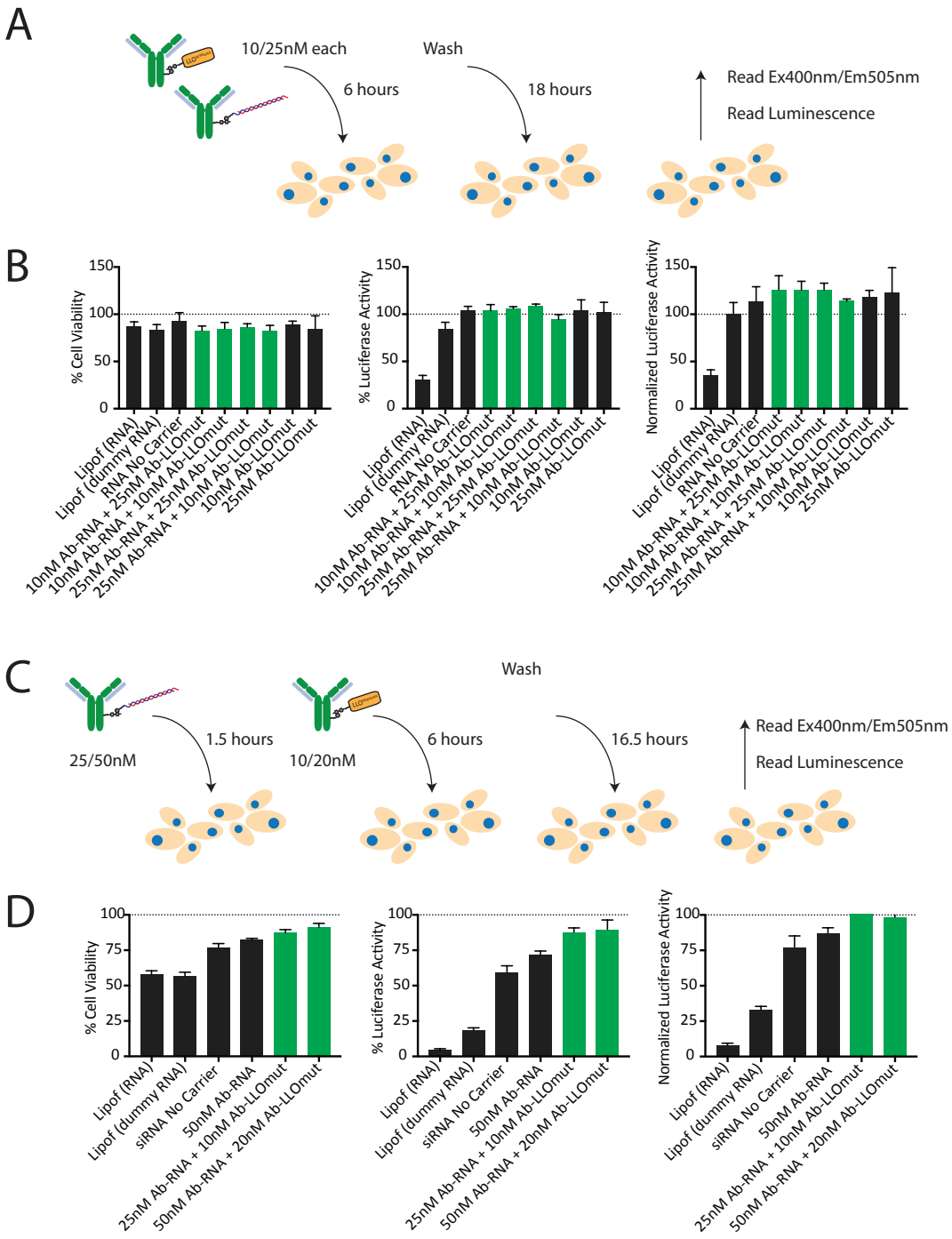

Figure 5.7 CD63Ab-siRNA and LLOmut Conjugate Co-Delivery: Simultaneous and Sequential Addition – Antibody conjugates targeting the CD63 receptor carrying siRNA and mutant LLO (non-PEGylated) delivered either simultaneously (top) or sequentially (bottom). (a) Schematic of simultaneous delivery of CD63Ab-siRNA and CD63Ab-LLOmut conjugates with varying concentration ratios. Cells were treated for 6 hours with conjugates, washed, then analyzed for luciferase activity. (b) (left to

right) Cell viability of treated cells, luciferase expression of treated cells, luciferase Expression normalized to cell viability. Black bars are controls and green are treated samples. (c) Schematic of sequential delivery of CD63Ab-siRNA conjugate for 1.5 hours, followed by CD63Ab-LLOmut conjugates with varying concentration ratios. Cells were treated for another 6 hours with conjugates, washed, then analyzed for luciferase activity. (d) (left to right) Cell viability of treated cells, luciferase expression of treated cells, luciferase Expression normalized to cell viability. Black bars are controls and green are treated samples.

LLO Conjugate Delivery: After conjugating the targeting siRNA with mutant LLO on its 4th domain cysteine, we examined knockdown via direct translocation of the LLOmut across the membrane (Figure 5.8). Again, there was no observed toxicity of the conjugate to mammalian cells, but there was no observed knockdown either. With this data, we concluded that the LLOmut either is not potent enough to translocate the membrane with siRNA or remains stuck to the surface of the cell and does not actually get internalized. With this, we postulated that there were several factors beyond those considered that could be impacting the delivery. Therefore, we moved forward with dosing a single conjugate complexed with an endosomal membrane disruptor.

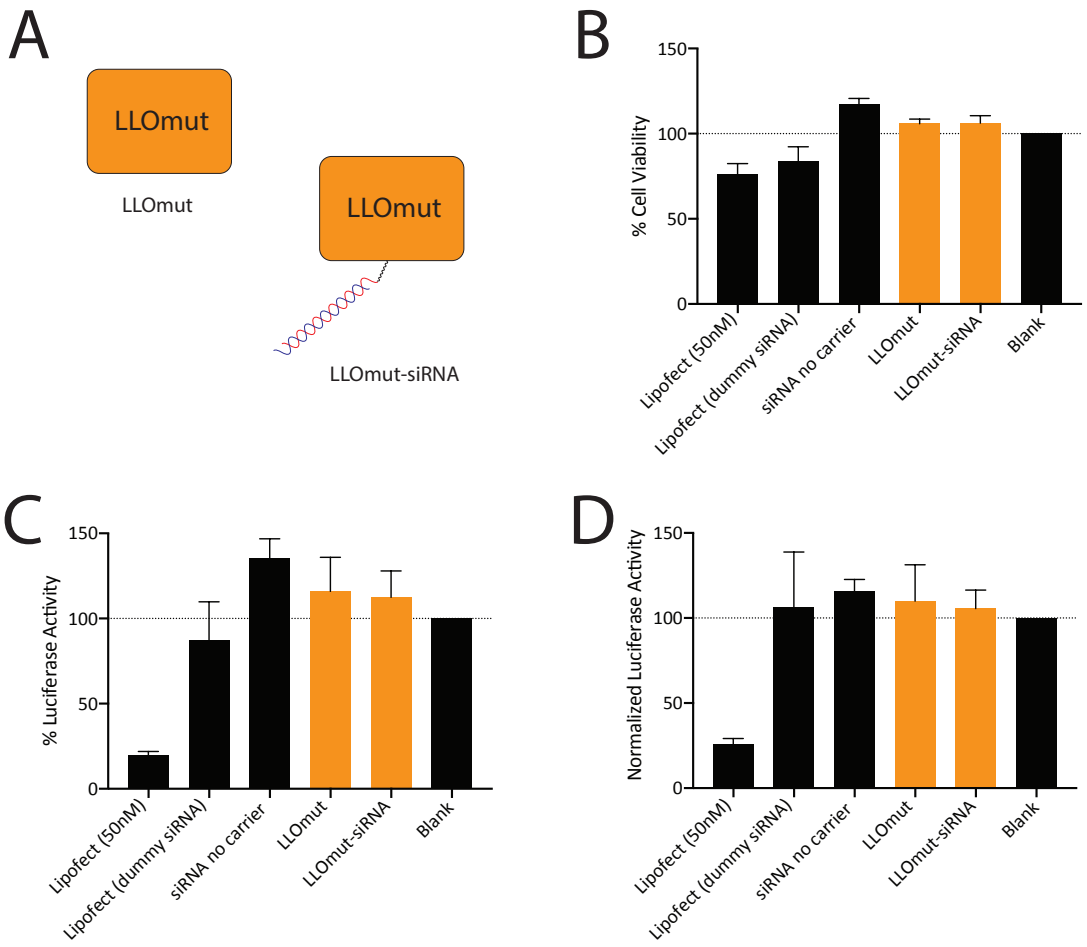

Figure 5.8 Conjugated LLOmut-siRNA Delivery – LLOmut conjugated directly with siRNA via 4th domain cysteine for non-targeted delivery to cells. Black bars are controls and yellow bars are treated samples (a) Schematic of LLOmut control and conjugated LLOmut-siRNA. (b) Cell viability of treated cells (c) Luciferase expression of treated cells (d) Luciferase Expression normalized to cell viability.

Ab-R9K Conjugate Delivery: Previous studies in siRNA conjugates have shown efficacy with antibodies complexed with siRNA via nucleic acid-binding proteins and peptides like polyamines and polyarginines. In this case, we looked at Her2Ab conjugates complexing siRNA with R9K, a known cell-penetrating peptide (CPP). We looked at these conjugates in two ways, by either conjugating siRNA directly to the antibody and complexing R9K, or directly conjugating R9K or complexing siRNA (Figure 5.9). Again, we examined multiple ratios and looked at their knockdown efficiency. Similar to other assays, there was no observed knockdown for any case.

This assay showed an abnormally high luciferase signal, indicating that the R9K could also be interfering with the assay kit. Future studies could parse out why the luciferase signal was high and analyze greater ratios of R9K and siRNA to see charge effects on the delivery efficiency.

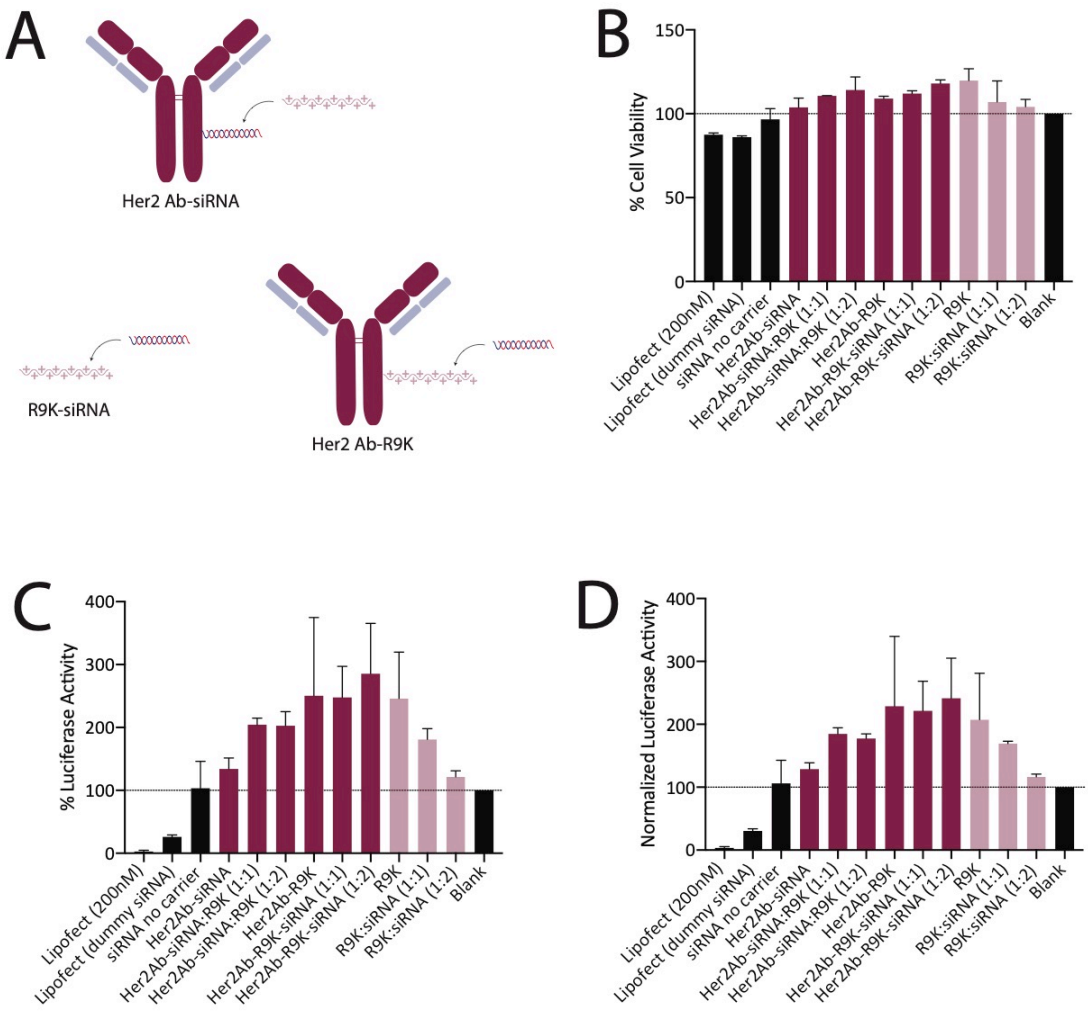

Figure 5.9 Her2Ab-R9K-siRNA Non-covalent conjugate delivery – Her2Ab conjugates covalently conjugated with R9K or siRNA, and complexed with siRNA or R9K, respectively. Dark pink bars show antibody conjugates, light pink bars show R9K-siRNA complexes, and black bars are controls. (a) Schematic of Ab conjugates and siRNA-R9K complexes (b) Cell viability of treated cells (c) Luciferase expression of treated cells (d) Luciferase Expression normalized to cell viability.

Discussion

In this chapter, we examined varying endocytic pathways, endosomal escape agents, and conjugation methods to co-deliver and study each components effect on knockdown efficiency. Unfortunately, we were not able to observe knockdown with any of the agents tried, but it did give us some insight into effective strategies for future studies.

We determined early on that potency of endosomal escape agents was not the most important factor in effectively delivering siRNA. When siRNA was directly complexed with Melittin, which has HC_{50} values in the low μM range, efficient knockdown was observed with only 50-100nM siRNA. However, with the LLOmut, with HC_{50} values in the high nanomolar range, was conjugated with siRNA, no knockdown was observed. This could be due to the membrane interaction of each membrane disruption agent, as the Melittin polyplex has a strong cationic charge and is likely taken up by macropinocytosis followed by endosomal escape, whereas the LLOmut conjugate binds cholesterol on the cell surface and forms a membrane bound pore. Additionally, more potent agents like LLO run into issues with outer membrane disruption because the agent is more potent than the dosing concentration of the antibody conjugate. More effective strategies for reversibly blocking the membrane interactions of the pore-forming toxins for those to be effectively incorporated into antibody conjugates.

I believe there is promise in the final complexation method that used the cationic R9K peptide with siRNA on an antibody conjugate. Putting both components on a single conjugate ensures that they are in the same intracellular compartment, and the ratio can be controlled with the complexation ratios. In future studies, this strategy could be

used with other cationic peptides and polymers with varying net charge to look at their endosomal escape efficacies. These conjugates could then be generated against different antibodies to look at their efficacy across different endocytic pathways. Later, dual-labeled conjugates with non-complexed endosomal escape agents could be developed using dual-labeling strategies to be discussed in chapter 6.

Materials & Methods

Homotypic Fusion Confocal Microscopy: To observe intracellular co-localization of co-delivered conjugates, SKOV3 cells were plated to ~75% confluency on MatTek 35mm glass-bottom dishes 24 hours prior to incubation. The cells were incubated with green-fluorescent TfRAb-dsDNA-AF488 and red-fluorescent TfRAb-AF647 conjugates at 50nM for 1 hour at 37°C in 5% CO_2. Following incubation, cells were washed with PBS, fixed with 4% paraformaldehyde, stained with Hoechst nuclear stain, and stored in PBS at 4°C prior to imaging. Dishes were imaged on a Zeiss LSM880 inverted confocal microscope with 405nm, 488nm, and 633nm lasers. Gain was determined based on an untreated cell control. Degree of co-localization was determined from the Coloc-2 plug-in in Fiji of red and green channels.

Knockdown Assay conditions: All knockdown assays used the following conditions unless stated otherwise. 15K SKOV3-Luc2 cells were plated in white Nunclon Delta coated flat bottom 96-well plates (ThermoFisher) 24 hours prior to the assay. Cells were treated with lipofectamine controls at a ratio of 75µL Lipofectamine per nmole of target siRNA (Sense strand: rGrGrA mCrGrA rGrGrA mCrGrA rGmCrA mCmUmU rCT*T; Antisense strand: rGrArA rGrUrG rCrUrC rGrUrC rCrUrC rGrUrC rCT*T) or dummy siRNA (Sense strand: rArArC rGrCrU rGrGrG rCrGrU rUrArA rUrCrA rAdTdT; Antisense strand: rUrUrG rArUrU rArArC rGrCrC rCrArG

rCrGrU rUdTdT) complexed at a 1:1 molar ratio. After 48 hours, cells were washed with PBS and replaced with 100µL fresh media (DMEM; high glucose, L-glutamine, No Phenol red, 10% FBS) and analyzed with the Promega ONE-GLO/Tox Luciferase Assay Kit. Fluorescence (cell viability) and luminescence (luciferase activity) signals were normalized to untreated controls. "Normalized Luciferase Activity" signals were luminescence signal normalized by cell count (i.e. fluorescence signal), then normalized to an untreated control.

Melittin-siRNA Complexation: For Melittin-siRNA complex delivery, 500nM or 1µM of double-stranded siRNA was complexed with 5µM or 20µM Melittin-SH in OPTI-MEM for 20 mins at RT. The solution was then diluted 1:10 into 100µL of DMEM + 10% FBS on SKOV3-Luc2 cells and incubated for 1 hour at 37°C. Cells were then washed with PBS and replaced with fresh DMEM for the remaining 47 hours.

Transferrin-Melittin Conjugates: For Transferrin (Tf) conjugate co-delivery, 200ng of double-stranded siRNA either conjugated to iron-loaded Tf or free in solution was incubated with 0, 1, or 5 molar equivalencies of Tf-Melittin conjugate in 100µL. The sample were incubated for 48 hours, replaced with fresh DMEM, and analyzed via Luc/Tox Luciferase Assay.

Antibody Conjugates + Chloroquine: For co-delivery of CatB cleavable Ab-siRNA conjugates with the lysosomotropic agent, Chloroquine (CQ), 100nM of conjugate was incubated with either 100µM CQ (TfRAb, CD63Ab, and TubAb), or 150µM (Her2Ab) for 24 hours at 37°C. The samples were then replaced with fresh DMEM and incubated for the remaining 24 hours at 37°C before analyzing via Luc/Tox Luciferase Assay.

CD63Ab-siRNA and CD63Ab-LLOmut Conjugate Dual Delivery: For co-delivery of CD63Ab-siRNA (CatB-cleavable) and CD63Ab-LLOmut (reducible) conjugates to HeLa-Luc2 cells, experimental conditions were examined with simultaneous or

sequential addition of the two conjugates. For simultaneous addition, either 10nM or 25nM of CD63Ab-siRNA and 10nM or 25nM of CD63Ab-LLOmut were incubated simultaneously for 6 hours at 37°C, washed with PBS, and replaced with fresh media and incubated at 37°C for the remaining 18 hours. For the sequential addition, either 25nM or 50nM of CD63Ab-siRNA was incubated for 1.5 hours at 37°C, followed by 10nM or 20nM CD63Ab-LLOmut for 6 hours at 37°C. The cells were then washed with PBS, replaced with fresh media, and incubated at 37°C for the remaining 16.5 hours.

LLOmut-siRNA Conjugates: For delivery of LLOmut-siRNA conjugates with no antibody carrier, 50nM of siRNA, LLOmut, or the conjugate were added to HeLa-Luc2 cells for 16 hours at 37°C, washed with PBS, replaced with fresh media, and incubated at 37°C for the remaining 8 hours.

Her2Ab-R9K Conjugates: For delivery of Her2Ab conjugates with R9K complexation with siRNA, antibodies were either conjugated with siRNA and complexed with R9K, or vice versa, at ratios of 1:1 or 1:2 at RT for 1 hour prior to assay. Then, 200nM of conjugate (based on protein) was incubated on cells at 37°C for 16 hours. Cells were washed with PBS, replaced with fresh media, and incubated at 37°C for the remaining 34 hours.

CHAPTER 6 – DUAL-LABELED ANTIBODY DRUG CONJUGATES FOR ORTHOGONAL CARGO RELEASE

Background

Antibody drug conjugates (ADCs) have emerged as a promising modality for the targeted delivery of drugs due to the powerful combination of antibody specificity and potency of certain chemotherapeutics and antibiotics. However, ADC aggregation due to non-specific conjugation and premature drug release remain key challenges in ADC development. Early generation ADCs therapeutic warheads were conjugated non-specifically to lysine residues on the surface of therapeutically relevant antibodies, which led to heterogeneous ADCs with a high propensity for aggregation, low tolerability, and ultimately poor efficacy.[14] This poor efficacy is further exacerbated by drug deconjugation in serum due to non-specific linker degradation.[109] To mitigate these issues, there has been a push for site-specific conjugation methods[9,15,17] that can generate homogeneous antibody bioconjugates (ABCs) with improved affinity, target receptor internalization, and reduced aggregation.

Methods for site-specific antibody conjugation[9] include maleimide conjugation to native cysteines in the hinge region of IgG1's,[198,199] C-terminal selenocysteines,[200] N-terminal serine oxidation and ligation,[201] ligation to Fab nucleotide binding sites,[202] glycan remodeling and glycoconjugation,[203-209] cystine re-bridging,[210-212] and engineering additional cysteines[14,109-111] or other reactive non-natural amino acids[18,112,113] into the constant region domains. Since codon optimization for efficient incorporation of non-natural amino acids can be difficult, peptide tags using natural amino acids have also been incorporated for chemoenzymatic ligation. Chemoenzymatic ligation involves the conjugation of a chemical substrate via an enzyme to a specific amino acid tag incorporated internally or terminally to the protein. Site-specific enzymatic conjugation strategies include microbial

transglutaminase (mTG),[13,14,23,115,116] butelase 1,[213] sortase A,[213,214] and formylglycine-generated enzyme (FGE).[25] New methods for site-specific conjugation to antibodies remain an active area of research.

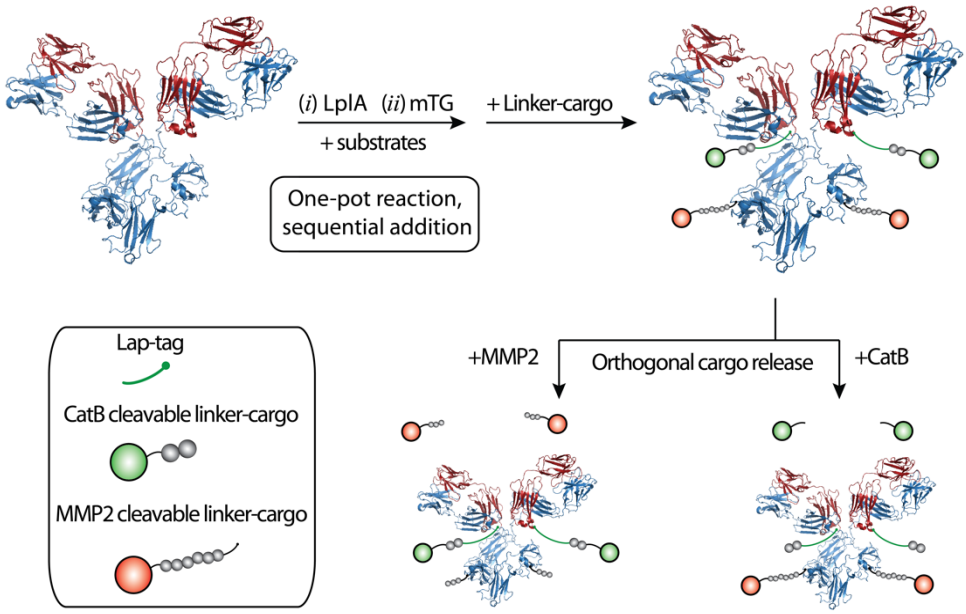

Figure 6.1 Schematic for Dual-Labeled Antibody Conjugates and Orthogonal Cleavage - The one-pot reaction of a dual site-specific assembly of an antibody bioconjugate possessing two cargo units that can be orthogonally released in response to specific enzyme triggers

In light of multi-drug resistant (MDR) cancers and antibacterial drug resistance, combination therapies have also become increasingly necessary to improve therapeutic outcomes[215]. Several groups have created dual-labeled[216] ADCs via multifunctional linkers or multiple conjugation sites for this purpose. For example, Seattle Genetics developed dual-labeled ADC's with two complementary tubulin inhibitors, MMAE and MMAF,[217] and showed significantly increased efficacy in a Hodgkin's lymphoma model. The single glycan in the heavy chain of antibodies has also been utilized for dual radiolabeling of antibodies[26] as well as incorporation of a radio-label and chemotherapeutic drug.[218] Additionally, other methods have utilized orthogonal enzymatic tags at multiple sites along the antibody, such as with multiple mTG-active

sites,[219] butelase A and sortase A,[213] and CLIP and SNAP tags.[220] We[221] and others[222,223] have incorporated multifunctional crosslinkers at a single site on proteins for examining intracellular conjugate processing. However, none of the conjugates in these examples incorporate orthogonal enzyme-triggered temporal control, in which one cargo needs to be released first to achieve a cooperative effect with the second.[215] By integrating orthogonal cleavage sites into site-specific dual-labeled antibodies, we can generate ABCs that can achieve programmable sequential controlled release.

In this work, we report the first example of a site-specific Lipoate-acid ligase A (LplA)-mediated ligation to an antibody via incorporation of a LplA acceptor peptide (LAP)-tag (GFEID**K**VWYDLDA) into the heavy and light chain of a humanized antiHer2 antibody, Trastuzumab. Furthermore, we demonstrate temporal control by designing site-specific dual-labeled antibody conjugates with controlled release properties via two orthogonal enzymatic cues (Figure 6.1). To do this, we utilized the mTG enzyme, along with LplA in a one-pot reaction to demonstrate attachment and release of two cargos at to two different sites on Trastuzumab via orthogonally cleavable bonds. This is shown with two fluorescent linkers, one cleavable by an extracellular protease, Matrix Metalloproteinase-2 (MMP-2), and the other cleavable by an intracellular protease, Cathepsin B (CatB). Following treatment with MMP-2 and CatB, we demonstrated orthogonal cargo release with either MMP-2 or CatB (Figure 6.1). This dual-labeled antibody platform will allow for sequential drug release from a single conjugate for cooperative drug combinations.

Results

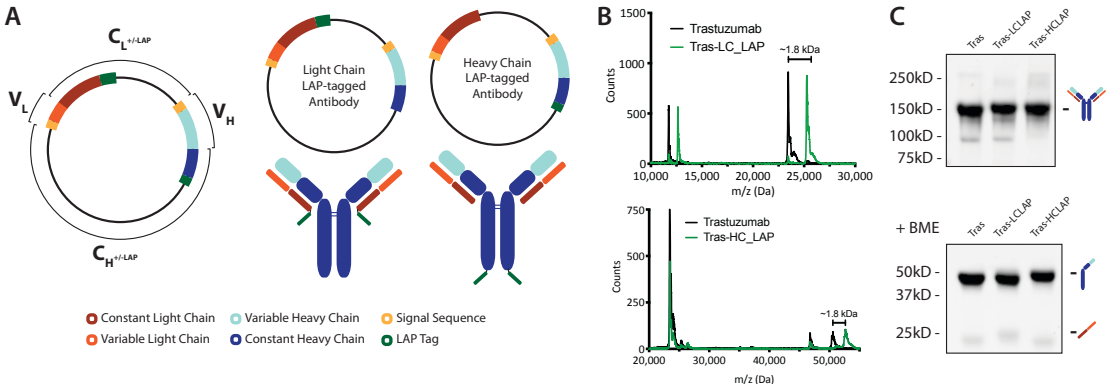

Figure 6.2 LAP-Tag incorporation into pVitro vector for simultaneous transfection and expression of light chain (LC) and heavy chain (HC) tagged Trastuzumab (A) Schematic representation of incorporation of LAP tag into pVitro dual-cassette vector. (B) MALDI-TOF MS of native (black), light-chain LAP-tagged (top, green) and heavy-chain (bottom, green) LAP-tagged antibody fragments (C) SDS-PAGE of (top) full-length and (bottom) reduced antibodies.

The LAP-tag (GFEID**K**VWYDLDA)[114] along with a GGGS flexible spacer at the N-terminal was cloned into the heavy chain (HC) and light chain (LC) C-termini of Trastuzumab. The pVitro dual-cassette expression vector system was used to transfect and express the heavy and light chains in a single vector (Figure 1A). The C-termini of each constant region chain was chosen for ease of swapping variable regions to generate LAP-tagged antibody conjugates against a new antigen, and for minimal inhibition of protein folding and antigen binding. Addition of the LAP-tag was verified with Sanger sequencing and MALDI-TOF mass spectrometry (Figure 6.2B). The MALDI of the reduced antibody conjugates shows the expected ~1.8 kDa mass shift for the addition of the 17-mer peptide (4-mer linker + 13-mer LAP-tag) as expected in both the light and heavy chains (Figure 6.2B). The extent of assembly and protein yield (~1-2 mg/L) of the LAP-tagged antibodies is comparable to that of the native antibody when expressed in the same cells (Figure 6.2C).

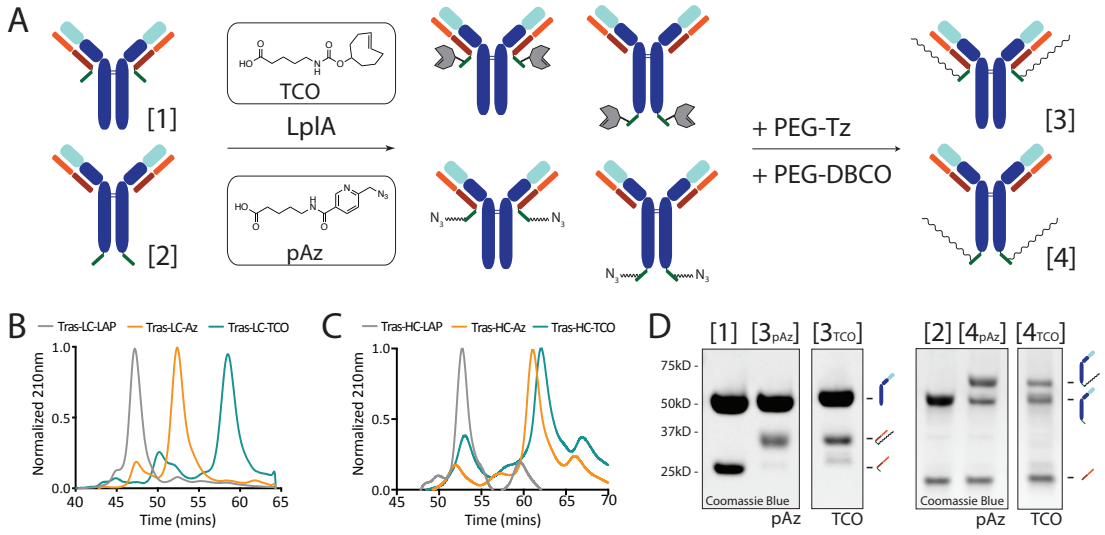

Figure 6.3 Efficient conjugation of antibodies with pAz and TCO substrates and Click-able PEGs (PEG-Tz and PEG-DBCO) via LplA - (A) Schematic representation of LplA two-step conjugation via TCO- and pAz-LAP tag substrates. (B) and (C) HIC traces of light and heavy chain modified antibodies functionalized with TCO and pAz-substrates via LplA. Hydrophobic shifts are indicative of functionalization (D) SDS-PAGE showing site-specific PEGylation of antibodies at light-chain (left) or heavy-chain (right) C-terminal.

To verify specificity, substrate scope and extent of reaction, LAP-tag modified antibodies were conjugated to picolyl-azide (pAz) and trans-cyclooctene (TCO) substrates via the LplA enzyme (Figure 6.2A). All conjugations were performed with 20 µM antibody, 10-fold excess substrate and 10 mol% LplA at 37°C for 90 minutes. Extent of conjugation was determined via hydrophobic interaction chromatography (HIC) (Figure 6.3B and C). Both pAz and TCO additions resulted in an increase in retention on the column relative to the LAP-tag modified antibody, an indication of greater hydrophobicity. The TCO modification resulted in a more hydrophobic bioconjugate relative to the pAz modified antibody. By measuring the area under the curve (AUC), conjugation efficiencies for the LC additions were calculated to be 86% for the pAz and 88% for TCO. Conjugation efficiencies for the HC additions were 82 % for the pAz substrate and 69 % for the TCO substrate. To verify that these

functional groups were accessible for conjugation after addition to the antibody, pAz and TCO functionalized antibodies were reacted with the corresponding large (5,000 MW) PEG-dibenzyl cyclooctyne (DBCO) or PEG-tetrazine to observe a gel shift via SDS-page (Figure 6.3D). Extent of reactions were calculated to be about 96% for the pAz substrate and 85% for the TCO substrate on the light chain LAP antibody, and 58% and 47% for the pAz and TCO substrates, respectively, on the HC LAP antibody. Successful conjugation indicates that the functional groups were accessible after attachment to the antibody. In general, we see that conjugation to the LC is more efficient than conjugation to the HC.

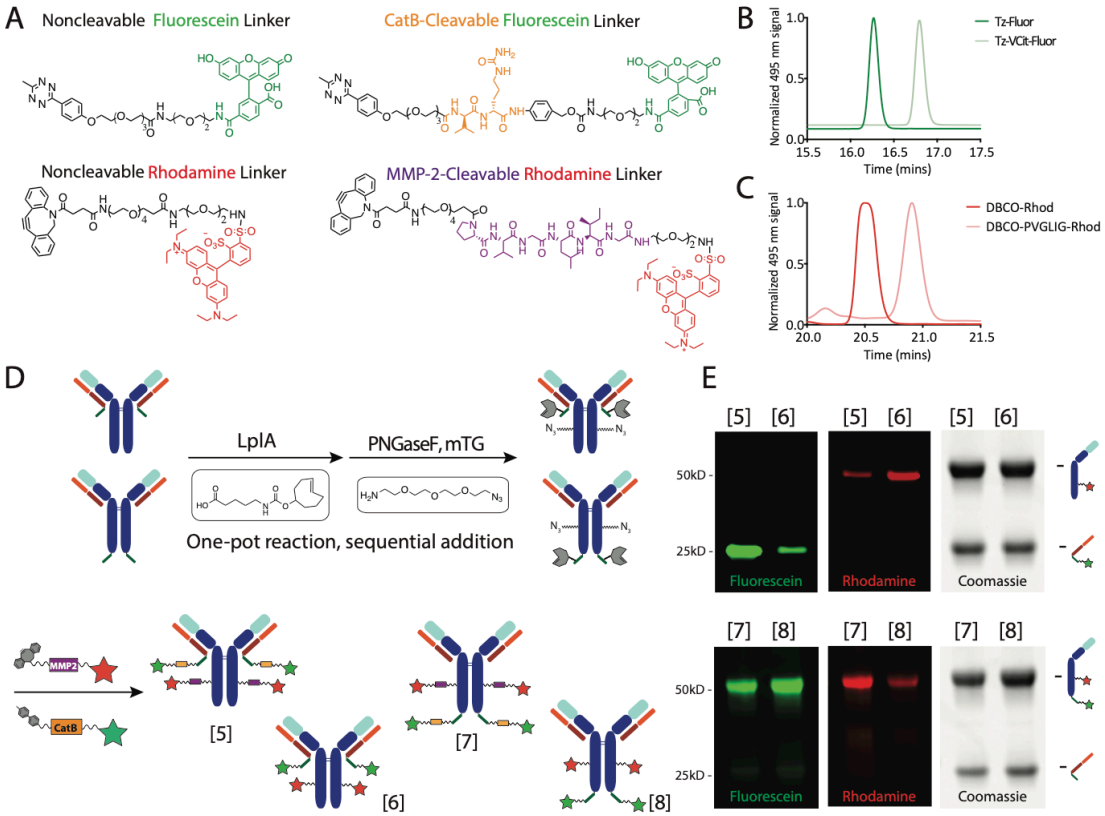

Figure 6.4 Dual-Labeled Antibodies via mTG and LplA – (A) Structures of fluorescein and rhodamine linkers with enzymatically labile sites or stable PEG controls. RP-HPLC traces of (B) purified fluorescein and (C) rhodamine linkers. (D) Schematic of a one-pot sequential labeling via LplA and mTG with TCO and pAz substrates, respectively, and subsequent modification with methyltetrazine and DBCO-functionalized fluorescent linkers. (E) Reduced SDS-PAGE of fluorescently-

labeled antibodies with fluorescein channel (green), rhodamine channel (red), and Coomassie channel (grey).

To demonstrate orthogonal labeling and sequential and orthogonal release from the ABCs, we synthesized fluorescein and rhodamine linkers, with and without cleavable sites, for facile detection of orthogonal cleavage from the ABCs. The valine-citrulline (VCit) peptide linkage has been verified previously to be cleaved by the intracellular enzyme, cathepsin B[224] and has been widely utilized in antibody drug conjugates. The PVGLIG peptide linkage was discovered via a large-scale screen of MMP's by Turk and colleagues[225] and used in a methotrexate-dextran conjugate by Chau, Tan and Langer[226] for enzyme-mediated drug release. This particular sequence was also chosen because none of the side-chains had reactive functional groups. Rhodamine linkers were functionalized with a DBCO group for strain-promoted copper-free "click" reaction with azide groups, and fluorescein linkers were functionalized with a methyltetrazine group for inverse electron demand Diels-Alder (IEDDA) reaction with TCO groups (Figure 6.4A). Detailed synthesis and characterization of the fluorescent linkers can be found in the Appendix (A.33-A.41). Linkers with peptide sequences (i.e. cleavable linkers) were slightly more hydrophobic than the non-cleavable linkers as determined via reverse-phase analytical HPLC (Figure 6.4B and C).

To demonstrate the compatibility of the LAP-tag with other site-specific modifications, as well as demonstrate sequential and orthogonal drug release, we adopted the mTG chemoenzymatic ligation as an additional, site-specific, conjugation method that does not require genetically encoding another conjugation site. Following deglycosylation of Trastuzumab with PNGase F to expose glutamine 295 (Q295) on the HC, conjugation via mTG leads to the generation of a thioester at Q295 that subsequently reacts with the primary amine substrate. This method of conjugation is orthogonal to LplA coupling of the lysine residue in the LAP-tag with valeric acid

substrates. Thus, we hypothesized that both enzymatic couplings could be performed in a one-pot reaction via sequential addition of the enzymes with a single purification step of both substrates and enzymes (Figure 6.4D). Fluorescent linkers synthesized with and without cleavable bonds in Figure 6.4A were used to verify reaction orthogonality (Figure 6.4D). Using both the cleavable and non-cleavable linkers, modified Trastuzumab was simultaneously labeled on the LAP-tag site, as well as the Q295 residue in Fc region and analyzed via fluorescent SDS-PAGE (Figure 6.4E). In the LC LAP-tagged Trastuzumab antibodies (Figure 6.4D, [5] and [6]), the LC shows green fluorescein fluorescence, and the HC shows red rhodamine fluorescence. There was no observed cross reactivity between the sites (Figure 6.4E). Additionally, in the HC LAP-tagged antibodies (Figure 6.4D, [7] and [8]), the HC showed both green and red fluorescence, indicating the two sites on the HC could be labeled simultaneously.

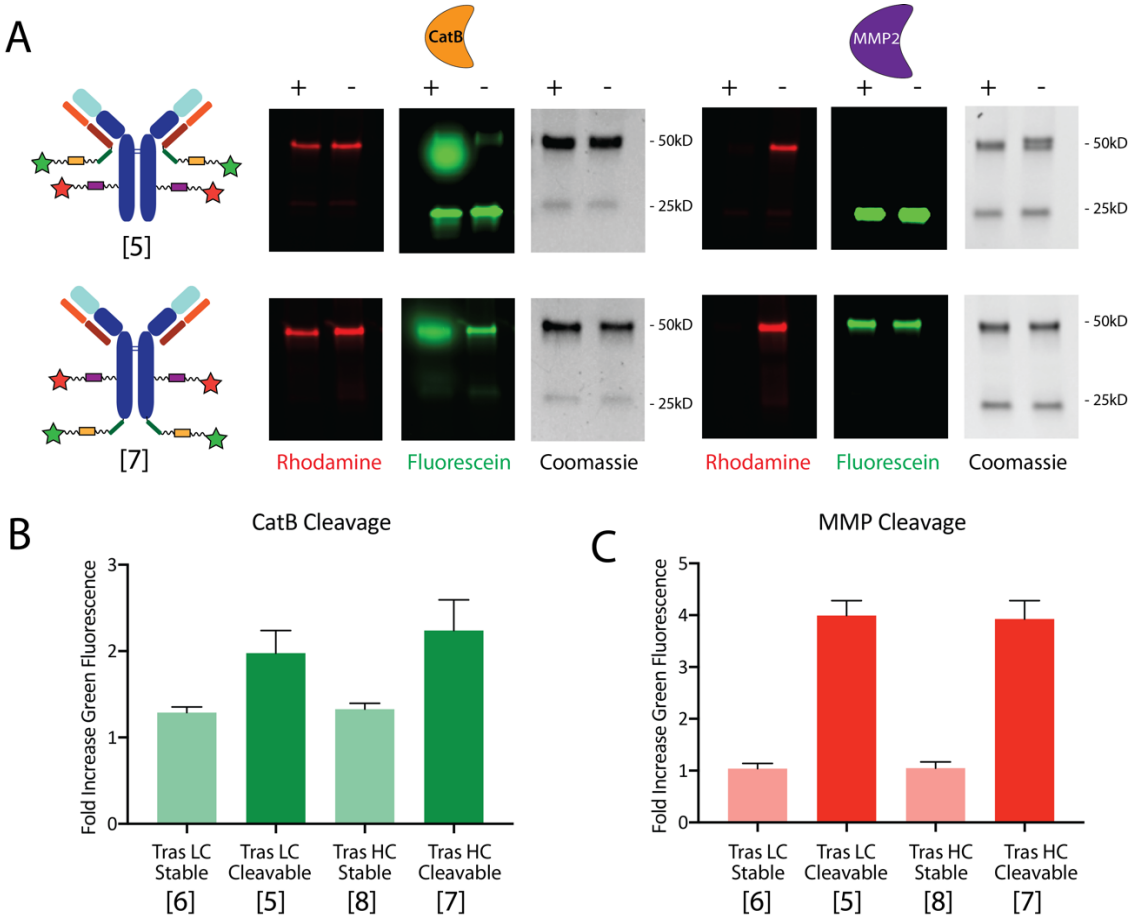

Figure 6.5 Enzymatic Cleavage of Linkers via CatB and MMP-2 – (A) Reduced SDS-PAGE of LC (top) and HC (bottom) dual-labeled antibodies treated with CatB and MMP-2. Fluorescein channel (green), rhodamine channel (red), and Coomassie channel (grey). Fluorescein cleavage by CatB generates a large green spot near the HC band. Rhodamine cleavage by MMP-2 leads to disappearance of the red band on the HC. (B) Green fluorescence de-quenching of cleavable conjugates relative to stable controls in the presence of CatB (C) Green fluorescence de-quenching of cleavable conjugates relative to stable controls in the presence of MMP-2.

To observe cleavage of the fluorescent linkers with the corresponding enzyme, antibodies were incubated with Cathepsin B (CatB, Sigma) and Matrix Metalloproteinase-2 (MMP-2, R&D Systems) and analyzed via fluorescent SDS-PAGE. In the presence of MMP-2, the red band is cleaved from the antibody with no apparent change in green fluorescence. Similarly, in the presence of CatB, the green band is partially cleaved from the antibody, generating free fluorescein that runs near

the heavy chain band (proof that free fluorescein runs at this position upon cleavage can be seen in the control in Appendix A.42) on SDS-PAGE (Figure 6.5A). No cross-cleavage was observed with either MMP-2 or CatB. As the fluorescein and rhodamine fluorophores undergo resonance energy transfer, the fluorescein is partially quenched when attached to the antibody and in proximity of rhodamine. Upon the addition of CatB, the fluorescein is cleaved from the molecule and is de-quenched. Similarly, upon the addition of MMP-2, the rhodamine is cleaved from the molecule, and the fluorescein is also de-quenched. Relative to the non-cleavable control, both the light chain and heavy chain LAP-tagged antibodies showed dequenching of green fluorescence upon addition of enzyme. With the addition of CatB, the antibodies showed ~ 2-fold increase in green fluorescence on the LC and HC tagged antibodies, respectively (Figure 6.5B). With the addition of MMP-2, the antibodies showed ~ 4-fold increase in green fluorescence on both the LC and HC tagged antibodies respectively (Figure 6.5C). These results thus demonstrate temporal control of cargo release via two orthogonal enzymatic cues on site-specific dual-labeled antibody conjugates.

Conclusions & Discussion

In this study, we generated site-specifically dual-labeled Trastuzumab bioconjugates, at two different sites via a one-pot reaction with orthogonally releasing linkers. The expression system developed in this work was used to generate Trastuzumab antibodies for dual chemoenzymatic ligation with LplA and mTG enzymes. Here, the LAP-tag was placed at the heavy and light chain C-termini; however, the LAP-tag could be moved to other locations on the antibody or at multiple sites for higher drug-antibody ratios. The fast kinetics of the LplA substrate addition to the antibody makes for rapid generation (~1-2 hours) of conjugates using click chemistry or fluorescent

substrates.[22,118,119,122] Additionally, the variable region swap method developed by Dodev and colleagues[98] allows for the straight-forward generation of antibodies against new antigens as shown in this work for Her2 and recently against polysialic acid[124]. This method, which involves simple transfection and generation of stable antibody-expressing 293F cells without viral components, allows the facile expression of antibodies for bioconjugation. The one-pot reaction demonstrated here utilizes two orthogonal chemistries with two orthogonal substrates. In this study, we used the TCO substrate with LplA, and an azido amine substrate with mTG. However, the Ting lab has generated several various substrates compatible with LplA variants[22,118,119,122], and mTG has been shown to be promiscuous to many amine-containing substrates[116]. Both enzymes are accessible to labs as the plasmid for $LplA^{W37V}$ is available on Addgene with protocol[227] for expression and purification, and mTG is cheap and accessible in meat glue formulations (Moo Glue, Modern Pantry). Quantitative labeling, though not achieved here, could be obtained through further optimization of reaction conditions with a different pair of substrates.

The orthogonal cleavage sites used in this study involve an extracellular protease, MMP-2, and an intracellular protease, CatB, which could be implicated in sequential drug release applications. With both extracellular and intracellular release triggers, it is possible to deliver drugs that need sequential release, such as the release of an efflux pump inhibitor followed by a hydrophobic chemotherapeutic drug, as could be necessary in multi-drug resistant (MDR) cancers[228]. This dual-labeling of a single antibody can also be utilized in imaging applications to examine uptake, trafficking, and intracellular cleavage of antibody conjugates[221,222]. The CatB-cleavable linker has been used in a large number of ADCs and has been shown to work with a variety of dipeptide cleavage sites, the most prominent being valine-citrulline used in this work.

The MMP-2 linker has not yet been utilized in an ADC but has been used in other polymer-drug conjugates for MMP2-triggered drug release. To the best of our knowledge, this work represents the first demonstration of antibody bioconjugates with two, orthogonal enzymatically cleavage sites at two different, site-specific, locations. By demonstrating orthogonal cleavage with extracellular and intracellular enzymes, this work holds great promise for the design of ADCs with sequential release properties and could be beneficial for disease applications that require cooperative drug combinations.

Materials & Methods

Materials. All chemicals and solvents were purchased from Millipore-Sigma and VWR unless stated otherwise. Chemical crosslinkers were purchased from BroadPharm (Az-PEG3-NH2, Cat#BP20580; TCO-NHS ester, BP-22417; NHS-PEG4-TCO, Cat# BP-22418; MeTzine-PEG5-NHS, BP-22945; DBCO-PEG4-NHS, BP-22288). Purified Cathepsin B enzyme was purchased from Millipore Sigma (Cat# C0150-2UN) and recombinant Matrix Metalloproteinase-2 was purchased from R&D Systems (Cat# 902-MP). Peptides were purchased from Genscript. DNA Primers were purchased from Integrated DNA Technologies (IDT). Materials for PCR and cloning were purchased from New England BioLabs. Gel electrophoresis materials were purchased from Bio-Rad. Plasmid for Trastuzumab antibody generation was purchased from Addgene (Plasmid# 61883). All sequencing was done by the Cornell Genomics Facility using the Applied Biosystems Automated 3730xl DNA Analyzer using Big Dye Terminator chemistry and ApliTaq-FS DNA Polymerase.

Cloning of LAP-tagged Antibodies. The "LAP Tag" and spacer (GGGS-GFEID**K**VWYDLDA) was incorporated into the heavy and light chain C-terminal of

the pVITRO-ch735-IgG1 vector [124] using 4 sequential PCR steps. The tag was added through the reverse primer, adding ~17-20 bases at a time. The following primers were used:

Heavy Chain LAP Tag:
FWD (ch735): ccgccacaggcgcgcactcccagattcagctgcagcaatc
REV1: aagccagatcctccgccTTTACCCGGAGACAGGGAGAGGC
REV2: accacaccttgtcgatctcgaagccagatcctccgccTTT
REV3: ACATCAggcgtccaggtcgtaccacaccttgtcgatctcg
REV4: ATGTCTGGCCAGCTAGCTGTACATCAggcgtccaggtcgt

Light Chain LAP Tag:
FWD (ch735): gggttccagctagccgcggtgatgtagtcatgacgcagac
REV1: aagccagatcctccgccACACTCTCCCCTGTTGAAGCTCT
REV2: accacaccttgtcgatctcgaagccagatcctccgccACA
REV3: TCCCTAggcgtccaggtcgtaccacaccttgtcgatctcg
REV4: CTGCTCCTAGGCGTACGGGATCCCTAggcgtccaggtcgt

PCR amplification was done with the Flash-Phusion enzyme master mix with an initial denaturation step for 30 sec at 98°C, followed by 30 cycles with denaturation for 10 sec at 98°C, and extension for 15 sec/kb at 72°C. The product was gel purified, and reamplified with 10ng of template for the 4 sequential amplifications.

To assemble the final vector, the following primers were used:
FWDvector: TCCCGTACGCCTAGGAGCAGGTTTCCCCAATGACACAAAA
REVvector: accgcggctagctggaacccagagcagcagaaacccaatg

FWDch735V_L: gggttccagctagccgcggtgatgtagtcatgacgcagac

REV4V_L: CTGCTCCTAGGCGTACGGGATCCCTAggcgtccaggtcgt

PCR amplification was done with the Flash-Phusion enzyme master mix with an initial denaturation step for 30 sec at 98°C, followed by 5 cycles with denaturation for 10 sec at 98°C, annealing for 15 sec starting at 55°C and decreasing 1°C per cycle, and extension time at 90% of the recommended 15 sec/kb which was 107 sec for the vector piece (FWDvector and REVvector) and 10 seconds for the light chain piece (FWDch735V_L and REV4V_L) at 72°C. The product was gel purified, and reamplified with 10ng of template for the 4 sequential amplifications. Following the touchdown protocol, 30 cycles of PCR were performed with denaturation for 1 sec at 98°C, annealing for 5 sec at 55°C and extension for 107 sec or 10 sec at 72°C respectively. Resulting PCR products were DpnI digested for 1 hour at 37°C. Then the digests were combined 1:1 to a total volume of 100 uL and incubated at RT for 1 hour. The reactions were cleaned up with the Qiagen PCR clean up protocol and eluted in 30 uL of water. The volume was brought to 100 uL with water and 2 uL of this reaction was used to transform NEB 10-beta chemically competent cells according to the manufacturer's protocol. After recovery, the cells were plated onto 300 µg/mL HyroB LB plates. Colonies were picked and grown in LB + 300µg/mL HygroB, mini-prepped, and verified with sanger sequencing.

To swap the variable regions from ch735 to Trastuzumab, the following primers were used:

TrasV_HFwd: ccgccacaggcgcgcactccGAGGTGCAGCTGGTGGAGTC

TrasV_HRev: GATGGGCCCTTGGTGCTAGCTGAGGAGACGGTGACAAGAG

TrasV_LFwd: gggttccagctagccgcggtGACATCCAGATGACCCAGTC

TrasV$_L$Rev: GATGGCGCCGCCACCGTACgtttgatCTCCAGCTTGGTAC

C$_H$Fwd: GCTAGCACCAAGGGCCCATCGGTCTTCCCCCTGGCACCCT

C$_H$Rev: accgcggctagctggaacccagagcagcagaaacccaatg

C$_L$Fwd: cgtacggtggcggcgccatctgtcttcatcttcccgccat

C$_L$Rev: ggagtgcgcgcctgtggcggccgccaccaagaagaggatc

Variable region pieces were amplified from pVitro1-Trastuzumab-IgG1 (Plasmid# 61883), and constant region pieces were amplified from the LAP-tag incorporated ch735 vector. PCR amplification was done with the Flash-Phusion enzyme master mix with an initial denaturation step for 30 sec 98°C, followed by 30 cycles with denaturation for 10 sec at 98°C, annealing for 15 sec at 60°C, and extension for 6 and 60 sec at 72°C for variable and constant region pieces, respectively. Resulting PCR products were DpnI digested for 2 hours, cleaned-up, and quantified via 260/280nm absorbance on a Tecan Nanoquant Plate. The purified pieces were mixed at a 1:1:1:1 molar ratio, ligated via Gibson, and transformed into NEB 10-beta chemically competent cells and plated onto 300µg/mL HygroB LB plates. Colonies were picked and grown in LB + 300µg/mL HygroB, mini-prepped, and verified with sanger sequencing.

Recovered pVITRO-Trastuzumab-IgG1-LAP vectors were re-transformed, midi-prepped, and transfected into HEK 293F suspension cells using Freestyle MAX reagent and selected with 50µg/mL HygroB for two weeks to generate a stable line. Stably expressing 293F cells were cultured in LAP-tagged antibody was purified from the 293F media using gravity column purification using protein A/G resin (ThermoFisher). The recovered antibody was buffer exchanged into PBS using Amicon 30kDa MWCO centrifugal columns and quantified via 280nm absorbance using a quartz NanoQuant plate (ext. coeff$_{280nm}$ = 210,000 M^{-1} cm^{-1}).

Sanger sequencing of constant heavy and light chain domains with LAP tag sequences.

BLACK & UPPERCASE – constant region DNA sequence

red & lowercase – LAP tag DNA sequence

C_H Region:

GCTAGCACCAAGGGCCCATCGGTCTTCCCCCTGGCACCCTCCTCCAAGAGC

ACCTCTGGGGGCACAGCGGCCCTGGGCTGCCTGGTCAAGGACTACTTCCCC

GAACCGGTGACGGTGTCGTGGAACTCAGGCGCCCTGACCAGCGGCGTGCA

CACCTTCCCGGCTGTCCTACAGTCCTCAGGACTCTACTCCCTCAGCAGCGT

GGTGACCGTGCCCTCCAGCAGCTTGGGCACCCAGACCTACATCTGCAACGT

GAATCACAAGCCCAGCAACACCAAGGTGGACAAGAAAGTTGAGCCCAAA

TCTTGTGACAAAACTCACACATGCCCACCGTGCCCAGCACCTGAACTCCTG

GGGGGACCGTCAGTCTTCCTCTTCCCCCCAAAACCCAAGGACACCCTCATG

ATCTCCCGGACCCCTGAGGTCACATGCGTGGTGGTGGACGTGAGCCACGA

AGACCCTGAGGTCAAGTTCAACTGGTACGTGGACGGCGTGGAGGTGCATA

ATGCCAAGACAAAGCCGCGGGAGGAGCAGTACAACAGCACGTACCGGGT

GGTCAGCGTCCTCACCGTCCTGCACCAGGACTGGCTGAATGGCAAGGAGT

ACAAGTGCAAGGTCTCCAACAAAGCCCTCCCAGCCCCCATCGAGAAAACC

ATCTCCAAAGCCAAAGGGCAGCCCCGAGAACCACAGGTGTACACCCTGCC

CCCATCCCGGGATGAGCTGACCAAGAACCAGGTCAGCCTGACCTGCCTGG

TCAAAGGCTTCTATCCCAGCGACATCGCCGTGGAGTGGGAGAGCAATGGG

CAGCCGGAGAACAACTACAAGACCACGCCTCCCGTGCTGGACTCCGACGG

CTCCTTCTTCCTCTACAGCAAGCTCACCGTGGACAAGAGCAGGTGGCAGCA

GGGGAACGTCTTCTCATGCTCCGTGATGCATGAGGCTCTGCACAACCACTA

CACGCAGAAGAGCCTCTCCCTGTCTCCGGGTAAAggcggaggatctggcttcgagatcga
caaggtgtggtacgacctggacgcc

C_L Region:

GTACGGTGGCGGCGCCATCTGTCTTCATCTTCCCGCCATCTGATGAGCAGT
TGAAATCTGGAACTGCCTCTGTTGTGTGCCTGCTGAATAACTTCTATCCCA
GAGAGGCCAAAGTACAGTGGAAGGTGGATAACGCCCTCCAATCGGGTAAC
TCCCAGGAGAGTGTCACAGAGCAGGACAGCAAGGACAGCACCTACAGCCT
CAGCAGCACCCTGACGCTGAGCAAAGCAGACTACGAGAAACACAAAGTCT
ACGCCTGCGAAGTCACCCATCAGGGCCTGAGCTCGCCCGTCACAAAGAGC
TTCAACAGGGGAGAGTGTggcggaggatctggcttcgagatcgacaaggtgtggtacgacctggacgcc

LplA Conjugation. 500µg of antibody was incubated at 20µM with 10mol% LplA, 200µM pAz or TCO-LAP, 1mM ATP, and 5mM $Mg(OAc)_2$ in PBS for 1.5 hours at 37°C. The reaction mixture was quenched with EDTA at a final concentration of 30mM. The extent of reaction was quantified via hydrophobic interaction chromatography (HIC) on a Tosoh TSK Phenyl-5PW column on a gradient of 100-40% high salt buffer (1.5M ammonium sulfate, 25mM phosphate, pH 7.0) in low salt buffer (18.75mM sodium phosphate, 25% v/v isopropanol, pH 7.0) over 60 mins.

For click reactions with corresponding PEG reagents, the quenched reaction was washed with PBS three times at 14,000 x g for 8 minutes in 500µL Amicon 30kDa MWCO centrifugal columns, recovered via inversion at 1,000 x g for 1 min, and quantified via 280nm absorbance using a quartz NanoQuant plate (ext. $coeff_{280nm}$ = 210,000 M^{-1} cm^{-1}). Recovered antibodies were incubated with a large excess (25 molar equivalencies) of 5,000 MW DBCO-PEG or MeTzine-PEG reagents overnight at 37°C. Reaction mixtures were then reduced, boiled, and run on a 4-20% Mini-Protean

TGX pre-cast protein gels (Bio-Rad) at 120V for 60 mins. Gels were stained with Bio-Safe® Coomassie, de-stained with water, and analyzed for a gel shift indicating a successful click reaction.

One-pot LplA and Transglutaminase Dual Conjugation. 500µg of antibody was incubated at 20µM with 10mol% LplA, 200µM pAz or TCO-LAP, 1mM ATP, and 5mM $Mg(OAc)_2$ in PBS for 1.5 hours at 37°C. After 1.5 hours, 200 wt% Moo Gloo (10U/g Ab), 160 molar equivalencies of NH_2-PEG_3-Az, and 0.6µL of PNGase F was added to the mixture for a final concentration of 12.5µM antibody in PBS with for 7 hours at 37°C. The reaction was washed with PBS three times at 14,000 x g for 8 minutes in 500µL Amicon 30kDa MWCO centrifugal columns to remove excess substrate and recovered via inversion at 1,000 x g for 1 min, then quantified via 280nm absorbance using a quartz NanoQuant plate (ext. $coeff_{280nm}$ = 210,000 M^{-1} cm^{-1}). Recovered antibodies were incubated with 10 molar equivalencies each of fluorescein and rhodamine linkers overnight at 37°C. The entire mixture was purified on 0.2mL NAb™ Protein A/G spin columns. The reaction mixture was added to the spin column and incubated for 10 mins at RT. After 10 mins, the column was centrifugated at 5,000 x g for 1 minute. The flow-through was then passed over the column two additional times. The mixture was washed 3 times with PBS, then eluted two times with 200µL 0.1M glycine (pH 2) into neutralizing 20µL 1M Tris (pH 8) and one time with 100µL 0.1M glycine into 10µL 1M Tris. The three eluted fractions were pooled and concentrated in 500µL Amicon 30kDa MWCO centrifugal columns with one spin at 14,000 x g for 15 mins, then recovered by inversion at 1,000 x g for 1 minute. The final dual-labeled conjugates were quantified on a quartz NanoQuant plate using 280nm, 498nm, and 565nm absorbances for antibody, fluorescein, and rhodamine concentrations, respectively (ext. $coeff_{280nm}$ = 210,000 M^{-1} cm^{-1}; ext.

coeff$_{498nm}$ = 30,900 M^{-1} cm^{-1}; ext. coeff$_{565nm}$ = 36,500 M^{-1} cm^{-1}). Correction factors for fluorescein and rhodamine signals at 280nm were 0.154 and 0.49, respectively.

Antibody Conjugate Cargo Release with Cathepsin B (CatB). Fluorescently labeled antibodies were incubated at 5μM with 0.025U of CatB in 10μL of in the recommended enzyme buffer (352mM K_2PO_4, 48mM Na_2PO_4, 4mM EDTA, 2mM Cysteine) for 48 hours at 37°C. Controls were incubated in buffer with an equal volume of enzyme storage solution (0.1% Brij 35) instead of enzyme. Samples were measured for fluorescence dequenching by measuring green fluorescence signal (494/521nm Ex/Em) normalized to red fluorescence (568/583nm Ex/Em), then normalized to controls without enzyme. The remainder of sample (5μL) was analyzed with fluorescent SDS-PAGE.

To verify that the large spot on SDS-PAGE is indeed the cleaved fluorophore, the cleavable fluorescein linker was incubated at 50μM with 0.2U of CatB or Brij 35 control in 10μL of the recommended enzyme buffer for 3 hours at 40°C. The linker was either run alone or mixed with 5μg of unlabeled antibody to verify that the cleaved fluorophore runs just below the heavy chain band (Figure S8).

Antibody Conjugate Cargo Release with MMP-2. MMP-2 enzyme was first activated at 0.1mg/mL with 1mM 4-aminophenylmercuric acid (APMA) for 1 hour at 37°C. Fluorescently labeled antibodies were incubated at 5μM with 0.01mg/mL enzyme in MMP-2 buffer (50mM Tris, 10mM $CaCl_2$, 150mM NaCl, 0.05% Brij 35) for 24 hours at 37°C. Samples were measured for fluorescence dequenching by measuring green fluorescence signal (494/521nm Ex/Em) normalized to red fluorescence (568/583nm Ex/Em), then normalized to controls without enzyme. The remainder of sample (5μL) was analyzed with fluorescent SDS-PAGE.

Fluorescent SDS-PAGE. Antibodies conjugated with fluorophores were analyzed via SDS-PAGE imaged for fluorescein and rhodamine fluorescence and co-stained with Coomassie Blue. 2.5µg of antibody was mixed 1:1 with Laemmli buffer with 5% (v/v) beta-mercaptoethanol (βME) and heated to 100°C for 10 mins. Samples were run on 4-20% Mini-Protean TGX pre-cast protein gels (Bio-Rad) at 120V for 60 mins. Fluorescent gels were first imaged on a ChemiDoc MP Imaging system (Bio-Rad) for fluorescein and rhodamine, then stained with Bio-Safe® Coomassie stain, de-stained with water, and imaged.

pAz Synthesis and Purification (Appendix A.29-A.30): The azide-functionalized LAP tag substrate (pAz, **7**) was synthesized and purified according to Uttamapinant *et. al.*[227] Briefly, 10g (51.27 mmol) of dimethyl 2,5-pyridine dicarboxylate (**1)** and 22.76 g (205.4 mmol) of anhydrous calcium chloride were solubilized in 300mL of 2:1 anhydrous THF:MeOH on ice. Then, 3.9 g (103.1 mmol) of $NaBH_4$ was slowly added to the reaction mixture and allowed to stir for 2 hours at 0°C. The reaction was quenched with 100mL ice-cold water, concentrated via rotary evaporation, extracted with chloroform, washed twice with water, and dried. Next, 1.2 g (7.14 mmol) of the recovered product, methyl 6-(hydroxymethyl)nicotinate (**2**), was solubilized in 72mL anhydrous DCM. Then, 4 mL (28.5 mmol) triethylamine (TEA) and 2.0 g (10.7 mmol) *p*-toluenesulfonyl chloride was added to the flask and stirred at RT for 3 hours. The mixture containing the tosylated product (**3**) was dried via rotary evaporation, re-solubilized in 72mL THF with 4.5 g (68.9 mmol) sodium azide, stirred at RT for 24 hours. The reaction mixture was extracted 3 times with ethyl acetate and water, and the organic layer was dried and purified via flash chromatography (Teledyne ISCO) on a gradient of 0-50% ethyl acetate in hexanes over 15 mins. Next, 394 mg (2.05 mmol) of the eluted product, methyl 6-(azidomethyl)nicotinate (**4**), was solubilized in

20.5 mL MeOH with 6.12mL of 1M LiOH and stirred at RT for 25 mins. The mixture was quenched with 210µL acetic acid and concentrated via rotary evaporation, then purified by flash chromatography on silica with isocratic ethyl acetate with 1% (v/v) acetic acid. Then, 300mg (1.68 mmol) of eluted product, 6-azidomethylnicotinic acid (**5**), was solubilized in 5mL anhydrous DMF with 352µL (2.5 mmol) TEA and 647 mg (2.5 mmol) N-N'-disuccinimidyl carbonate for 3 hours at RT. The reaction mixture was dried and purified via flash chromatography on silica using 1:1 isocratic hexanes:ethyl acetate to yield the succinimidyl ester of 6-azidomethyl nicotinic acid (**6**). Next, 100mg (0.36 mmol) of **6**, 76 mg (0.65 mmol) of aminovaleric acid, and 90µL (0.65 mmol) TEA were stirred together for 3 hours at RT in 1mL DMF. The final product, 5-(6-(azidomethyl)nicotinamido) pentanoic acid or pAz (**7**), was purified via flash chromatography on silica with isocratic ethyl acetate with 1% acetic acid. The final product was verified with H^1-NMR and LCMS (**Figure S1**).

TCO-LAP Synthesis and Purification (Appendix A.31-A.32)*:* The TCO-functionalized LAP tag substrate (TCO-LAP, **8**) synthesis protocol was adapted from Liu *et. al*[121]. Briefly, 6mg (0.0227 mmol) of TCO-NHS ester was incubated with 2.8mg (0.0239 mmol) of aminovaleric acid in 2:1 DMSO:PBS overnight at RT. The reaction mixture was purified via RP-HPLC on a gradient of 25-60% AcN + 0.1% TFA in H_2O + 0.1% TFA over 14 mins on a C18 semiprep RP-HPLC column. The product (**8**) eluted at ~11 mins and mass was verified via LC-MS (**Figure S2**).

Fluorescein Linker Synthesis. To synthesize the fluorescein cleavable and stable linkers, first 9.2 mg (19.5 µmol) of Fluorescein-NHS was solubilized in 194µL of anhydrous DMSO with 14.4 mg (97.2 µmol) bis-PEG_2-NH_2 and 5.4µL (38.9 µmol) TEA for 3 hours at RT. The resulting Fluorescein-PEG_2-NH_2 (**9**) was purified on a

C18 RP-HPLC semiprep column on a gradient of 5-65% AcN in H_2O with 0.1% TFA over 20 mins, dried, and verified with LCMS. The product eluted at ~11 mins.

For the stable linker (**10**), 2 mg (3.95 μmol) of Fluorescein-PEG_2-NH_2 (**9**) was incubated in 181μL anhydrous DMSO with 2.76μL (19.8 μmol) TEA and 2.1 mg (3.95 μmol) NHS-PEG_4-MeTzine at RT for 3 hours. The final product was purified on a C18 RP-HPLC semiprep column on a 5-95% gradient of AcN + 0.1% TFA in H_2O + 0.1% TFA. The product (**10**) eluted at 16.25 mins and mass was verified via LC-MS (**Figure S3**).

For the CatB-cleavable linker (**13**), 5.9 mg (11.63 μmol) of Fluorescein-PEG_2-NH_2 (**9**) was incubated with 233 μL of anhydrous DMSO with 6.48 μL (46.50 μmol) triethylamine and 8.9 mg (11.63 μmol) of Fmoc-Val-Cit-PAB-PNP ester at RT for 1.5 hours to generate **11**. Removal of Fmoc protecting group was performed by the addition of 23.90 μL of piperidine. Deprotection via piperidine was carried out at RT for 30 minutes. The final product (**12**) was purified on a C18 RP-HPLC semiprep column on a linear gradient of 5-35% AcN in H_2O with 0.1% TFA over 40 mins, dried, and verified with LCMS. The product eluted at ~31.5 mins.

Val-Cit-PAB-PEG_2-Fluorescein (**12**) (1.60 mg, 1.76 μmol) was incubated with 70.2 μL of anhydrous DMSO with 12.23 μL (17.56 μmol) triethylamine and NHS-PEG_5-MeTzine (0.94 mg, 1.76 μmol) at RT for 5 hours. The final product (**13**) was purified on a C18 RP-HPLC semiprep column on a linear gradient of 5-55% AcN in H_2O with 0.1% TFA over 50 mins, dried, and verified with LCMS. The product eluted at ~40.5 mins.

Rhodamine Linker Synthesis. To synthesize the rhodamine cleavable and stable linkers, first 5 mg (8.68 μmol) of Rhodamine sulfonyl chloride was incubated with (43.4 μmol) bis-PEG_2-NH_2 and (43.4 μmol) TEA in 113μL DMF for 16 hours at RT.

The resulting Rhodamine-PEG_2-NH_2 (**14**) was purified on a C18 RP-HPLC semiprep column on a 5-95% gradient of AcN + 0.1% TFA in H_2O + 0.1% TFA. The product (**14**) eluted at ~15 mins and the mass was verified via LC-MS.

For the stable linker (**15**), 1.5 mg (2.2 µmol) of Rhodamine-PEG_2-NH_2 (**14**) was incubated in 151µL anhydrous DMSO with 15.2µL (10.9 µmol) TEA and 2.1 mg (3.3 µmol) NHS-PEG_4-DBCO for 3 hours at RT. The final product (**15**) was purified on a C18 RP-HPLC semiprep column on a gradient of 5-65% AcN in H_2O with 0.1% TFA over 20 mins, dried, and verified with LCMS (**Figure S5**). The product eluted at ~20.5 mins and was quantified via absorbance at 565nm (ext. $coeff_{565nm}$ = 36,500 M^{-1} cm^{-1}).

For the MMP-2-cleavable linker (**19**), 0.8 mg (1.03 µmol) of Fmoc-PVGLIG-OH (Genscript, **16**) was incubated with 2.1 µmol each DIC and N-hydroxysuccinimide in 28.5µL anhydrous DMF for 1 hour. After 1 hour, 1.29 µmol of rhodamine-PEG_2-NH_2 (**14**) and TEA were added to the mixture to a final volume of 62µL. The mixture was incubated overnight at RT to yield **17**, then Fmoc-deprotected with 10% (v/v) piperidine. The NH_2-PVGLIG-Rhodamine (**18**) product was purified via RP-HPLC on a 5-95% gradient of AcN + 0.1% TFA in H_2O + 0.1% TFA. The two product isomers eluted at 17.2 and 18.1 mins, were quantified via absorbance at 565nm (ext. $coeff_{565nm}$ = 36,500 M^{-1} cm^{-1}) and mass was verified via LC-MS. The eluted product (**18**) (0.4mg; 0.33 µmol) was then solubilized in dry DMSO, and incubated with 0.5 µL (3.3 µmol) TEA and 0.49 µmol NHS-PEG_4-DBCO in 114µL dry DMSO for 3 hours at RT. The final product (**19**) was purified on a C18 RP-HPLC semiprep column on a gradient of 5-65% AcN in H_2O with 0.1% TFA over 20 mins, dried, and verified with LCMS (**Figure S6**). The product eluted at ~21 mins and was quantified via absorbance at 565nm (ext. $coeff_{565nm}$ = 36,500 M^{-1} cm^{-1}).

CHAPTER 7 – CONCLUSIONS AND FUTURE DIRECTIONS

Antibody therapeutics are among the fastest growing field of biologics in the market currently and show no signs of slowing down. The target specificity, evolvability, and range of therapeutic mechanisms available with antibodies make it an unparalleled protein therapeutic for a huge host of disease targets. With the current display technologies available, antibodies can be evolved for better affinity and binding site variability against any extracellular target. Some argue that the accessible extracellular disease markers and targets have already been identified, and thus the future of antibodies lies optimization of antibodies against existing targets. This can be done by enhancing affinity, modulating the binding site, inducing a more enhanced secondary response, building bispecific and multi-targeting antibodies, and incorporating better conjugation sites onto antibodies to deliver drugs.

The antibody drug conjugate (ADC) branch of antibody-based therapeutics is a relatively new field but has been growing very quickly. After the discovery that site-specific, homogeneous ADCs are better tolerated in animals and humans, the field of site-specific antibody conjugation has seen rapid growth. However, the increased complexity of site-specific ADCs tends to lead to more purification steps and thus an increase in cost in an already expensive biologic. This can possibly be circumvented with reaction pairs or chemoenzymatic ligations with fast kinetics, quantitative yields, and strong serum stability. Currently, the most commonly used site-specific conjugation technique is through engineered cysteine residues. These are easy to incorporate into antibodies, but maleimide chemistry can lead to premature drug release and systemic toxicity. However, there has been a large amount of work to stabilize the thio-succinimide linkage.

Chemoenzymatic methods are an alternative means for coupling cargo to antibodies with stable linkages. These can form stable amide bonds or incorporate "click chemistry" functional groups that are aromatically stabilized after conjugation. This does not alleviate the purification problem though and could be even more rigorous to remove the added enzyme. Work like FGE ligation from the Bertozzi lab with co-translationally modified antibodies is an effective means to minimize purification, and other systems that could incorporate bio-orthogonal functional groups onto antibodies in this way would be effective. The FGE method is great, but not optimal, because the corresponding substrate, the HIPS reagent, has limited stability in aqueous solution and difficult to work with.

The purification problem is further amplified with more complicated ADCs, such as those with multiple cargo on a single antibody. There are a number of strategies to do this, including methods discussed in this dissertation. Our work is unique in incorporating cleavable linkers with orthogonal cleavage sites to a single antibody, but we still suffer from incomplete reaction conversion using the microbial transglutaminase (mTG) and lipoic acid ligase (LplA) enzymes. I believe this can be circumvented though with more antibody, which would allow us to use higher reaction concentrations and drive them to completion. Additionally, the instability of the trans-cyclooctene could be an attributing factor for a lack of reaction conversion. I think developing these more complex ADCs will be very important in the field of biologics delivery, where a lack of non-toxic modalities for endosomal translocation still plagues the field.

The emergence of N-acetylgalactosamine (GalNAc)-siRNA conjugates and their efficacy has really enlightened the community in the benefits of targeted conjugate

therapeutics over particle-based carriers in delivering certain biologics. However, making effective conjugates to target beyond the liver continues to be a challenge. Based on the theory that the GalNAc conjugates work so well because of the high abundance and fast recycling of the ASGPR, it's going to be difficult to find another receptor ligand pair in another disease that works just as well. It is possible that higher affinity binding ligands could prompt different internalization pathways depending on the epitope, as has been seen with Transferrin-receptor targeted antibodies, but this would require quite a bit of screening and optimization. RNA aptamers may provide an alternative to this antibody screening method, as large RNA libraries are available and target siRNAs can be easily added to the sequence. However, instability of RNA conjugates is still a major variable in RNA conjugates, as the location and number of chemical modifications varies from sequence to sequence. Collaborations with companies or research groups with RNA synthesis capabilities could be helpful in studying these delivery methods. Either way, for ligand-receptor pairs with lower abundance and internalization rates, endosomal escape is still the major barrier to effective delivery.

There are a large host of reagents available with membrane-disrupting capabilities for endosomal escape; but applying these reagents in a way that does not disrupt the outer membrane or elicit an immune response is still very difficult. Antimicrobial peptides and bacterial toxins are excellent pore-formers but are not specific to the endosomal membrane and need to be protected and later deprotected by an endosomal-specific reagent. Additionally, these can illicit an immune response in circulation as they are derived from pathogens. I feel the future lies in incorporating small, potent, hydrophobic, synthetic endosomal escape domains into the conjugate. These small hydrophobic domains must be incorporated in such a way though that they are only

uncovered once the conjugate reaches the endosomal compartment, likely from cleavage by an endosomal protease. These hydrophobic domains can then be used to drag the RNA across the endosomal membrane into the cytosol. They should be synthetic though, as to not induce an immunological response or be degraded in the endosomal compartment. These should also be attached in a way that keeps the siRNA attached to the endosomal escape domain but is released from the targeting ligand. This way, the siRNA is covalently attached to the escape domain and is not reliant on passive leakage from the endosome following pore formation in the endosomal membrane. Furthermore, better understanding of endosomal and lysosomal trafficking must be investigated to better understand the limitations in efficient intracellular delivery.

With this, despite being unable to produce a functional antibody conjugate for siRNA delivery and endosomal escape, I remain hopeful for the future of RNA-based therapeutics. Transient gene therapies don't come with the ethical issues of permanent genetic manipulation in technologies like CRISPR, but still lead to gene knockdown long enough for disease mediation. The first RNAi-mediated therapy was FDA-approved in 2018, and I feel the next 10 years will bring a host of new, targeted, RNAi-mediated carriers.

APPENDIX

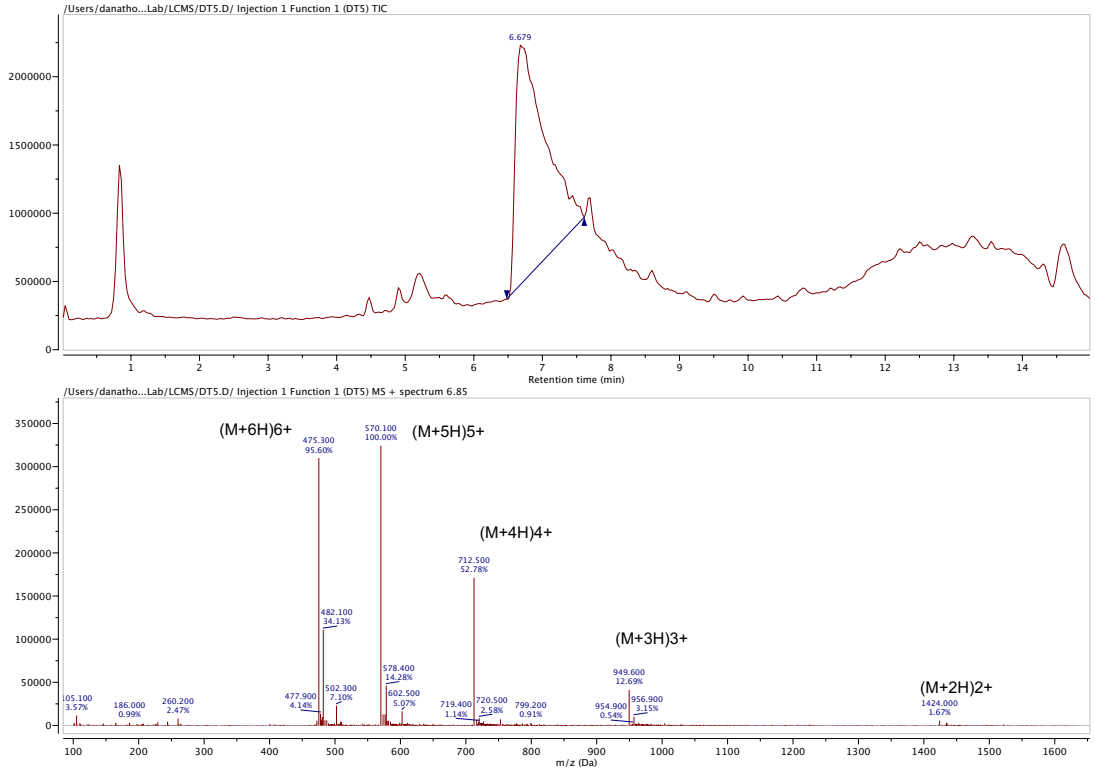

Appendix A.1 LCMS analysis of parent Melittin peptide. TIC trace for elution time of peptide (6.679 mins) and corresponding mass spectra. Expected mass 2845.74. Detected $(M+2H)^{2+}$ 1424.000, $(M+3H)^{3+}$ 949.600, $(M+4H)^{4+}$ 712.500, $(M+5H)^{5+}$ 570.100, $(M+6H)^{6+}$ 475.300.

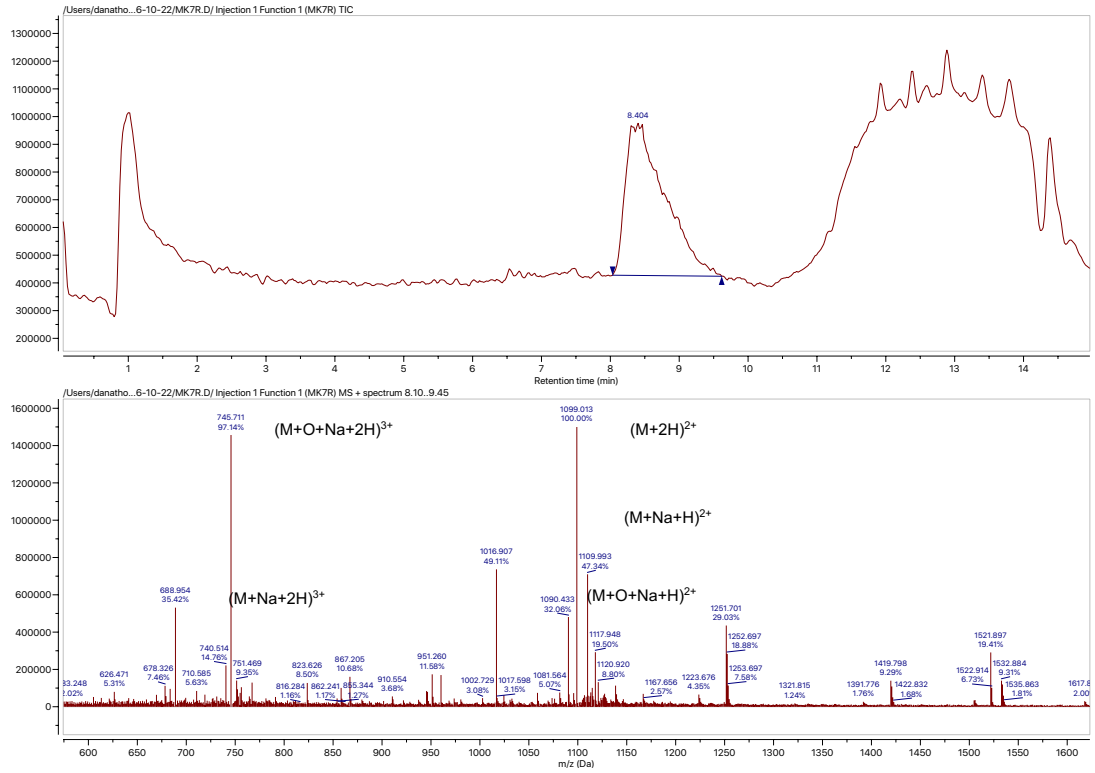

Appendix A.2 LCMS analysis of parent MK7R, truncated Melittin peptide analog. TIC trace for elution time of peptide (8.404 mins) and corresponding mass spectra. Some apparent oxidation of presumably tryptophan residue was detected. Expected mass of parent peptide 2195.32. Expected mass of singly oxidized peptide 2227.31. Detected $(M+2H)^{2+}$ 1099.013, $(M+O+Na+2H)^{3+}$ 745.711.

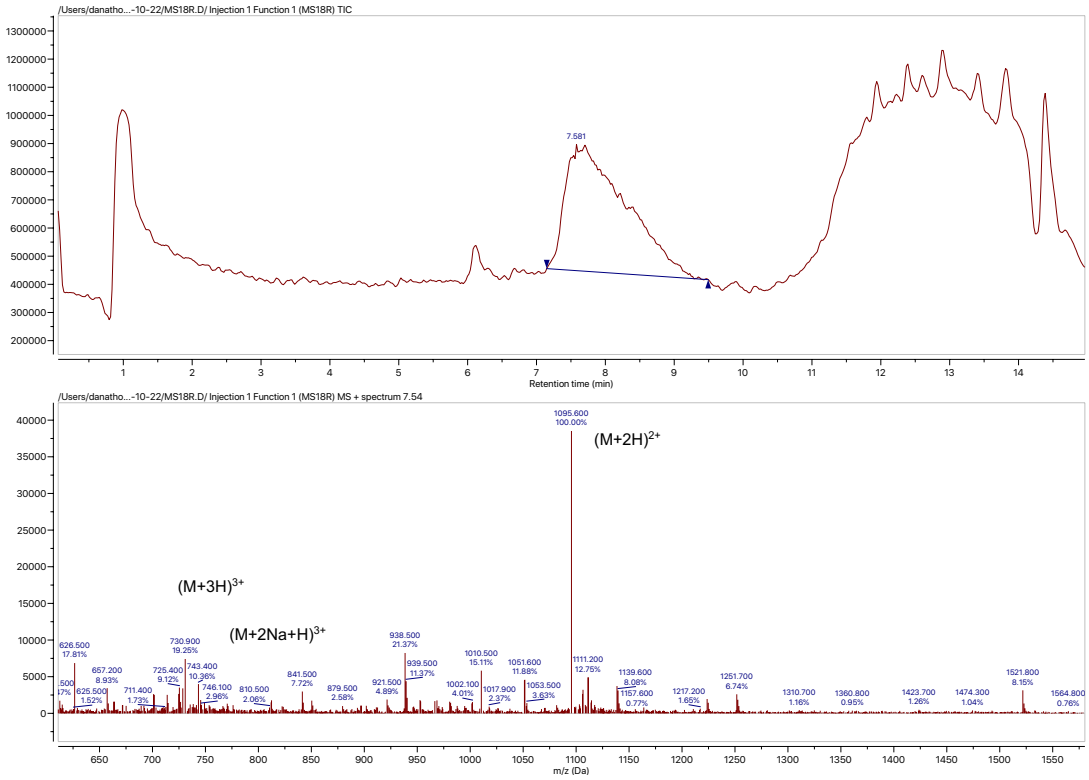

Appendix A.3 LCMS analysis of parent MS18R, truncated Melittin peptide analog. TIC trace for elution time of peptide (7.581 mins) and corresponding mass spectra. Expected mass 2188.36. Detected $(M+2H)^{2+}$ 1095.600, $(M+3H)^{3+}$ 730.900.

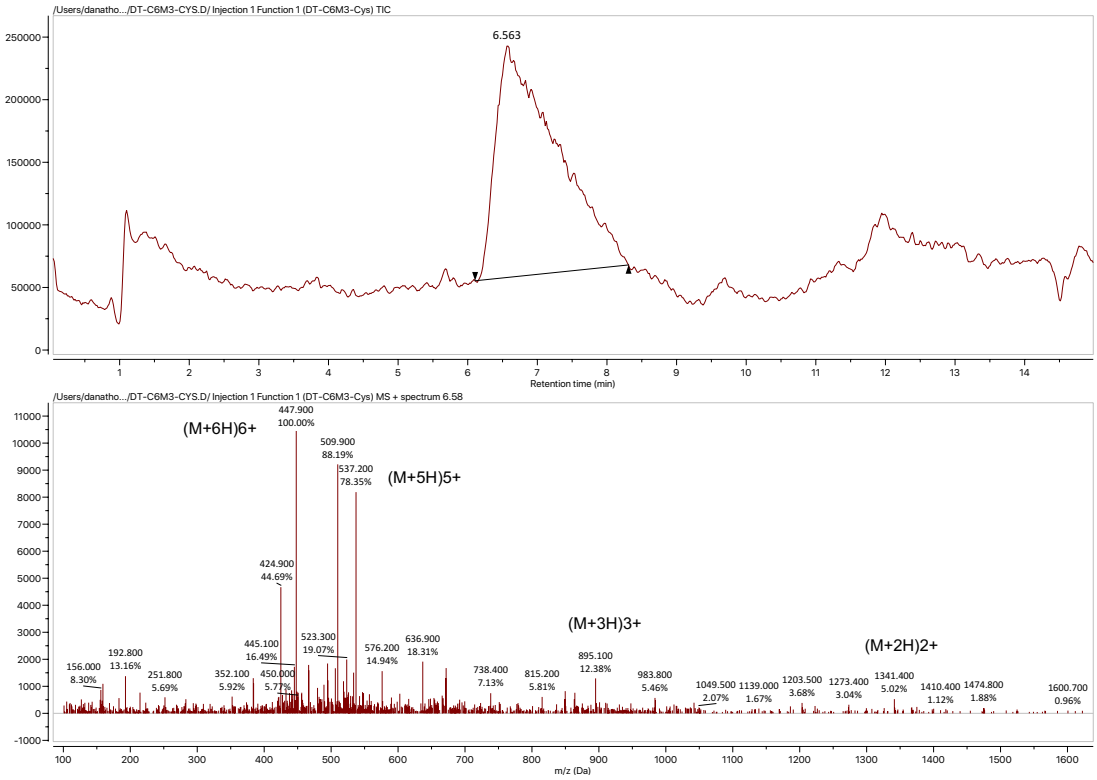

Appendix A.4 LCMS analysis of C6M3 Parent Peptide. TIC trace for elution time of C6M3 (6.563 mins) and corresponding mass spectra. Expected mass 2681.57. Detected $(M+2H)^{2+}$ 1341.400, $(M+3H)^{3+}$ 895.100, $(M+4H)^{4+}$ 671.800, $(M+5H)^{5+}$ 537.200, $(M+6H)^{6+}$ 447.900.

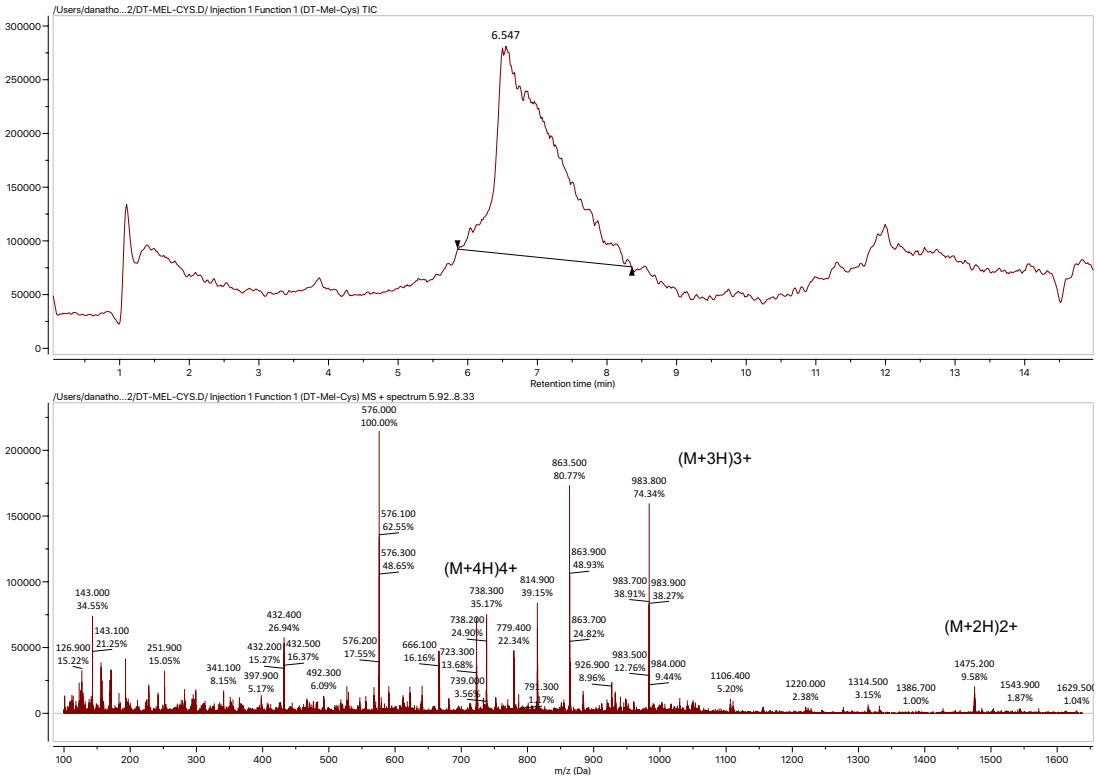

Appendix A.5 LCMS analysis of parent Mel-Cys peptide. TIC trace for elution time of peptide (6.547 mins) and corresponding mass spectra. Expected mass 2948.75. Detected $(M+2H)^{2+}$ 1475.200, $(M+3H)^{3+}$ 983.800, $(M+4H)^{4+}$ 738.300

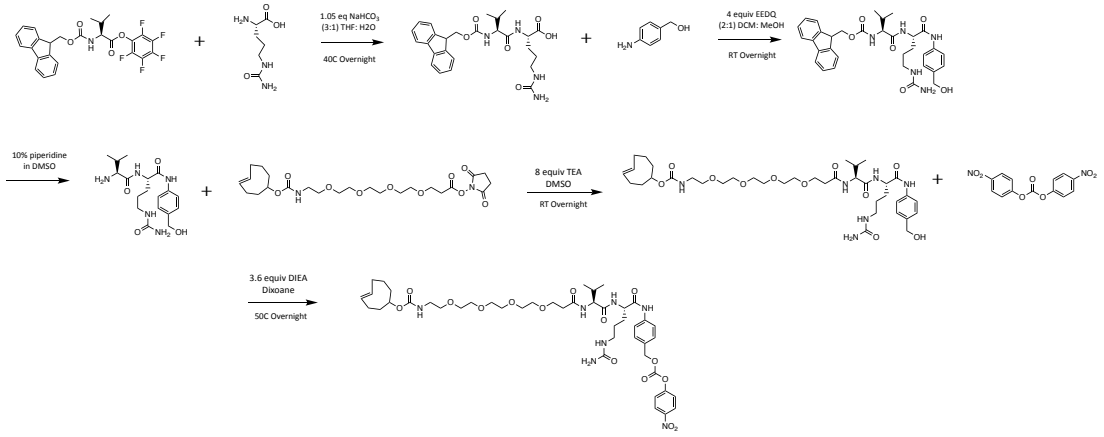

Appendix A.6 Synthesis Scheme of TCO-functionalized, amine-reactive, self-immolative, CatB-cleavable linker with Phe-Cit cleavable site.

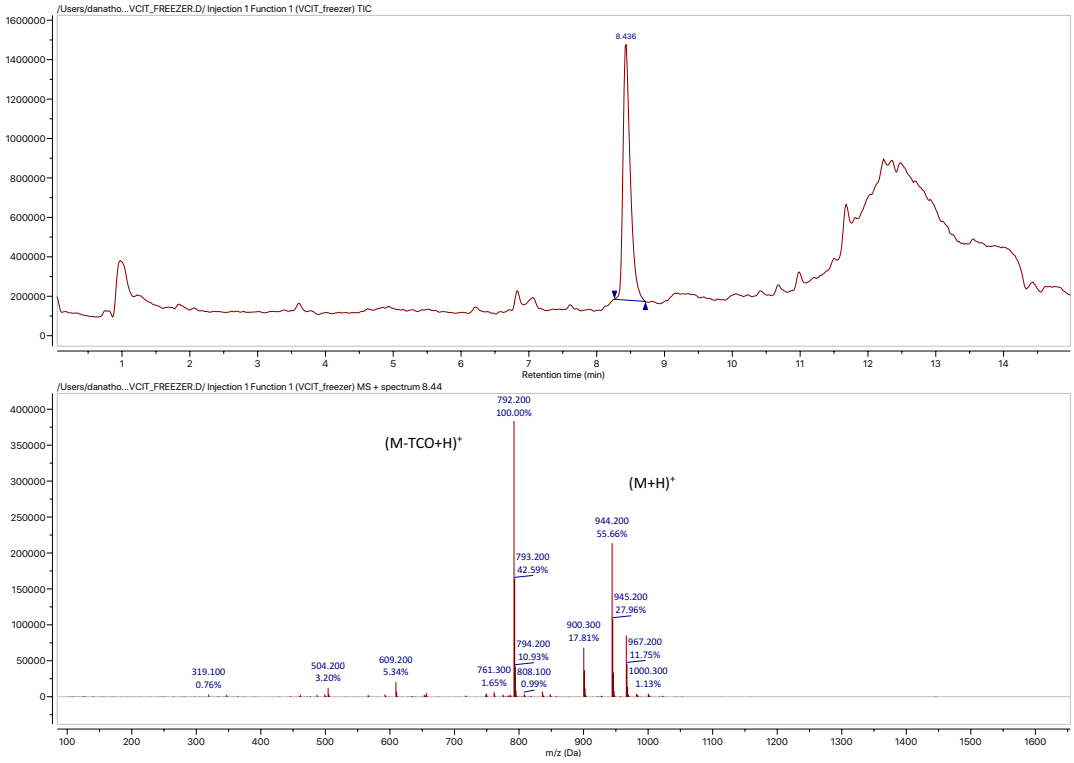

Appendix A.7 LCMS analysis of TCO-functionalized, amine-reactive, self-immolative, CatB-cleavable linker with Val-Cit cleavable site. TIC trace for elution time of linker (8.436 mins) and corresponding mass spectra. Fragmentation tends to occur at carbamate bond, generating a fragment lacking the TCO mass (-153.09). Expected mass 943.45. Detected $(M+H)^+$ 944.200.

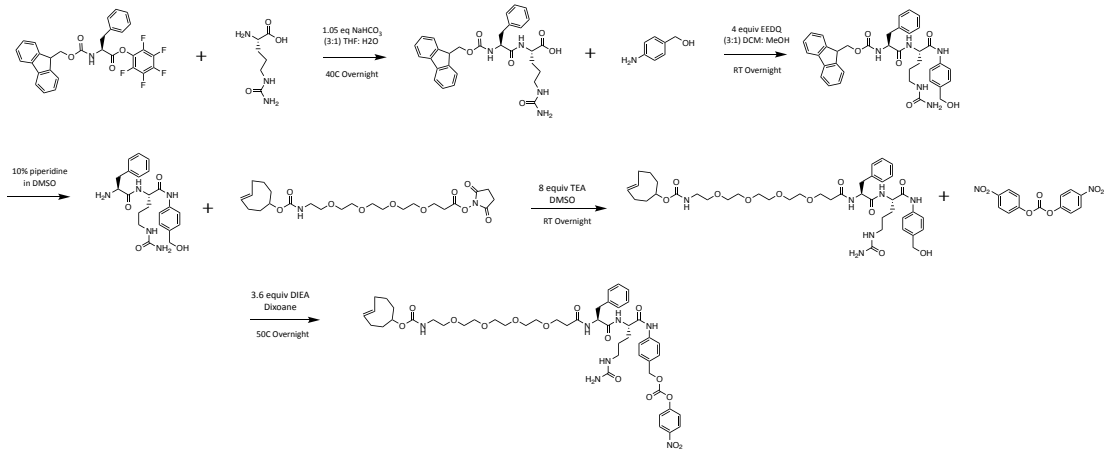

Appendix A.8 Synthesis Scheme of TCO-functionalized, amine-reactive, self-immolative, CatB-cleavable linker with Phe-Cit cleavable site.

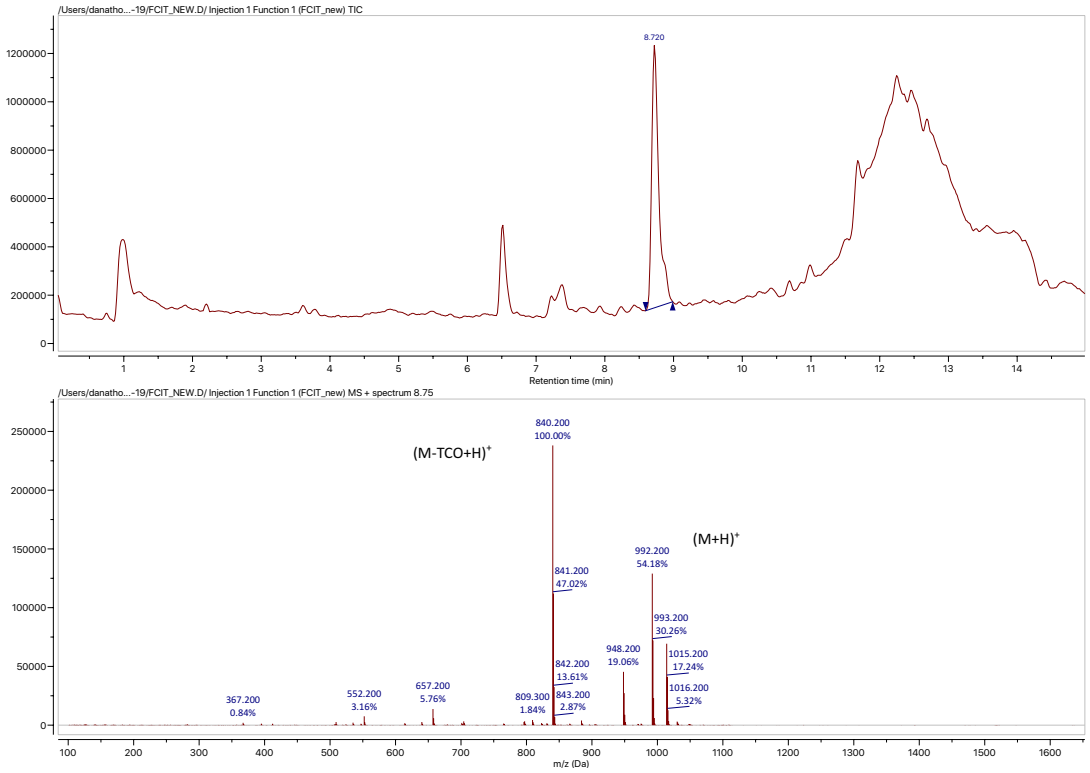

Appendix A.9 LCMS analysis of TCO-functionalized, amine-reactive, self-immolative, CatB-cleavable linker with Phe-Cit cleavable site. TIC trace for elution time of linker (8.720 mins) and corresponding mass spectra. Fragmentation tends to occur at carbamate bond, generating a fragment lacking the TCO mass (-153.09). Expected mass 991.45. Detected $(M+H)^+$ 992.200.

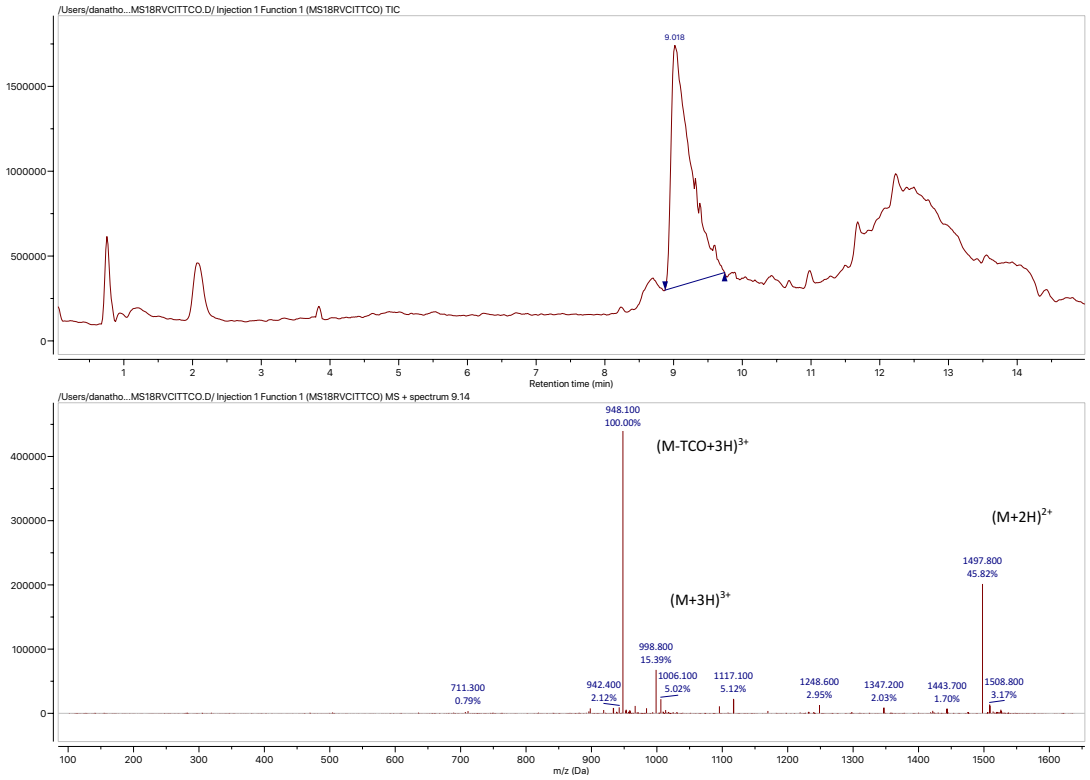

Appendix A.10 LCMS analysis of MS18R, truncated Melittin peptide analog, conjugated with CatB cleavable, TCO-functionalized linker with Val-Cit cleavable site. TIC trace for elution time of peptide conjugate (9.081 mins) and corresponding mass spectra. Fragmentation tends to occur at carbamate bond, generating a fragment lacking the TCO mass (-153.09). Expected mass 2992.78. Detected $(M+2H)^{2+}$ 1497.800, $(M+3H)^{3+}$ 998.800.

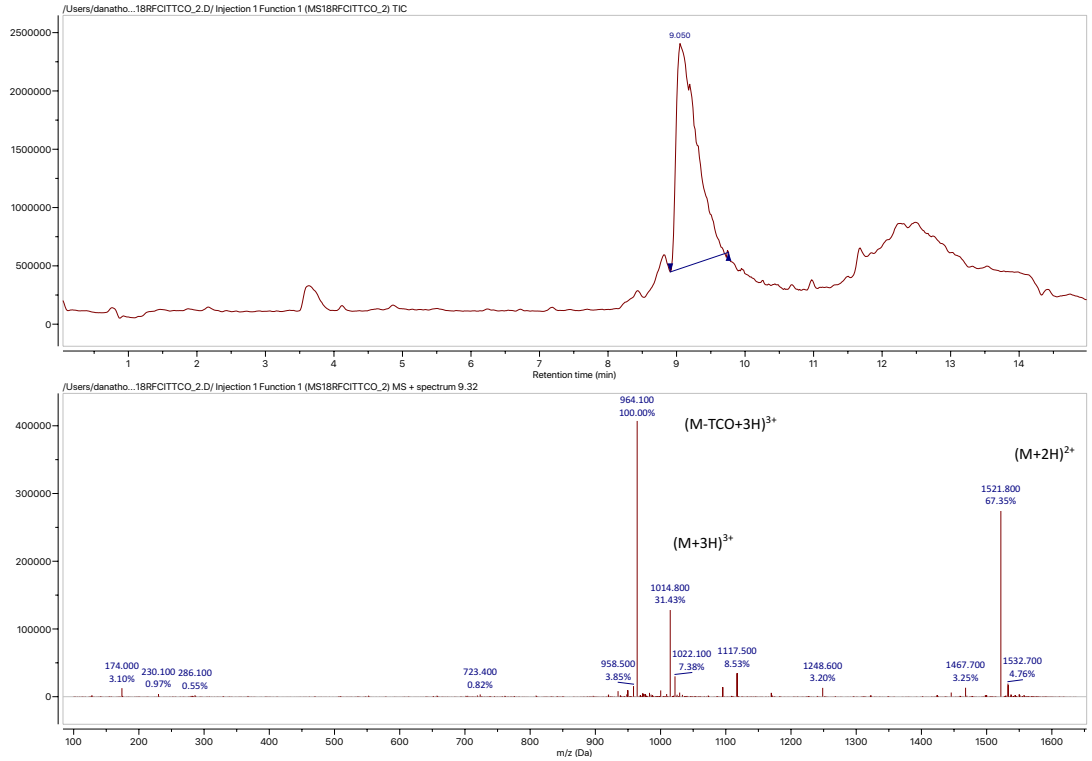

Appendix A.11 LCMS analysis of MS18R, truncated Melittin peptide analog, conjugated with CatB cleavable, TCO-functionalized linker with Phe-Cit cleavable site. TIC trace for elution time of peptide conjugate (9.060 mins) and corresponding mass spectra. Fragmentation tends to occur at carbamate bond, generating a fragment lacking the TCO mass (-153.09). Expected mass 3040.78. Detected $(M+2H)^{2+}$ 1521.800, $(M+3H)^{3+}$ 1014.800.

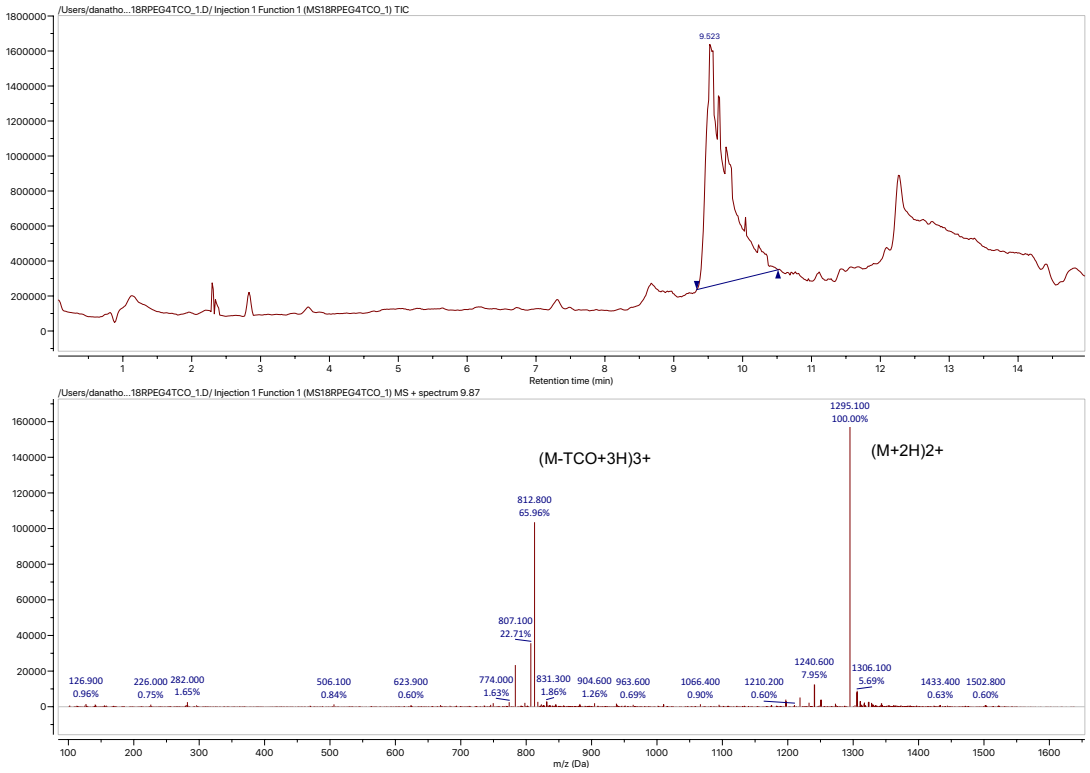

Appendix A.12 LCMS analysis of MS18R, truncated Melittin peptide analog, conjugated with stable, PEG, TCO-functionalized linker. TIC trace for elution time of peptide conjugate (9.523 mins) and corresponding mass spectra. Fragmentation tends to occur at carbamate bond, generating a fragment lacking the TCO mass (-153.09). Expected mass 2588.59. Detected $(M+2H)^{2+}$ 1295.100.

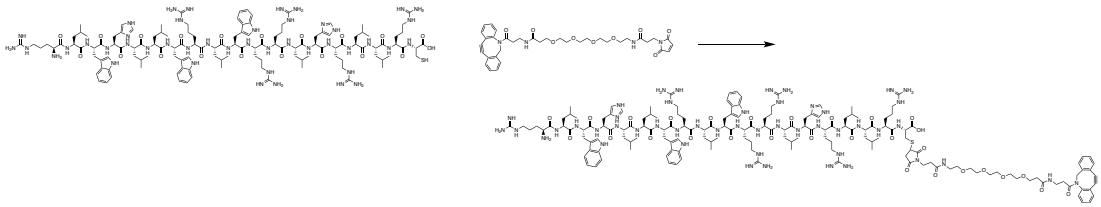

Appendix A.13 Reaction Scheme for C6M3-MAL-PEG4-DBCO Synthesis

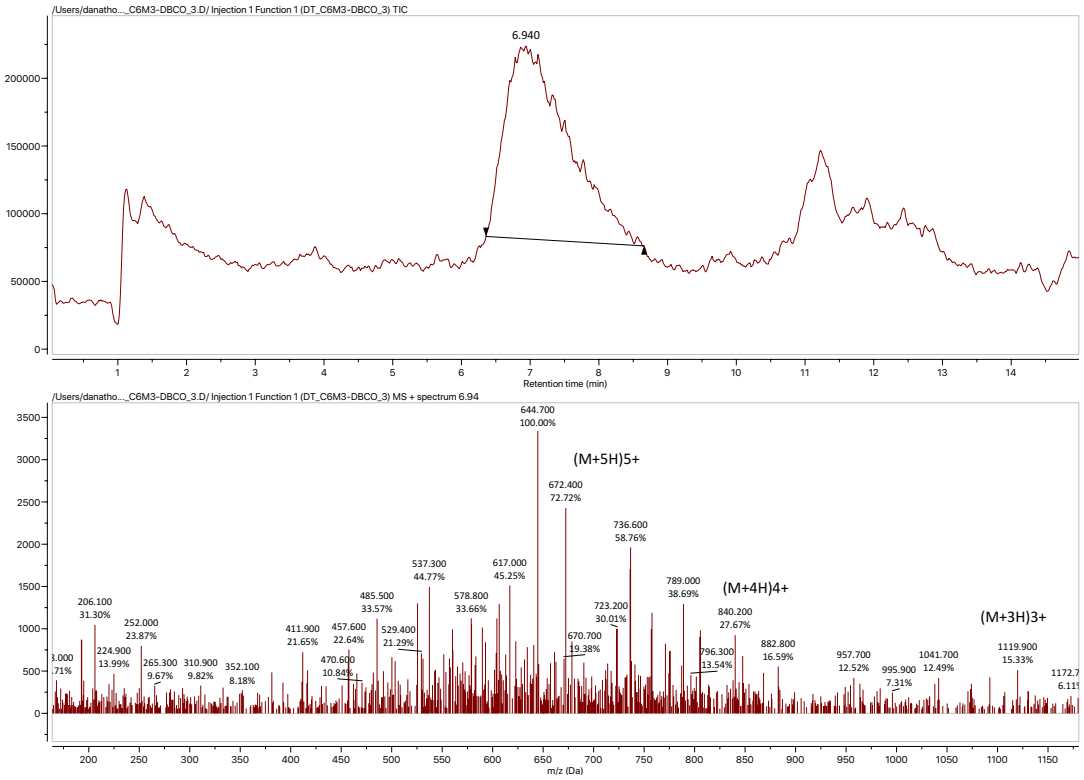

Appendix A.14 LCMS analysis of C6M3-MAL-PEG4-DBCO. TIC Trace for elution time of product (6.940 mins) and corresponding mass spectra. Expected mass 3355.87. Detected $(M+3H)^{3+}$ 1119.900, $(M+4H)^{4+}$ 840.200, $(M+5H)^{5+}$ 672.400.

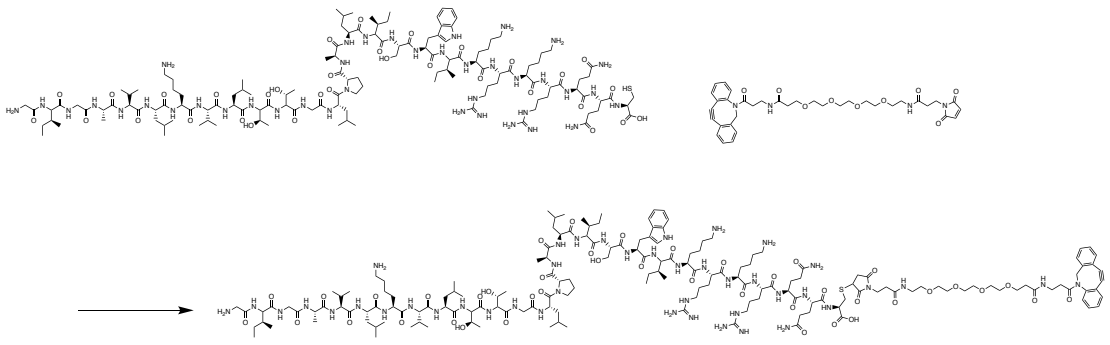

Appendix A.15 Reaction Scheme for Mel-MAL-PEG4-DBCO Synthesis

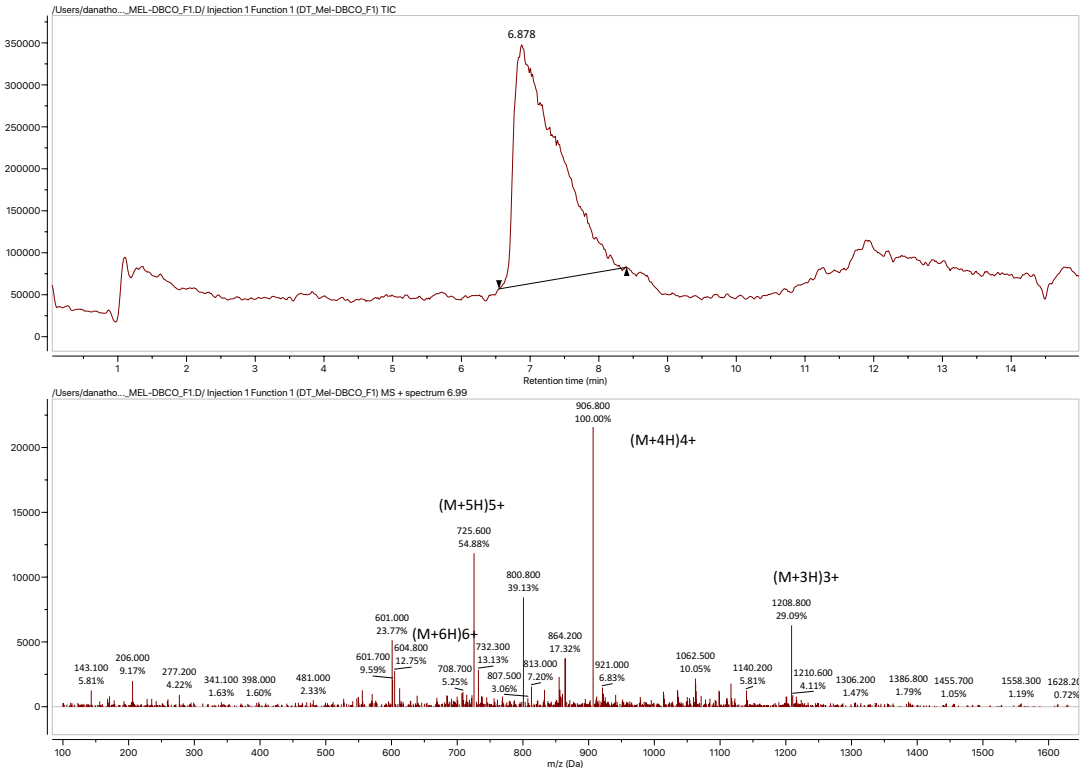

Appendix A.16 LCMS analysis of Mel-MAL-PEG4-DBCO peptide. TIC trace for elution time of peptide (6.878 mins) and corresponding mass spectra. Expected mass 3623.05. Detected $(M+3H)^{3+}$ 1208.800, $(M+4H)^{4+}$ 906.800, $(M+5H)^{5+}$ 725.600

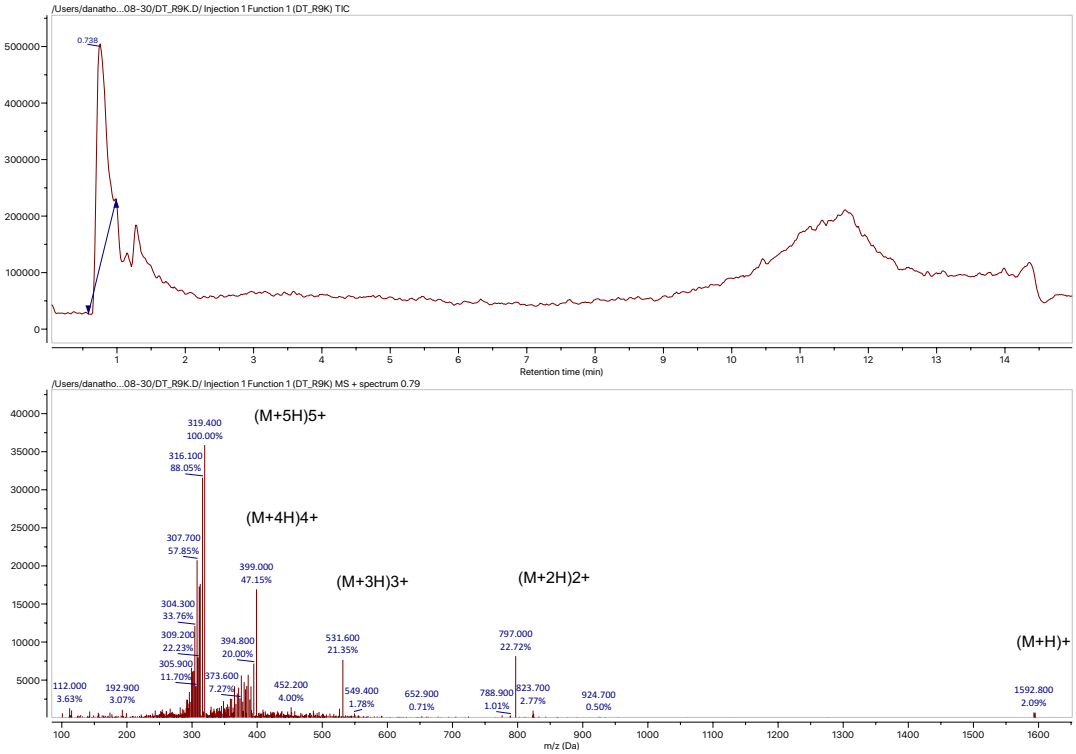

Appendix A.17 LCMS analysis of Parent R9K peptide. TIC trace for elution time of R9K (0.738 mins) and corresponding mass spectra. Expected mass 1592.04. Detected $(M+H)^{+}$ 1592.800, $(M+2H)^{2+}$ 797.000, $(M+3H)^{3+}$ 531.600, $(M+4H)^{4+}$ 399.000, $(M+5H)^{5+}$ 319.400.

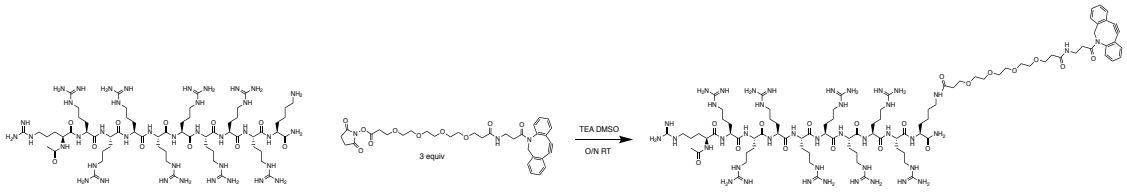

Appendix A.18 Reaction scheme for R9K-PEG4-DBCO Synthesis.

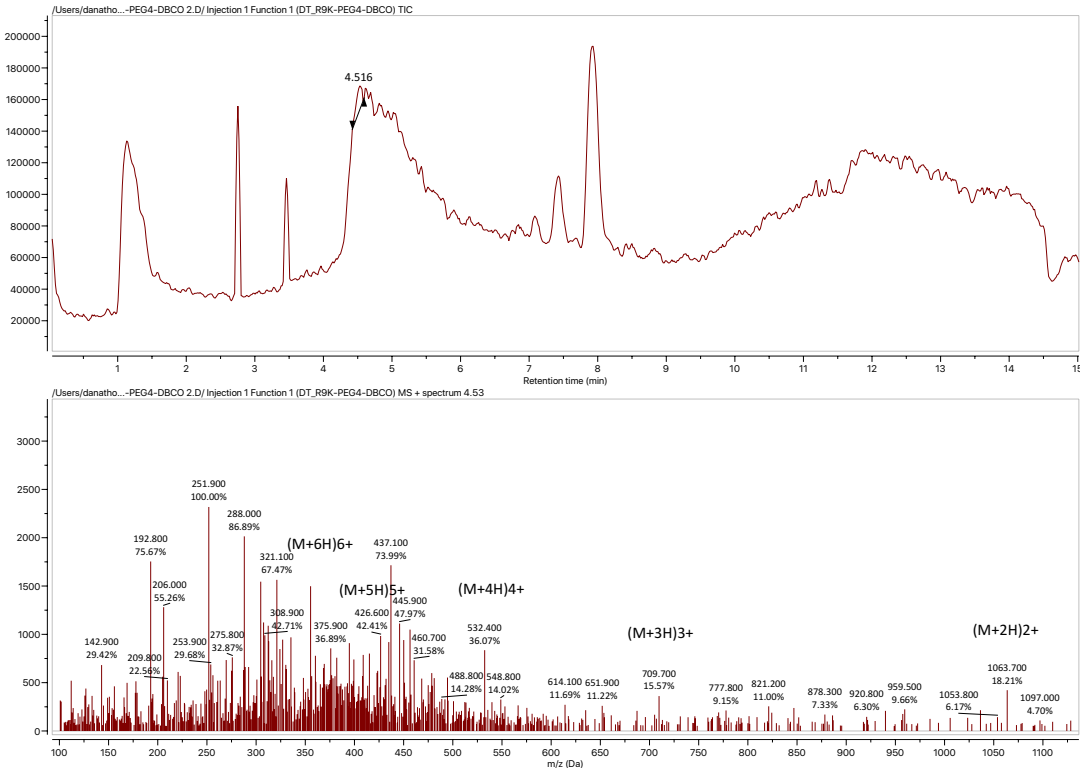

Appendix A.19 LCMS of R9K-PEG4-DBCO Reaction Mixture. TIC trace for elution mixture and corresponding mass spectra. Product elution time is underlined in black (4.516 mins). Expected Mass 2126.28. Detected $(M+2H)^{2+}$ 1063.700, $(M+3H)^{3+}$ 709.700, $(M+4H)^{4+}$ 532.400, $(M+5H)^{5+}$ 426.600.

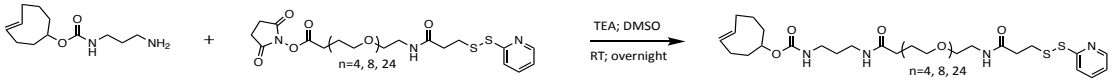

Appendix A.20 Reaction Scheme for TCO-functionalized, reducible linker synthesis with varying PEG lengths. n = 4, 8, or 24 PEG units.

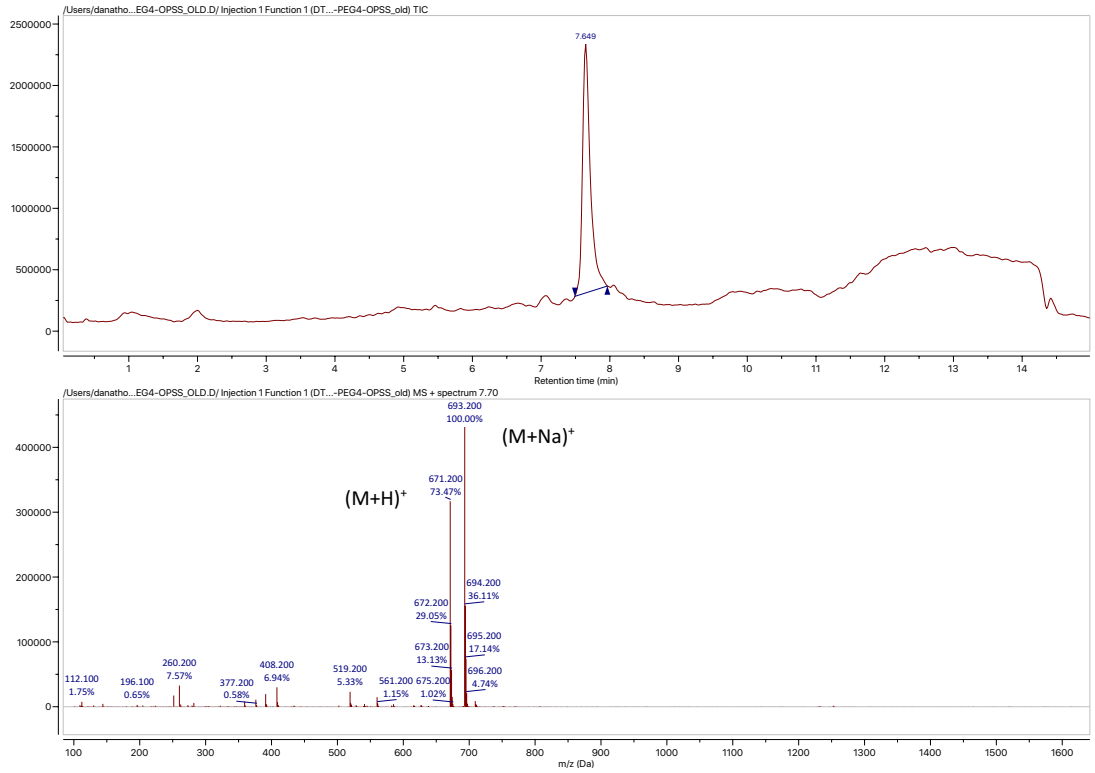

Appendix A.21 LCMS analysis of TCO-PEG$_4$-OPSS, reduction sensitive linker. TIC trace for elution time of linker (7.649 mins) and corresponding mass spectra. Expected mass 670.31. Detected $(M+H)^+$ 671.200, $(M+Na)^+$ 693.200.

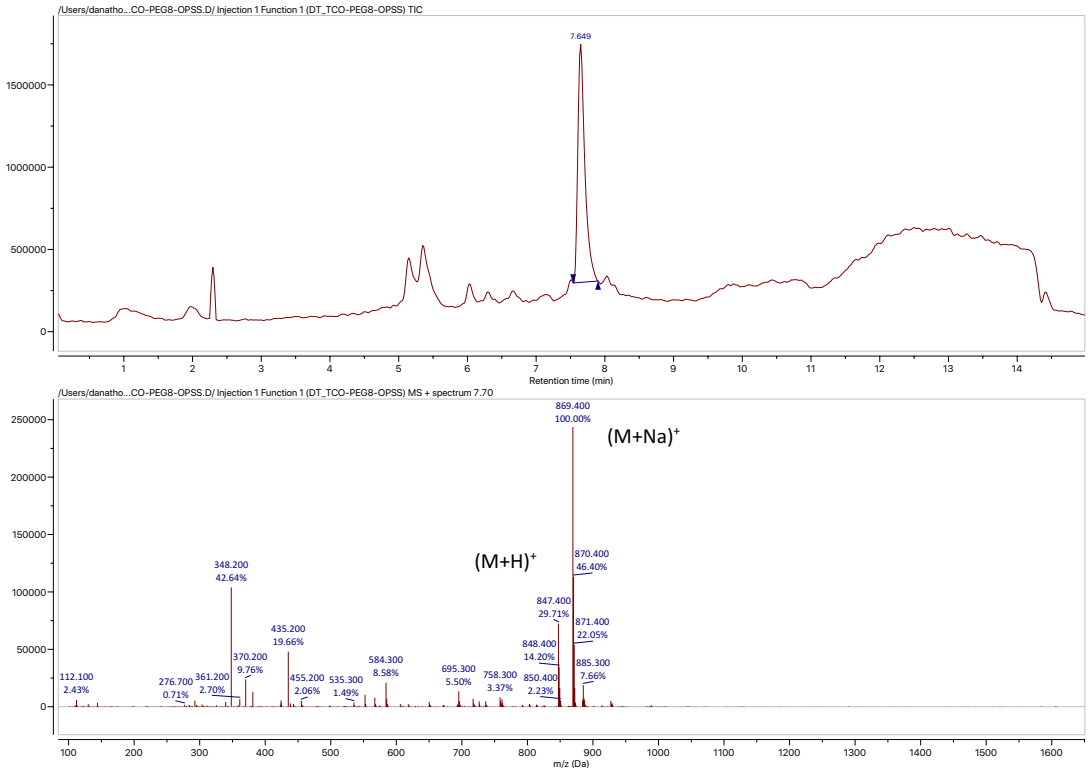

Appendix A.22 LCMS analysis of TCO-PEG$_8$-OPSS, reduction sensitive linker. TIC trace for elution time of linker (7.649 mins) and corresponding mass spectra. Expected mass 846.41. Detected $(M+H)^+$ 847.400, $(M+Na)^+$ 869.400.

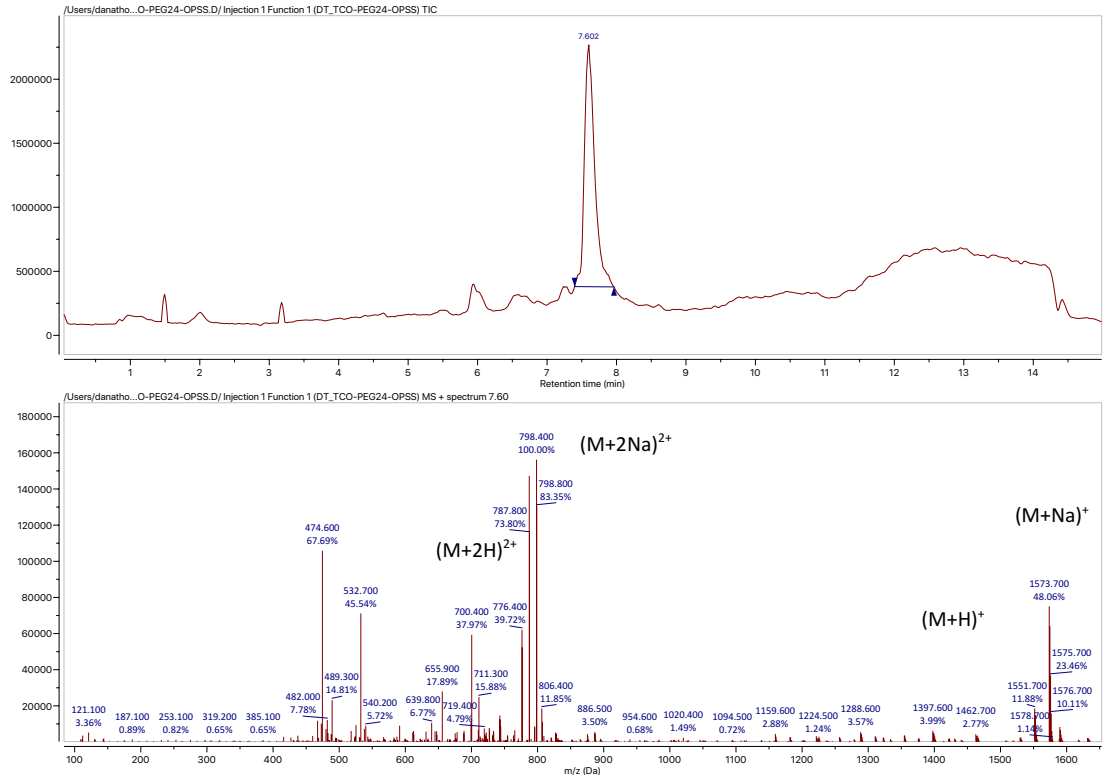

Appendix A.23 LCMS analysis of TCO-PEG$_{24}$-OPSS, reduction sensitive linker. TIC trace for elution time of linker (7.602 mins) and corresponding mass spectra. Expected mass 1550.83. Detected $(M+H)^+$ 1551.700, $(M+Na)^+$ 1573.700, $(M+2H)^{2+}$ 787.800, $(M+2Na)^{2+}$ 798.400.

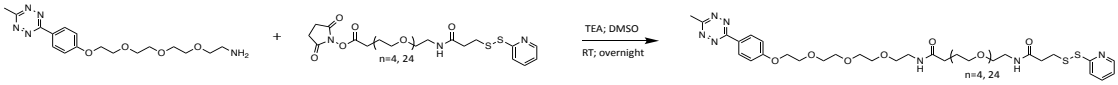

Appendix A.24 Reaction Scheme for methyl tetrazine-functionalized, reducible linker synthesis with varying PEG lengths. n = 4 or 24 PEG units.

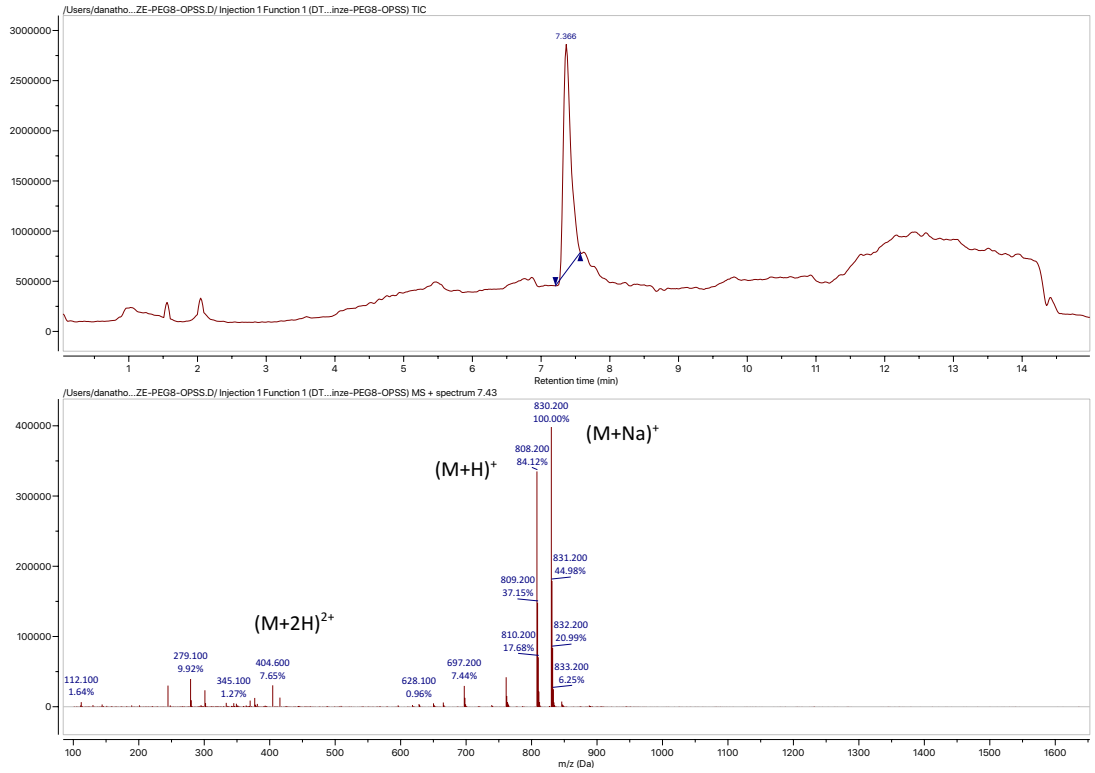

Appendix A.25 LCMS analysis of MeTzine-PEG$_8$-OPSS, reduction sensitive linker. TIC trace for elution time of linker (7.366 mins) and corresponding mass spectra. Expected mass 807.33. Detected $(M+H)^+$ 808.200, $(M+Na)^+$ 830.200, $(M+2H)^{2+}$ 404.600.

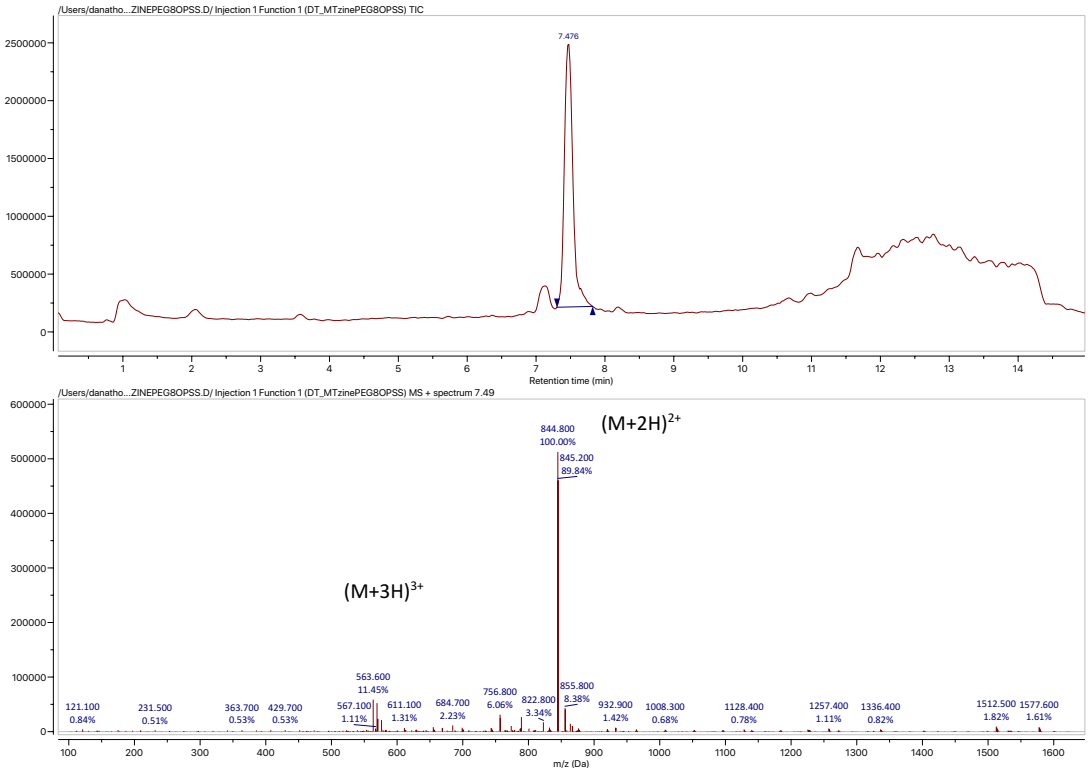

Appendix A.26 LCMS analysis of MeTzine-PEG$_{28}$-OPSS, reduction sensitive linker. TIC trace for elution time of linker (7.476 mins) and corresponding mass spectra. Expected mass 1687.85. Detected $(M+2H)^{2+}$ 844.800, $(M+3H)^{3+}$ 563.600.

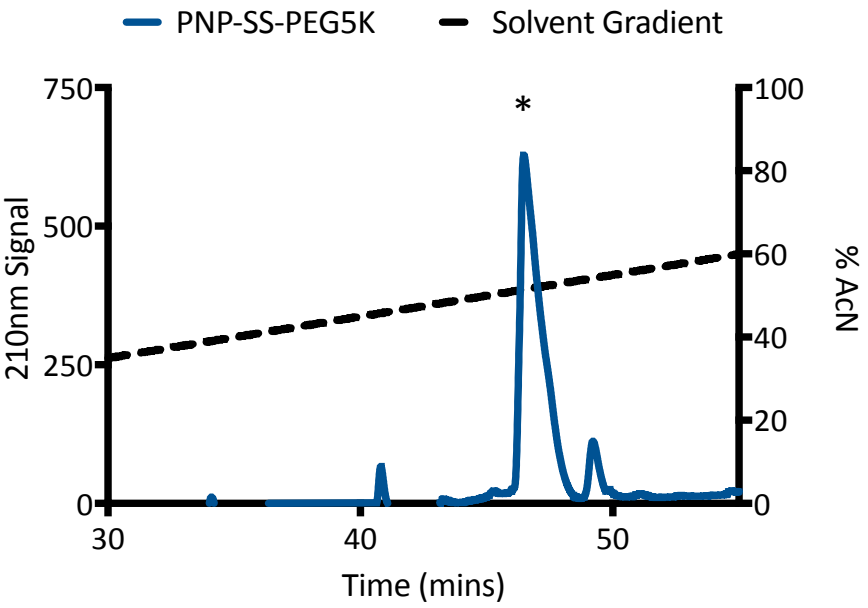

Appendix A.27 HPLC Trace of Amine-reactive, reduction sensitive PEGylation reagent on a C18 column on a gradient of AcN in water.

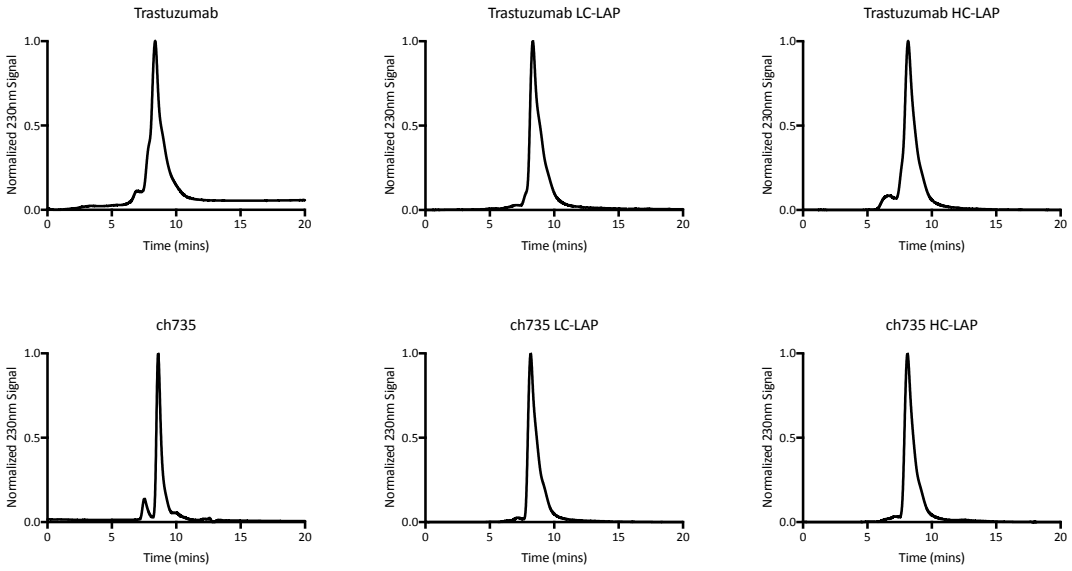

Appendix A.28 Size Exclusion Chromatography Traces of Antibodies purified from 293F cells, with or without LAP tag incorporated. All antibodies elute at ~9 mins and show few aggregates across both antibody types, with and without the LAP tag.

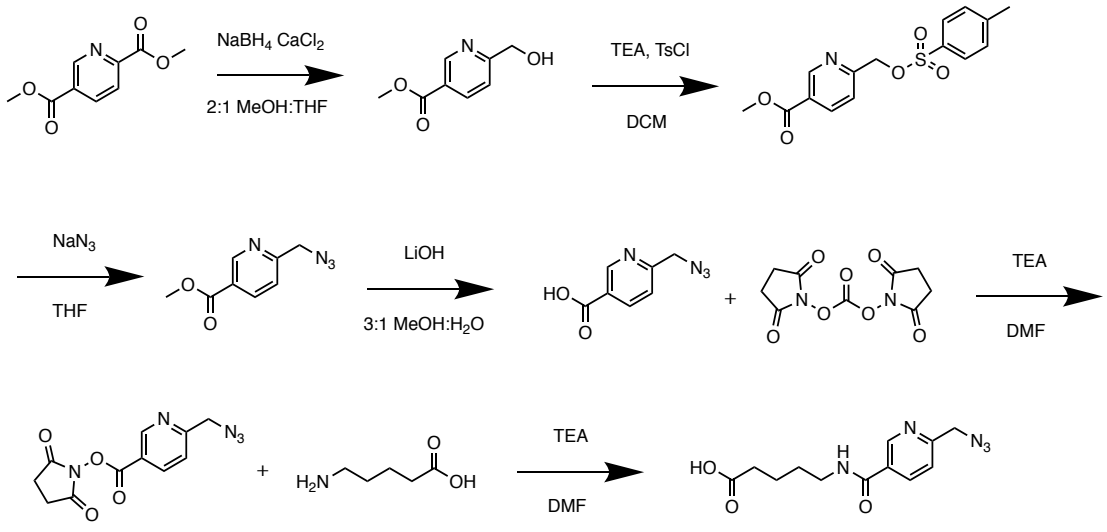

Appendix A.29 Synthesis Scheme for pAz substrate for LplA chemoenzymatic ligation.

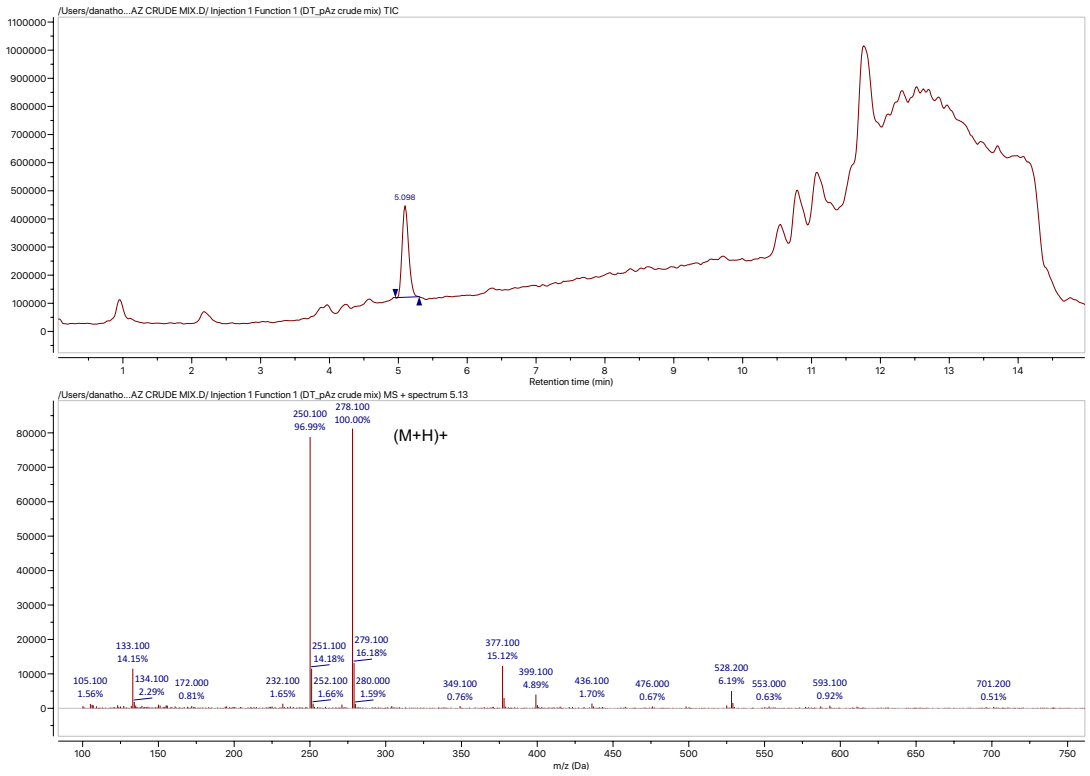

Appendix A.30 LCMS analysis of pAz substrate for LplA chemoenzymatic ligation. TIC trace for elution time of linker (5.098 mins) and corresponding mass spectra. Expected mass 277.12. Detected $(M+H)^+$ 278.100.

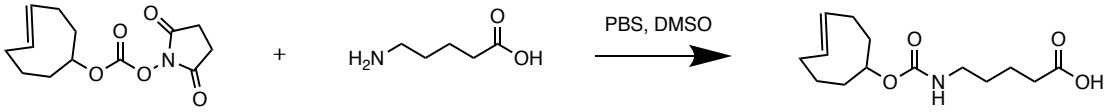

Appendix A.31 Synthesis Scheme for TCO-LAP substrate for LplA chemoenzymatic ligation.

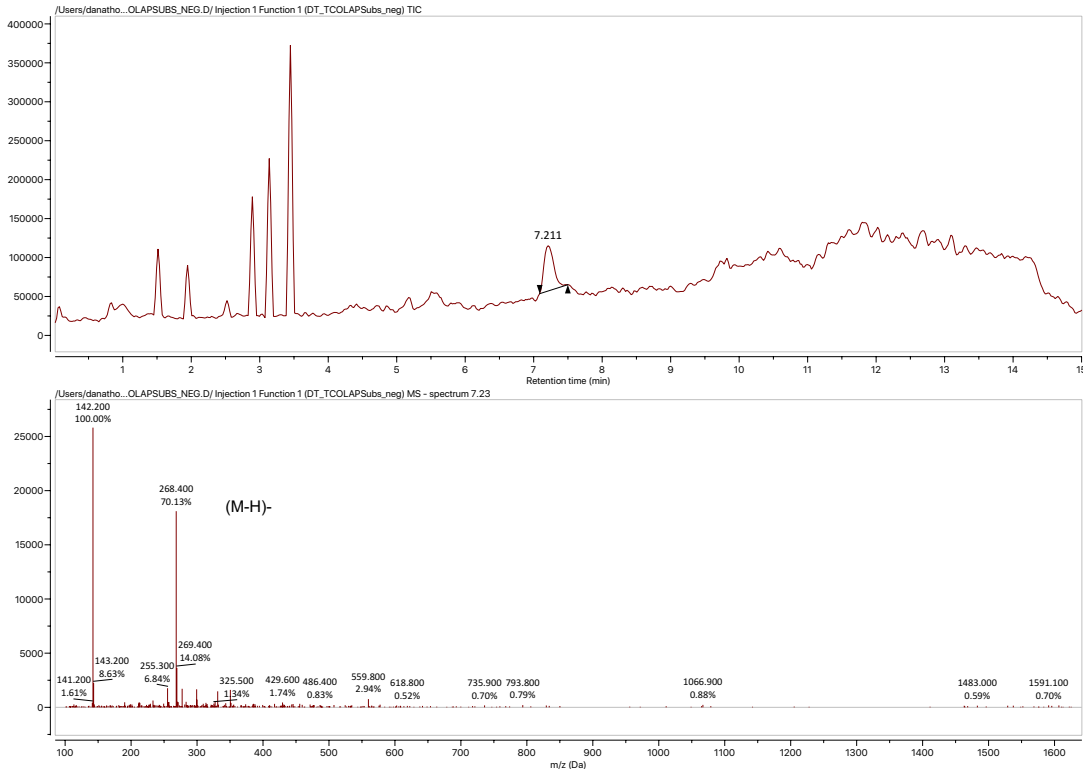

Appendix A.32 LCMS analysis of TCO-LAP substrate for LplA chemoenzymatic ligation. TIC trace for elution time of linker (7.211 mins) and corresponding mass spectra. Expected mass 269.16. Detected $(M-H)^-$ 268.400.

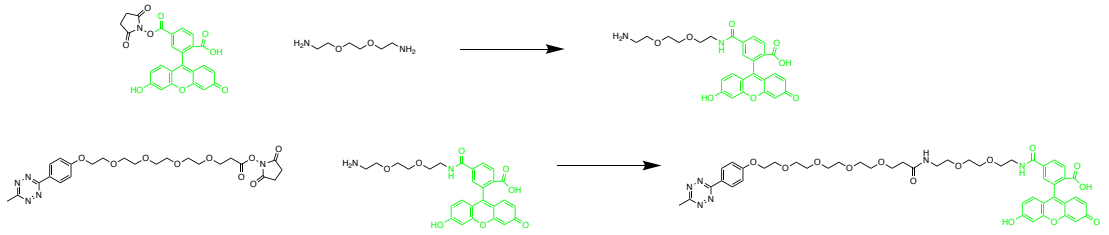

Appendix A.33 Synthesis Scheme for MeTzine-PEG$_4$-Fluorescein, Stable, non-cleavable Fluorescent

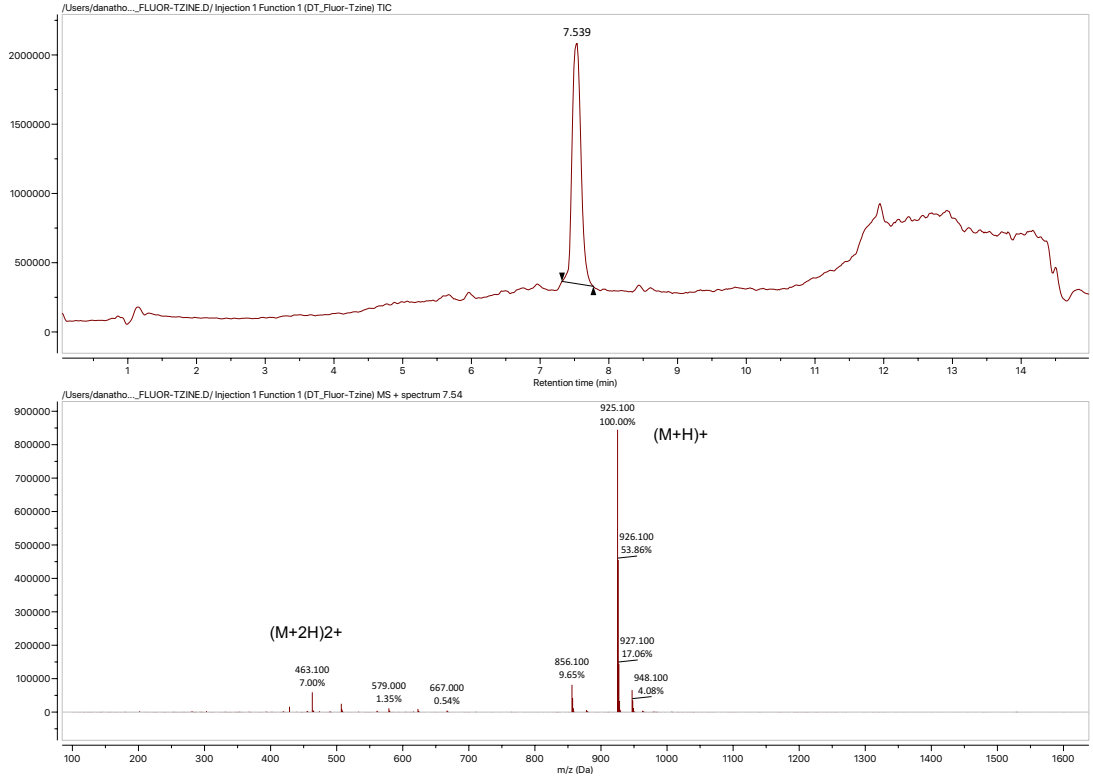

Appendix A.34 LCMS analysis of MeTzine-PEG$_4$-Fluorescein, Stable, non-cleavable Fluorescent Linker. TIC trace for elution time of linker (7.539 mins) and corresponding mass spectra. Expected mass 924.35. Detected $(M+H)^+$ 925.100, $(M+2H)^{2+}$ 463.100

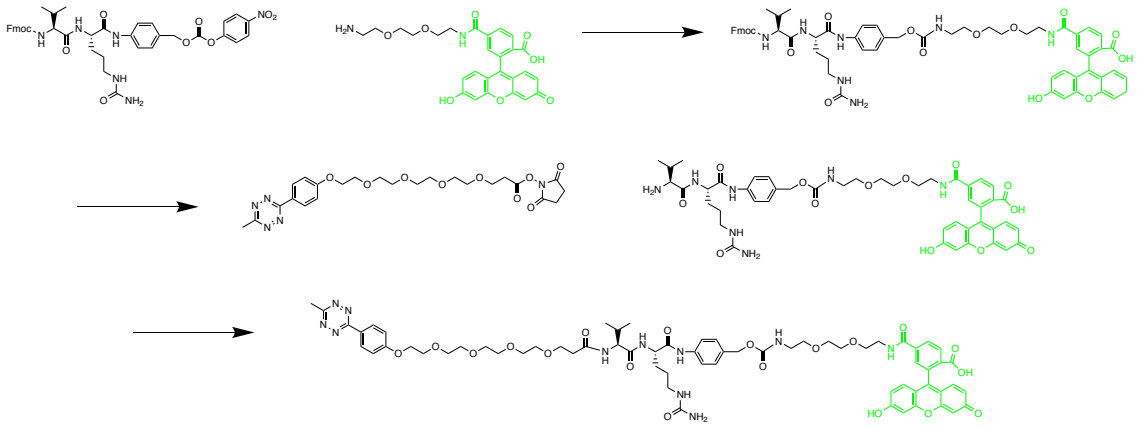

Appendix A.35 Synthesis Scheme for MeTzine-Val-Cit-Fluorescein, CatB-cleavable Fluorescent Linker.

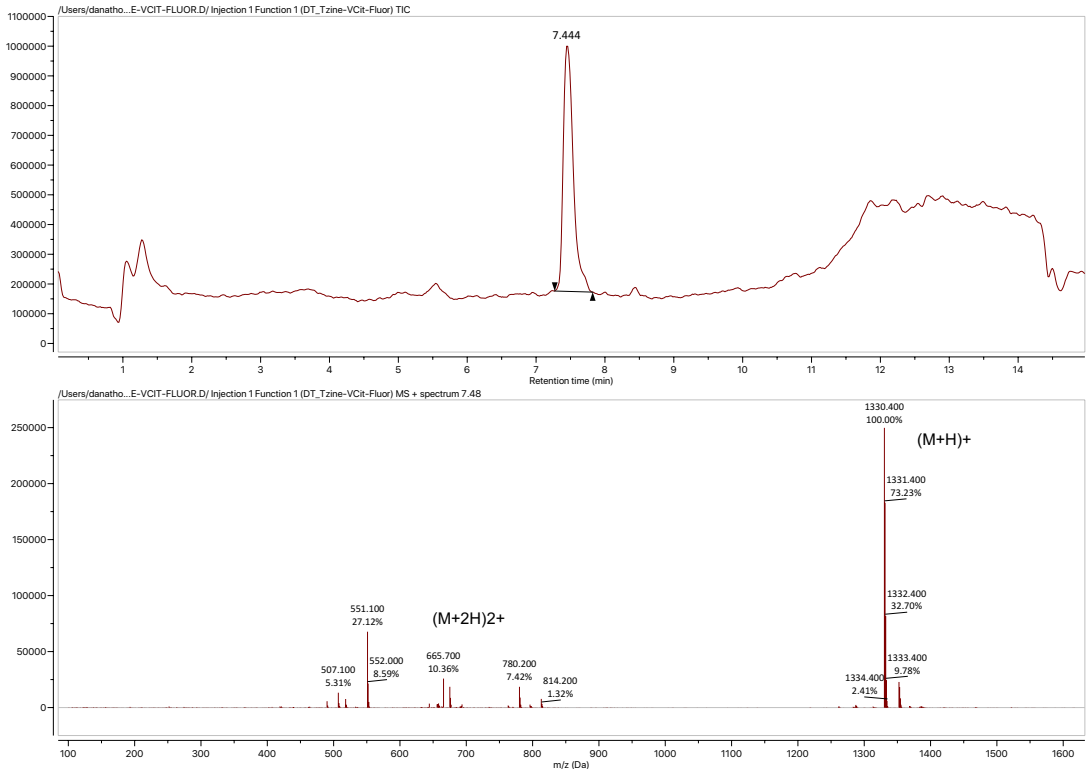

Appendix A.36 LCMS analysis of MeTzine-Val-Cit-Fluorescein, CatB-cleavable Fluorescent Linker. TIC trace for elution time of linker (7.444 mins) and

corresponding mass spectra. Expected mass 1329.56. Detected $(M+H)^+$ 1330.400, $(M+2H)^{2+}$ 665.700

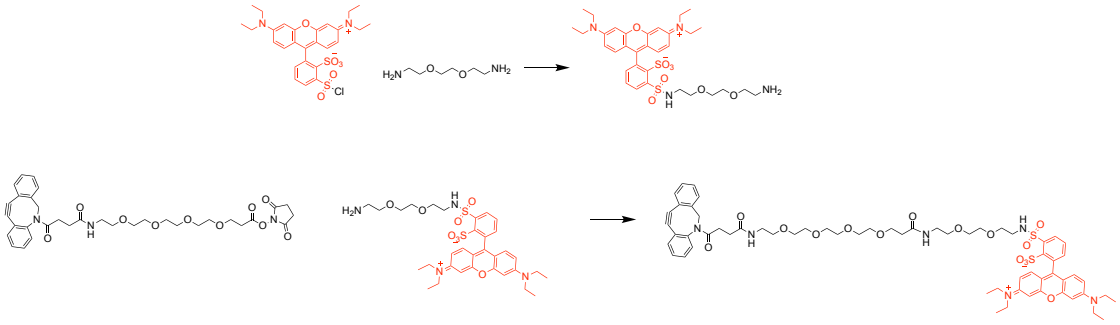

Appendix A.37 Synthesis scheme for DBCO-PEG_4-Rhodamine, stable, non-cleavable Fluorescent Linker.

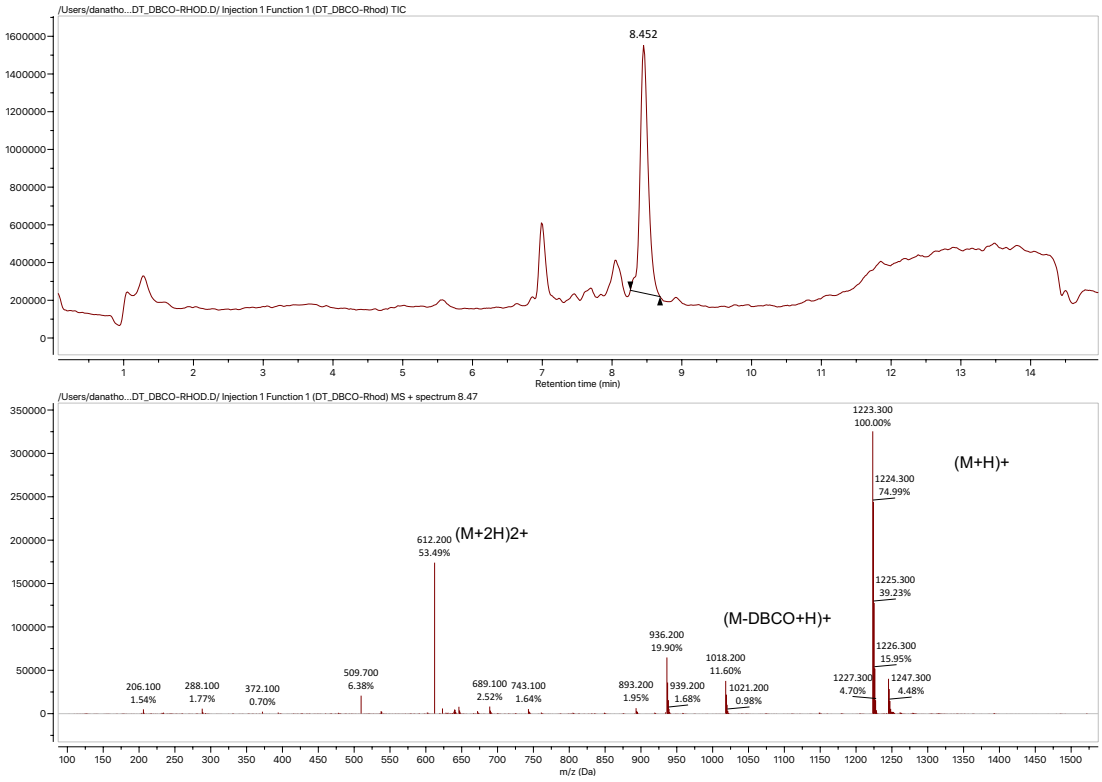

Appendix A.38 LCMS analysis of DBCO-PEG_4-Rhodamine, stable, non-cleavable Fluorescent Linker. TIC trace for elution time of linker (8.452 mins) and corresponding mass spectra. DBCO tends to fragment at the tertiary amide on the DBCO ring (M-187.1). Expected mass 1222.35. Detected $(M+H)^+$ 1223.300, $(M+2H)^{2+}$ 612.200

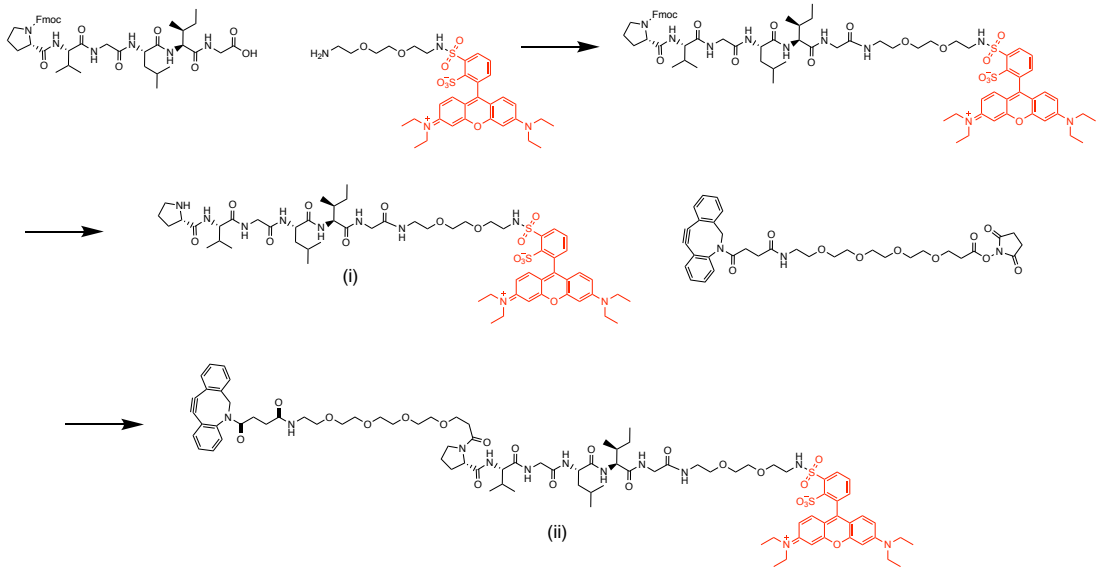

Appendix A.39 Synthesis scheme for Rhodamine-PVGLIG-PEG$_4$-DBCO, the MMP-2 cleavable Fluorescent Linker.

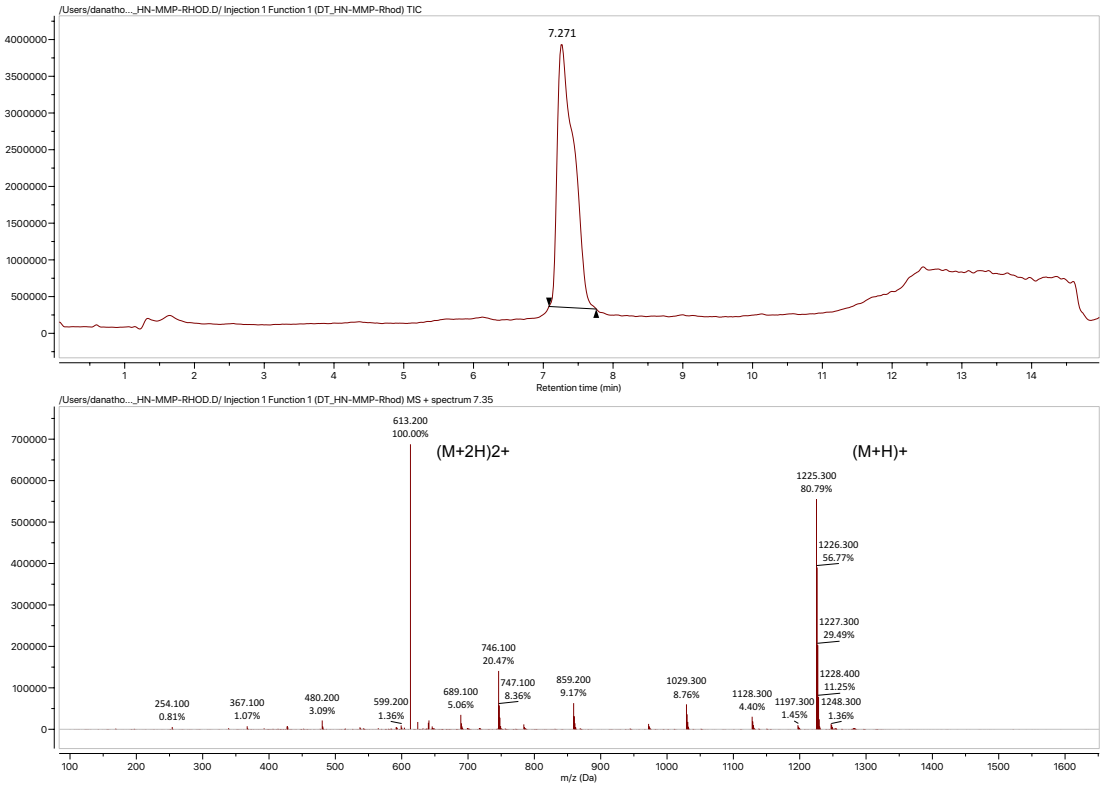

Appendix A.40 LCMS analysis of Rhodamine-PVGLIG-NH2, intermediate product [Appendix 39(i)] for synthesis of MMP-2 cleavable Fluorescent Linker. TIC trace for elution time of linker (7.271 mins) and corresponding mass spectra. Expected mass 1224.59. Detected $(M+H)^{+}$ 1225.300, $(M+2H)^{2+}$ 613.200.

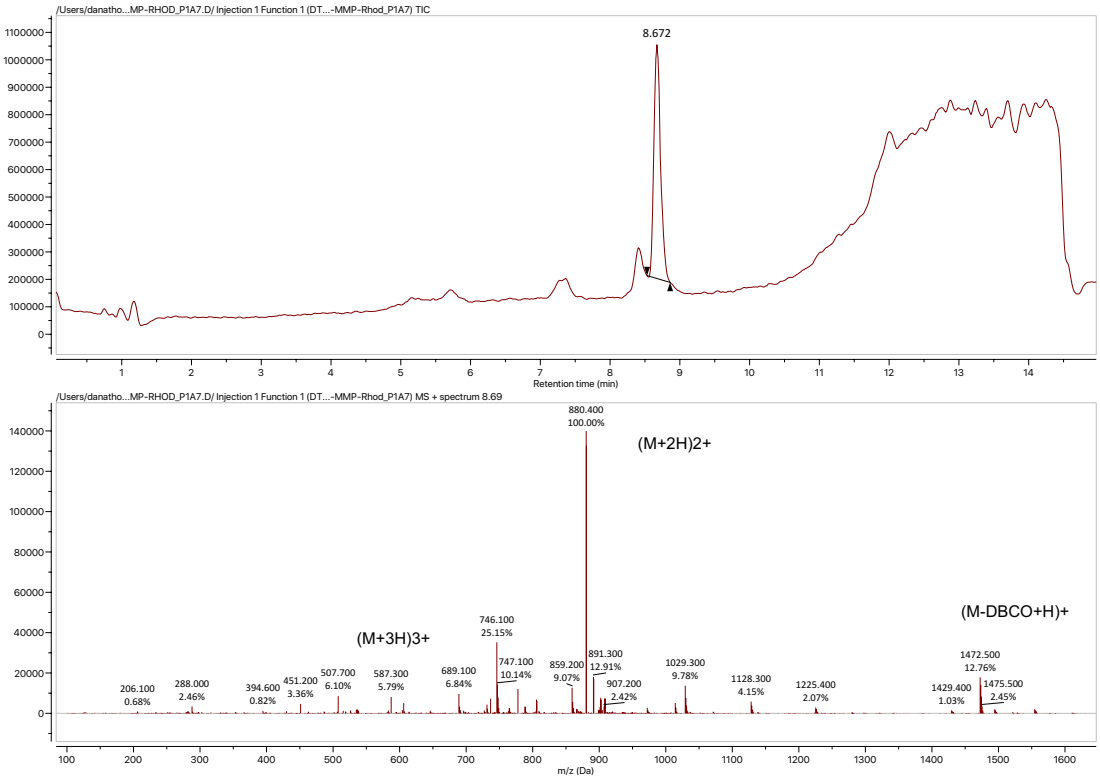

Appendix A.41 LCMS analysis of final Rhodamine-PVGLIG-PEG$_4$-DBCO, the MMP-2 cleavable Fluorescent Linker [Appendix 39(ii)]. TIC trace for elution time of linker (8.672 mins) and corresponding mass spectra. DBCO tends to fragment at the tertiary amide on the DBCO ring (M-187.1). Expected mass 1758.83. Detected $(M+2H)^{2+}$ 880.400, $(M+3H)^{3+}$ 587.300.

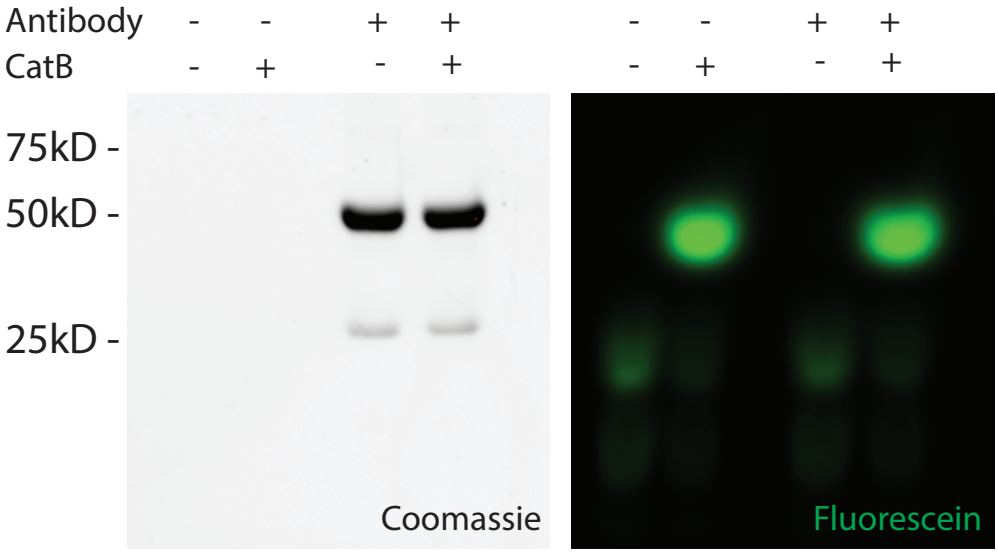

Appendix A.42 SDS-PAGE of antibody and Tzine-Val-Cit-Fluorescein Linker control. (Left) Coomassie stain for protein (Right) Fluorescein channel for linker. Non-conjugated linker was treated with CatB and analyzed on SDS-PAGE for band location relative to the antibody.

REFERENCES

1. Carter, P. J. Potent antibody therapeutics by design. *Nat Rev Immunol* **6,** 343–357 (2006).
2. Weiner, G. J. Building better monoclonal antibody-based therapeutics. *Nature Publishing Group* **15,** 361–370 (2015).
3. Köhler, G. & Milstein, C. Continuous cultures of fused cells secreting antibody of predefined specificity. *Nature* **256,** 495–497 (1975).
4. Scott, A. M. *et al.* A phase I clinical trial with monoclonal antibody ch806 targeting transitional state and mutant epidermal growth factor receptors. *Proceedings of the National Academy of Sciences* **104,** 4071–4076 (2007).
5. Scott, A. M., Wolchok, J. D. & Old, L. J. Antibody therapy of cancer. 1–10 (2012). doi:10.1038/nrc3236
6. Johnson, P. & Glennie, M. The mechanisms of action of rituximab in the elimination of tumor cells. *Seminars in Oncology* **30,** 3–8 (2003).
7. Byrd, J. C. *et al.* The mechanism of tumor cell clearance by rituximab in vivo in patients with B-cell chronic lymphocytic leukemia: evidence of caspase activation and apoptosis induction. *Blood* **99,** 1038–1043 (2002).
8. Hodi, F. S. *et al.* Improved Survival with Ipilimumab in Patients with Metastatic Melanoma. *New England Journal of Medicine* **363,** 711–723 (2010).
9. Beck, A., Goetsch, L., Dumontet, C. & Corvaïa, N. Strategies and challenges for the next generation of antibody–drug conjugates. *Nature Publishing Group* **16,** 315–337 (2017).
10. LoRusso, P. M., Weiss, D., Guardino, E., Girish, S. & Sliwkowski, M. X. Trastuzumab Emtansine: A Unique Antibody-Drug Conjugate in Development for Human Epidermal Growth Factor Receptor 2-Positive Cancer. *Clinical Cancer Research* **17,** 6437–6447 (2011).
11. Zein, N., Sinha, A. M., McGahren, W. J. & Ellestad, G. A. Calicheamicin gamma 1I: an antitumor antibiotic that cleaves double-stranded DNA site specifically. *Science* **240,** 1198–1201 (1988).
12. Godwin, C. D., Gale, R. P. & Walter, R. B. Gemtuzumab ozogamicin in acute myeloid leukemia. **31,** 1855–1868 (2017).
13. Strop, P. *et al.* Location Matters: Site of Conjugation Modulates Stability and Pharmacokinetics of Antibody Drug Conjugates. *Chemistry & Biology* **20,** 161–167 (2013).
14. Junutula, J. R. *et al.* Site-specific conjugation of a cytotoxic drug to an antibody improves the therapeutic index. *Nature Biotechnology* **26,** 925–932 (2008).
15. Lotze, J., Reinhardt, U., Seitz, O. & Beck-Sickinger, A. G. Peptide-tags for site-specific protein labelling in vitro and in vivo. *Molecular BioSystems* **12,** 1731–1745 (2016).
16. Zhou, Z. *et al.* Genetically Encoded Short Peptide Tags for Orthogonal Protein Labeling by Sfp and AcpS Phosphopantetheinyl Transferases. *ACS Chemical Biology* **2,** 337–346 (2007).

17. Rabuka, D. Chemoenzymatic methods for site-specific protein modification. *Current Opinion in Chemical Biology* **14,** 790–796 (2010).
18. Zimmerman, E. S. *et al.* Production of Site-Specific Antibody–Drug Conjugates Using Optimized Non-Natural Amino Acids in a Cell-Free Expression System. *Bioconjugate Chemistry* **25,** 351–361 (2014).
19. Hallam, T. J., Wold, E., Wahl, A. & Smider, V. V. Antibody Conjugates with Unnatural Amino Acids. *Mol. Pharmaceutics* **12,** 1848–1862 (2015).
20. Xiao, H. *et al.* Genetic Incorporation of Multiple Unnatural Amino Acids into Proteins in Mammalian Cells. *Angewandte Chemie International Edition* **52,** 14080–14083 (2013).
21. Wang, K. *et al.* Optimized orthogonal translation of unnatural amino acids enables spontaneous protein double-labelling and FRET. *Nature Chemistry* **6,** 393–403 (2014).
22. Cohen, J. D., Zou, P. & Ting, A. Y. Site-Specific Protein Modification Using Lipoic Acid Ligase and Bis-Aryl Hydrazone Formation. *ChemBioChem* **13,** 888–894 (2012).
23. Jeger, S. *et al.* Site-Specific and Stoichiometric Modification of Antibodies by Bacterial Transglutaminase. *Angewandte Chemie International Edition* **49,** 9995–9997 (2010).
24. Antos, J. M. *et al.* Site-Specific N- and C-Terminal Labeling of a Single Polypeptide Using Sortases of Different Specificity. *Journal of the American Chemical Society* **131,** 10800–10801 (2009).
25. Rush, J. S. & Bertozzi, C. R. New Aldehyde Tag Sequences Identified by Screening Formylglycine Generating Enzymes in Vitroand in Vivo. *Journal of the American Chemical Society* **130,** 12240–12241 (2008).
26. Zeglis, B. M. *et al.* Enzyme-Mediated Methodology for the Site-Specific Radiolabeling of Antibodies Based on Catalyst-Free Click Chemistry. *Bioconjugate Chemistry* **24,** 1057–1067 (2013).
27. Mahalingam, S. M. *et al.* Evaluation of a Centyrin-Based Near-Infrared Probe for Fluorescence-Guided Surgery of Epidermal Growth Factor Receptor Positive Tumors. *Bioconjugate Chemistry* **28,** 2865–2873 (2017).
28. Rossin, R. *et al.* In Vivo Chemistry for Pretargeted Tumor Imaging in Live Mice. *Angewandte Chemie International Edition* **49,** 3375–3378 (2010).
29. Adumeau, P. *et al.* Site-Specifically Labeled Antibody–Drug Conjugate for Simultaneous Therapy and ImmunoPET. *Mol. Pharmaceutics* **15,** 892–898 (2018).
30. van Buggenum, J. A. G. L. *et al.* A covalent and cleavable antibody-DNA conjugation strategy for sensitive protein detection via immuno-PCR. *Scientific Reports* **6,** 22675 (2016).
31. Kazane, S. A. *et al.* Site-specific DNA-antibody conjugates for specific and sensitive immuno-PCR. *Proceedings of the National Academy of Sciences* **109,** 3731–3736 (2012).
32. Baltimore, D. *et al.* A prudent path forward for genomic engineering and germline gene modification. *Science* **348,** 36–38 (2015).
33. Dowdy, S. F. Overcoming cellular barriers for RNA therapeutics. *Nature Biotechnology* **35,** 222–229 (2017).

34. Rinaldi, C. & Wood, M. J. A. Antisense oligonucleotides: the next frontier for treatment of neurological disorders. *Nature Publishing Group* 1–13 (2017). doi:10.1038/nrneurol.2017.148
35. Opalinska, J. B. & Gewirtz, A. M. Nucleic-acid therapeutics: basic principles and recent applications. *Nat Rev Drug Discov* **1,** 503–514 (2002).
36. Muntoni, F. & Wood, M. J. A. Targeting RNA to treat neuromuscular disease. 1–17 (2011). doi:10.1038/nrd3459
37. Elbashir, S. M. *et al.* Duplexes of 21-Nucleotide RNAs Mediate RNA Interference in Cultured Mammalian Cells. *Nature* **411,** 494–498 (2001).
38. Fire, A. *et al.* Potent and specific genetic interference by double-stranded RNA in Caenorhabditis elegans. *Nature* **391,** 806–811 (1998).
39. Kenski, D. M. *et al.* siRNA-optimized Modifications for Enhanced In Vivo Activity. *Molecular Therapy — Nucleic Acids* **1,** e5 (2012).
40. Watts, J., Deleavy, G. & Damha, M. Chemically modified siRNA: tools and applications. *Drug Discovery Today* **13,** 842–855 (2008).
41. Robbins, M., Judge, A. & MacLachlan, I. siRNA and Innate Immunity. *Oligonucleotides* **19,** 89–102 (2009).
42. Eckstein, F. Nucleoside Phosphorothioates. *Journal of the American Chemical Society* **88,** 4292–4294 (1966).
43. Crooke, S. T., Wang, S., Vickers, T. A., Shen, W. & Liang, X.-H. Cellular uptake and trafficking of antisense oligonucleotides. *Nature Biotechnology* **35,** 230–237 (2017).
44. Matsuda, S. *et al.* siRNA Conjugates Carrying Sequentially Assembled Trivalent N-Acetylgalactosamine Linked Through Nucleosides Elicit Robust Gene Silencing In Vivoin Hepatocytes. *ACS Chemical Biology* **10,** 1181–1187 (2015).
45. Gilleron, J. *et al.* Image-based analysis of lipid nanoparticle–mediated siRNA delivery, intracellular trafficking and endosomal escape. *Nature Biotechnology* **31,** 638–646 (2013).
46. Wittrup, A. *et al.* Visualizing lipid-formulated siRNA release from endosomes and target gene knockdown. *Nature Biotechnology* **33,** 870–876 (2015).
47. Juliano, R. L. The delivery of therapeutic oligonucleotides. *Nucleic Acids Research* **44,** 6518–6548 (2016).
48. Stewart, M. P., Lorenz, A., Dahlman, J. & Sahay, G. Challenges in carrier-mediated intracellular delivery: moving beyond endosomal barriers. *WIREs Nanomed Nanobiotechnol* **8,** 465–478 (2015).
49. Blain, J. C. & Szostak, J. W. Progress Toward Synthetic Cells. *Annual Review of Biochemistry* **83,** 615–640 (2014).
50. Varkouhi, A. K., Scholte, M., Storm, G. & Haisma, H. J. Endosomal escape pathways for delivery of biologicals. *Journal of Controlled Release* **151,** 220–228 (2011).
51. Miller, D. K., Griffiths, E., Lenard, J. & Firestone, R. A. Cell killing by lysosomotropic detergents. *The Journal of Cell Biology* **97,** 1841–1851 (1983).
52. Pack, D. W., Putnam, D. & Langer, R. Design of imidazole-containing endosomolytic biopolymers for gene delivery. *Biotechnology and Bioengineering* **67,** 217–223 (2000).

53. Moreira, C. *et al.* Improving chitosan-mediated gene transfer by the introduction of intracellular buffering moieties into the chitosan backbone. *Acta Biomaterialia* **5,** 2995–3006 (2009).
54. Marsh, M. & Helenius, A. in **36,** 107–151 (Elsevier, 1989).
55. Wiley, D. C. & Skehel, J. J. The Structure and Function of the Hemagglutinin Membrane Glycoprotein of Influenza Virus. *Annual Review of Biochemistry* **56,** 365–394 (1987).
56. Horth, M. *et al.* Theoretical and functional analysis of the SIV fusion peptide. *The EMBO Journal* **10,** 2747–2755 (1991).
57. Maxfield, F. R. Weak bases and ionophores rapidly and reversibly raise the pH of endocytic vesicles in cultured mouse fibroblasts. *The Journal of Cell Biology* **95,** 676–681 (1982).
58. Cheng, J. *et al.* Structure−Function Correlation of Chloroquine and Analogues as Transgene Expression Enhancers in Nonviral Gene Delivery. *Journal of Medicinal Chemistry* **49,** 6522–6531 (2006).
59. Veldhoen, S., Laufer, S. D., Trampe, A. & Restle, T. Cellular delivery of small interfering RNA by a non-covalently attached cell-penetrating peptide: quantitative analysis of uptake and biological effect. *Nucleic Acids Research* **34,** 6561–6573 (2006).
60. Wadia, J. S., Stan, R. V. & Dowdy, S. F. Transducible TAT-HA fusogenic peptide enhances escape of TAT-fusion proteins after lipid raft macropinocytosis. *Nature Medicine* **10,** 310–315 (2004).
61. Terwilliger, T. C. & Eisenberg, D. The Structure of Melittin (II. Interpretation of the Structure). *Journal of Biological Chemistry* (1981). doi:10.2210/pdb1mlt/pdb
62. Dempsey, C. E. The actions of melittin on membranes. *Biochimica et Biophysica Acta (BBA) - Reviews on Biomembranes* **1031,** 143–161 (1990).
63. Othon, C. M., Kwon, O.-H., Lin, M. M. & Zewail, A. H. Solvation in protein (un)folding of melittin tetramer–monomer transition. *Proceedings of the National Academy of Sciences* **106,** 12593–12598 (2009).
64. Lee, M. T., Hung, W. C., Chen, F. Y. & Huang, H. W. Mechanism and kinetics of pore formation in membranes by water-soluble amphipathic peptides. *Proceedings of the National Academy of Sciences* **105,** 5087–5092 (2008).
65. Goto, Y. & Hagihara, Y. Mechanism of the conformational transition of melittin. *Biochemistry* **31,** 732–738 (2002).
66. Ogris, M., Carlisle, R. C., Bettinger, T. & Seymour, L. W. Melittin Enables Efficient Vesicular Escape and Enhanced Nuclear Access of Nonviral Gene Delivery Vectors. *Journal of Biological Chemistry* **276,** 47550–47555 (2001).
67. Tan, Y.-X. *et al.* Truncated peptides from melittin and its analog with high lytic activity at endosomal pH enhance branched polyethylenimine-mediated gene transfection. *J. Gene Med.* **14,** 241–250 (2012).
68. Rozema, D. B. *et al.* Dynamic PolyConjugates for targeted in vivo delivery of siRNA to hepatocytes. *Proceedings of the National Academy of Sciences* **104,** 12982–12987 (2007).
69. Rozema, D. B., Ekena, K., Lewis, D. L., Loomis, A. G. & Wolff, J. A. Endosomolysis by Masking of a Membrane-Active Agent (EMMA) for

Cytoplasmic Release of Macromolecules. *Bioconjugate Chemistry* **14,** 51–57 (2003).
70. Wong, S. C. *et al.* Co-Injection of a Targeted, Reversibly Masked Endosomolytic Polymer Dramatically Improves the Efficacy of Cholesterol-Conjugated Small Interfering RNAs In Vivo. *Nucleic Acid Therapeutics* **22,** 1–11 (2012).
71. Tweten, R. K., Parker, M. W. & Johnson, A. E. in *Pore-Forming Toxins* **257,** 15–33 (Springer, Berlin, Heidelberg, 2001).
72. Heuck, A. P., Savva, C. G., Holzenburg, A. & Johnson, A. E. Conformational Changes That Effect Oligomerization and Initiate Pore Formation Are Triggered throughout Perfringolysin O upon Binding to Cholesterol. *Journal of Biological Chemistry* **282,** 22629–22637 (2007).
73. Rossjohn, J., Feil, S. C., McKinstry, W. J., Tweten, R. K. & Parker, M. W. Structure of a Cholesterol-Binding, Thiol-Activated Cytolysin and a Model of Its Membrane Form. *Cell* **89,** 685–692 (1997).
74. Koster, S. *et al.* Crystal structure of listeriolysin O reveals molecular details of oligomerization and pore formation. *Nature Communications* **5,** 1–14 (2014).
75. Pirie, C. M., Liu, D. V. & Wittrup, K. D. Targeted Cytolysins Synergistically Potentiate Cytoplasmic Delivery of Gelonin Immunotoxin. *Molecular Cancer Therapeutics* **12,** 1774–1782 (2013).
76. Pirie, C. M., Hackel, B. J., Rosenblum, M. G. & Wittrup, K. D. Convergent Potency of Internalized Gelonin Immunotoxins across Varied Cell Lines, Antigens, and Targeting Moieties. *Journal of Biological Chemistry* **286,** 4165–4172 (2011).
77. Yang, N. J. *et al.* Antibody-Mediated Neutralization of Perfringolysin O for Intracellular Protein Delivery. *Mol. Pharmaceutics* **12,** 1992–2000 (2015).
78. Yang, N. J. *et al.* Cytosolic delivery of siRNA by ultra-high affinity dsRNA binding proteins. *Nucleic Acids Research* **45,** 7602–7614 (2017).
79. Ecker, D. M., Jones, S. D. & Levine, H. L. The therapeutic monoclonal antibody market. *mAbs* **7,** 9–14 (2014).
80. Reichert, J. M., Rosensweig, C. J., Faden, L. B. & Dewitz, M. C. Monoclonal antibody successes in the clinic. *Nature Biotechnology* **23,** 1073–1078 (2005).
81. Marks, J. D. *et al.* By-passing Immunization: Human Antibodies from V-gene Libraries Displayed on Phage. *Journal of Molecular Biology* 1–17 (2003).
82. McCafferty, J., Griffiths, A. D., Winter, G. & Chiswell, D. J. Phage antibodies: filamentous phage displaying antibody variable domains. *Nature* **348,** 552–554 (1990).
83. Bradbury, A. R. M. & Marks, J. D. Antibodies from phage antibody libraries. *Journal of Immunological Methods* **290,** 29–49 (2004).
84. Zahnd, C. *et al.* Directed in VitroEvolution and Crystallographic Analysis of a Peptide-binding Single Chain Antibody Fragment (scFv) with Low Picomolar Affinity. *Journal of Biological Chemistry* **279,** 18870–18877 (2004).
85. Hanes, J., Schaffitzel, C., Knappik, A. & Plückthun, A. Picomolar affinity antibodies from a fully synthetic naive library selected and evolved by ribosome display. *Nature Biotechnology* **18,** 1287–1292 (2000).
86. Hanes, J., Jermutus, L., Weber-Bornhauser, S., Bosshard, H. R. & Pluckthun, A. Ribosome display efficiently selects and evolves high-affinity antibodies in

vitro from immune libraries. *Proceedings of the National Academy of Sciences* **95,** 14130–14135 (1998).
87. Schaffitzel, C. *et al.* In vitro generated antibodies specific for telomeric guanine-quadruplex DNA react with Stylonychia lemnae macronuclei. *Proceedings of the National Academy of Sciences* **98,** 8572–8577 (2001).
88. Jermutus, L., Honegger, A., Schwesinger, F., Hanes, J. & Pluckthun, A. Tailoring in vitro evolution for protein affinity or stability. *Proceedings of the National Academy of Sciences* **98,** 75–80 (2001).
89. Boder, E. T., Midelfort, K. S. & Wittrup, K. D. Directed evolution of antibody fragments with monovalent femtomolar antigen-binding affinity. *Proceedings of the National Academy of Sciences* **97,** 10701–10705 (2000).
90. Boder, E. T. & Wittrup, K. D. Yeast surface display for screening combinatorial polypeptide libraries. *Nature Biotechnology* **15,** 553–557 (1997).
91. Lonberg, N. Human antibodies from transgenic animals. *Nature Biotechnology* **23,** 1117–1125 (2005).
92. Green, L. L. *et al.* Antigen–specific human monoclonal antibodies from mice engineered with human Ig heavy and light chain YACs. *Nature Genetics* **7,** 13–21 (1994).
93. Salles, G. *et al.* Phase 1 study results of the type II glycoengineered humanized anti-CD20 monoclonal antibody obinutuzumab (GA101) in B-cell lymphoma patients. *Blood* **119,** 5126–5132 (2012).
94. Dalle, S. *et al.* Preclinical Studies on the Mechanism of Action and the Anti-Lymphoma Activity of the Novel Anti-CD20 Antibody GA101. *Molecular Cancer Therapeutics* **10,** 178–185 (2011).
95. Cartron, G. *et al.* Obinutuzumab (GA101) in relapsed/refractory chronic lymphocytic leukemia: final data from the phase 1/2 GAUGUIN study. *Blood* **124,** 2196–2202 (2014).
96. Bowles, J. A. *et al.* Anti-CD20 monoclonal antibody with enhanced affinity for CD16 activates NK cells at lower concentrations and more effectively than rituximab. *Blood* **108,** 2648–2654 (2006).
97. Lohse, S. *et al.* Recombinant Dimeric IgA Antibodies against the Epidermal Growth Factor Receptor Mediate Effective Tumor Cell Killing. *The Journal of Immunology* **186,** 3770–3778 (2011).
98. Dodev, T. S. *et al.* A tool kit for rapid cloning and expression of recombinant antibodies. *Scientific Reports* **4,** (2014).
99. Ilieva, K. M. *et al.* Functionally Active Fc Mutant Antibodies Recognizing Cancer Antigens Generated Rapidly at High Yields. *Front. Immunol.* **8,** 4892–18 (2017).
100. Dall'Ozzo, S. *et al.* Rituximab-Dependent Cytotoxicity by Natural Killer Cells: Influence of FCGR3A Polymorphism on the Concentration-Effect Relationship. *Cancer Research* **64,** 4664–4669 (2004).
101. Lefebvre, M.-L., Krause, S. W., Salcedo, M. & Nardin, A. Ex Vivo-activated Human Macrophages Kill Chronic Lymphocytic Leukemia Cells in the Presence of Rituximab: Mechanism of Antibody-dependent Cellular Cytotoxicity and Impact of Human Serum. *Journal of Immunotherapy* **29,** 388–397 (2006).

102. Hernandez-Ilizaliturri, F. J. *et al.* Neutrophils Contribute to the Biological Antitumor Activity of Rituximab in a Non-Hodgkin's Lymphoma Severe Combined Immunodeficiency Mouse Model. *Clinical Cancer Research* **9,** 5866–5873 (2003).
103. Beers, S. A. & Glennie, M. J. Neutrophils: 'neu players' in antibody therapy? *Blood* **122,** 3093–3094 (2013).
104. Sievers, E. L. & Senter, P. D. Antibody-Drug Conjugates in Cancer Therapy. *Annual Review of Medicine* **64,** 15–29 (2013).
105. Prescher, J. A. & Bertozzi, C. R. Chemistry in living systems. *Nature Chemical Biology* **1,** 13–21 (2005).
106. Kolb, H. C., Finn, M. G. & Sharpless, K. B. Click Chemistry: Diverse Chemical Function from a Few Good Reactions. *Angewandte Chemie International Edition* **40,** 2004–2021 (2001).
107. Huisgen, R. 1,3-Dipolar Cycloadditions. *Angewandte Chemie International Edition* **2,** 565–598 (1963).
108. Blackman, M. L., Royzen, M. & Fox, J. M. Tetrazine Ligation: Fast Bioconjugation Based on Inverse-Electron-Demand Diels−Alder Reactivity. *Journal of the American Chemical Society* **130,** 13518–13519 (2008).
109. Shen, B.-Q. *et al.* Conjugation site modulates the in vivo stability and therapeutic activity of antibody-drug conjugates. *Nature Biotechnology* **30,** 184–189 (2012).
110. Jeffrey, S. C. *et al.* A Potent Anti-CD70 Antibody–Drug Conjugate Combining a Dimeric Pyrrolobenzodiazepine Drug with Site-Specific Conjugation Technology. *Bioconjugate Chemistry* **24,** 1256–1263 (2013).
111. Voynov, V. *et al.* Design and Application of Antibody Cysteine Variants. *Bioconjugate Chemistry* **21,** 385–392 (2010).
112. Tian, F. *et al.* A general approach to site-specific antibody drug conjugates. *Proceedings of the National Academy of Sciences* **111,** 1766–1771 (2014).
113. VanBrunt, M. P. *et al.* Genetically Encoded Azide Containing Amino Acid in Mammalian Cells Enables Site-Specific Antibody–Drug Conjugates Using Click Cycloaddition Chemistry. *Bioconjugate Chemistry* **26,** 2249–2260 (2015).
114. Puthenveetil, S., Liu, D. S., White, K. A., Thompson, S. & Ting, A. Y. Yeast Display Evolution of a Kinetically Efficient 13-Amino Acid Substrate for Lipoic Acid Ligase. *Journal of the American Chemical Society* **131,** 16430–16438 (2009).
115. Lhospice, F. *et al.* Site-Specific Conjugation of Monomethyl Auristatin E to Anti-CD30 Antibodies Improves Their Pharmacokinetics and Therapeutic Index in Rodent Models. *Mol. Pharmaceutics* **12,** 1863–1871 (2015).
116. Dennler, P. *et al.* Transglutaminase-Based Chemo-Enzymatic Conjugation Approach Yields Homogeneous Antibody–Drug Conjugates. *Bioconjugate Chemistry* **25,** 569–578 (2014).
117. Fontana, A., Spolaore, B., Mero, A. & Veronese, F. M. Site-specific modification and PEGylation of pharmaceutical proteins mediated by transglutaminase. *Advanced Drug Delivery Reviews* **60,** 13–28 (2008).

118. Liu, D. S. *et al.* Computational design of a red fluorophore ligase for site-specific protein labeling in living cells. *Proceedings of the National Academy of Sciences* **111,** E4551–E4559 (2014).
119. Uttamapinant, C. *et al.* A fluorophore ligase for site-specific protein labeling inside living cells. *Proceedings of the National Academy of Sciences* **107,** 10914–10919 (2010).
120. Uttamapinant, C. *et al.* Fast, Cell-Compatible Click Chemistry with Copper-Chelating Azides for Biomolecular Labeling. *Angewandte Chemie International Edition* **51,** 5852–5856 (2012).
121. Liu, D. S. *et al.* Diels–Alder Cycloaddition for Fluorophore Targeting to Specific Proteins inside Living Cells. *Journal of the American Chemical Society* **134,** 792–795 (2011).
122. Cohen, J. D., Thompson, S. & Ting, A. Y. Structure-Guided Engineering of a Pacific Blue Fluorophore Ligase for Specific Protein Imaging in Living Cells. *Biochemistry* **50,** 8221–8225 (2011).
123. Hildreth, J. E. K., Derr, D. & Azorsa, D. O. Characterization of a Novel Self-Associating Mr 40,000 Platelet Glycoprotein. *Blood* **77,** 121–132 (1991).
124. Cox, E. C. *et al.* Antibody-mediated endocytosis of polysialic acid enables intracellular delivery and cytotoxicity of a glycan-directed antibody-drug conjugate. *Cancer Research* canres.3119.2018 (2019). doi:10.1158/0008-5472.CAN-18-3119
125. Bertelsen, V. & Stang, E. The Mysterious Ways of ErbB2/HER2 Trafficking. *Membranes* **4,** 424–446 (2014).
126. Pols, M. S. & Klumperman, J. Trafficking and function of the tetraspanin CD63. *Experimental Cell Research* **315,** 1584–1592 (2009).
127. Dozier, J. & Distefano, M. Site-Specific PEGylation of Therapeutic Proteins. *IJMS* **16,** 25831–25864 (2015).
128. Fire, A. *et al.* Potent and specific genetic interference by double-stranded RNA in Caenorhabditis elegans. *Nature* **391,** 806–811 (1998).
129. Davis, M. E. The First Targeted Delivery of siRNA in Humans via a Self-Assembling, Cyclodextrin Polymer-Based Nanoparticle: From Concept to Clinic. *Mol. Pharmaceutics* **6,** 659–668 (2009).
130. Gonzalez, H., Hwang, S. J. & Davis, M. E. New Class of Polymers for the Delivery of Macromolecular Therapeutics. *Bioconjugate Chemistry* **10,** 1068–1074 (1999).
131. Hu-Lieskovan, S., Heidel, J. D., Bartlett, D. W., Davis, M. E. & Triche, T. J. Sequence-Specific Knockdown of EWS-FLI1 by Targeted, Nonviral Delivery of Small Interfering RNA Inhibits Tumor Growth in a Murine Model of Metastatic Ewing's Sarcoma. *Cancer Research* **65,** 8984–8992 (2005).
132. Hwang, S. J., Bellocq, N. C. & Davis, M. E. Effects of Structure of β-Cyclodextrin-Containing Polymers on Gene Delivery. *Bioconjugate Chemistry* **12,** 280–290 (2001).
133. Popielarski, S. R., Mishra, S. & Davis, M. E. Structural Effects of Carbohydrate-Containing Polycations on Gene Delivery. 3. Cyclodextrin Type and Functionalization. *Bioconjugate Chemistry* **14,** 672–678 (2003).
134. Pun, S. H. *et al.* Cyclodextrin-Modified Polyethylenimine Polymers for Gene Delivery. *Bioconjugate Chemistry* **15,** 831–840 (2004).

135. Reineke, T. M. & Davis, M. E. Structural Effects of Carbohydrate-Containing Polycations on Gene Delivery. 1. Carbohydrate Size and Its Distance from Charge Centers. *Bioconjugate Chemistry* **14,** 247–254 (2003).
136. Hafez, I. M., Maurer, N. & Cullis, P. R. On the mechanism whereby cationic lipids promote intracellular delivery of polynucleic acids. *Gene Therapy* **8,** 1188–1196 (2001).
137. Hafez, I. M., Ansell, S. & Cullis, P. R. Tunable pH-Sensitive Liposomes Composed of Mixtures of Cationic and Anionic Lipids. *Biophysical Journal* **79,** 1438–1446 (2000).
138. Huang, L. & Liu, Y. In Vivo Delivery of RNAi with Lipid-Based Nanoparticles. *Annu. Rev. Biomed. Eng.* **13,** 507–530 (2011).
139. Jayaraman, M. *et al.* Maximizing the Potency of siRNA Lipid Nanoparticles for Hepatic Gene Silencing In Vivo. *Angewandte Chemie International Edition* **51,** 8529–8533 (2012).
140. Love, K. T. *et al.* Lipid-like materials for low-dose, in vivo gene silencing. *Proceedings of the National Academy of Sciences* **107,** 9915–9915 (2010).
141. Mahon, K. P. *et al.* Combinatorial Approach to Determine Functional Group Effects on Lipidoid-Mediated siRNA Delivery. *Bioconjugate Chemistry* **21,** 1448–1454 (2010).
142. Sato, Y. *et al.* A pH-sensitive cationic lipid facilitates the delivery of liposomal siRNA and gene silencing activity in vitro and in vivo. *Journal of Controlled Release* **163,** 267–276 (2012).
143. Xu, Y. & Szoka, F. C. Mechanism of DNA Release from Cationic Liposome/DNA Complexes Used in Cell Transfection †,‡. *Biochemistry* **35,** 5616–5623 (1996).
144. Zhang, J., Fan, H., Levorse, D. A. & Crocker, L. S. Ionization Behavior of Amino Lipids for siRNA Delivery: Determination of Ionization Constants, SAR, and the Impact of Lipid p K a on Cationic Lipid−Biomembrane Interactions. *Langmuir* **27,** 1907–1914 (2011).
145. Zhang, S., Zhi, D. & Huang, L. Lipid-based vectors for siRNA delivery. *Journal of Drug Targeting* **20,** 724–735 (2012).
146. Zimmermann, T. S. *et al.* RNAi-mediated gene silencing in non-human primates. *Nature* **441,** 111–114 (2006).
147. Urban-Klein, B., Werth, S., Abuharbeid, S., Czubayko, F. & Aigner, A. RNAi-mediated gene-targeting through systemic application of polyethylenimine (PEI)-complexed siRNA in vivo. *Gene Therapy* **12,** 461–466 (2004).
148. Kichler, A. Gene transfer with modified polyethylenimines. *J. Gene Med.* **6,** S3–S10 (2004).
149. Kircheis, R., Wightman, L. & Wagner, E. Design and gene delivery activity of modified polyethylenimines. *Advanced Drug Delivery Reviews* **53,** 341–358 (2001).
150. Richards Grayson, A. C., Doody, A. M. & Putnam, D. Biophysical and Structural Characterization of Polyethylenimine-Mediated siRNA Delivery in Vitro. *Pharm Res* **23,** 1868–1876 (2006).

151. Thomas, M. *et al.* Full deacylation of polyethylenimine dramatically boosts its gene delivery efficiency and specificity to mouse lung. *Proceedings of the National Academy of Sciences* **102,** 5679–5684 (2005).
152. Werth, S. *et al.* A low molecular weight fraction of polyethylenimine (PEI) displays increased transfection efficiency of DNA and siRNA in fresh or lyophilized complexes. *Journal of Controlled Release* **112,** 257–270 (2006).
153. Wittrup, A. & Lieberman, J. Knocking down disease: a progress report on siRNA therapeutics. *Nature Reviews Genetics* **16,** 543–552 (2015).
154. Hajj, K. A. & Whitehead, K. A. Tools for translation: non-viral materials for therapeutic mRNA delivery. *Nature Publishing Group* **2,** 1–17 (2017).
155. Alexis, F., Pridgen, E., Molnar, L. K. & Farokhzad, O. C. Factors Affecting the Clearance and Biodistribution of Polymeric Nanoparticles. *Mol. Pharmaceutics* **5,** 505–515 (2008).
156. Nielsen, C., Kjems, J., Sørensen, K. R., Engelholm, L. H. & Behrendt, N. Advances in targeted delivery of small interfering RNA using simple bioconjugates. *Expert Opinion on Drug Delivery* **11,** 791–822 (2014).
157. Nair, J. K. *et al.* Multivalent N -Acetylgalactosamine-Conjugated siRNA Localizes in Hepatocytes and Elicits Robust RNAi-Mediated Gene Silencing. *Journal of the American Chemical Society* **136,** 16958–16961 (2014).
158. McNamara, J. O. *et al.* Cell type–specific delivery of siRNAs with aptamer-siRNA chimeras. *Nature Biotechnology* **24,** 1005–1015 (2006).
159. Wheeler, L. A. *et al.* Inhibition of HIV transmission in human cervicovaginal explants and humanized mice using CD4 aptamer-siRNA chimeras. *Journal of Clinical Investigation* **121,** 2401–2412 (2011).
160. Berezhnoy, A., Castro, I., Levay, A., Malek, T. R. & Gilboa, E. Aptamer-targeted inhibition of mTOR in T cells enhances antitumor immunity. *Journal of Clinical Investigation* **124,** 188–197 (2013).
161. Song, E. *et al.* Antibody mediated in vivo delivery of small interfering RNAs via cell-surface receptors. *Nature Biotechnology* **23,** 709–717 (2005).
162. Baumer, S. *et al.* Antibody-Mediated Delivery of Anti-KRAS-siRNA In Vivo Overcomes Therapy Resistance in Colon Cancer. *Clinical Cancer Research* **21,** 1383–1394 (2015).
163. Sugo, T. *et al.* Development of antibody-siRNA conjugate targeted to cardiac and skeletal muscles. *Journal of Controlled Release* **237,** 1–13 (2016).
164. Ma, Y. *et al.* Humanized Lewis-Y Specific Antibody Based Delivery of STAT3 siRNA. *ACS Chemical Biology* **6,** 962–970 (2011).
165. Cuellar, T. L. *et al.* Systematic evaluation of antibody-mediated siRNA delivery using an industrial platform of THIOMAB-siRNA conjugates. *Nucleic Acids Research* **43,** 1189–1203 (2014).
166. Baumer, N. *et al.* Antibody-coupled siRNA as an efficient method for in vivo mRNA knockdown. *Nature Protocols* **11,** 22–36 (2015).
167. Peer, D., Zhu, P., Carman, C. V., Lieberman, J. & Shimaoka, M. Selective gene silencing in activated leukocytes by targeting siRNAs to the integrin lymphocyte function-associated antigen-1. *Proceedings of the National Academy of Sciences* **104,** 4095–4100 (2007).

168. Yao, Y. D. *et al.* Targeted Delivery of PLK1-siRNA by ScFv Suppresses Her2 Breast Cancer Growth and Metastasis. *Science Translational Medicine* **4,** 130ra48–130ra48 (2012).
169. Kumar, P. *et al.* T Cell-Specific siRNA Delivery Suppresses HIV-1 Infection in Humanized Mice. *Cell* **134,** 577–586 (2008).
170. Kingston, R. E., Chen, C. A. & Rose, J. K. Calcium Phosphate Transfection. *Current Protocols in Molecular Biology* **63,** 9.1.1–9.1.11 (2003).
171. Parmar, R. *et al.* 5′-(E)-Vinylphosphonate: A Stable Phosphate Mimic Can Improve the RNAi Activity of siRNA-GalNAc Conjugates. *ChemBioChem* **17,** 985–989 (2016).
172. Layzer, J. M. *et al.* In vivo activity of nuclease-resistant siRNAs. *RNA* **10,** 766–771 (2004).
173. Matias, C. *et al.* Citrate and albumin facilitate transferrin iron loading in the presence of phosphate. *Journal of Inorganic Biochemistry* **168,** 107–113 (2017).
174. Khvorova, A. & Watts, J. K. The chemical evolution of oligonucleotide therapies of clinical utility. *Nature Biotechnology* **35,** 238–248 (2017).
175. Zak, O. *et al.* Iron Release from Recombinant N-lobe and Mutants of Human Transferrin. *Biochemistry* **34,** 14428–14434 (1995).
176. Zelikin, A. N., Ehrhardt, C. & Healy, A. M. Materials and methods for delivery of biological drugs. *Nature Chemistry* **8,** 997–1007 (2016).
177. Whitehead, K. A., Langer, R. & Anderson, D. G. Knocking down barriers: advances in siRNA delivery. *Nat Rev Drug Discov* **8,** 129–138 (2009).
178. Schellinger, J. G. *et al.* Melittin-grafted HPMA-oligolysine based copolymers for gene delivery. *Biomaterials* **34,** 2318–2326 (2013).
179. Bettinger, T., Carlisle, R. C., Read, M. L., Ogris, M. & Seymour, L. W. Peptide-mediated RNA delivery: a novel approach for enhanced transfection of primary and post-mitotic cells. *Nucleic Acids Research* **29,** 3882–3891 (2001).
180. Boeckle, S., Wagner, E. & Ogris, M. C- versus N-terminally linked melittin-polyethylenimine conjugates: the site of linkage strongly influences activity of DNA polyplexes. *J. Gene Med.* **7,** 1335–1347 (2005).
181. Chen, C.-P., Kim, J.-S., Steenblock, E., Liu, D. & Rice, K. G. Gene Transfer with Poly-Melittin Peptides. *Bioconjugate Chemistry* **17,** 1057–1062 (2006).
182. Meyer, M. *et al.* Synthesis and Biological Evaluation of a Bioresponsive and Endosomolytic siRNA−Polymer Conjugate. *Mol. Pharmaceutics* **6,** 752–762 (2009).
183. Melikov, K. & Chernomordik, L. V. Arginine-rich cell penetrating peptides: from endosomal uptake to nuclear delivery. *Cell. Mol. Life Sci.* **62,** 2739–2749 (2005).
184. Nagahara, H. *et al.* Transduction of full-length TAT fusion proteins into mammalian cells: TAT-$p27^{Kip1}$ induces cell migration. *Nature Medicine* **4,** 1449–1452 (1998).
185. Margus, H., Padari, K. & Pooga, M. Cell-penetrating Peptides as Versatile Vehicles for Oligonucleotide Delivery. *Molecular Therapy* **20,** 525–533 (2016).

186. Najjar, K. *et al.* Unlocking Endosomal Entrapment with Supercharged Arginine-Rich Peptides. *Bioconjugate Chemistry* **28,** 2932–2941 (2017).
187. Mandal, M. & Lee, K.-D. Listeriolysin O-liposome-mediated cytosolic delivery of macromolecule antigen in vivo: enhancement of antigen-specific cytotoxic T lymphocyte frequency, activity, and tumor protection. *Biochimica et Biophysica Acta (BBA) - Biomembranes* **1563,** 7–17 (2002).
188. Saito, G., Amidon, G. L. & Lee, K.-D. Enhanced cytosolic delivery of plasmid DNA by a sulfhydryl-activatable listeriolysin O/protamine conjugate utilizing cellular reducing potential. *Gene Therapy* **10,** 72–83 (2003).
189. Werkmeister, J. A., Hewish, D. R., Kirkpatrick, A. & Rivett, D. E. Sequence requirements for the activity of membrane-active peptides. *The Journal of Peptide Research* **60,** 232–238 (2002).
190. Phan, N. N., Li, C. & Alabi, C. A. Intracellular Delivery via Noncharged Sequence-Defined Cell- Penetrating Oligomers. *Bioconjugate Chemistry* **29,** 2628–2635 (2018).
191. Verherstraeten, S. *et al.* Perfringolysin O: The Underrated Clostridium perfringens Toxin? *Toxins* **7,** 1702–1721 (2015).
192. Polekhina, G., Giddings, K. S., Tweten, R. K. & Parker, M. W. Insights into the action of the superfamily of cholesterol-dependent cytolysins from studies of intermedilysin. *Proceedings of the National Academy of Sciences* **102,** 600–605 (2005).
193. Liu, D. V., Yang, N. J. & Wittrup, K. D. A Nonpolycationic Fully Proteinaceous Multiagent System for Potent Targeted Delivery of siRNA. *Molecular Therapy — Nucleic Acids* **3,** e162 (2014).
194. Rozema, D. B. *et al.* Protease-triggered siRNA delivery vehicles. *Journal of Controlled Release* **209,** 57–66 (2015).
195. Naganawa, A., Ichikawa, Y. & Isobe, M. Synthetic studies on tautomycin: Synthesis of 2,3-Disubstituted Maleic Anhydride Segment. *Tetrahedron* **50,** 8969–8982 (1994).
196. Xing, Y., Smith, A. M., Agrawal, A., Ruan, G. & Nie, S. Molecular profiling of single cancer cells and clinical tissue specimens with semiconductor quantum dots. *International Journal of Nanomedicine* **1,** 473–481 (2006).
197. Mayor, S. & Pagano, R. E. Pathways of clathrin-independent endocytosis. *Nature Reviews Molecular Cell Biology* **8,** 603–612 (2007).
198. Doronina, S. O. *et al.* Development of potent monoclonal antibody auristatin conjugates for cancer therapy. *Nature Biotechnology* 778–784 (2003).
199. Hamblett, K. J. *et al.* Effects of Drug Loading on the Antitumor Activity of a Monoclonal Antibody Drug Conjugate. *Clinical Cancer Research* 7063–7070 (2004).
200. Patterson, J. T., Asano, S., Li, X., Rader, C. & Barbas, C. F., III. Improving the Serum Stability of Site-Specific Antibody Conjugates with Sulfone Linkers. *Bioconjugate Chemistry* **25,** 1402–1407 (2014).
201. Thompson, P. *et al.* Hydrolytically Stable Site-Specific Conjugation at the N-Terminus of an Engineered Antibody. *Bioconjugate Chemistry* **26,** 2085–2096 (2015).

202. Lac, D. *et al.* Covalent Chemical Ligation Strategy for Mono- and Polyclonal Immunoglobulins at Their Nucleotide Binding Sites. *Bioconjugate Chemistry* **27,** 159–169 (2016).
203. Zuberbühler, K., Casi, G., Bernardes, G. J. L. & Neri, D. Fucose-specific conjugation of hydrazide derivatives to a vascular-targeting monoclonal antibody in IgG format. *Chemical Communications* **48,** 7100–3 (2012).
204. Ekholm, F. S. *et al.* Introducing Glycolinkers for the Functionalization of Cytotoxic Drugs and Applications in Antibody-Drug Conjugation Chemistry. *ChemMedChem* **11,** 2501–2505 (2016).
205. Okeley, N. M. *et al.* Metabolic Engineering of Monoclonal Antibody Carbohydrates for Antibody–Drug Conjugation. *Bioconjugate Chemistry* **24,** 1650–1655 (2013).
206. Zhou, Q. *et al.* Site-Specific Antibody–Drug Conjugation through Glycoengineering. *Bioconjugate Chemistry* **25,** 510–520 (2014).
207. Li, X., Fang, T. & Boons, G.-J. Preparation of Well-Defined Antibody-Drug Conjugates through Glycan Remodeling and Strain-Promoted Azide-Alkyne Cycloadditions. *Angewandte Chemie International Edition* **53,** 7179–7182 (2014).
208. Qasba, P. K. Glycans of Antibodies as a Specific Site for Drug Conjugation Using Glycosyltransferases. *Bioconjugate Chemistry* **26,** 2170–2175 (2015).
209. van Geel, R. *et al.* Chemoenzymatic Conjugation of Toxic Payloads to the Globally Conserved N-Glycan of Native mAbs Provides Homogeneous and Highly Efficacious Antibody–Drug Conjugates. *Bioconjugate Chemistry* **26,** 2233–2242 (2015).
210. Bryant, P. *et al.* In Vitro and In Vivo Evaluation of Cysteine Rebridged Trastuzumab–MMAE Antibody Drug Conjugates with Defined Drug-to-Antibody Ratios. *Mol. Pharmaceutics* **12,** 1872–1879 (2015).
211. Behrens, C. R. *et al.* Antibody–Drug Conjugates (ADCs) Derived from Interchain Cysteine Cross-Linking Demonstrate Improved Homogeneity and Other Pharmacological Properties over Conventional Heterogeneous ADCs. *Mol. Pharmaceutics* **12,** 3986–3998 (2015).
212. Maruani, A. *et al.* A plug-and-play approach to antibody-based therapeutics via a chemoselective dual click strategy. *Nature Communications* **6,** 6645 (2015).
213. Harmand, T. J. *et al.* One-Pot Dual Labeling of IgG 1 and Preparation of C-to-C Fusion Proteins Through a Combination of Sortase A and Butelase 1. *Bioconjugate Chemistry* 1–5 (2018). doi:10.1021/acs.bioconjchem.8b00563
214. Beerli, R. R., Hell, T., Merkel, A. S. & Grawunder, U. Sortase Enzyme-Mediated Generation of Site-Specifically Conjugated Antibody Drug Conjugates with High In Vitro and In Vivo Potency. *PLoS ONE* **10,** e0131177–17 (2015).
215. Hu, C.-M. J. & Zhang, L. Nanoparticle-based combination therapy toward overcoming drug resistance in cancer. *Biochemical Pharmacology* **83,** 1104–1111 (2012).
216. Maruani, A., Richards, D. A. & Chudasama, V. Dual modification of biomolecules. *Org. Biomol. Chem.* **14,** 6165–6178 (2016).

217. Levengood, M. R. *et al.* Orthogonal Cysteine Protection Enables Homogeneous Multi-Drug Antibody-Drug Conjugates. *Angew. Chem.* **129,** 751–755 (2016).
218. Adumeau, P. *et al.* Site-Specifically Labeled Antibody–Drug Conjugate for Simultaneous Therapy and ImmunoPET. *Mol. Pharmaceutics* **15,** 892–898 (2018).
219. Spycher, P. R. *et al.* Dual, Site-Specific Modification of Antibodies by Using Solid-Phase Immobilized Microbial Transglutaminase. *ChemBioChem* **18,** 1923–1927 (2017).
220. Wollschlaeger, C. *et al.* Simultaneous and Independent Dual Site-Specific Self-Labeling of Recombinant Antibodies. *Bioconjugate Chemistry* 1–9 (2018). doi:10.1021/acs.bioconjchem.8b00545
221. Sorkin, M. R., Walker, J. A., Brown, J. S. & Alabi, C. A. Versatile Platform for the Synthesis of Orthogonally Cleavable Heteromultifunctional Cross-Linkers. *Bioconjugate Chemistry* **28,** 907–912 (2017).
222. Lee, B.-C. *et al.* FRET Reagent Reveals the Intracellular Processing of Peptide-Linked Antibody–Drug Conjugates. *Bioconjugate Chemistry* **29,** 2468–2477 (2018).
223. Anami, Y. *et al.* Enzymatic conjugation using branched linkers for constructing homogeneous antibody–drug conjugates with high potency. *Org. Biomol. Chem.* **15,** 5635–5642 (2017).
224. Dubowchik, G. M. *et al.* Cathepsin B-Labile Dipeptide Linkers for Lysosomal Release of Doxorubicin from Internalizing Immunoconjugates: Model Studies of Enzymatic Drug Release and Antigen-Specific In Vitro Anticancer Activity. *Bioconjugate Chemistry* **13,** 855–869 (2002).
225. Turk, B. E., Huang, L. L., Piro, E. T. & Cantley, L. C. Determination of protease cleavage site motifs using mixture-based oriented peptide libraries. *Nature Biotechnology* **19,** 661–667 (2001).
226. Chau, Y., Tan, F. E. & Langer, R. Synthesis and Characterization of Dextran−Peptide−Methotrexate Conjugates for Tumor Targeting via Mediation by Matrix Metalloproteinase II and Matrix Metalloproteinase IX. *Bioconjugate Chemistry* **15,** 931–941 (2004).
227. Uttamapinant, C., Sanchez, M. I., Liu, D. S., Yao, J. Z. & Ting, A. Y. Site-specific protein labeling using PRIME and chelation-assisted click chemistry. *Nature Protocols* **8,** 1620–1634 (2013).
228. Salomon, P. L. & Singh, R. Sensitive ELISA Method for the Measurement of Catabolites of Antibody–Drug Conjugates (ADCs) in Target Cancer Cells. *Mol. Pharmaceutics* **12,** 1752–1761 (2015).